THE GEOCHEMISTRY OF UNDERSATURATED ARC LAVAS FROM THE TABAR-FENI ISLAND GROUPS, PAPUA NEW GUINEA

by

ALLEN KEN KENNEDY

B.S. (honors), La Trobe University, Melbourne, Australia
(1976)

SUBMITTED TO THE DEPARTMENT OF EARTH
ATMOSPHERIC, AND PLANETARY SCIENCES
IN PARTIAL FULFILLMENT OF THE
REQUIREMENTS FOR THE
DEGREE OF

DOCTOR OF PHILOSOPHY
at the
MASSACHUSETTS INSTITUTE OF TECHNOLOGY
February 1988

Signature of
Author_____
Department of Earth, Atmospheric,
and Planetary Sciences
February 10, 1988

Certified by_____
Stanley R. Hart
Thesis Supervisor

Accepted
by_____
Chairman, Department Committee on Graduate Students

THE GEOCHEMISTRY OF UNDERSATURATED ARC LAVAS FROM THE TABAR-FENI ISLAND GROUPS, PAPUA NEW GUINEA

by

ALLEN KEN KENNEDY

SUBMITTED TO THE DEPARTMENT OF EARTH
ATMOSPHERIC, AND PLANETARY SCIENCES IN
PARTIAL FULFILLMENT OF THE REQUIREMENTS
FOR THE DEGREE OF DOCTOR OF PHILOSOPHY

ABSTRACT

The undersaturated lavas from the Tabar-Feni island chain in Papua New Guinea, are highly enriched in large ion lithophile elements (LILE), depleted in high field strength elements (HFSE) and have Nd, Sr and Pb isotopes typical of arc lavas.

Experimental results (1 atm), major element, trace element, and mineral chemistry show that the fractionation of the undersaturated Lihir lavas is dominated by the removal at low pressures of a cpx-rich assemblage. The isotopic data for Lihir is consistent with a cogenetic origin for this suite. Elements normally considered incompatible have high bulk partition coefficients in both primitive and evolved lavas. This results in crossing REE patterns, primitive lavas with higher abundances of incompatible elements than evolved lavas. Changes in trace element partitioning in apatite microphenocrysts which nucleate at the crystal-liquid interface of rapidly growing clinopyroxene phenocrysts are responsible for this effect.

In the Feni islands three groups of lavas have different major element, trace element and isotopic compositions. When these samples are projected onto the oliv-diop-neph and oliv-plag-diop faces of the pseudoquarternary of Sack et al. (1987), they plot as well separated evolutionary trends. The compositions of the Tabar-Feni lavas is consistent with a polybaric fractionation under high oxygen fugacities (Ni-NiO to H-M), of olivine at moderate to high pressure followed by differentiation of different cpx-rich assemblages within the crust, at pressures between 1 atmosphere and 5 kb.

The Sr, Pb and Nd isotopic data for the Feni lavas requires at least 3 isotopically distinct components. AFC is suggested by increasing $^{87}Sr/^{86}Sr$ and decreasing, $^{143}Nd/^{144}Nd$ and $^{206}Pb/^{204}Pb$, coupled with decreasing Sc and increasing Ba. Phonolitic tephrites from Feni evolve by mixing, and one endmember is poorly constrained.

The Tabar-Feni lavas have isotopic composition and trace element ratios that are similar to those found in calc-alkaline, tholeiitic and undersaturated arc lavas that have no identifiable crust/sediment isotopic signature. The combined data from all island groups produces a negative correlation between HFSE depletion and LILE enrichment. Mixing between two arc source components, with one derived from OIB and one from MORB, or both derived from OIB explains this correlation.

There has been no plate subduction for >20 my in the Tabar-Feni region and there is no seismic evidence for a detached plate beneath these islands. Therefore, magmas with arc signatures can be generated in a tectonic setting where there is <u>no</u> subducting slab and there is <u>no</u> present influx of fluids from a slab.

Thesis Supervisor: Stanley R. Hart
Professor of Geology and Geochemistry.

TABLE OF CONTENTS

LIST OF FIGURES

LIST OF TABLES

ACKNOWLEDGEMENTS

I am grateful to Stan Hart for, providing an environment of scientific freedom, patience during rewrites, isotopic and geochemical insight, almost instantaneous feedback during the last six months, financial backing, a good sense of humor, and time. I would like to thank Fred Frey for friendship, interest in my scientific development, a willingness to discuss anything at any time, an open attitude to new ideas, free access to INAA and financial support. Nobu Shimizu provided the chance to explore the world of the ion microprobe and the complexity of geological processes. I am especially grateful for the opportunity to learn a skill that can be built into a career. Thanks to Tim Grove for use of experimental furnaces, instruction on the microprobe and petrologic discussion. Thanks go to Ted Madden for being on both my generals and thesis committees, and to Bob Kay for interesting discussion during the thesis defense.

Thanks to Ken Burrhus for an education in electronics and in mass spectrometer diagnostics and surgery. Thanks also for many an enjoyable afternoon or morning tea discussing the outside world. Thanks to Ila for patiently teaching me INNA and for supplying good food and company on other occassions. Many thanks go to Steve Recca for help with the microprobe at all hours, unfailing enthusiasm, help with computing/computer problems large and small, and a lot of enjoyable conversation.

Thanks go to my office mates, both past and present, Tom Juster, Dave Gerlach and Jane Selverstone for putting up with me, and for making my time at MIT far more enjoyable than I would have imagined.

Thanks go to Levent Gulen for friendship, help with mass spectrometry and clean lab techniques, and for a lot of good conversations. Thanks to Wally Johnson and Bob Heming for samples and enthusiasm.

Vincent Salters, Mike Baker, Yan Song, Ro Kinzler and Peter Tilke have helped me keep MIT in perspective. I have enjoyed our times together and I consider myself lucky to have such great friends.

Thanks also go to the other folks of the 12th, 11th and 10th floors and to the afternoon tea crowd.

Thanks to my mother, for teaching me to value myself, education, and life. I cannot thank you enough.

Special thanks to my wife, Reneau, who has shared my life in Boston. Thanks for camping holidays, both across the USA and England, for showing me Idaho and Oregon, for celebrations at the Hilton, and for support when I needed it most. Thanks for drafting, typing, and editing. I would never have made it without you. Thanks for all the love.

INTRODUCTION

Location

The Tabar-Feni island groups are located adjacent to, and northeast of, the Tertiary island arc of New Ireland in northeastern Papua New Guinea (Figure I-1). These island groups form a 260 km linear chain, which trends northwest-southeast, and is approximately parallel to the coast of New Ireland at a distance of 50-70 km. Each island group is 70 km from the next group and consists of two or more closely spaced islands.

The Tabar group, situated at the northwest end of the chain, contains the islands of Simberi, Tatau and Tabar, which form a linear north-south trend, with Tabar closest to New Ireland. This oblique alignment also occurs in the Lihir and Tanga island groups. Mahur, Masahet and Lihir are the islands of the Lihir group, which is named after the largest and southern-most island. The Tanga island group consists of the northern island of Boang, Malendok island, and four small islands, Lif, Bitlik, Bitbok and Tefa, which are situated just south of Malendok. The Feni group, at the other end of the Tabar-Feni island chain, is comprised of Babase and

Figure I-1 Locality map for Tabar-Feni islands.

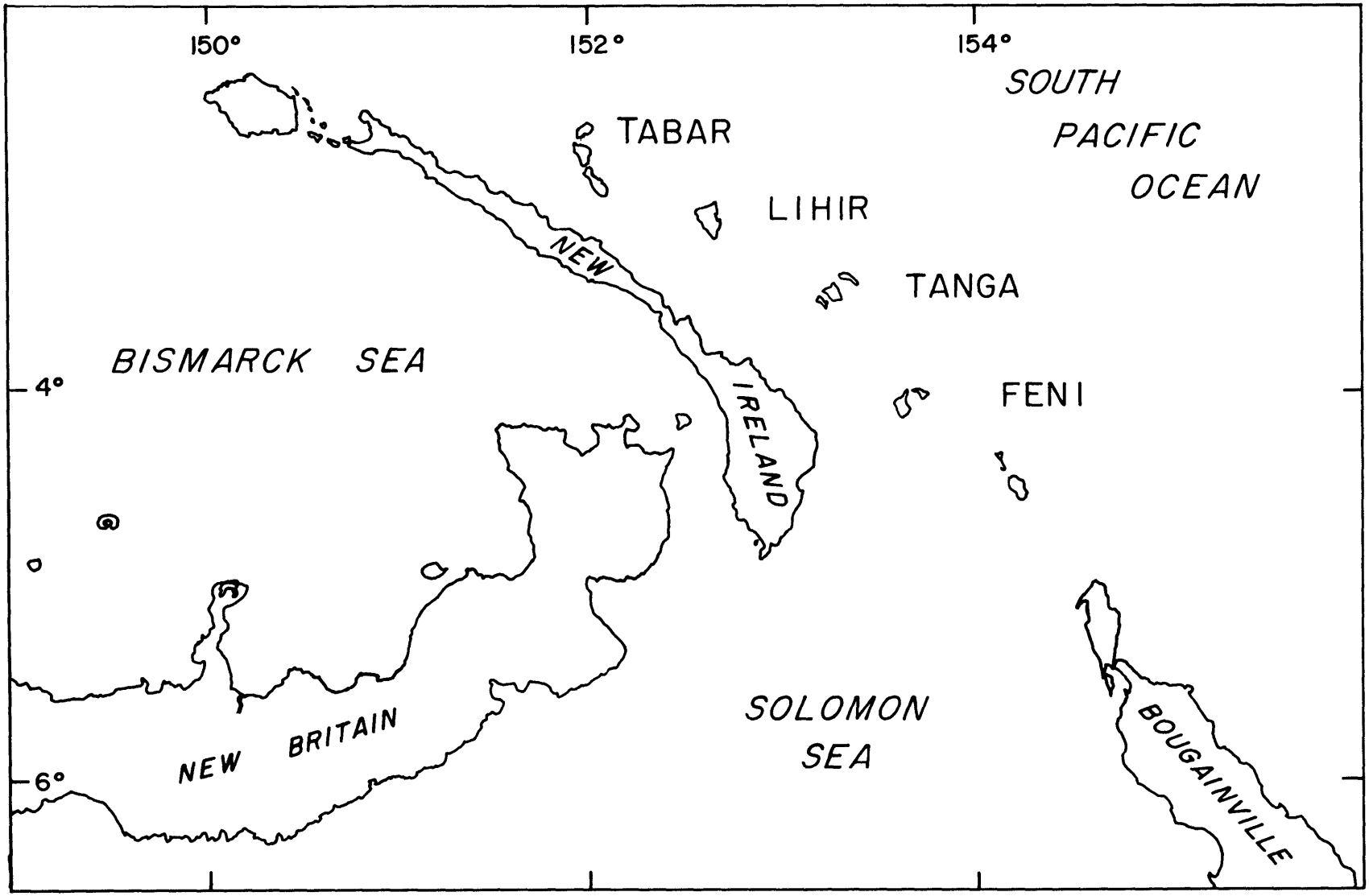
150°
152°
154°
SOUTH
PACIFIC
OCEAN
TABAR
LIHIR
TANGA
FENI
NEW
IRELAND
BISMARCK SEA
4°
6°
NEW BRITAIN
SOLOMON
SEA
BOUGAINVILLE

Ambitle islands. The Green islands, a group of small coral atolls, form an extension of the main chain and probably are the result of submarine volcanic activity. The island of Buka, in the Bougainville islands, is on the extension of this trend, however, no alkaline rocks have been reported in this volcanic and seismically active region, which is typically calc-alkaline. All of the Tabar-Feni islands are less than 200 km^2 and have low relief due to extensive erosion and the development of a number of small volcanoes on some islands (Wallace et al. 1983). The maximum elevation of 700 m occurs on the largest island, Lihir.

The major islands within each group are deeply eroded volcanic complexes of Cainozoic age. Most lavas and volcaniclastic deposits are Pliocene to Pleistocene, although pre-Middle Miocene rocks are found in the Tabar islands. Five samples from various islands have K-Ar ages of 0.19-1.53 my and qtz-trachytes are the youngest extrusive rocks in each island group and represent the cessation of volcanic activity (Wallace et al. 1983). Hydrothermal springs occur mainly within the Quaternary caulderas of each of the island groups and are associated with gold deposits on Lihir and Simberi islands.

Tectonic setting

The thickness of the crust in NE Papua New Guinea has been determined in a number of seismic studies (Wiebenga 1973, Finlayson and Cull 1973, and by Gulf Oil Research and Development (1973), see Wallace et al. 1983). The Lihir and Feni island groups are associated with crustal thicknesses of 20 km and 30/35 km respectively, and a stepwise increase in seafloor depth from 1600 m to 2400 m.

The eastern portion of Papua New Guinea is one of the most seismically active regions on earth, however, the Tabar-Feni islands show only moderate seismic activity (Denham 1973, Figure 4 and the BMR Earthquake Data File 1960-1979). Epicenters are usually shallower than 30 km in the Tabar to Tanga region and are often associated with observable faults or the extension of these faults (Hohnen 1978). Earthquakes, located at depths >350 km, are centered below the Feni island group and are associated with the deepest portion of the Solomon Sea plate which is being subducted under the islands of New Britain and Bougainville.

Papua New Guinea is a tectonically complex region, where the convergence of the Indo-Australian and Pacific plates, at rates of 9-14 cm yr^{-1} (Johnson and Molnar 1972, Curtis 1973, Krause 1973, Taylor 1975), and the presence of a least two minor plates between these major plates (Johnson 1979), has combined to produce a variety of tectonic regimes and one of the most volcanically active regions in the circum-Pacific.

At least six interpretrations exist for the distribution of plate boundaries in Papua New Guinea and the Solomon islands (see Johnson 1979 for a review, Coleman and Packham 1976, Angus-Leppan et al. 1983).

There are three distinct models of the arrangement of plate boundaries in the Tabar-Feni region. Coleman and Packham (1976) suggested that the Tabar-Feni island chain is separated from New Ireland by a major tectonic boundary, however there is little seismic or structural justification for this conclusion. Curtis (1973b) suggested a plate boundary to the east of the Tabar-Feni island chain in the vicinity of the Lyra-Kilinailau trough as well as a boundary to the west of New Ireland. This configuration requires an unlikely plate geometry and New Ireland and the Tabar-Feni island groups to be separated from the Pacific plate. As with the previous model, there is little seismic evidence for a plate boundary east of New Ireland, although the existence of troughs both to the east and west of the Tabar-Feni islands suggest that this region is tectonically active. The third model (Johnson and Molnar 1972), has no plate boundaries to the east of New Ireland and has the boundary of the Pacific plate with the Solomon Sea and Bismark plates to the west of Bougainville and New Ireland. The distribution of shallow earthquake epicenters matches this geometry.

Calc-alkaline volcanic rocks last erupted on New Ireland in the Tertiary. These rocks represent the last subduction-related volcanic activity (Hohnen 1978). New

Ireland is an extinct arc segment, and at present, there is no evidence for the existence of a subducted slab beneath New Ireland or the Tabar-Feni island groups. This plate fragment has been tectonically stable for the past 15 my (Falvey and Pritchard 1986).

Nomenclature

The Tabar-Feni rocks are dominantly undersaturated alkali-rich mafic volcanics. The alkaline nature of these rocks, which is unusual in an arc setting, was first noted by Glaessner (1915) and these rocks have subsequently been studied by Johnson et al. (1976), Arculus et al. (1978), Perfit et al. (1978), Heming (1979), Perfit et al. (1982) and Wallace et al. (1983).

The Tabar-Feni rocks are extremely varied in major element composition. The classification scheme used in this paper is the Total Alkali Silica (TAS) diagram (Le Maitre 1984). The TAS diagram for the rocks analyzed in this study is shown in Figure I-2. Alkali and transitional basalts, trachybasalts (Hy- and Ne-), phonolitic tephrites and trachytes are the most abundant rock types and have been found in most island groups. The frequency of occurence is, however, variable on the larger islands. For example, while mafic clinopyroxene-rich rocks with restricted major element compositions are abundant on Lihir, evolved rocks are scarce. In contrast, the lavas from Ambitle, in the Feni islands,

Figure I-2

TAS diagram of Tabar-Feni lavas.

Fields are: F Foidite; B Basalt; S1 Trachybasalt;
U1 Tephrite and Basanite; U2 Phonolitic Tephrite;
U3 Tephritic Phonolite; Ph Phonolite; T Trachyte;
S2A & S2B Trachyandesite, A Mugearite,Shoshonite
B Benmorite,Latite;
O1 Basaltic Andesite; O2 Andesite; O3 Dacite;
R Rhyolite;
Pc Picrobasalt.

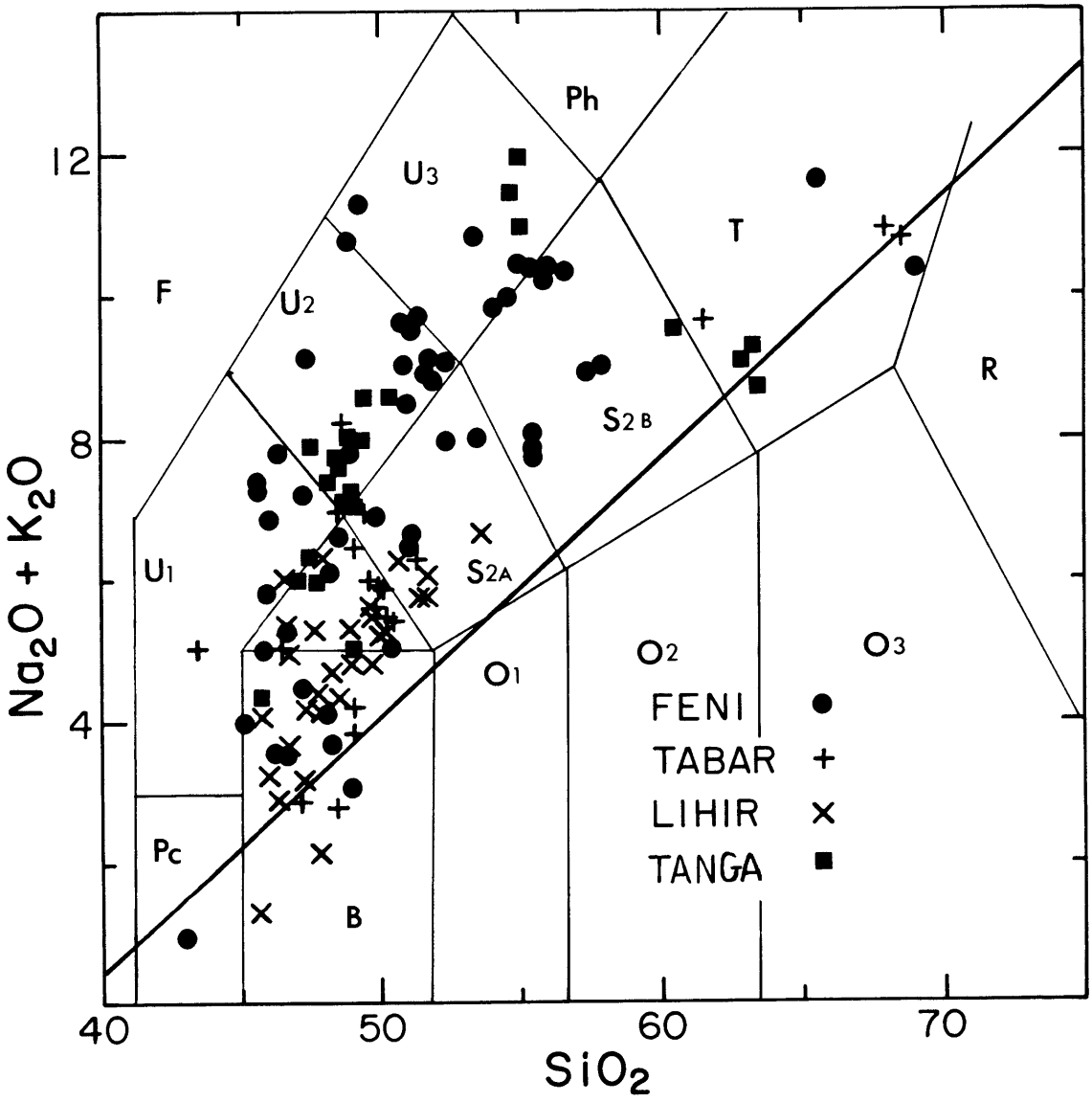
Ph
U3
T
F
U2
R
S2B
U1
S2A
O1
O2
O3
Pc
B
FENI
TABAR
LIHIR
TANGA
12
8
4
40
50
60
70
Na2O + K2O
SiO2

show a wide range of compositions and evolved lavas are more abundant than primitive lavas.

Apart from the qtz-trachytes and a few hyp-normative samples from Lihir and Tabar, all the analysed samples from these islands are ne-normative (Wallace et al. 1983). The exact degree of undersaturation is difficult to assess without petrographic study, as the high Fe^{3+}/Fe^{2+} measured by Heming (1979) and Wallace et al. (1983) biases the calculated norms toward high magnetite contents, and hypersthene and quartz normative compositions.

Throughout the text, samples are referred to as primitive, evolved, parental and primary. These are defined as follows: 1) Primary lavas are in equilibrium with a lherzolitic mantle and have not been modified prior to eruption. These magmas have high Ni and high Mg/(Mg+Fe). Very few primary lavas are present in the analysed samples, 2) Primitive lavas are taken as lavas with MgO > 6%, or the lavas with highest MgO in a single fractionation sequence. 3) Evolved lavas have undergone some fractionation relative to the primitive lavas of a fractionation sequence, and in general, this refers to lavas with < 6% MgO, 4) Parental magmas or lavas can fractionate by some process to an evolved composition.

The following chapters each deal with one aspect of the genesis and evolution of undersaturated arc lavas from the Tabar-Feni islands. The topics covered are: 1) experimental

and major element constraints on the genesis of Lihir lavas, 2) trace element and isotopic constraints on the genesis and evolution of Lihir lavas, 3) the major element chemistry and petrology of the Feni lavas, 4) crystal fractionation, magma mixing and assimilation in the Feni lavas, and 5) the mantle source of undersaturated lavas from the Tabar-Feni island chain.

CHAPTER 1

EXPERIMENTAL AND MAJOR ELEMENT CONSTRAINTS ON THE GENESIS AND EVOLUTION OF LAVAS FROM LIHIR

Introduction

Lihir Island, which is located in northeast Papua New Guinea, off the coast of New Ireland, is the largest island in the Lihir island group, and part of the Tabar-Feni chain. The four Pleistocene-Holocene volcanic island groups forming this chain are situated 30-50 km east of New Ireland and parallel to the coast (Figure 1-1). Lihir is a Pliocene to Holocene volcanic complex which has five recognizable volcanic segments: Londolovit block, the Wurtol wedge, and three younger volcanoes, Huniho, Kinami, and Luise. Lavas from this chain of islands have trace element characteristics that are typical of island arcs. They are highly enriched in LILE and depleted in HFSE relative to the REE, and are SiO_2 undersaturated, and this is unusual in an arc setting. Most of the erupted rocks have high measured H_2O, CO_2, Cl and Fe_2O_3/FeO ratios (Heming 1979, Wallace et al. 1983). The presence of hauyne as the principal feldspathoid also suggests a S-rich magma (Baldridge et al. 1981). The Lihir rocks are cpx-rich alkali basalts which contain abundant phenocrysts (15-50%) of clinopyroxene, olivine, plagioclase, and Ti-magnetite. Evolved rocks with higher alkali contents contain biotite and/or amphibole. Analyzed samples from Lihir do not show the geochemical diversity of samples from other island groups in the T-F chain (Wallace et al. 1983),

Figure 1-1

Map of eastern Papua New Guinea showing the location of the Tabar-Feni island chain, which contains the Tabar, Lihir, Tanga and Feni island groups, the presently active subduction zones of New Britain and Bougainville, crustal thicknesses measured at Lihir and Feni and the location of inferred faults (Wiebenga 1973) that delimit the New Ireland Basin. The boundary of the Ontong-Java Plateau is after Exon and Tiffin (1982).

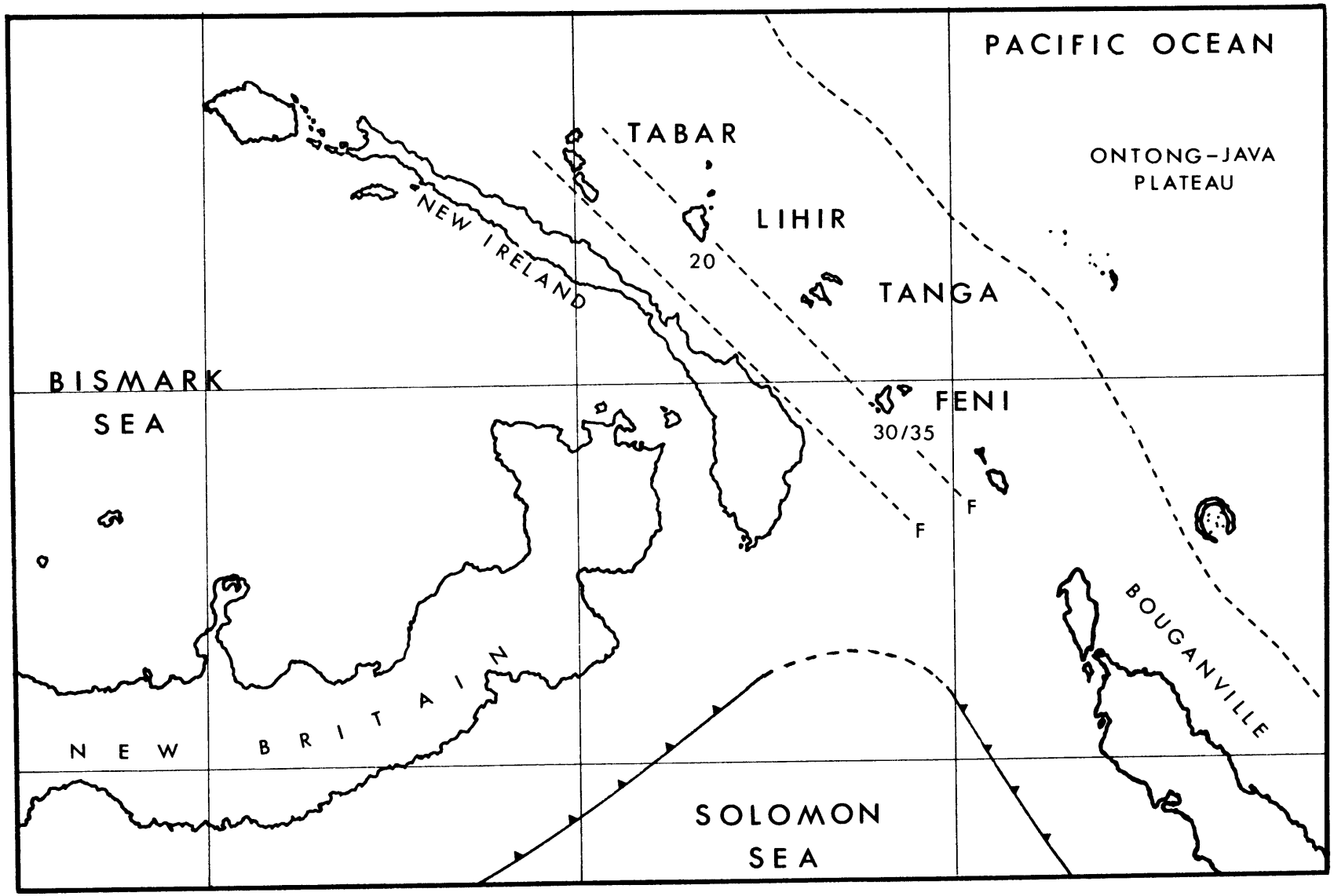
PACIFIC OCEAN
TABAR
ONTONG-JAVA
PLATEAU
LIHIR
NEW IRELAND
20
TANGA
BISMARK
SEA
FENI
30/35
F
F
BOUGANVILLE
NEW BRITAIN
SOLOMON
SEA

and fractional crystallization is the principal process controlling major element compositional variation.

The Luise lavas (L7, 10, 14, 22, 23 and 25, and LH1/11, 15, 17, 20, 21, 28, 29 and 30 of Wallace et al. 1983) can be separated into two groups. One group, which will be referred to as primitive (L7, L10 and L14), has low SiO_2 (<48.5%), high MgO (>5.8%) and CaO (>11.0%), and has undergone enrichment of incompatible elements during fractionation. The second group will be refered to as evolved lavas. These rocks have fractionated substantial amounts of clinopyroxene and show a depletion in elements normally considered incompatible relative to the primitive group. The lavas show minor differences in major and trace element chemistry both within and between volcanic units. The samples from the Londolovit block (L3, 6, 8 and 78LH1) are, in general, more magnesian and calcic, and are enriched in Cr, Sc and Ni relative to lavas of similar MgO content from the other units. L3 has very low abundances of Rb and K_2O and may have low alkalis because of alkali mobility during post-eruptive alteration. Lavas from Kinami volcano (L12, 13 and LH1/19, 24, 27) are similar to the primitive group from Luise, showing a similar enrichment of incompatible elements. Only three samples from Huniho were analyzed by Wallace et al. (1983) and one of these, LH1/9, was analyzed for most trace elements. This lava has primitive major element characteristics (MgO 6.85%, CaO 12.6% and SiO_2 47.1%), but is

depleted in incompatible elements like the evolved lavas from Luise.

The AFM diagram (Figure 1-2) has been traditionally used to examine the degree of Fe-enrichment in various rock series and to separate arc rocks into the tholeiitic and calc-alkaline rock series (Kuno 1968, Irvine and Baragar 1978). The Lihir lavas, average experimental glasses and individual analyses of glasses in experiment 7 are plotted in this diagram. Although the T-F rocks are undersaturated, projection onto this diagram shows a number of features that are typical of tholeiitic and calc-alkaline arc rocks. The T-F rocks have moderate iron enrichment with only a few samples plotting in the tholeiitic field of Irvine and Baragar (1978) and showing the degree of iron enrichment that occurs in rocks from the New Britain volcanoes (Johnson et al. 1978, Fig. 4). The Lihir lavas, which plot in the tholeiitic field, have higher iron and magnesium and lower alkali contents than the other T-F lavas. Many of the Lihir samples plot outside the field encompassing all other T-F lavas.

In subsequent sections, the lavas are separated into primitive and evolved groups based on major element criteria (Introduction) and trace element criteria (see Table 2.1). Samples have been designated as primitive (P) or evolved (E) in Table 2.1.

Figure 1-2

AFM diagram showing Lihir lavas (▽), average compositions of experimental glasses (■) and individual analyzes of disequilibrium glasses from experiment 7 (▲). Field for all other T-F lavas. Pigeonitic-Hyperthenic and Tholeiitic-Calc-alkaline boundaries are from Kuno (1968), and Irvine and Baragar (1978).

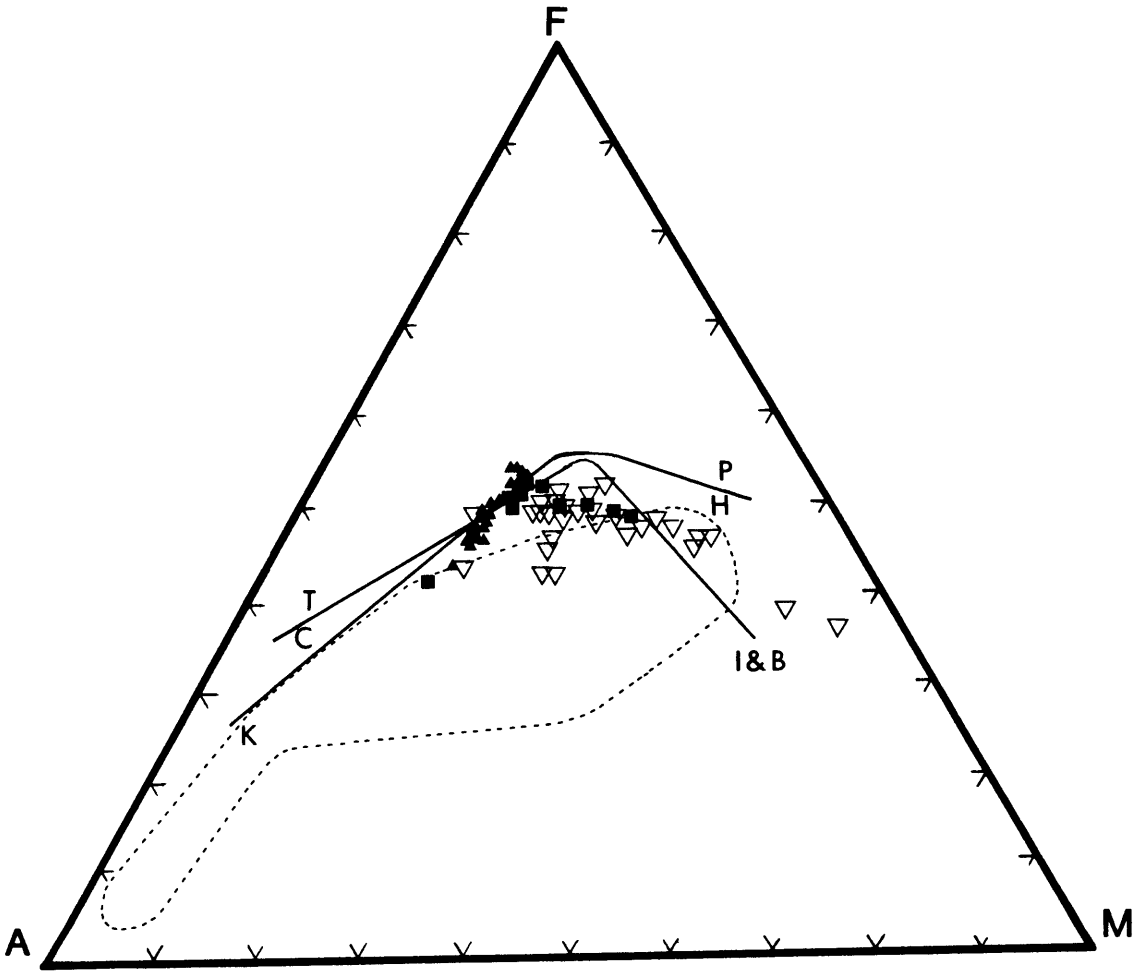
F
A
M
P
H
T
C
K
I&B

Usually, the last erupted lava on each of the larger islands is a qtz-trachyte which Wallace et al. (1983) proposed were crustal melts. Seismic data shows that the crust beneath Lihir is <20 km and possibly as thin as 15 km (Wiebenga, 1973). This limits the depth of crustal crystal fractionation to <7 kb.

Overview of relevant experimental studies

The evolution of a lava is dependent on a large number of parameters such as: the phases crystallizing, the order of phase appearance, and the proportions of phases. Each of these factors must be considered if a suite of lavas is to be understood. Pressure, fO_2 and H_2O control the order of appearance of olivine, plagioclase, spinel, clinopyroxene and amphibole in undersaturated lavas and the resultant fractionation trends. At 1 atm pressure and fO_2 less than Ni-NiO, the first phase on the liquidus in systems with low H_2O (<1%), is usually olivine for alkali basalts and basanites (Ford and MacDonald 1978, Cawthorn et al. 1973, Duke 1974, Graham 1980, and Mahood and Baker 1986). However, if the sample has high Al_2O_3 (18%) or CaO content, the first phase on the liquidus may become plagioclase (Baker and Eggler 1983, Humphries 1980) or clinopyroxene (Graham 1980).

With increasing water content or pressure, clinopyroxene stability is enhanced and the appearance of plagioclase is suppressed by up to 100 °C (Spulber and Rutherford 1983,

Graham 1980). Plagioclase crystallized in water-rich systems is enriched in anorthite (Eggler 1972, Sekine et al. 1979). In general, higher pressure reduces the primary phase volume of olivine (Stolper 1980, Takahashi and Kushiro 1983, Presnall et al. 1979), however, an increase in H_2O has the opposite effect (Kushiro 1972). Magnetite is a liquidus or near liquidus phase in undersaturated lavas if fO_2 is high (>Ni-NiO), and it may exercise a major influence on the development of the iron enrichment trends characteristic of some suites (Humphries 1980, Grove and Kinzler 1986). Two other constraints that may produce compositional variation in evolved lavas are changing phase proportions with change in pressure of crystallization (Grove and Baker 1984) and the effect of other elements (such as F, Cl and S) which control the the type of feldspathoid that crystallizes from undersaturated lavas (Carmichael et al. 1974).

This paper uses the results of 1 atm melting experiments, to model the genesis and evolution of the Lihir lavas. The major element compositions of the more primitive lavas are similar to 78LH1 and the evolution of these rocks under low P conditions can be studied with 1 atm melting experiments. These rocks have a greater degree of iron enrichment than samples from other islands in the T-F chain.

A series of 1 atm experiments along the QFM buffer and at higher oxygen fugacities were performed to allow comparison of melt and mineral compositions and the order of

phase appearance between anhydrous 1 atm experiments and the natural samples. These experiments also address the following questions: 1) What is the relationship between the cpx-rich basalts, which are common throughout the islands, and the tephritic phonolites and trachytes which are uncommon? 2) Under what conditions are the Mg-rich olivines and clinopyroxenes in equilibrium with the lavas, or are they xenocrystal? 3) What are appropriate major element partition coefficients for cpx-rich alkali basalts? and, 4) How much variation is produced in the position of multiple saturation surfaces by changing fO_2?

Fractionation of magnetite from undersaturated magmas enriches the residual liquids in SiO_2, expecially if magnetite crystallizes early in the fractionation sequence. In contrast, Mahood and Baker (1985) have suggested crystal fractionation at higher pressure results in an increase in normative nepheline. Examination of the degree of enrichment in SiO_2 during 1 atm crystallization was another problem addressed in this study.

Experimental Methods

Experiments were perfomed on sample 78LH1 (from Lihir Island), which is a K-rich basalt and is one of the least evolved alkalic basalts. This basalt, and all of the Lihir samples, have low Ni, Cr and Mg/Fe, suggesting a prior episode of olivine fractionation. The presence of cumulate

xenoliths, that usually lack olivine, indicate that magma chamber processes have affected most of the erupted samples. Low pressure fractionation of these magmas is best assessed by examining a relatively primitive sample which is similar to most of the analyzed samples, rather than a primary melt with a different major element composition. 78LH1, which contains (25%) phenocrysts, clinopyroxene (22%), Ti-magnetite (2%), olivine (0.8%) and plagioclase (0.2%), was selected and powdered in a WC shatterbox. Arc lavas and undersaturated lavas rarely exhibit Fe-enrichment (Carmichael et al. 1974). This results from crystal fractionation of magnetite at fO_2 between QFM and Ni-NiO (Ewart 1982, Johnson et al. 1978, Carmichael and Ghiorso 1986). Melting experiments were carried out at different fO_2 to assess the variation of melt chemistry produced by magnetite crystallization.

Experimental Conditions

Disks of the powdered sample were produced in an XRF pellet press using Elvanol as a binding agent. Small fragments of these pellets (50 mg-100 mg) were fused, using an oxygen-natural gas torch, to 0.004" Fe-Pt loops, which had been electroplated with Fe to reduce Fe loss. Experiments were performed in a Deltech DT31VT gas mixing furnace at MIT, using a mixture of CO_2 and H_2 to control oxygen fugacity, which was measured with a ZrO_2-CaO electrolyte cell calibrated at the Fe-FeO, Ni-NiO and Cu-Cu_2O buffers. Gas

flow rates were maintained at 0.3 ml/sec with a manometer system, and the oxygen fugacity was controlled to 0.1 log units of the desired value. Temperature was monitored with a Pt-10Rh thermocouple calibrated against the melting points of NaCl, Au and Pd on the IPTS temperature scale (Biggar 1972). Experiment duration varied between 22 and 24 hours for near liquidus experiments and up to 264 hours for lower temperature runs. Samples were quenched by dropping into H_2O. Analysis of the 1191°C experimental glass showed that loss of sodium was approximately 10% for this run. Volatilization of sodium is a major problem in 1-atm wire loop experiments on undersaturated, alkali-rich lavas, such as 78LH1, especially at low oxygen fugacity, high gas flow rates, long run times, low degrees of crystallinity, and at high temperatures. In these experiments, the partial pressure of sodium in the furnace atm was elevated by suspension of a porcelain crucible containing Na_2SiO_3 above the experimental charge (Tormey et al. 1987).

Some alkali and phosphorus loss still occurred in all runs, as equilibrium is unlikely between continuously replenished gas atmosphere and the experimental charge. Mass balance calculations (Table 1.1) suggest that sodium loss was approximately 10% or less in the high temperature experiments, and approximately 5% in the lower temperature and higher fO_2 charges. It is impossible to assess the exact amount of sodium lost, because of the presence of (<10 and usually <5 volume %) unequilibrated cores in the larger

Table 1.1

Experimental Conditions				Calculated Phase Proportions (wt%)							
Expt#	Duration(hrs)	Temp.(°c)$^{\phi}$	-log fO_2^{ϕ}	Glass	Oliv	Cpx	Plag	Ti-Mag	ΔNa_2O	X^2	Phases
1	24	1191	8.50	100					-.22		g
2	24	1172	8.67	99.95	.05				-.13	0.7	g,o
3	24	1155	8.93	91	1	8			-.04	0.4	g,o,c
4	22	1136	9.21	84	1	15			+.04	0.3	g,o,c
5	72	1137	9.19	84	2	14			+.07	0.3	g,o,c,p
6	48	1127	9.22	76	2	20	2		+.10	1.0	g,o,c,p
7	76	1119	9.31	70	2	26	3		+.08	0.5	g,o,c,p,m
8	96	1109	9.49	69	3	22	6		+.16	0.7	g,o,c,p,m
†11	168	1137	8.99	81	1	18	0.2		-.18	1.3	g,o,c,p
†12	168	1135	8.80	76	1	20	2		-.12	1.3	g,o,c,p
†13	264	1135	8.23	70	2	24	5	.07	-.05	1.0	g,o,c,p,m
†14	192	1115	8.57	50	2	34	10	3	+.03	0.3	g,o,c,p,m
				*75.1	0.8	21.6	0.5	2			

ϕ Temperatures and fO_2 calculated from the average of ~20 readings

+ Phase proportions calculated using Simplex algorithm (Kostal et al., 1986) assuming the bulk composition of each run to be equal to the major element analysis of 78LH1

* Data from point count (total no. pts 2400) of 78LH1 ΔNa_2O difference in wt% Na_2O between calculated and original content negative represents loss X^2 calculated as $\sum_{n=1}^{i}$ (observed-calculated)^2 for major elements

† expts of f_{O_2} > QFM

(g) glass (o) div (c) cpx (p) plag (m) mag

crystals. Since the melt and overgrowths of all phases were analyzed in each charge, a mass balance calculation (Bryan 1986, Kostal et al. 1986) gives the approximate Na loss and the mode, and this is given in Table 1.1 along with the run conditions. This calculation does not account for the unreacted cores within larger crystals. Comparison of P_2O_5 and the calculated degree of crystallinity showed that P_2O_5 may have been lost from experiment 14. P_2O_5 loss was confirmed by analysis of the glass at the rim of the charge (0.6% P_2O_5) and center of the charge (0.8% P_2O_5). The higher value is consistent with the degree of crystallinity and with the incompatible nature of this element. The P_2O_5 contents, given in Table 1.2, were derived from the analysis of glass near the center of the charge whenever lower P_2O_5 contents were identified in glass from the edge of the charge.

Analytical Techniques

Experimental glasses and phases were analyzed with the MIT MAC-5 microprobe and its replacement, the JEOL 733 Superprobe, using an accelerating voltage of 15 kv, a sample current of 10 nA currents and the same set of standards. Glasses were analyzed with 10 um spot size to minimize Na loss, and crystals were analyzed with either a 10 um or <1 um beam. Data reduction was performed on line, using the correction procedures given in Bence and Albee (1968), and Albee and Ray (1970). The same microprobe techniques were

Table 1.2

Average Glass Composition

Exp#	n	SiO_2	TiO_2	Al_2O_3	Fe_2O_3	FeO$^{\phi}$	MnO	MgO	CaO	Na_2O	K_2O	P_2O_5	Total	Fe2+/Mg	%Norm Ne
1	13	48.5	.86	13.5	1.76	9.45	.24	7.50	12.7	2.32	2.13	.40	99.39	.707	4.59
		.6*	.08	.4		.16+	.06	.16	.5	.18	.14	.04			
2	14	48.4	.83	13.5	1.82	9.34	.22	7.04	12.2	2.42	2.21	.41	98.47	.744	4.30
		.7	.09	.2		.34	.05	.14	.6	.20	.06	.04			
3	9	48.3	.90	14.8	1.78	9.28	.22	6.11	11.7	2.70	2.45	.49	98.73	.853	5.56
		.5	.08	.7		.27	.04	.15	.7	.13	.07	.06			
4	11	48.3	.91	15.5	1.81	9.39	.23	5.37	10.9	3.03	2.74	.50	98.71	.981	6.99
		.3	.04	.4		.34	.10	.22	.2	.16	.09	.06			
5	13	48.6	.91	15.4	1.82	9.36	.22	5.31	10.8	3.06	2.66	.50	98.71	.989	6.29
		.8	.04	1.3		.56	.08	.37	.5	.22	.14	.06			
6	10	47.7	.98	15.6	2.06	9.93	.23	4.69	10.3	3.30	2.86	.56	98.31	1.19	8.27
		.5	.08	.3		.26	.06	.12	.5	.17	.13	.06			
7	18	40.0	.95	15.7	1.98	9.38	.22	4.37	9.3	3.48	3.43	.62	98.41	1.20	7.73
		1.1	.09	.4		.60	.06	.27	.4	.15	.25	.06			
8	14	48.2	.99	15.5	1.94	9.90	.24	4.53	10.1	3.47	3.34	.62	98.82	1.23	9.97
		1.8	.14	.5		1.50	.05	.51	1.5	.38	.79	.11			
11	9	49.4	1.00	15.3	2.01	9.76	.21	4.94	10.4	2.83	2.90	.52	99.28	1.11	3.65
		.6	.08	.5		.30	.06	.19	.4	.19	.09	.05			
12	11	49.5	1.00	15.3	2.32	9.51	.22	4.59	9.8	3.05	3.15	.48	98.88	1.16	4.49
		.6	.12	.3		.62	.03	.14	.3	.22	.09	.12			
13	8	49.9	1.04	15.4	2.85	8.63	.23	4.59	9.1	3.22	3.37	.52	98.81	1.05	4.05
		.7	.06	.2		.42	.04	.16	.4	.10	.16	.05			
14	12	51.6	.79	16.9	2.33	6.70	.26	3.56	7.4	4.14	4.66	.79	99.37	1.10	8.19
		.5	.08	1.1		.60	.04	.38	.7	.22	.49	.06			

n no. of analysis used to calculate means and standard deviations

* standard deviations are 2σ of the mean

\+ standard deviations of total Fe as FeO

ϕ FeO, Fe_2O_3 calculated according to Kilinc et al. (1983) using experimental conditions

used on thin sections of 78LH1 and other samples from the T-F Islands. The compositions of the experimental phases reported in Tables 1.2 through 1.5 are the averages of different rim overgrowths or patches of glass. The number of analyses and the standard deviation on the mean is also given.

Major element data for samples in Table 2.1 were obtained as averages of duplicate analyses by X-ray fluorescence at the University of Massachusetts (Rhodes 1983) and the Bureau of Mineral Resources, Australia (see Wallace et al. 1983).

Analysis of experimental run products

The experiments were isothermal synthesis experiments; therefore, there was no attempt to prove equilibrium. However, the experiments produced values for Fe-Mg exchange distribution coefficients that were similar in both long and short experiments. The final state of each experiment is not true equilibrium, but rather an approach toward it. Five experiments were (4, 5, 11, 12, 13) run at essentially constant temperature (1135-1137 °C) for durations ranging between 22 and 264 hours. Three of these experiments were run at fO_2 close to the Ni-NiO buffer, and two at QFM oxygen fugacities. The Fe/Mg partitioning between the experimental liquids and phases is constant within errors, with the exception of clinopyroxene in run 13 which was run at

Table 1.3

Average Olivine Compositions

Exp #	n	SiO_2	TiO_2	Al_2O_3	FeO	MnO	MgO	CaO	Cr_2O_3	NiO	Total	Fo
2	5	39.5	.04	.05	18.3	.38	42.0	.67	.02	.01	101.01	80
		.5*	.03	.02	.6	.04	.7	.06	.05	.02		
3	4	35.2	.04	.05	19.2	.37	40.7	.66	0	0	100.28	78
		.5	.03	.02	.6	.03	1.4	.09				
4	4	38.6	.05	.04	21.2	.44	39.0	.60	0	.02	99.96	76
		1.3	.02	.02	.7	.10	.7	.16		.05		
5	3	39.0	.06	.08	21.9	.45	39.2	.64	.02	0	101.25	75
		.5	.01	.03	.1	.09	.9	.2	.05			
6	5	38.7	.05	.06	24.6	.46	36.3	.68	0	.01	100.78	72
		.6	.05	.04	.6	.04	.9	.01		.04		
7	4	38.5	.05	.06	23.3	.52	37.4	.62	0	.01	100.59	74
		1.6	.04	.06	.2	.02	.9	.1		.05		
8	4	38.6	.05	.05	24.1	.58	37.4	.46	0	.06	101.27	73
		.5	.02	.02	.7	.07	.3	.07		.02		
11	4	38.6	.03	.04	24.9	.51	37.0	.51	.03	.03	101.49	73
		.5	.02	.03	.6	.04	.9	.08	.04	.06		
12	3	38.6	.03	.10	24.7	.44	36.8	.46	0	.09	101.25	72
		.3	.01	.03	.3	.02	.3	.04		.04		
13	3	38.9	.05	.11	22.3	.51	39.4	.38	.03	.07	101.75	75
		.4	.1	.02	.2	.07	.7	.04	.02	.05		
14	6	39.3	.08	.39	21.9	.62	38.0	.97	0	.04	101.25	74
		1.7	.02	.2	1.0	.18	2.0	.5		.04		

Magnetite Compositions

Exp #	n	SiO_2	TiO_2	Al_2O_3	Fe_2O_3	FeO	MnO	MgO	CaO	Cr_2O_3	NiO_2	Total	
7	1	.14	5.33	8.04	34.88	44.1	.43	5.73	.6	.24	.3	99.02	Resorbed
8	1	.24	6.08	8.26	33.55	45.86	.39	4.90	.07	.2	.04	99.59	Resorbed
13	1	.24	3.33	7.93	37.48	43.76	.41	5.59	.15	.28	.03	99.20	
14	1	.19	4.57	7.53	35.96	44.46	.45	5.23	.14	.07	0	98.62	

n,* As in Table 2

Table 1.4

Average Clinopyroxene Compositions

Exp #	n	SiO_2	TiO_2	Al_2O_3	FeO	MnO	MgO	CaO	Na_2O	Cr_2O_3	Total	Mg/(Mg+Fe)	^aAlVI	$Fe_2O_3^+$	FeO^+
3	4	51.8	.44	3.28	6.01	.09	15.7	22.0	.26	.26	99.96	.823	.051	.91	5.19
		.5*	.03	1.4	.52	.04	.8	1.6	.08	.10		.01			
4	3	51.3	.44	3.65	6.19	.14	15.1	21.8	.33	.24	99.27	.813	.063	.79	5.48
		1.0	.05	.66	.44	.09	.5	2.0	.14	.13		.01			
5	5	50.8	.53	3.52	6.62	.11	14.9	22.6	.26	.24	99.65	.800	.045	1.65	5.13
		.8	.08	.5	1.0	.08	.5	.5	.09	.08		.02			
6	6	49.6	.66	4.97	7.78	.17	13.6	22.2	.39	.09	99.56	.759	0.77	1.88	6.08
		1.3	.07	1.2	.9	.05	.5	1.6	.18	.11		.02			
7	8	49.4	.71	5.08	8.47	.18	13.3	21.7	.44	.04	99.33	.732	.081	1.85	6.80
		1.0	.04	.35	.66	.06	.9	1.2	.1	.06		.01			
8	4	48.1	.85	6.21	8.99	.19	12.6	22.4	.50	0	99.90	.714	.087	3.14	6.17
		.7	.07	.6	.5	.03	.3	.9	.07			.01			
11	7	51.5	.52	3.42	6.85	.16	15.2	22.1	.27	.12	99.66	.797	.058	.69	5.63
		1.4	.10	.61	1.6	.11	1.1	.3	.23	.08		.04			
12	7	51.1	.52	3.42	6.96	.15	15.0	22.4	.25	.09	99.95	.789	.047	1.48	5.63
		.7	.12	.74	.70	.06	.4	.4	.06	.07		.02			
13	6	48.9	.75	5.13	8.46	.17	13.5	22.2	.41	.05	100.06	.728	.057	3.45	5.35
		1.0	.26	1.4	.38	.03	.8	.8	.25	.09		.03			
14	9	49.0	.68	4.92	8.5	.18	13.7	22.5	.38	.01	99.86	.753	.058	3.20	5.61
		1.7	.04	2.0	1.4	.07	1.6	.9	.06	.03		.006			

n,* As in Table 2

+ Fe_2O_3, FeO calculated using the method of Papike et al., 1974

a AlVI calculated using the method of Lindsley and Andersen, 1983

Table 1.5

Average Plagioclase Compositions

Exp #	n	SiO_2	Al_2O_3	FeO^+	MgO	CaO	Na_2O	K_2O	Total	Ca/Na	An	Ab	Or
5	6	50.0	31.7	.69	.17	14.4	2.67	.47	100.17	2.99	.729	.243	.027
		.4*	.5	.12	.01	.6	.22	.08					
6	10	49.6	31.1	.75	.16	14.2	2.74	.52	99.13	2.87	.719	.252	.028
		.8	.3	.18	.06	.4	.22	.07					
7	8	51.9	29.7	1.02	.13	12.6	3.52	.70	99.63	1.98	.627	.321	.042
		1.0	.7	.16	.12	.6	.26	.17					
8	9	52.4	29.5	1.04	.14	12.3	3.74	.81	100.00	1.82	.613	.338	.049
		1.8	1.0	.22	.10	.9	.48	.08					
11	9	50.4	31.6	.75	.18	14.3	2.77	.54	100.49	2.86	.717	.251	.032
		.7	.7	.14	.09	.7	.13	.13					
12	9	50.2	31.5	.96	.20	14.4	2.71	.56	100.49	2.93	.721	.245	.034
		1.4	.6	.15	.08	.4	.16	.08					
13	6	51.2	30.1	1.25	.22	13.3	3.25	.75	100.10	2.26	.662	.293	.044
		1.6	1.1	.40	.20	1.2	.46	.19					
14	11	51.6	29.8	1.27	.15	12.7	3.43	.82	99.79	2.05	.639	.313	.048
		1.2	.7	.32	.05	.9	.43	.16					

+ as analyzed n,* as in Table 2

considerably higher oxygen fugacities (Figure 1-3a,b).

The attainment of consistent results for Fe-Mg exchange does not prove equilibrium, but demonstrates a close approach to exchange equilibrium (Figure 1-3). The calculated degree of crystallinity increased slightly with experiment duration as the amount of clinopyroxene increased (Table 1.1) and as plagioclase appeared. The width of the equilibrium overgrowth increased at the expense of the unreacted cores from 3-5 um to 15-25 um with increasing run time.

In experiments run below 1127 C, olivine was chemically homogeneous, but all other phases had unequilibrated cores often surrounded by 5-15 um overgrowth rims. These rims recorded exchange Kds close to those produced in the higher temperature experiments. Plagioclase crystals had much smaller overgrowth rims and contained up to 1.5% FeO.

The variability of the overgrowth composition was assessed by examination of the 1 sigma values for each element reported in Tables 1.3 through 1.5. The largest 1 sigma values occur for phases from the lowest temperature experiments. Experiment 7 shows considerable variation in glass composition; the individual analyses are plotted on an AFM diagram in Figure 1-2. Higher SiO_2, K_2O, P_2O_5, Al_2O_3 and Na_2O, accompanied by lower MgO, FeO, TiO_2 and CaO, is often recorded during crystal fractionation in natural samples and this type of trend occurs in the evolved T-F lavas. Experiment 7 did not have an unusual distribution of experimental phases, nor did the glass compositions show any

Figure 1-3

Fe^{2+}/Mg of average clinopyroxenes (a) and olivines (b) plotted against Fe^{2+}/Mg of average experimental glass compositions. Lines shown for reference have gradients labeled. All Fe as Fe^{2+} in olivine. Fe^{2+} in clinopyroxene calculated from stoichiometric constraints (Papike et al. 1974). Symbols as follows: (▲) QFM experiments, (●) QFM to Ni-NiO experiments.

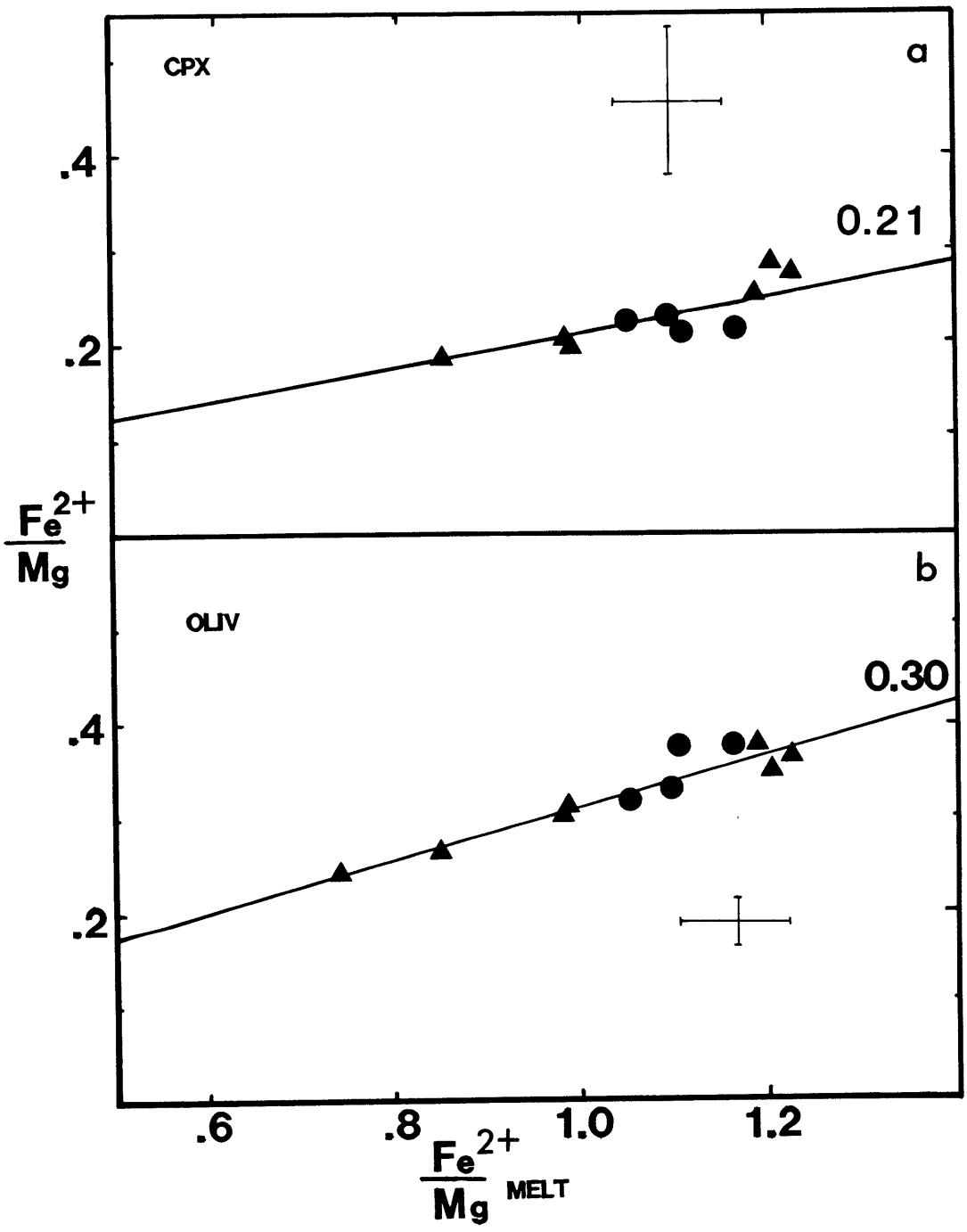
CPX
a
0.21
.4
.2
$\frac{Fe^{2+}}{Mg}$
b
OLIV
0.30
.4
.2
.6
.8
1.0
1.2
$\frac{Fe^{2+}}{Mg}$ MELT

relationship to the distribution of phases within the charge. The experimental phases within this charge were not as homogeneous as those analysed in the other experiments, however this discrepancy was minor in comparison to the inhomogeneity of the glasses. Presently, there is no explanation for this observation, as temperature gradients, separation of crystals from liquid, and diffusional effects, can be ruled out. The lower P_2O_5, Na_2O and K_2O suggest alkali-P_2O_5 loss, but this is inconsistent with lower SiO_2 in the same analysis.

Experimental Results

The 1 atm, QFM, anhydrous liquidus is at 1175 °C for 78LH1 and olivine is the liquidus phase followed by clinopyroxene at approximately 1155 °C, plagioclase at approximately 1137 °C and Ti-magnetite at 1110 °C. At >1 logfO_2 unit higher oxygen fugacity, Ti-magnetite can be found in the experimental changes at temperatures as high or higher than 1137 °C, suggesting that 0.5 logfO_2 units variations in fO_2 can drastically effect the temperature of appearance of Ti-magnetite in these undersaturated magmas. A single Ti-magnetite phenocryst was found and analyzed in runs 7 and 8, however in both cases the Ti-magnetite phenocryst was undergoing resorption. All analyzed experimental glasses, which contain magnetite (7, 8, 13, 14), had higher silica contents and lower iron contents than experiments at the same

temperature but with lower fO_2. Experiment 14 had the highest SiO_2, K_2O and Al_2O_3, lowest CaO, MgO and P_2O_5.

Measured partition coefficients for Fe^{2+}/Mg between olivine and clinopyroxene and the average composition for each experimental liquid are shown in Figures 1-3a and 1-3b. Olivine and clinopyroxene partitioning was calculated using the Fe^{3+}/Fe^{2+} ratio predicted by the equation of Sack et al. (1980) and the coefficients of Kilinc et al. (1983). The olivine coefficient is equal to 0.3, which is consistent with the work of Roedder and Emslie (1970), and many subsequent studies. Olivines in runs 7 and 11 are homogeneous in composition however, the calculated partition coefficients are respectively higher and lower, but within error of the value derived from the other experiments. A higher K_2O content in the melt is expected to lower the distribution coefficient (Foley and Green 1986), however this was not apparent in experiment 14, which had the highest K_2O content, and this effect may not become apparent until higher K_2O contents are reached. Olivines in the Lihir lavas, like those from all of the T-F lavas, are more magnesian (Fo 70-91) than with the experimental olivines (Fo 72-80). This results from the lower Fe^{2+} of the highly oxidized lavas.

The Fe^{2+}/Mg partition coefficient between clinopyroxene and melt ranges between 0.22 and 0.28, with an average value of 0.26. These values overlap with values found in 1 atmospheric experiments in MORB, saturated arc lavas, and undersaturated lavas (Grove and Bryan 1983, Grove and Baker

1984, Mahood and Baker 1986, and Sack et al. 1987). The average rim overgrowth composition for the clinopyroxenes from each experiment is plotted in Figure 1-5 along with analyzed clinopyroxenes for 78LH1. The experimentally produced clinopyroxenes show the same compositional variation as the natural clinopyroxenes, with increasing Al_2O_3, FeO*, Na_2O and TiO_2, and decreasing MgO, but do not show the complex zoning found in the natural mineral. These compositional changes are typical of clinopyroxene in undersaturated lavas (Baldridge et al. 1981) and are the result of increasing Acmite, CaTi-Tschermak and CaAl-Tschermak components. The compositions of natural cpx overlap with experimental clinopyroxenes, with the latter having slightly lower Al_2O_3 and FeO* contents that result from kinetic effects caused by different growth rates in the experiments and natural system (Grove and Bence 1976, Tsuchiyama 1981). The experimental clinopyroxenes have a limited range of MgO contents (12.5-15.7%) compared with the natural phenocrysts (11.2-18.6%). The magnesian cores of the natural phenocrysts are best explained by higher fO_2 in the natural samples, although a xenocrystal origin cannot be completely ruled out. The overall similarity of experimental and natural clinopyroxenes suggests that most of the growth of the natural clinopyroxenes occurred at pressures close to 1 atm, or that the pressure effect on the compositional evolution of the clinopyroxenes in this suite of rocks is difficult to detect.

Figure 1-4

Ca/Na of average plagioclases and experimental glasses, with experiments numbered. Errors shown are 2 sigma errors calculated from the averaged data in experiment 6. The line shown for comparison has gradient of 1.45.

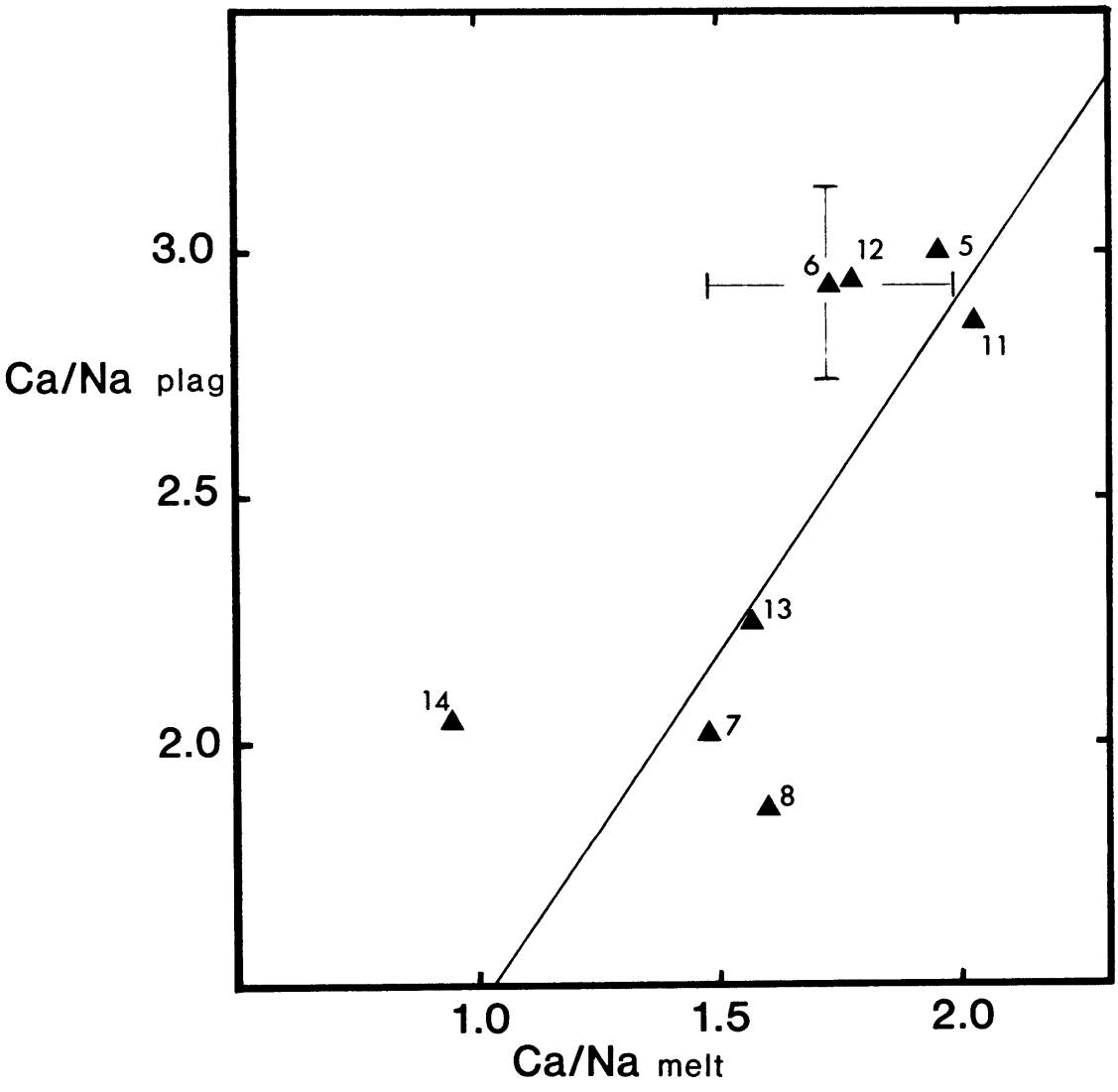
3.0
2.5
2.0
Ca/Na plag
1.0
1.5
2.0
Ca/Na melt
6
12
5
11
13
14
7
8

The presence of abundant sector-zoned clinopyroxene in the Lihir lavas is typical of what occurs in many undersaturated lavas (Larsen 1981, Downes 1974) and is commonly interpreted as a kinetic effect (Nakamura 1973, Shimizu 1981) resulting from rapid isothermal growth (Kouchi et al. 1983). This interpretation is supported by the presence of trapped melt, olivine, magnetite and plagioclase in many clinopyroxene phenocrysts and ubiquitous microphenocrysts of apatite that occur within clinopyroxene phenocrysts. These microphenocrysts probably grow from a supersaturated water-rich melt at the crystal-melt interface (Watson 1980). The P_2O_5 concentrations of the Lihir lavas are too low to crystallize apatite under 1 atm anhydrous conditions. Grove and Bryan (1983) describe experiments where there is a rapid increase in the proportion of cpx. High Al^{VI} contents in magnesian clinopyroxene is consistently used to argue for high pressure crystallization of this phase (Mahood and Baker 1986, Duda and Schminke 1985). The magnesian clinopyroxenes from 78LH1 all have low Al^{VI}, indicating they have crystallized at low pressures. The rim composition is normally enriched in Fe, Na and Al and depleted in Mg and Cr, and this can be seen in Figure 1-5. In some instances, the clinopyroxenes show the growth of discrete zones, with Fe-rich clinopyroxene overgrown by a more magnesian composition. This type of growth could be interpreted as the result of magma mixing (Barton et al.

1982) or could result from skeletal crystal morphology during growth.

Plagioclase in the experimental charges shows moderate compositional variation (An 60-75) in comparison to the natural phenocrysts in 78LH1 (An 58-86). The Ca/Na partition coefficient for the seven highest temperature experiments containing plagioclase ranges between 1.66 and 1.13 (Figure 1-4). In the lowest temperature run (#14) at 1115°C, the plagioclase overgrowth rim compositions are very consistent (Table 1.5), however, the distribution coefficient is 2.17 and contrasts with the value of 1.13 obtained from the lowest temperature experiment at QFM oxygen fugacity. The higher value in this experiment, which is typical of the values calculated from the data of Sack et al. (1987) for melts of similar composition (K-14, K-15 and SSC-2). At present there is no simple explanation for the calcic compositions of plagioclase within this experiment. There is a decrease of the measured partition coefficient with decreasing temperature, and the values are within the range of values (1.0-1.8) calculated from the experimental data of Mahood and Baker (1986). Tormey et al. 1987, in experiments on primitive tholeiites from the Kane Fracture Zone, obtained an average Ca/Na partition coefficient of 1.2.

The plagioclase phenocrysts of the Lihir lavas have a wider range of anorthite content (An 30-86) (Wallace et al. 1983) and this is consistent with the high water contents of the lavas resulting in An-rich plagioclase (Johannes 1978).

Figure 1-5

Variation in natural clinopyroxene compositions occuring in 78LH1. The lower end of numbered lines markes the average experimental clinopyroxene compositions which are given for comparison.

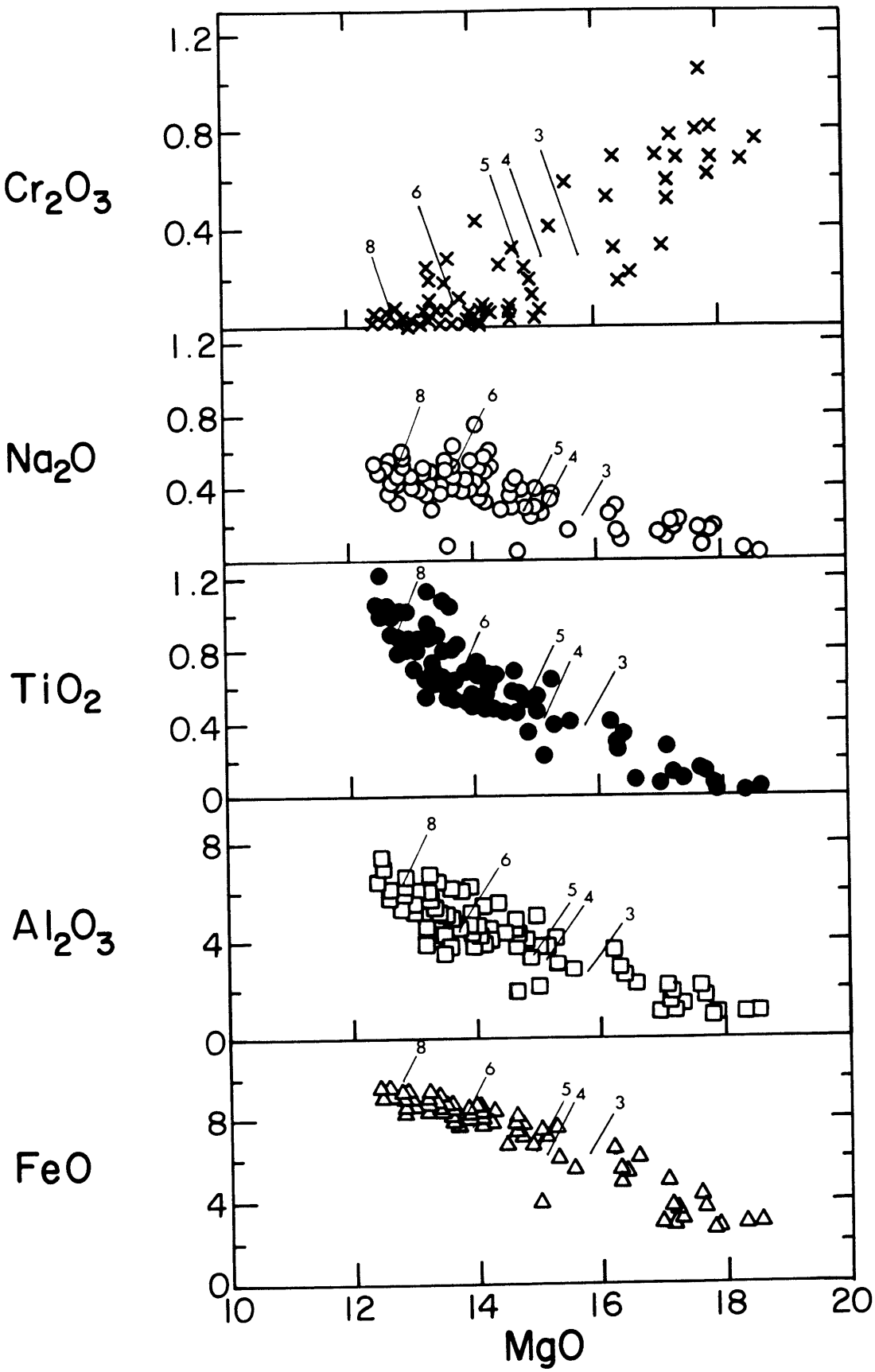
Cr2O3
Na2O
TiO2
Al2O3
FeO
MgO
1.2
0.8
0.4
0
8
4
10
12
14
16
18
20
8
6
5
4
3

Ti-magnetite in the Lihir lavas contains Al, Cr, and Mg, as minor constituents, and have low Al contents which is typical of spinel in arc rocks. The experimental Ti-magnetites are fairly uniform in composition and are richer in magnesium and aluminum, and poorer in titanium than most of the natural examples (Wallace et al. 1983).

Comparison of experimental and natural liquid lines of descent

The analyzed experimental glass compositions represent a series of 1 atm anhydrous melt compositions that can be compared with the Lihir lavas and the other Tabar-Feni lavas, and with a hypothetical liquid line of descent calculated from the measured partition coefficients and calculated modes (Table 1.1). The 1 atm experiment glasses all have increasing normative ne with decreasing temperature. Experiment 14, has highest SiO_2 (51.5%), high alkalis, Na_2O (4.14%), K_2O (4.66%) and is still ne-normative (8%). The experimental liquids show an increase of feldspar components with crystallization. Qtz-trachytes cannot be produced from ne-normative magmas by crystal fractionation at low pressure because of the low pressure thermal divide (Yoder and Tilley 1962). Al_2O_3, P_2O_5, TiO_2 and the alkalis increase continuously, and MgO and CaO decrease continuously with increasing crystallinity (decreasing temperature), while SiO_2 shows relatively little variation in the QFM experiments

Figure 1-6

Major element compositions of natural lavas (▽) and experimental glasses (▲) plotted against MgO. Curves show numerical fractionation models discussed in the text and the labeled tick-marks correspond to the percent of melt crystallized. The fractionation models use phase proportions from the experiments (Table 1.1) and the measured Fe^{2+}/Mg exchange distribution coefficients for olivine and clinopyroxene, and the Ca/Na exchange distribution coefficient for plagioclase. A set of phase compositions are calculated for each liquid composition and then 1% of the original mass of liquid is reduced by subtraction of this assemblage. A new liquid is calculated and the process is repeated. The curve labeled with 50 is calculated for fO_2 = QFM. The sudden change in direction of this calculated liquid line of descent occurs when Ti-magnetite is added to the fractionating assemblage. The other calculated liquid line of descent is for fO_2 = Ni-NiO, with Ti-magnetite crystallizing throughout.

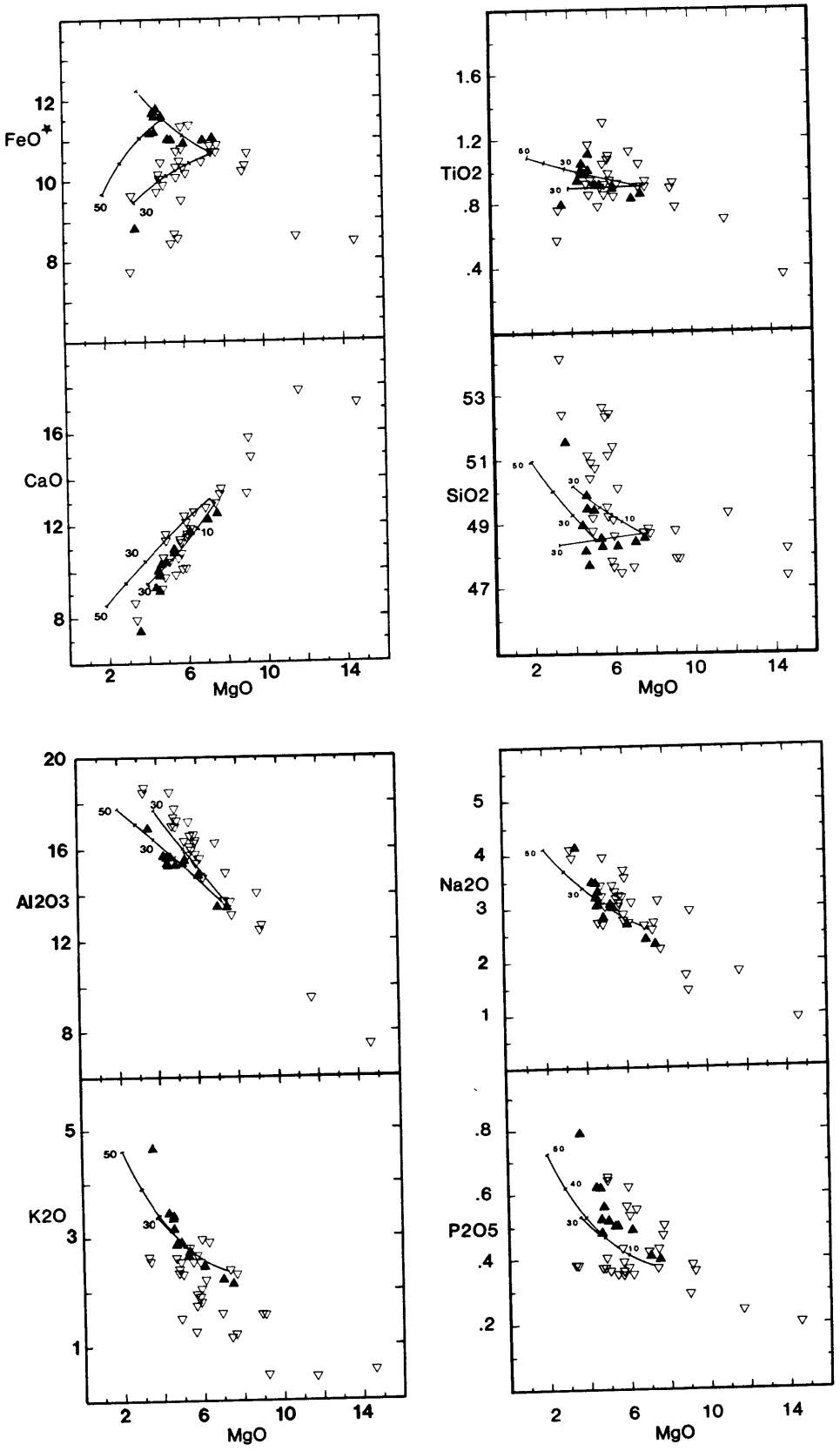
FeO*
12
10
8
50
30
CaO
16
12
8
30
10
MgO
2
6
10
14
TiO2
1.6
1.2
.8
.4
SiO2
53
51
49
47
Al2O3
20
16
12
8
K2O
5
3
1
P2O5
.8
.6
.4
.2
Na2O
5
4
3
2
1
40

until plagioclase is a stable phase and then it decreases by approximately 0.5%, (Figures 1-6a through 1-6g). In these experiments FeO* remains essentially constant until 30% crystallinity and then increases, but not consistently. TiO_2 initially behaves as a moderately incompatible element and increases down temperature until Ti-magnetite crystallizes.

The experiments at higher fO_2 have a higher calculated abundance of clinopyroxene and degree of crystallinity than the QFM experiments at the same temperature. These glasses have higher SiO_2 and K_2O, and lower CaO and MgO. The highest fO_2 experiment has abundant Ti-magnetite and the most evolved glass composition with high SiO_2, Al_2O_3 and alkalis, and low FeO* and TiO_2 (Table 1.2). This increase in crystallinity with increasing oxygen fugacity cannot be completely explained by the crystallization of Ti-magnetite, as the lower CaO and MgO of these liquids require the simultaneous crystallization of clinopyroxene. The high phenocryst content of many of the T-F lavas may reflect crystallization in response to a sudden increase in oxygen fugacity. The Lihir lavas have higher Al_2O_3 and lower K_2O and Na_2O than the experimental glasses at a similar MgO content, suggesting a different fractionation history, parental compositions, or conditions of fractionation. The higher Al_2O_3 and Na_2O, and lower FeO* of the natural lavas, can be interpreted as fractionation at higher pressures, or higher partial pressure of H_2O or higher fO_2 using the experiments of Duke (1974), Mahood and Baker (1986), Spulber and Rutherford (1983).

Calculated liquid lines of descent, which are derived from the calculated phase proportions (Table 1.1), and the major element distribution coefficients, for both the QFM and higher fO_2 experiments, are shown as tick-marked lines in Figure 1-6. The tick-marks show percent of liquid crystallized. These calculations followed the method of Grove and Donelly-Nolan (1986) and use an average composition for clinopyroxene, plagioclase and Ti-magnetite, and exchange distribution coefficients of 1.37 for Ca/Na plagioclase, 0.3 for Fe/Mg olivine. The Fe^{2+}/Mg distribution coefficient for clinopyroxene was taken as 0.25 for modeling the QFM liquid line of descent and 0.29 for the higher fO_2 model. None of the modeled liquid lines of descent are similar to the analyzed glass compositions and the Lihir lavas for SiO_2, CaO, FeO, Al_2O_3 and Na_2O, suggesting that the experiments are poor approximations to the equilibrium evolution of the natural samples. The natural lavas have higher Al_2O_3 and SiO_2, and lower FeO* at a similar MgO content to the calculated liquid line of descent and experimental glasses. This discrepancy could result from early crystallization of Ti-magnetite and higher An content of plagioclase in the natural samples, or crystallization of amphibole in the lavas. Since Ti-magnetite is present in the primitive lavas of the islands, the fO_2 during crystallization was extremely high and was close to the Ni-NiO buffer. The experiments have higher plagioclase proportions than the natural lavas and this could explain the lower Al_2O_3 and Na_2O of the

calculated liquid lines of descent. Two other factor have been virtually ignored is the above discussion and they are: the effect of fractionation at higher pressures and the possibility that 78LH1 is not a liquid. The general effects of higher pressure fractionation has been previously discussed (p35-37), and it can be concluded that higher pressure crystallization can explain the poor fit of the natural and hypothetical models. 78LH1 is phenocryst-rich, however it is typical of the Lihir lavas and is not depleted in incompatible elements (see chapter 2) as would be expected if it had accumulated phenocrysts.

Comparison of the experimental and natural lavas using projection schemes

The Lihir lavas and the experimental data can be compared on the ternary projections from the psuedoquarternary mineral projection scheme for undersaturated magmas of Sack et al. (1987). The plotting osition of samples in the oliv-diop-neph projection is highly dependent on the Fe^{3+}/Fe^{2+} ratio used, and hence on the oxygen fugacity and degree of alteration (Sack et al. 1987). High Fe_2O_3 contents result in the sample plotting closer to the olivine apex. To make a meaningful comparison between the natural samples and experiments, it is essential to use an Fe^{3+}/Fe^{2+} ratio that accurately reflects the conditions of crystallization. This is relatively easy for the experiments

Figure 1-7

Olivine-Diopside-Nepheline (a) and Olivine-Plagioclase-Diopside (b) projections of the pseudo-quarternary projection scheme of Sack et al. (1987). The 1 atm, QFM, olivine + high-Ca pyroxene + plagioclase cotectics of Sack et al. (1987) and Mahood and Baker (1986) are shown along with the experimental glasses and proposed cotectics for 1 atm QFM and Ni-NiO from experiments on 78LH1 in Figure 1-7a. In Figure 1-7b the experimental data is shown along with a fractionation trend which passes through the data set of Sack et al. (1987). No clearly defined trend could be discerned for the Mahood and Baker (1986) data and was therefore not shown. Note that this projection does not distinguish differences in fO_2.

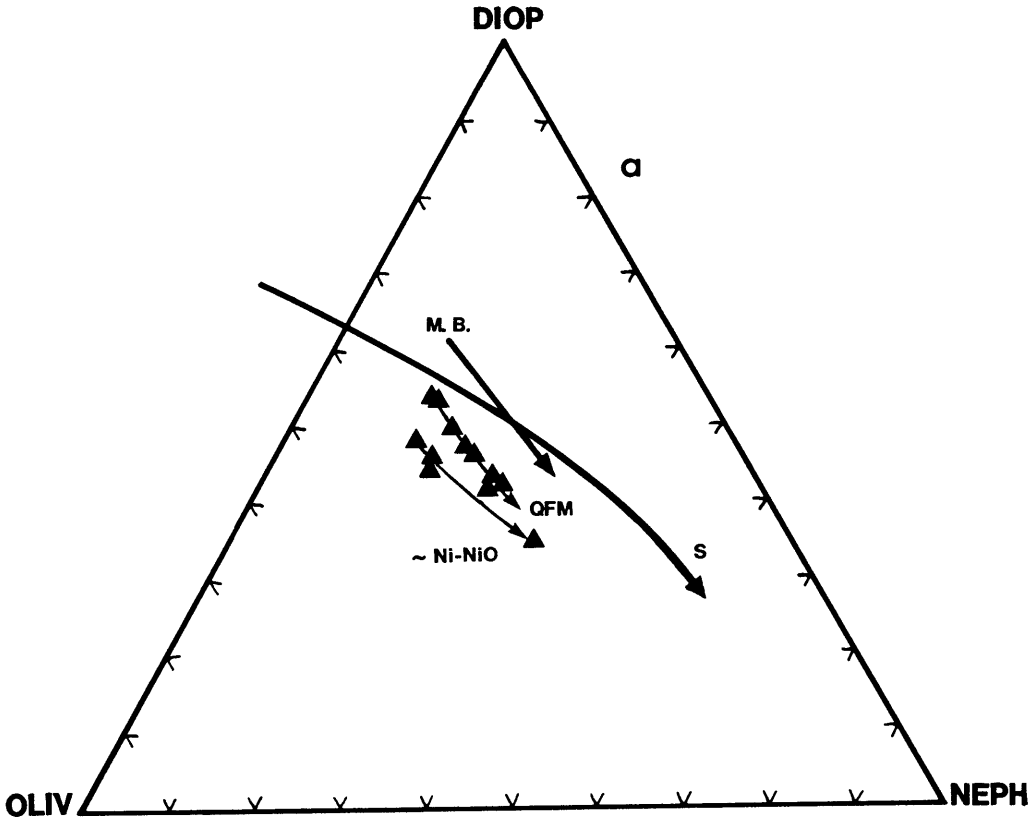
DIOP
a
M. B.
QFM
~ Ni-NiO
S
OLIV
NEPH

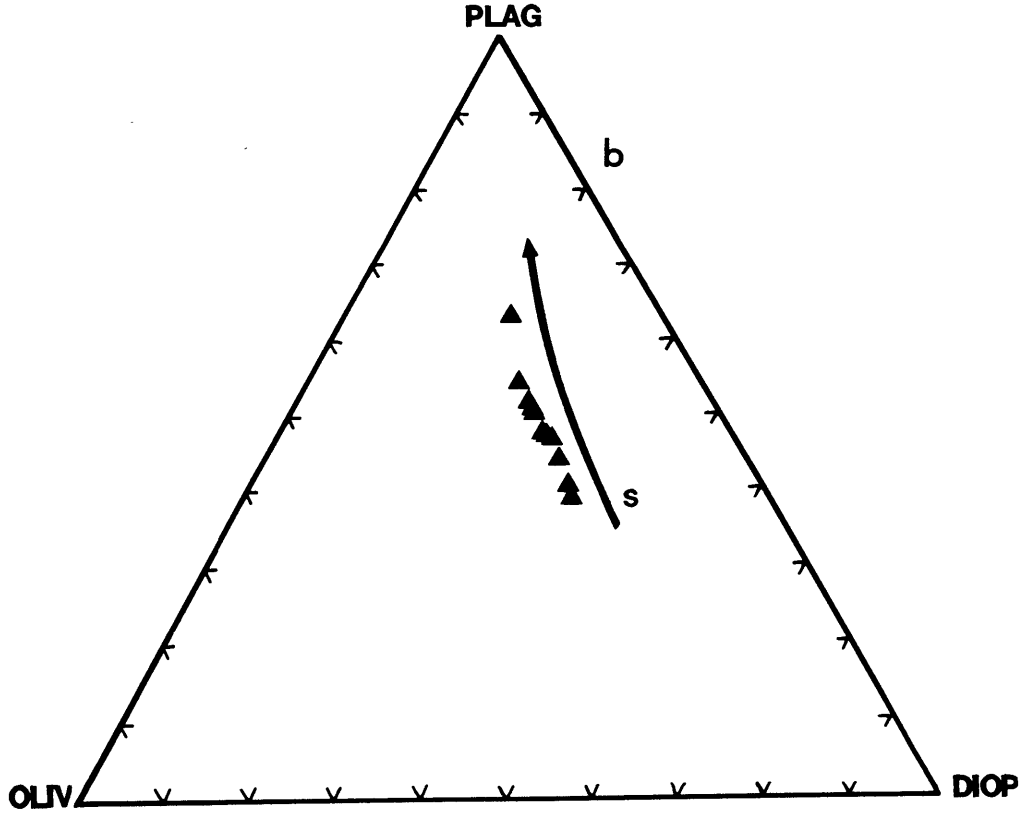
PLAG
b
s
OLIV
DIOP

where the Fe^{3+}/Fe^{2+} ratio can be calculated using the empirical relationship between Fe^{3+}/Fe^{2+}, fO_2, temperature and melt composition of Sack et al. (1980) with the updated coefficients of Kilinc et al. (1983). Assessing the true oxidation state of the Lihir lavas is more difficult. Measured Fe^{3+}/Fe^{2+} values are exceptionally high in lavas from the T-F islands, and are typically close to unity, and rarely less than 0.5 (Heming 1979 and Wallace et al. 1983). The unusually high fO_2 required to produce the high measured Fe^{3+}/Fe^{2+} in the lavas and minerals may result from the influx of water into a shallow magma chamber (Luhr and Carmichael 1985), from disassociation of H_2O during magma ascent (Foley et al. 1986), or from post-eruptive alteration during crystallization. The experimental glasses, Lihir lavas, and the anhydrous 1 atm QFM oliv-diop-plag saturation boundary (Sack et al. 1987) are plotted in Figures 1-7a and 1-7b on the oliv-diop-neph and oliv-plag-diop projections. The constancy of the Fe^{2+}/Mg exchange distribution coefficient for olivine/melt in these experiments, and those of previous workers (Roeder and Emslie 1970, Mahood and Baker 1986, Sack et al. 1987), allows the calculation of the Fe^{3+}/Fe^{2+} ratio of a melt in equilibrium with olivine. Provided some assumptions are made, this approach can be used to <u>estimate</u> the Fe^{3+}/Fe^{2+} of the Lihir lavas. If the olivines are xenocrystal, it is unlikely that they will provide an accurate estimate of the Fe^{3+}/Fe^{2+} ratio. Phenocryst-poor lavas which contain olivines that record

compositional zoning in Fe/Mg are rare in arc settings. However, some lavas with these characteristics occur in the T-F island chain. This method has been used on samples from the Feni islands, and the calculated Fe^{3+}/Fe^{2+} values are close to those measured by Heming (1979) and Wallace et al. (1983). Given the Fo-rich composition of olivines, both phenocryst and microphenocryst, in lavas from the T-F island chain, the measured Fe^{3+}/Fe^{2+} ratio has been used in the calculation of projection components.

The two points connected with a tie-line in the oliv-diop-neph projection (Figure 1-9a) are the positions calculated for a single sample but with a Fe^{3+}/Fe^{2+} ratio of 0.15 for the point closest to the diop apex and the measured ratio for the other. The large displacement emphasizes the need for accurate measurement of the oxidation state of iron when this projection scheme is used.

The 1 atm oliv-cpx-plag saturated experimental glasses, produced at oxygen fugacities close to the QFM buffer, form a well defined trend toward the nepheline apex, with decreasing temperature. This projected saturation surface parallels the multiple saturation boundary of the experiments of Mahood and Baker (1986) on sample 38, an undersaturated lava from Pantelleria, but is offset to higher olivine proportions as a result of the higher MgO contents of these glasses and the slightly higher fO_2. The experiments close to the Ni-NiO buffer have higher Fe^{3+}/Fe^{2+} and calculated olivine proportions and their positions in this projection can be

used to infer that the trend shown by the lower fO_2 is simply translated towards the olivine apex at higher oxygen fugacities.

The three projected oliv-cpx-plag multiple saturation boundaries, discussed in the previous paragraph, show systematic differences to the saturation boundary of Sack et al. (1987). This is to be expected since bulk compositional differences in MORB experiments (Walker et al. 1979, Grove and Bryan 1983, and Tormey et al. 1987) produce both displacement and crossing of the oliv-cpx-plag multiple saturation surfaces in the oliv-plag-diop-qtz pseudoquarternary of Walker et al. (1979). In subsequent discussions, any reference to a multiple saturation boundary will refer to the oliv-cpx-plag boundary derived in the experiments on 78LH1.

Ankaramitic lavas and cpx-rich cumulate nodules occur on Lihir. It is necessary to separate cumulate samples and late stage differentiates from lavas that possibly represent primitive liquids before examining crystal fractionation using the projection schemes. Since fractionation is dominated by clinopyroxene crystallization, CaO vs SiO_2 and Al_2O_3 vs SiO_2 diagrams provide an easy way of assessing the relationship between samples. In Figure 1-8 the Lihir samples fall on two trends, one representing accumulation crystallization of clinopyroxene, and the other crystal fractionation of clinopyroxene, magnetite and minor amounts of olivine, plagioclase and amphibole. Samples with low SiO_2

Figure 1-8

Al_2O_3 vs SiO_2 (a) and CaO vs SiO_2 (b) of the Lihir lavas. Arrows show the effects of differentiation and accumulation of clinopyroxene. Samples discussed in the text are numbered.

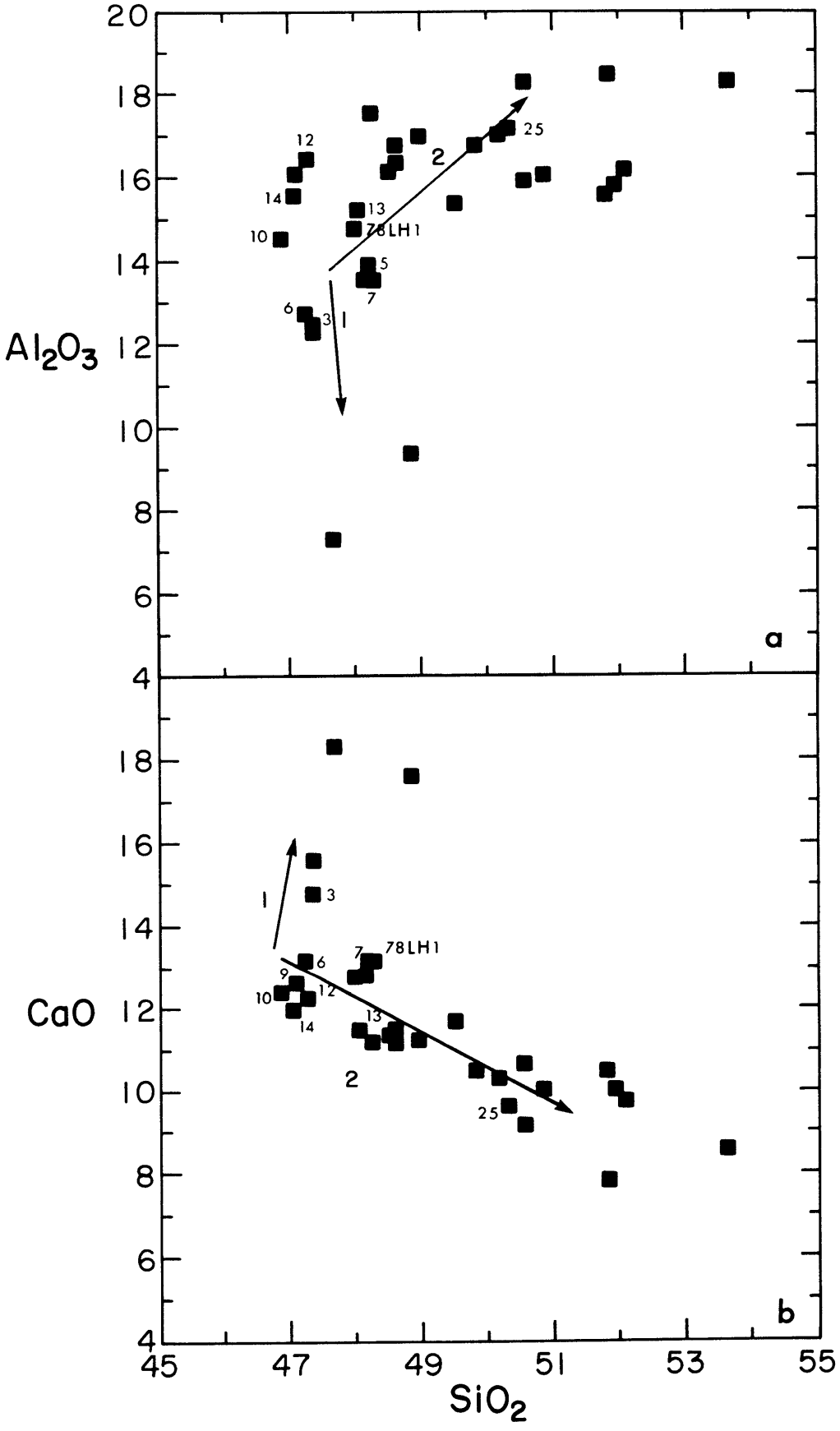
20
18
16
14
12
10
8
6
4
Al_2O_3
12
14
13
78LH1
10
5
7
6
3
1
2
25
a
18
16
14
12
10
8
6
4
CaO
1
3
7
78LH1
6
9
10
12
14
13
2
25
b
45
47
49
51
53
55
SiO_2

and CaO and Al_2O_3 contents close to the values at the intersection of the two trends are good candidates for being parental liquids. On the basis of trace element chemistry (chapter 2), L6 and L7 have parental compositions. Samples that are considered parental liquids have been labeled to aid discussion of fractionation within the Lihir lavas. Also labeled is L25, a more evolved sample, which will be in trace element models of crystal fractionation.

In the oliv-diop-neph projection (Figure 1-9a), most of the Lihir lavas plot as a group to the olivine side of both QFM and Ni-NiO experimental glasses and with lower calculated ne proportions, in a region between the 1 atm saturation surface and the high pressure oliv-cpx-opx saturation surface proposed by Sack et al. (1987). The projected positions of these lavas in the olivine field suggests that olivine should be the first mafic phase to crystallize in these lavas at 1 atm. However, the mafic lavas from Lihir, like those from the other islands, have clinopyroxene as the most abundant phase and only minor olivine. Some samples from Lihir have accumulated clinopyroxene and plot in the diopside field. The labeled samples that are the most primitive liquids plot closer to the experimental multiple saturation surface than the more evolved samples, and scatter along the saturation surface from qtz-normative compositions (L6) to moderately high nepheline contents (L10). This scatter of the primitive lavas results from substantial differences in K_2O, and hence projected ne-content, of the lavas. The K_2O content of the

Figure 1-9

Olivine-Diopside-Nepheline (a) and
Olivine-Plagioclase-Diopside
(b) projections showing Lihir lavas and cotectics and fractionation trends given in Figure 1-7. Numbering as for Figure 1-8. Fields A and B are amphiboles and biotites analyzed in the T-F lavas. A tie line connects the plotting positions of a single sample with Fe^{2+}/Fe^{3+}=0.9 and with the measured value 0.5. The high pressure multiple saturation boundary suggested by Sack et al. (1987) is also shown. The fractionation vector drawn from F7 towards the olivine apex in Figure 1-9a shows the direction of fractionation in this projection for the evolved lavas.

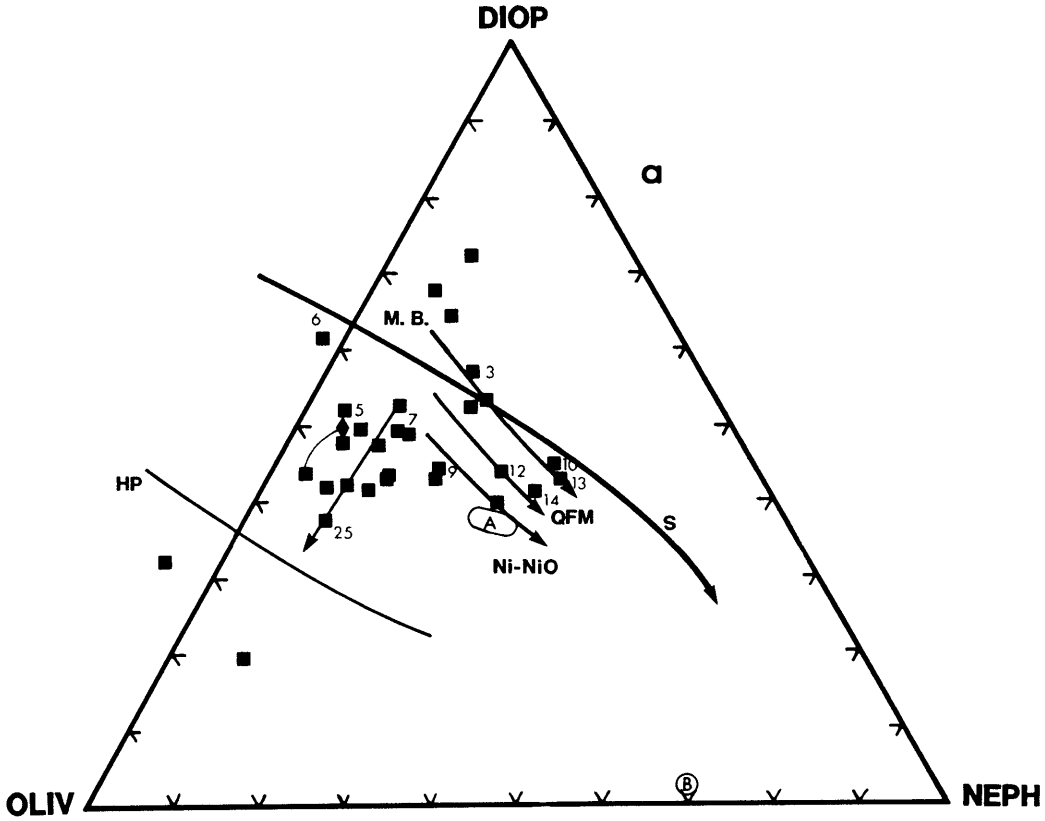
DIOP
a
M. B.
6
3
5
7
9
12
10
13
14
25
HP
QFM
Ni-NiO
S
A
B
OLIV
NEPH

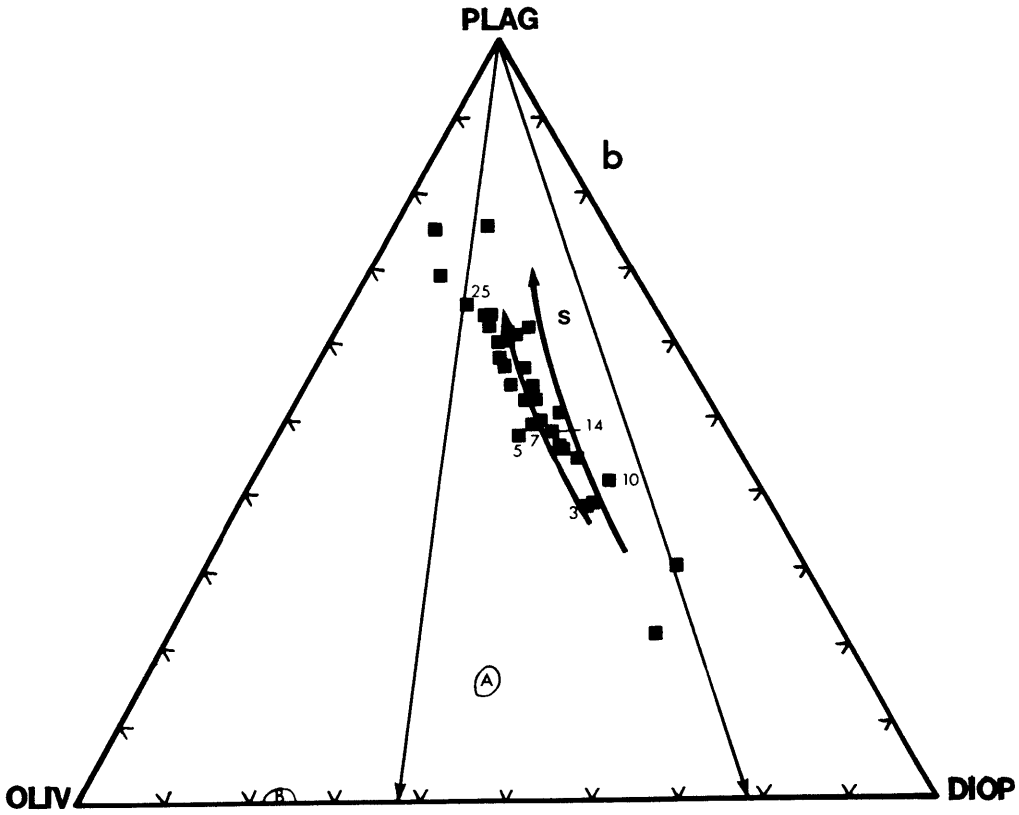
PLAG
b
25
S
14
5
7
10
3
A
B
OLIV
DIOP

Lihir lavas increases only slightly while Al_2O_3 and SiO_2 increase substantially during fractionation (Figure 1-6). This change in the composition of the liquid produces a decrease in the proportion of nepheline and an increase on the calculated proportion of plagioclase. Therefore, the fractionation trend exhibited by the Lihir lavas is parallel to the oliv-diop edge of this projection.

The evolution of the Lihir samples shown in Figure 1.9b, is toward the oliv-plag edge, and this results in a constantly increasing oliv/diop ratio. The natural samples and the experimental glasses form a slightly curved array that trends almost directly away from the diop apex and the lack of scatter, and the well defined nature of this trend, reflects a saturation surface in the 4-component system. Projection of the evolved samples through plagioclase results in these samples plotting to the olivine side of the 1 atm anhydrous multiple saturation boundary. The plotting position is sensitive to relatively small variations in bulk composition for evolved samples, especially phenocryst-rich lavas that have variable Fe^{3+}/Fe^{2+}. The projected positions of the Lihir lavas is consistent with a polybaric fractionation under high oxygen fugacities, of olivine and clinopyroxene at moderate pressure, and differentiation at lower pressure of an assemblage containing clinopyroxene, amphibole and phlogopite. This evolutionary model is supported by the low Ni, V and Sc in most of the lavas, by

the duplication of phenocryst compositions in the experiments, and by the presence of amphibole and biotite in some of the lavas.

Major element constraints on generation of the Lihir Lavas

None of the Lihir lavas have Ni contents of primary magmas, and the major element chemistry has been modified by removal of olivine and clinopyroxene. The absence of primary magmas makes the interpretation of the melting conditions; pressure, degree of partial melting, and residual source mineralogy difficult. The assumption that a parental magma has undergone low pressure fractional crystallization to produce the observed compositional specturm is supported by the experimental results, and by the presence of cpx-rich cumulate nodules. Since lavas from the other islands in the chain have similar major element chemistry to those from Lihir, it is possible to gain insight into the petrogenesis of the Lihir lavas by examining the primitive lavas from the other islands.

Primitive potassic alkali-basalts from the Feni group are similar to the Lihir lavas, having high CaO/Al_2O_3, low SiO_2, and the same mineralogy, although they usually have higher alkali contents and slightly lower iron. SiO_2 undersaturated magmas generated at high pressures usually have high CO_2 (Wyllie 1979). Previous studies of alkalic basalt suites (Frey et al. 1978, Sun and Hanson 1975, and

Clague and Frey 1982) concluded that this type of basalt is a partial melt of a garnet-peridotite and that the degree of partial melting increases with increasing SiO_2 content of the melt. The major element trends in the relatively few primitive magmas of the T-F are similar to those exhibited by the Honolulu volcanic series (Clague and Frey 1980). CaO and SiO_2 are negatively correlated (Bultitude and Green 1968), and this may indicate changes in the degree of melting of a single source. The Al_2O_3/CaO and CaO/MgO ratios of the Lihir lavas respectively range between 0.9 and 1.3, and, 1.5 and 2.0. These lavas consistently have lower Al_2O_3/CaO and higher CaO/MgO at a similar SiO_2 content than the Honolulu volcanic series and the C-series undersaturated lavas of Grenada (Thirwall and Graham 1984). The lower Al_2O_3/CaO and higher CaO/MgO and Sc, is consistent with a greater proportion of clinopyroxene entering the melt during partial melting. The effects of volatile content on melt compositions produced by partial melting of mantle have been studied experimentally (Eggler and Holloway 1977, Wyllie 1979, and Ryabchikov et al. 1981). The experimental data, however, for systems containing variable CO_2 and H_2O are not consistent (see BVSP 1981 p 553). A major constraint can be placed on the pressure of generation of the Lihir lavas since undersaturated lavas cannot be generated at pressures below 10 kb (Jaques and Green 1980, and Wyllie 1979).

Discussion

The previous sections have shown that the evolution of the Lihir lavas is toward a plagioclase-rich composition and the oliv-diop edge of the oliv-diop-neph projection of Sack et al. (1987), and toward compositions with lower calculated ne proportions. At the same time, there is limited increase in the K_2O abundance of the derivative lavas. The fractionation of amphibole or biotite, two low silica potassic phases that are present in some of the Lihir lavas (Wallace et al. 1983), in addition to clinopyroxene, magnetite, and minor plagioclase, could supress the enrichment of K_2O. The crystallizing assemblage in both the lavas and 1 atm experiments is dominated by clinopyroxene, and this phase is responsible for the decreasing CaO and increasing Al_2O_3 of this suite. The trace element geochemistry, which is discussed elsewhere, shows that biotite fractionation is unlikely. The projected position of amphibole and biotite from the T-F lavas (Figure 1-9) is consistent with removal of amphibole being responsible for the evolution of the lavas toward the oliv-diop boundary and toward silica saturation.

Amphibole is an early crystallizing phase in the Aleutians, and the Lesser Antilles and Japan (Conrad and Kay 1984, Kay and Kay 1985, Arculus and Wills 1980, Dostal et al. 1983), with the order of phase appearance being olivine, then clinopyroxene, then amphibole and plagioclase, with oxides

crystallizing at different positions depending on the fO_2. Experimental studies have shown that amphibole is stabilized by the presence of H_2O in a melt in undersaturated lavas (Cawthorn et al. 1973, Helz 1976); the Lihir lavas are exceptionally rich in volatiles. Grove and Kinzler (1986) have pointed out the difficulty of deriving calc-alkaline derivatives from ne-normative compositions by removal of an assemblage containing amphibole, as amphibole has a composition close to the melt. This requires prohibitively large amounts of fractionation to produce relatively minor changes in the composition of the residual liquid. The applicability of this model to the Lihir case, is dependent on the difference in composition of the amphibole and melt. For the Lihir lavas, the difference is sufficiently large, as the lavas typically have SiO_2 contents >47%, while the amphiboles normally have 40%.

The position of the lavas in Figures 1-9a and 1-9b, relative to the position of amphibole and clinopyroxene, is such that the removal of a assemblage dominated by clinopyroxene and amphibole from a parental lava similar to L7, will produce the observed trend toward lower ne-normative compositions. Although this type of crystal fractionation is successful, it is not completely general since the fractionation direction is dependent on the initial position of the lava when amphibole becomes a liquidus phase. Alkali-rich lavas, which have higher calculated nepheline proportions than amphibole, will continue to evolve towards

more ne-normative compositions, while others will evolve towards the region where most Lihir samples plot.

The early evolution (primitive samples of chapter 2) of the Lihir lavas appears to be dominated by olivine removal, and this period is followed by fractionation of clinopyroxene and magnetite, and/or by clinopyroxene, amphibole, plagioclase, apatite and magnetite crystallization.

Conclusions

The 1 atm experimental results, major element chemistry, and the low Al^{VI} of clinopyroxenes, show that the fractionation of the Lihir lavas is dominated by the removal at low pressures of a cpx-rich assemblage that also contains magnetite, plagioclase, apatite, and amphibole. The observed suite of lavas have all undergone substantial olivine crystallization, although the only evidence for this process is the low MgO, Cr and Ni contents. The cpx-rich basalts evolve towards plag-rich compositions, however the trachytic lavas cannot be derived by fractional crystallization. The alkali-rich tephritic phonolites could be derived by fractionation of an assemblage which contained little or no amphibole, as this would allow the major element composition to evolve beyond the composition of amphibole in the oliv-diop-neph projection. If amphibole appears early in the fractionation sequence the magma will evolve toward the olivine apex in the oliv-diop-neph projection.

Projection of the experiments, lavas and phases onto the projections of the Sack et al. (1987), show that lavas evolve toward lower nepheline, olivine and diopside, and higher plagioclase proportions. The crossing of experimentally determined multiple saturation surfaces suggests that the position of these surfaces is dependent upon the bulk composition of the system. Increasing oxygen fugacity produces a shift of the projected position of the oliv-cpx-plag multiple saturation surface toward the olivine apex of the oliv-diop-neph projection, but has no observable effect on the position of this surface in the oliv-plag-diop projection. The variation in the calculated oliv/diop ratio of the primitive Lihir lavas can be interpreted as resulting from variations in the fO_2 in the vicinity of the Ni-NiO buffer. This conclusion is supported by the magnesian phenocrysts of the lavas and the ubiquitous presence of Ti-magnetite in the lavas. The variation in calculated nepheline proportions results from early fractionation of these lavas and from heterogeneity of the primary lavas.

The evolved lavas from Lihir have undergone crystallization of an amphibole bearing assemblage which drives the composition of most of these lavas in the direction opposite to that produced by the anhydrous, 1 atm experiments. Fractionation of clinopyroxene, amphibole and Ti-magnetite at shallow levels is the dominant process controlling the major element evolution of the Lihir lavas, and by analogy, the lavas from the other T-F islands.

Appendix 1: Mass balance

Mass balance calculations are consistently used in the geological literature and numerous methods exist for the solution of this type of problem (Ax=b where the equation is in matrix form). Least Squares (L.S.), either in constrained or unconstrained form, is the most common method (Chayes 1968, Bryan 1969, Gray 1973, Le Maitre 1979, Reid et al. 1973, Albarede and Provost 1977) and linear programming and the simplex algorithm have also been used (Wright and Doherty 1970, Banks 1979, Kostal et al. 1986). Unfortunately, the unconstrained L.S. solution of a mass balance problem can result in negative proportions and total proportions unequal to 1.0, and the constrained forms usually require a priori information to produce meaningful results (Reid et al. 1973, Albarede and Provost 1977). The simplex algorithm, which has been used here, has great flexibility in the constraints that can be imposed upon the solution. The constraints of positive proportions that sum to 1.0 can easily be applied as a second term to the error function that is used to produce a least squares solution. This flexibility can be a limitation of this method, as it is possible to produce almost any result by adding unwarranted constraints, thus the validity of the results must be carefully examined before use.

The problem of closure and the resultant correlation of errors, and the need for stoichiometric constraints in mineral components, are additional problems (Chayes 1962, Le Maitre 1982) that must be addressed in this type of calculation. The application of constraints which force all components to be positive, is a necessity if realistic results are to be obtained (Wright and Doherty 1970). However, such constraints can cover a serious error in the model assumptions (Reid et al. 1973, Le Maitre 1982, Stormer and Nicholls 1978). For this reason, proportions were calculated using both the unconstrained and constrained equations and then compared. Whenever an unconstrained solution gave negative proportions more negative than $-1e^{-6}$ or a total outside of the range 99.5% to 100.5% the constrained solution, which for each phase was typically within 5% of the unconstrained proportion, was adopted.

The microprobe data used in the calculation of phase proportions has not been normalized to 100 wt% since this is equivalent to a complex weighting of the mass balance equations. Because of the importance of Fe^{3+}/Fe^{2+} in the crystallization of Ti-magnetite from the experimental liquids, the value of this ratio in the melt and cpx has been estimated respectively with the methods of Kilinc et al. (1983) and Papike et al. (1974). Olivine was assumed to contain only ferrous iron. The contribution of plagioclase was ignored, and the proportion of ferric and ferrous iron in Ti-magnetite was calculated using stoichiometric constraints.

The mass balance of experimental charges must also take into account loss of Na_2O, K_2O, P_2O_5 and iron from the experimental charge and the low levels of some elements in various phases. It was assumed that K_2O loss was insignificant in these experiments and that P_2O_5 was not lost from the experiments close to the QFM buffer. In the highest fO_2 experiments, the P_2O_5 content of the glasses at the rim of the experimental charges were substantially lower than the levels measured at the center of the charges, or in regions of high crystallinity. The values used in the calculations, and presented in the tables, are averages from the center of the charges where loss is at a minimum. Iron loss was taken to be negligible in these experiments, as the mass balance calculations did not indicate a deficit in total iron. The Na_2O loss was assumed to be equal to the difference between the calculated Na_2O and the starting Na_2O, although this assumes the mass balance solution is correct. The greatest calculated deficiences were 8% for the highest temperature experiment and 7% for run experiment 11. All other runs had discrepancies of 5% or lower. Similar results for sodium loss were obtained when Na_2O was included as a separate component and weighted to produce an exact fit for this element. Low concentration levels can result in the calculation of unrealistic estimates of means and standard deviations (Albarede and Provost 1977) and this is a potential problem in mass balance calculations that use minor or trace elements. The weighting scheme used circumvents

this problem by assigning small weights to low concentration elements such as MnO.

Weighted mass balance equations produce a more statistically meaningful result than unweighted equations that assume equal relative errors for all elements (Reid et al. 1973) and the weights are usually derived from estimates of the unit variance (Hamilton 1964). If the uncertainties on the various elements in the component matrix (A) are unknown, the estimates of the normalized unit variances of each element in the b vector are used to weight each equation. If the uncertainties on each element in each component are known, as in the case where these values are the averages of multiple analyses, then the weighting assigned to each mass balance equation is given by equation 11 of Reid et al. (1973). Although this method is the most rigorous, the resultant proportions are in no way guaranteed to be more accurate than those of the simpler methods. To assess whether this method is truly superior to the simpler methods of unit weighting and weighting with only the uncertainties of the elements in the b vector, the phase proportions of experiment 12 were calculated with each method and compared to one another and the proportions as estimated during microprobe analysis. The unit weighting method gives unrealistic estimates of the olivine and plagioclase proportions and negative proportions and will not be considered further. The plagioclase percentage (7%) obtained by using the weights calculated from the b vector

uncertainties appears to be too high when compared to the experimental charge and the more complex weighting scheme, which uses the uncertainties from both the A matrix and b vector is adopted as the best method.

These weighting schemes all ignore the effect of covariances that result from the closed nature of the components and b vector. Chayes (1960) has shown that closure results in higher negative correlations than would be calculated from an open data set, and this results in an overestimation of the variance. A priori information about the proportions have not been included in the form of constraint equations since the size of the experimental charges and the distribution of glasses within microprobed sections makes point counting unrealistic. The calculated weights used require an initial estimate of the correct proportions, and the program is used to iterate toward the final solution. This iterative process is relatively painless as convergence is usually achieved in two or three iterations.

The calculated weights from the second and third weighting schemes are fairly similar and assign larger weights to the more abundant elements, SiO_2, Al_2O_3, FeO, Fe_2O_3, CaO, K_2O and MgO, whereas as the elements with low abundances are lightly weighted and this is intuitively comforting. Much of the similarity between these two schemes can be attributed to the lower standard deviations on the elements in the analysed glass component and b vector, and

the large proportion of liquid in the charges. The calculated weights derived by combining the A matrix and b vector uncertainties become the best estimate of the true weights in highly crystalline charges; this method should be used in preference to the other methods under these circumstances. Comparison of results normally uses chi-squared values, however this method was not adopted here because of the complexity introduced by the constraints of positive values for each proportion. Chi-squared is normally evaluated using this distribution for the degrees of freedom for each model and an adopted probability. Since the different mass balance equations have different degrees of freedom because of different numbers of phases and different numbers of imposed constraints, i.e. positive proportions and/or non negative proportions the chi-squared values are not comparable. Under these circumstances the best measure to compare is the sum of the deviations squared, as presented in Table 1.1, or the calculated probabilities.

CHAPTER 2

TRACE ELEMENT AND ISOTOPIC CONSTRAINTS ON THE GENESIS AND EVOLUTION OF THE LIHIR LAVAS

Introduction

The major element chemistry of lavas from Lihir, the largest island in the Tabar-Feni island chain, Papua New Guinea (PNG), and the results of 1 atm anhydrous crystallization experiments on a Lihir lava (Kennedy et al. 1987), suggest that crystal fractionation of clinopyroxene, amphibole, Ti-magnetite and apatite has been the dominant process influencing the evolution of this suite of undersaturated basalts and tephrites, and that two separate evolutionary sequences exist in the Lihir lavas. In this chapter trace element and isotope data is used to examine: 1) simple crystal fractionation models for both evolutionary trends, 2) the relationship between or decoupling of major elements, trace elements and isotopes, 3) the possibility of mixing, AFC, open and closed system crystallization and boundary layer crystallization, producing the observed trace element trends, i.e., the crossing REE patterns of primitive and evolved lavas, 4) the generation of arc characteristics, particularly variation of Ba/La, and 5) The lower La/Yb of lavas from Lihir when compared to lavas of similar major element composition from the other Tabar-Feni islands.

Analytical methods

Data for major elements and Ni, Y, Zr, Nb, were obtained as averages of duplicate analyses by X-ray fluorescence at the University of Massachusetts (Rhodes 1983) and the Bureau of Mineral Resources (B.M.R.), Australia (see Wallace et al. 1983); Hf, Co, Sc, Na, Th, Cr, and REE by INAA (Ila and Frey, 1984); K, Rb, Cs, Sr, Ba, Sm, and Nd, were obtained by isotope dilution (Hart and Brooks, 1977) for samples analysed for isotopic compositions. Isotope analysis was performed at MIT using techniques modified from those of Richard et al. (1976) and Manhes et al. (1978). $^{87}Sr/^{86}Sr$ is normalized to $^{86}Sr/^{88}Sr=0.1194$ and $^{87}Sr/^{86}Sr=0.70800$ for Eimer and Amend $SrCO_3$. $^{143}Nd/^{144}Nd$ is normalized to $^{146}Nd/^{144}Nd=0.7129$ and $^{143}Nd/^{144}Nd=0.51264$ for BCR-1. The 2 sigma error from in-run statistics are <0.00003 for $^{87}Sr/^{86}Sr$ and <0.000025 for $^{143}Nd/^{144}Nd$ and typical reproducibility is respectively 0.000025 and 0.00002. Pb isotope mass fractionation was corrected using duplicate analyses of NBS 981, since in-run statistics are better than 0.015% amu^{-1} and reproducibility is better than 0.05% amu^{-1}.

Major element evolution of the Lihir lavas

It is important to identify lavas that represent parental magmas before examining crystal fractionation using the trace element and isotopic data. The CaO and SiO_2 vs MgO

diagrams (Figure 2-1) provide an easy way of assessing the relationship between samples. In the CaO vs MgO figure the Lihir samples fall along a single fractionation trend that results from crystal fractionation of clinopyroxene. Samples with SiO_2 <48% and MgO >5.8% (Table 2.1) are primitive magmas. Primitive samples have been labeled in this diagram and will be referred to as the primitive group throughout this chapter. These lavas have high Fe_2O_3* and CaO, low Al_2O_3 and SiO_2, and higher Ni than the evolved lavas. The Ni abundance suggests that the primitive lavas have undergone olivine fractionation. The lavas with MgO >8% are phenocryst-rich samples that have accumulated cpx and olivine, and are consequently not representative of parental liquids. The primitive lavas have constant SiO_2 and increasing Fe/Mg, with decreasing MgO, and have fractionated only minor amounts of magnetite. In chapter 1, cumulate lavas were identified using Al_2O_3 and CaO vs SiO_2 diagrams and those samples are not considered further. Any sample with CaO/Al_2O_3 >1.2 and CaO >14% is considered a cumulate and these lavas plot in the Diopside phase volume in the Oliv-Diop-Neph projection of chapter 1. L25, which is also labeled in Figure 2-1, has lower CaO and higher SiO_2 and Al_2O_3 as a result of fractionation of clinopyroxene, magnetite, plagioclase and amphibole, and is representative of the evolved lavas.

Figure 2-1

CaO vs MgO (a) and SiO_2 vs MgO (b) of the Lihir lavas. Samples discussed in the text are numbered. Additional samples from Wallace et al. (1983).

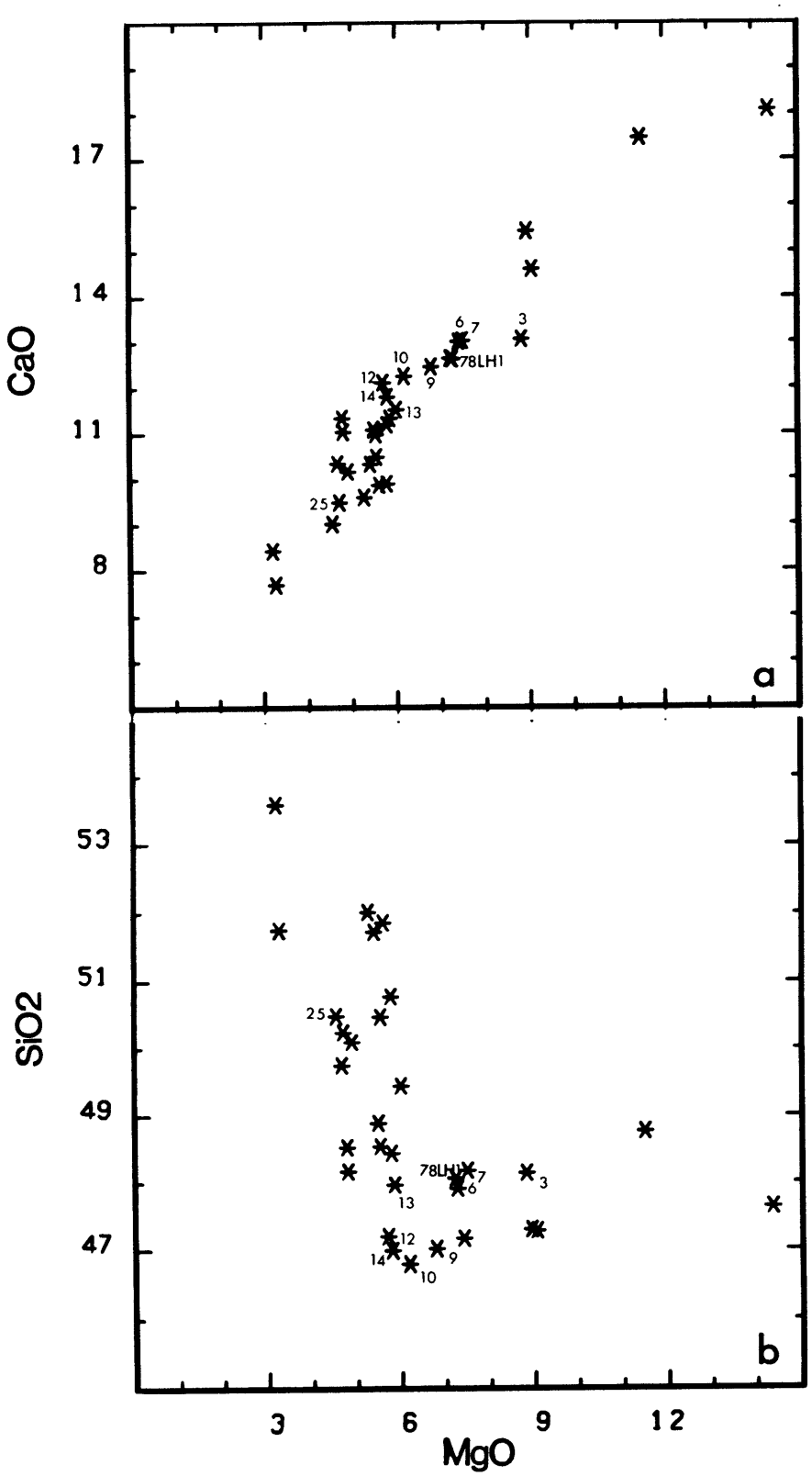
CaO
17
14
11
8
a
SiO2
53
51
49
47
b
3
6
9
12
MgO
78LH1
25
14
12
13
10
9
7
6
3

General trace element and isotopic characteristics of the Lihir lavas

The Lihir lavas are enriched in Sr (950-1780 ppm) relative to most island arc basalts (IAB) and oceanic island basalts (OIB). These rocks have normal arc K/Rb, Ba/La and Sr/La ratios as defined by Morris and Hart (1983, Table 2.4) with respective ranges of 300-500, 10-20, and 85-130, and are depleted in HFSE with concentrations typical of arc rocks (Perfit et al. 1980), i.e. Nb <3 ppm, Hf <2 ppm, and TiO_2 <1.2 %. The Sr, Nd and Pb isotopes of the Lihir lavas are typical of arcs (Table 2.1) and similar to tholeiitic and calc-alkaline rocks from PNG (Johnson et al. 1985, Page and Johnson 1974, DePaolo and Johnson 1979, White and Patchett 1984, Hamilton et al. 1983) and other intra-oceanic arcs (von Drach et al. 1986, Morris and Hart 1983, DePaolo and Wasserburg 1977, Kay et al. 1986, Staudigel et al. in press). The Sr and Nd isotopic compositions overlap with those from the Feni islands, but like samples from the Tabar and Tanga island groups, extend to higher $^{87}Sr/^{86}Sr$. The Lihir samples plot to the high $^{87}Sr/^{86}Sr$ side of the mantle array (Figure 2-2) and this may have resulted from contamination by seawater (Hawkesworth 1982). Lihir island has active geothermal springs with a seawater component (Wallace et al. 1983) and this may result in contamination during eruption and cooling. However, analysis of a leached powder of L3 gave the same isotopic composition as the

Table 2.1

Major Element, Trace Element and Isotopic Analyses of Lihir Lavas

Group	P	P	P	P	P	P	P	P	E	E	E	E
	L3	L6	L7	78LH1	L10	L12	L13	L14	L16	L22	L23	L25
SiO_2	47.4	47.24	47.98	48.14	46.87	47.27	48.04	47.06	48.51	52.09	50.17	50.32
TiO_2	0.76	0.90	1.03	0.89	0.91	1.06	0.93	0.96	1.08	0.77	0.93	1.00
Al_2O_3	12.5	12.69	14.75	13.50	14.51	16.41	15.19	15.55	16.12	16.16	17.01	17.15
Fe_2O_3	11.7	11.70	11.74	11.90	12.44	11.49	11.32	12.42	11.80	9.24	10.84	11.02
MnO	0.21	0.21	0.19	0.24	0.23	0.21	0.22	0.22	0.21	0.18	0.21	0.21
MgO	9.1	7.47	7.33	7.28	6.24	5.77	5.92	5.86	5.85	5.33	4.96	4.77
CaO	14.7	13.12	12.74	12.76	12.36	12.22	11.45	11.92	11.31	9.70	10.27	9.59
Na_2O	2.9	2.15	2.68	2.55	3.05	3.16	3.51	3.64	2.73	3.37	2.98	3.17
K_2O	0.44	2.23	1.13	2.35	2.85	1.86	2.91	1.77	2.01	2.75	2.28	2.37
P_2O_5	0.36	0.49	0.42	0.37	0.54	0.55	0.52	0.61	0.37	0.35	0.36	0.40
H_2O	2.0	1.2	2.0	1.3	0.57	1.2	0.12	1.3	1.8	0.66	1.5	0.96
CO_2	0.3	0.3	0.3	0.3	0.03	0.05	0.1	0.4	0.2	0.1	0.3	0.01
Fe^{2+}/Fe^{3+}	1.22	1.51	1.00	-	1.30	1.13	0.97	0.95	1.11	1.01	1.20	1.22
Rb	12.0	43.5	36.9	58.2	58.2	128	59.0	59.0	40.0	49.4	39.5	40.0
Sr	1196	1120	1049	1659	1397	1430	1440	1780	1140	948	1089	1021
Ba	187	168	135	199	255	265	270	390	175	239	249	220
Cs	1.16	0.85	0.54	0.78	0.86	1.10	0.76	1.0	0.00	224	0.75	0.43
V	308	313	287	320	347	251	275	264	234	113	226	235
Cr	119	221	124	158	33.0	24	94.0	18	47	33	21.8	12.7
Co	45	0.0	0.0	0.0	50	0.0	0.0	0.0	0.0	32	37	37
Ni	40	40	27	41	25	14	20	14	16	22	16	14
Sc	53.5	46.1	46.8	42.5	31	21	24	15	30	68	25.5	24.5
Zn	82	89	76	95	91	74	72	77	78	16.5	78	93
Ga	13.5	15	15.5	0.00	16.5	17.5	16.5	17.0	16.5	20	17.0	17.5
Y	15	17	18	0.00	19	21	19	19	19	66	20	24
Zr	45	70	70	86	57	74	67	65	32	1.5	60	70
Nb	1.5	1.5	0.51	2.7	1.5	2.0	2.0	2.0	1.5	0.00	1.0	1.0
Hf	1.4	1.8	1.8	1.70	1.9	1.9	1.6	1.8	0.00	0.00	1.9	2.1
U	0.0	0.0	0.00	0.00	0.00	0.83	0.94	0.00	0.00	0.00	0.00	0.00
Th	0.6	0.7	0.7	0.9	1.1	1.4	1.4	1.4	0.00	0.00	0.00	0.92
La	11.8	12.2	10.6	12.4	13.8	15.4	17.1	18.8	12.0	11.0	10.1	10.4
Ce	26.0	28.4	25.9	29.7	32.3	36.0	42.4	42.5	32.0	23.0	23.10	25.10
Nd	16.1	18.4	18.0	18.78	21.1	21.4	24.1	27.7	16.0	15.0	15.0	16.6
Sm	4.09	4.78	4.76	4.72	5.40	5.46	5.22	6.36	0.00	3.38	3.94	4.41
Eu	1.27	1.53	1.53	1.50	1.70	1.73	1.66	1.97	0.00	0.00	1.34	1.42
Tb	0.66	0.63	0.64	0.75	0.58	0.76	0.68	.77	0.00	0.00	0.56	0.64
Yb	1.2	1.8	1.7	1.6	1.8	2.0	1.71	1.70	0.00	0.00	2.0	2.3
Lu	0.21	0.27	0.27	0.24	0.25	0.00	0.00	0.00	0.00	0.00	0.31	0.35
$^{87}Sr/^{86}Sr$	0.704241*	0.703862	0.703822	0.703950	0.703961	0.704094	0.000000	0.000000	0.000000	0.704128	0.704008	0.703954
$^{143}Nd/^{144}Nd$	0.512967	0.512990	0.512982	0.513013	0.512976	0.512998	0.000000	0.000000	0.000000	0.512961	0.513035	0.512968
$^{206}Pb/^{204}Pb$	18.738	0.000	0.000	18.740	18.743	18.756	0.000	0.000	0.000	18.741	18.754	18.743
$^{207}Pb/^{204}Pb$	15.550	0.000	0.000	15.540	15.556	15.550	0.000	0.000	0.000	15.541	15.569	15.539
$^{208}Pb/^{204}Pb$	38.402	0.000	0.000	38.364	38.378	38.392	0.000	0.000	0.000	33.335	38.441	38.330

Major element data from XRF analysis, except for K_2O which was obtained by isotope dilution and Na_2O from INAA in samples L3-L10, L22-25 and 78LH1 Major element analyses normalized to 100% anhydrous. K, Rb, Sr, Ba, Cs, Sm, Nd analyzed by isotope dilution in samples where isotope compositions given. *$^{87}Sr/^{86}Sr$ after acid washing, L3 .704250. Ni, Zn, Ga, Y, Zr, Nb, by XRF. REE, U, Th in L12-14 by spark source mass spectrometry, all other samples by INAA. Hf, Cr, Co, Sc by INAA except for samples L12-22 by XRF. H_2O, CO_2, Fe^{2+}/Fe^{3+} after Wallace et al., (1983).

unleached powder, and ion microprobe studies of clinopyroxenes from the Tabar-Feni lavas give Sr partition coefficients that are similar to those found in equilibrium experiments (Ray et al. 1983), suggesting that the Sr isotopic composition and concentrations have not changed since crystallization. Mixing between a depleted arc component similar to the New Britain volcanics, and an enriched component with higher $^{87}Sr/^{86}Sr$ and lower $^{143}Nd/^{144}Nd$, which is similar to the enriched component found in the Feni islands (Kennedy 1986), is another alternative.

The Lihir lavas have homogeneous Pb isotopic composition (Figure 2-3) with the spread in all three ratios being less than the normal quoted fractionation error of .05% amu^{-1}. The data plots on the upper edge of the Pacific MORB field and overlaps with the fields for other intra-oceanic arcs (Kay et al. 1978, Gill 1984, Ewart and Hawkesworth 1987, Meijer 1976, Sun 1980, Morris and Hart 1983). The Pb isotopic composition of samples from Lihir are similar to those of lavas from the islands of Tanga and Tabar (not shown), but are distinct from Feni lavas (Figure 2-3). The $^{206}Pb/^{204}Pb$ values are intermediate between those of Feni or Bougainville, and the Rabaul volcanics from East New Britain; these possible endmembers may have been mixed in the Tabar-Feni region.

Figure 2-2

$^{143}Nd/^{144}Nd$ vs $^{87}Sr/^{86}Sr$ of Lihir samples (▲) and fields for lavas from the other Tabar-Feni island groups, the Mariana, Aleutian and New Britain arcs, and Walvis Ridge. Bulk Earth is marked for reference. Data for the fields is from McCulloch and Perfit (1981), Morris and Hart (1983), von Drach et al. (1986), DePaolo and Wasserburg (1977), Richardson et al. (1982), White and Patchett (1984) and unpublished data. Two sigma errors are also shown for reference.

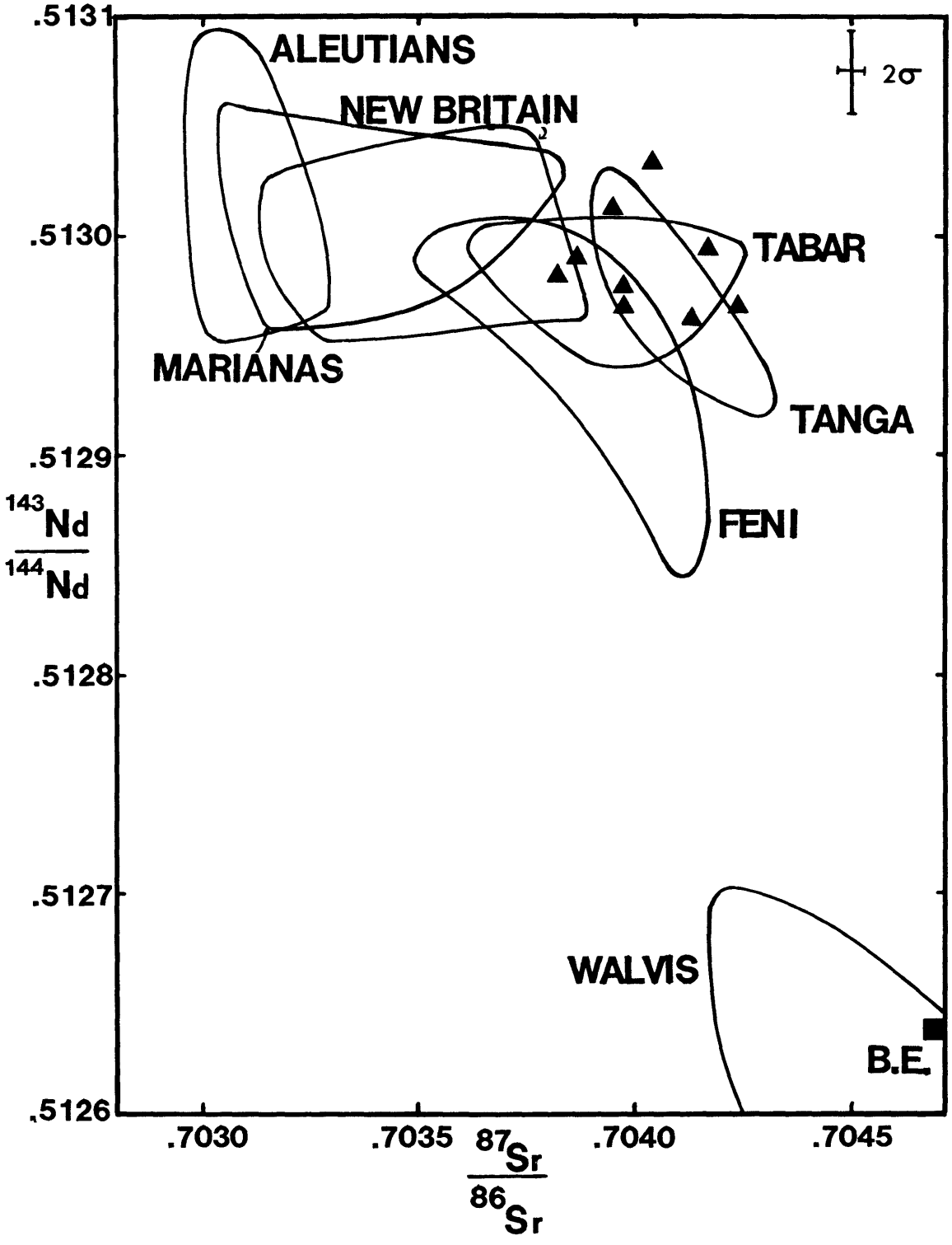
.5131
.5130
.5129
.5128
.5127
.5126
143Nd/144Nd
.7030
.7035
.7040
.7045
87Sr/86Sr
2σ
ALEUTIANS
NEW BRITAIN
TABAR
MARIANAS
TANGA
FENI
WALVIS
B.E.

Figure 2-3

$^{207}Pb/^{204}Pb$ and $^{208}Pb/^{204}Pb$ vs $^{206}Pb/^{204}Pb$ for Lihir samples and fields for other Papua New Guinea and Pacific arcs, Pacific MORB, Walvis Ridge and Samoa lavas. Data from references in Figure 2-2 and Ewart and Hawkesworth (1987), White et al. (1987), Johnson et al. (1985).

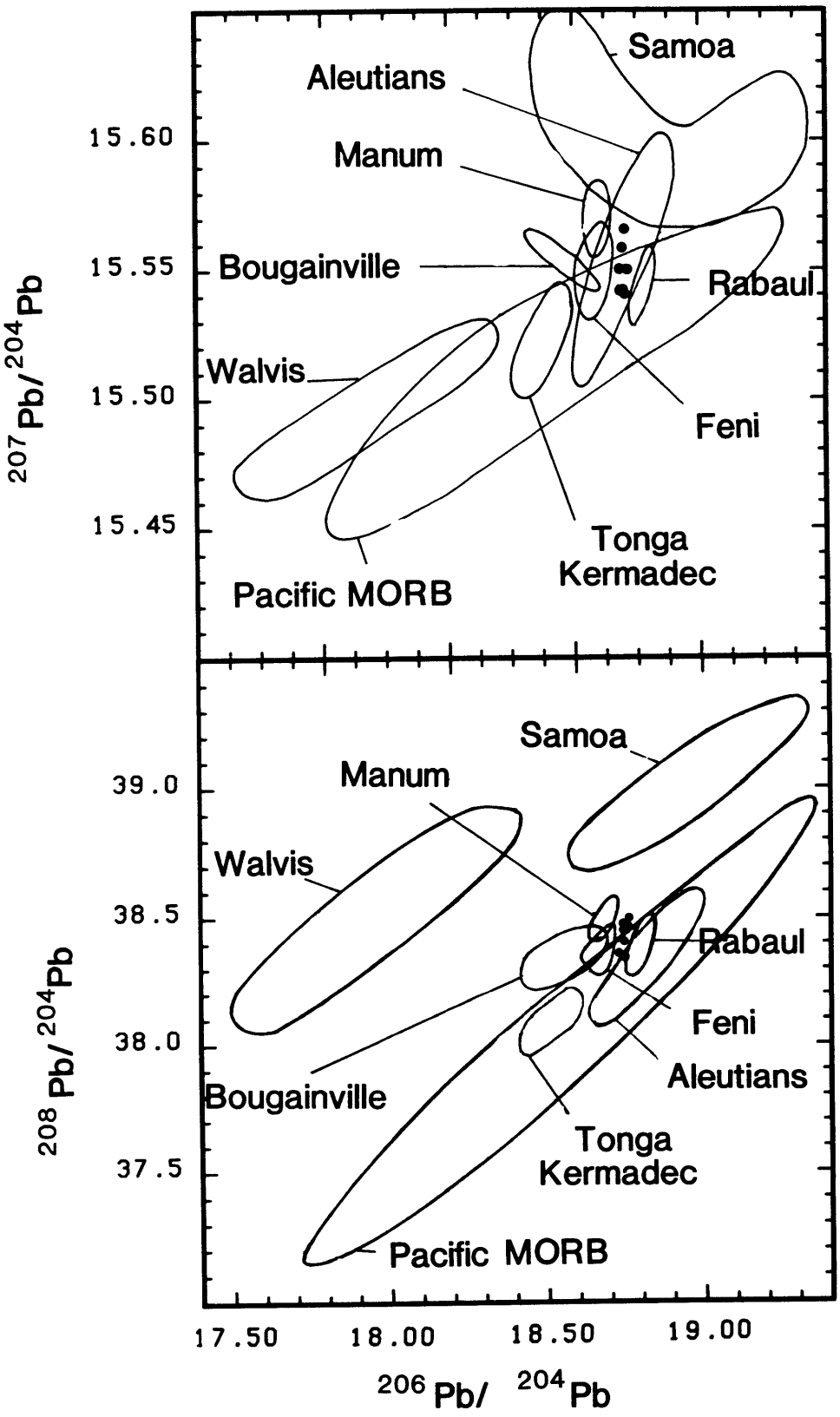
Samoa
Aleutians
Manum
Bougainville
Rabaul
Walvis
Feni
Tonga
Kermadec
Pacific MORB
15.60
15.55
15.50
15.45
$^{207}Pb/^{204}Pb$
Samoa
Manum
Walvis
Rabaul
Feni
Aleutians
Bougainville
Tonga
Kermadec
Pacific MORB
39.0
38.5
38.0
37.5
$^{208}Pb/^{204}Pb$
17.50
18.00
18.50
19.00
$^{206}Pb/^{204}Pb$

Comparison of Lihir lavas with other Tabar-Feni lavas

The Tabar-Feni lavas, like most SiO_2 undersaturated lavas, are enriched in incompatible elements having (La/Yb)c.n. >3. However, this level of enrichment is moderate when compared to the enrichment found in many undersaturated suites from continental and arc environments (Downes 1984, Mertes and Schminke 1985, DeFino et al. 1986, Wyers and Barton 1987, Saunders et al. 1987, Wheller et al. 1987). The Lihir lavas have lower alkalies, Sr, Ba, LREE and higher HREE and Sc than most lavas from the Feni, Tanga and Tabar island groups. The REE patterns for seven Lihir lavas are shown in Figures 2-5a and 2-5b. The field for all lavas, other than qtz-trachytes, from the other Tabar-Feni islands is also shown. A qtz-trachyte from the Feni islands is drawn for comparison in both figures, and this type of lava is the last magma erupted on each of the major islands in the chain. From the light to middle REE, the REE patterns all have convex upwards curvature. A concave upwards curvature for the HREE is suggested by the reduction of slope between Tb and Yb, and Yb and Lu, and, (Yb/Lu)c.n. <1.0 in many lavas, and this characteristic has previously been used to support metasomatic enrichment of a previously depleted mantle source (Hickey and Frey 1982). The evolved Lihir lavas have lower LREE than lavas from the other Tabar-Feni islands (Figure 2-4) and this may result from: 1) accumulation of clinopyroxene, 2) a source region depleted

Figure 2-4

Trace element abundance patterns for lavas from different volcanic units of Lihir normalized to L7, a primitive lava from Luise volcano; the data is from Table 2.1, and the L9 data is from Wallace et al. (1983).

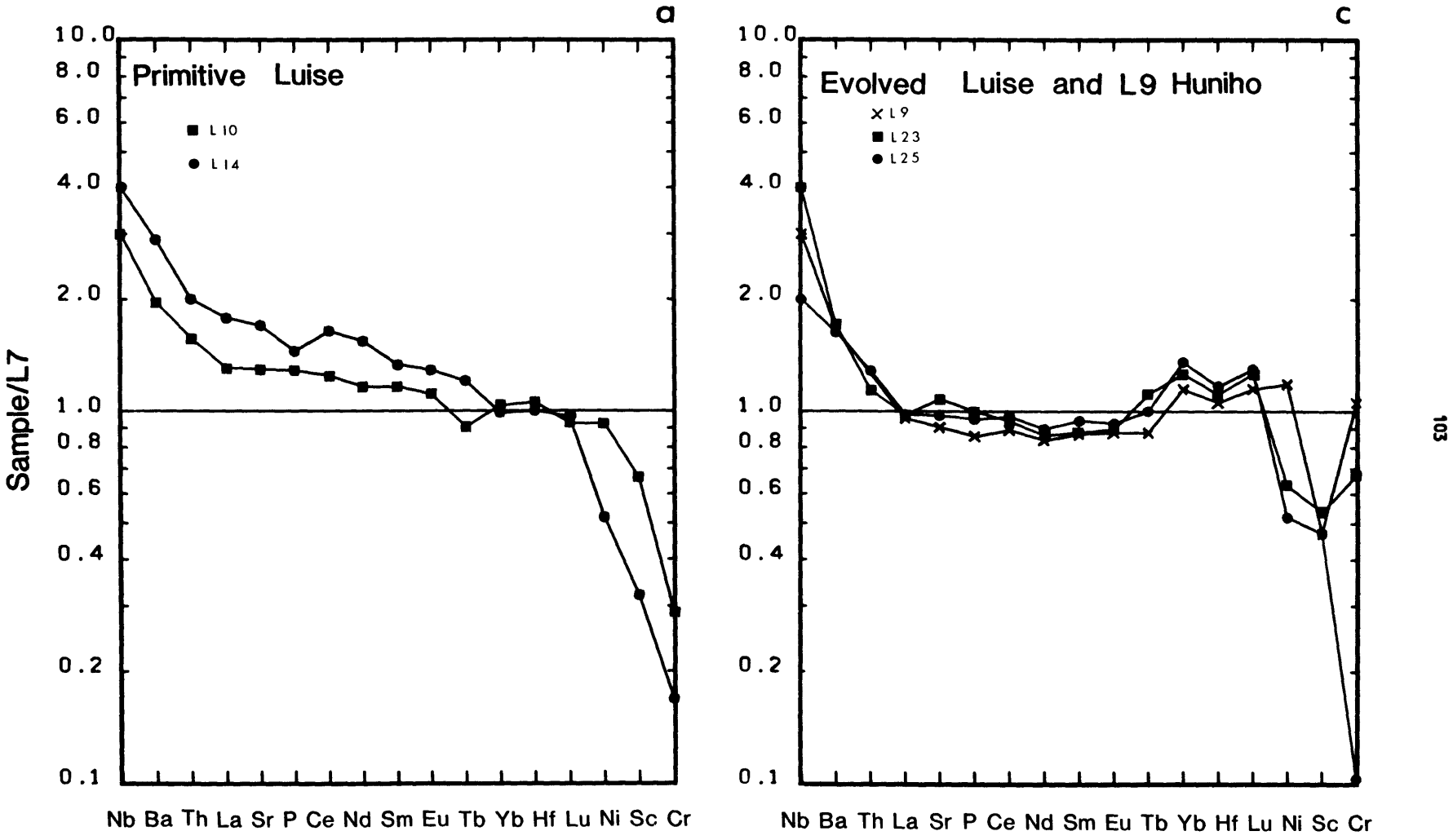
a
Primitive Luise
L10
L14
Sample/L7
10.0
8.0
6.0
4.0
2.0
1.0
0.8
0.6
0.4
0.2
0.1
Nb Ba Th La Sr P Ce Nd Sm Eu Tb Yb Hf Lu Ni Sc Cr
c
Evolved Luise and L9 Huniho
L9
L23
L25
10.0
8.0
6.0
4.0
2.0
1.0
0.8
0.6
0.4
0.2
0.1
Nb Ba Th La Sr P Ce Nd Sm Eu Tb Yb Hf Lu Ni Sc Cr

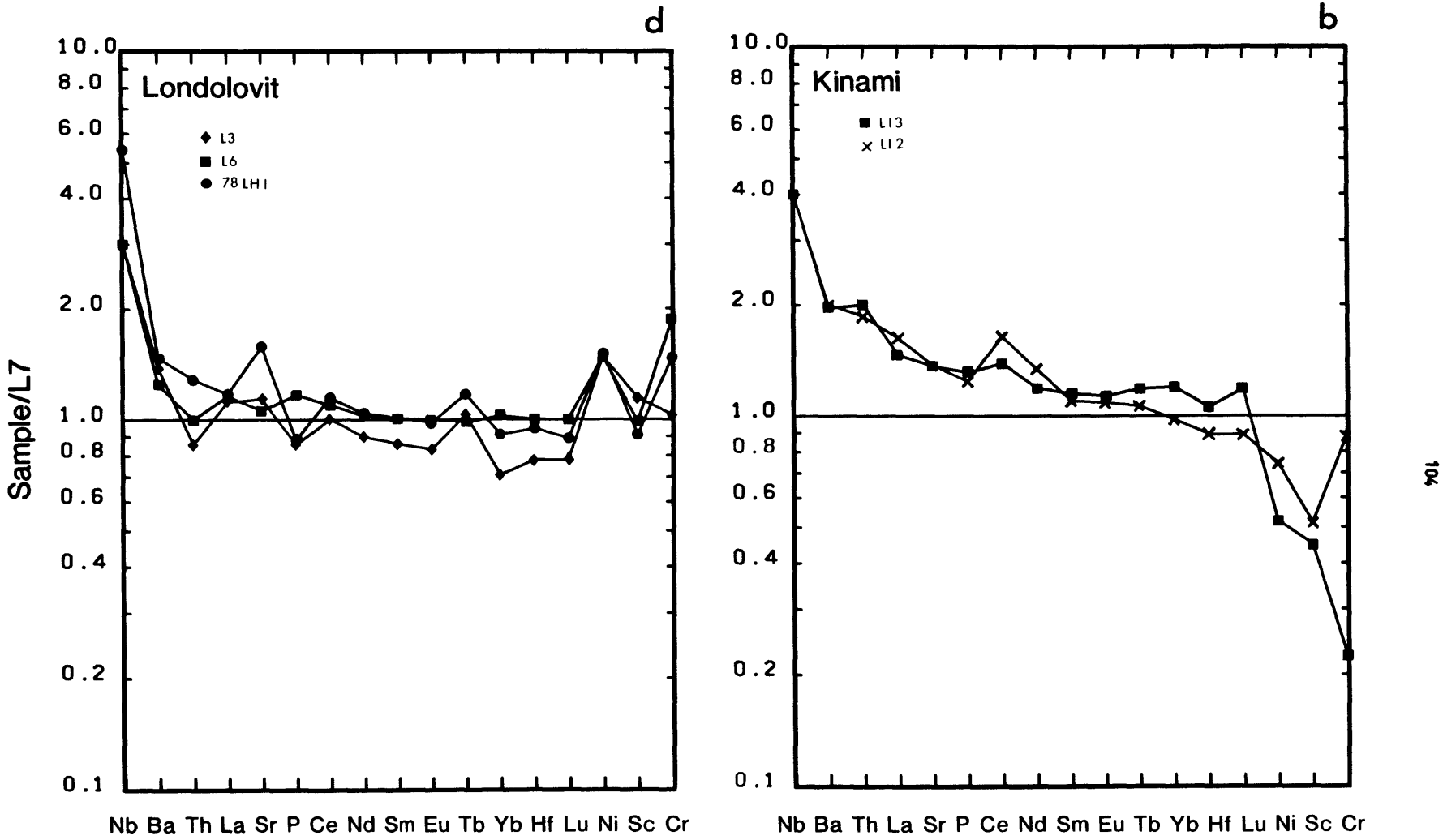
d
Londolovit
L3
L6
78 LH 1
Sample/L7
10.0
8.0
6.0
4.0
2.0
1.0
0.8
0.6
0.4
0.2
0.1
Nb Ba Th La Sr P Ce Nd Sm Eu Tb Yb Hf Lu Ni Sc Cr
b
Kinami
LI 3
LI 2
10.0
8.0
6.0
4.0
2.0
1.0
0.8
0.6
0.4
0.2
0.1
Nb Ba Th La Sr P Ce Nd Sm Eu Tb Yb Hf Lu Ni Sc Cr

Figure 2-5

Chondrite normalized REE patterns for a) primitive lavas and b) evolved lavas. The field enclosed by dashed lines and is for primitive lavas from other Tabar-Feni islands. A qtz-trachyte from the Feni islands is shown for comparison.

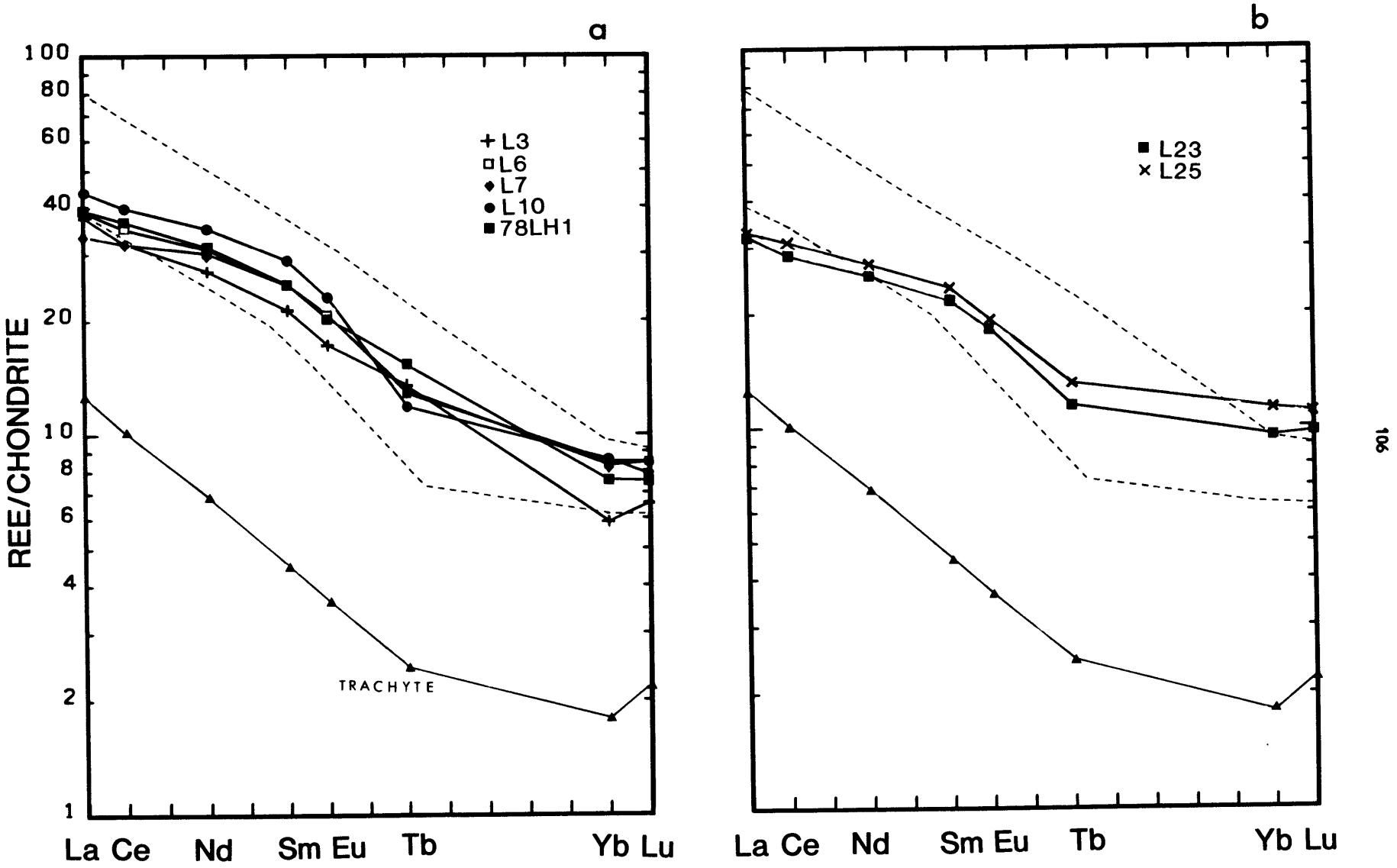
a
b
REE/CHONDRITE
100
80
60
40
20
10
8
6
4
2
1
+ L3
□ L6
◆ L7
● L10
■ 78LH1
TRACHYTE
■ L23
× L25
La Ce Nd Sm Eu Tb Yb Lu
La Ce Nd Sm Eu Tb Yb Lu

in LREE and enriched in HREE, relative to the source for the other Tabar-Feni lavas, 3) a higher degree of partial melting, and from 4) a less evolved composition.

The higher HREE contents of the evolved lavas when compared to the primitive lavas, cannot be explained by the accumulation of clinopyroxene, as the Ds for the HREE in this phase are too low to increase the HREE concentrations by a factor of two. If apatite, which is a ubiquitous accessory phase found within clinopyroxene phenocrysts in most lavas, is also considered, the increase in HREE could be easily explained. A number of problems exist with the accumulation hypothesis. First, both clinopyroxene and apatite have higher Ds for Yb than Lu and accumulation of these phases, if they have crystallized in equilibrium with a LREE enriched melt, they should produce convex upward curvature of the HREE and a (Yb/Lu)c.n. ratio that is greater than the original melt. Second, the lavas from Lihir that have the highest HREE contents, have the lowest CaO/Al_2O_3 ratios, and have undergone substantial clinopyroxene fractionation (Figure 2-1); lavas with similar major element compositions from Lihir and the other islands have different LREE/HREE ratios.

The possibility of a more depleted source or a higher degree of partial melting are not independent problems, since the REE pattern resulting from a lower degree of melting of one source may be identical to the REE pattern resulting from a higher degree of melting of a more enriched source (Albarede and Tamagnan 1986). Wallace et al. (1983) have

separated the primitive erupted lavas into three groups, which are found on most of the islands, based principally on LREE/HREE and LILE/LREE ratios. Kennedy (1986) has shown that mixing is common, and that a variety of endmembers are required. The existence of a number of parental magma compositions in the Tabar-Feni islands cannot be debated, given the isotopic and trace element data. The degree of depletion of HFSE and enrichment of LILE is unlikely to be similar for each mantle source region along the 150 km length of the island chain. A high degree of partial melting would explain the lower incompatible element concentrations in the Lihir lavas, however SiO_2 and Al_2O_3/CaO are not higher as would be expected for higher degrees of melting (Bultitude and Green 1968, Clague and Frey 1982) of a similar source.

Isotopic and trace element characteristics of individual lavas

The island of Lihir is comprised of 5 volcanic units which are: the Wurtol wedge, the Londolovit block, and the remanents of 3 volcanoes, Kinami, Huniho and Luise (Wallace et al. 1983). The Pb isotopes are homogeneous, and Nd isotopes are restricted in range (Table 2.1). The range in $^{87}Sr/^{86}Sr$ (0.70382-0.70424) is larger and this variation is not completely consistent with any simple relationship between isotopes and trace elements. The lack of a simple relationship between trace elements and isotopic composition

in arc lavas has been attributed to contamination by material from the magma conduit during ascent (Kay and Kay, 1985), by seawater (von Drach et al. 1986), or by contamination within the magma chamber (Myers and Sinha 1985) or by variations in metasomatism by fluids derived from the slab (Davidson 1987). The isotopic composition of the Lihir eruptives have not changed with time as samples from the oldest (Londolovit, L3, L6 and 78LH1) and youngest (Luise, L7, L22, L23 and L25) volcanic units have similar isotopic composition ranges. Evidence for a cogenetic relationship between lavas from these groups is present in the isotopic data. The primitive and evolved lavas, L10 and L25 have identical Sr, Pb and Nd isotopic composition. If the primitive and evolved lavas are not related by a fractionation process, then parents of the evolved samples and derivatives from the primitive lavas are not present in the analyzed suite.

The abundances of alkali elements (Cs, Rb, K), Sr and P_2O_5, and the ratios of these elements are variable in the Lihir lavas (Table 2.1), for example L13 and L14 are depleted in K relative to other lavas, however L13 is enriched in Rb. In some instances, lavas with similar REE patterns and major element chemistry have different isotopic composition. 78LH1 has higher Sr/Ba, Rb/Ba and K_2O/Ba and higher $^{143}Nd/^{144}Nd$ than the other primitive Lihir lavas, although its major element composition is similar to other lavas in this group (Figure 2-1). The isotopic and trace element heterogeneity of some of the Lihir samples requires several parental

lavas, however the trace element evolution of this suite can be examined by separating the lavas into primitive (L6, L7, L10, L12, L13, L14 and 78LH1) and evolved groups.

The trace element abundances of various Lihir lavas have been normalized against L7, a primitive lava from Luise volcano that has low SiO_2, high MgO, low trace element abundances and a CaO content which suggests this lava has not accumulated clinopyroxene (Figure 2-4). This normalization removes the characteristic enrichment and depletions of arc lavas, and provided the correct order of incompatibility is chosen, allows easy examination of the effects of differentiation. The order of elements along the abscissa in Figure 2-4 is based on the assumption of L10 and L14 being derived from a lava with similar trace element abundances to L7. The primitive Luise (L7, L10 and L14, Figure 2-4a) and Kinami (L12, L13, Figure 2-4b) lavas have similar trace element patterns and the incompatible elements (Nb to Tb) increase as the compatible elements (Tb to Cr) decrease, as would be expected during fractional crystallization. The evolved lavas from Luise, L23 and L25, and sample LH1/9 from Huniho have remarkably consistent trace element patterns (Figure 2-4c) that are markedly different to those of the primitive samples. These lavas have similar or lower abundances of Sr, P, LREE and MREE and moderate enrichment of the HREE, Rb, Ba, K and Nb relative to L7. If L7 is typical of the parent for the evolved lavas, then a different fractionation process must be responsible for the

trace element evolution of the evolved and primitive lavas. The primitive lavas show a greater enrichment of the incompatible elements than the evolved lavas (Figure 2-4) and this can only occur if the bulk partition coefficients (D) for the LREE and MREE are higher in the evolved lavas than in the primitive lavas. The opposite must be true for the bulk partition coefficients for the HREE, which are enriched in the evolved lavas, relative to L7 and the other primitive lavas. LH1/9 (Wallace et al. 1983), which is included in the evolved group because of its similar trace element abundances and characteristics, has the most primitive major element chemistry of the evolved lavas (Figure 2-1). This sample has trace element abundances intermediate between L23 and L25, two highly evolved samples within this group, and is unlikely to be parental to the evolved lavas unless the bulk D is approximately equal to 1.0 for all trace elements during fractionation. The degree of enrichment of incompatible trace elements does not correlate well with the degree of major element evolution in the Lihir lavas. The highest abundances of incompatible elements are found in some of the lavas with relatively primitive major element composition. For example, L14, which has the highest Sr, Ba, Th and LREE of the samples in Table 2.1, has intermediate MgO (5.85%) and low SiO_2 (47%).

Samples from the Londolovit block (L3, L6, 78LH1) are more magnesian than L7. They are enriched in Ni and Cr relative to L7, and are included in the primitive group and,

they are not enriched in the HREE. L3 has higher LREE/HREE with (La/Yb)c.n. =6.4 and is more depleted in the HREE than other Lihir lavas. Fractionation of apatite or amphibole could increase La/Yb and decrease the HREE, however L3 has a La/Eu ratio that is similar to the other lavas and does not show the depletion of the MREE expected with fractionation of these phases. A high H_2O content of 2.1% and extremely low K_2O and Rb contents may indicate that L3 is altered, however lavas with similar depletions of the HREE, but without the depletion of K_2O and Rb, and high H_2O, are found throughout the Tabar-Feni islands (Wallace et al. 1983, chapter 3) and are a distinct magma type.

Correlations between trace elements

The Lihir data shows several features that suggest a genetic relationship between most of the primitive lavas, despite their $^{87}Sr/^{86}Sr$ isotopic variability. Excellent positive correlations between incompatible elements are normally found in undersaturated lavas, when such trends pass through the origin on element-element diagrams, partial melting or fractional crystallization may be responsible for the trace element variation. The LREE correlate positively with P_2O_5 (Figure 2-6a) and Th (not shown). The data arrays have intercepts close to zero, however this trend is complex, with the lowest P_2O_5 and REE concentrations in lavas which have accumulated clinopyroxene and olivine, the highest

Figure 2-6

a) Nd and Sm vs P_2O_5 for Lihir lavas showing good positive correlation

b) K_2O vs P_2O_5 showing poor positive correlation of primitive samples (numbered) and negative correlation of evolved samples. The arrow indicates the direction of fractionation within the evolved group.

c) Sr vs Ba showing excellent positive correlation in primitive lavas (numbered), with the exception of 78LH1, and the lower Sr abundance of evolved lavas. Evolved lavas with MgO <5.5% are encircled by a dotted boundary.

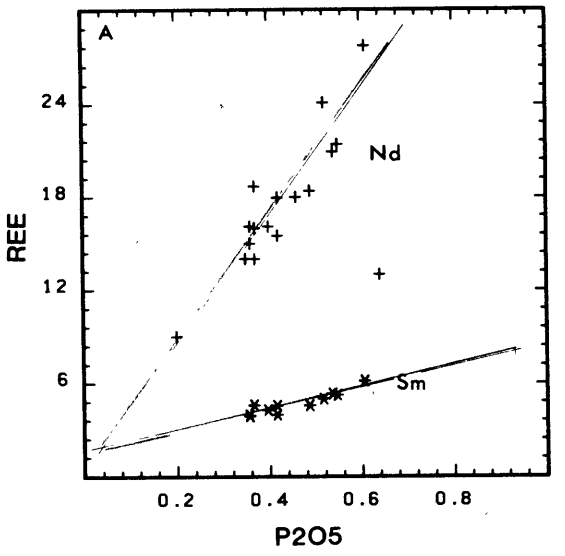
A
24
18
12
6
REE
Nd
Sm
0.2
0.4
0.6
0.8
P2O5

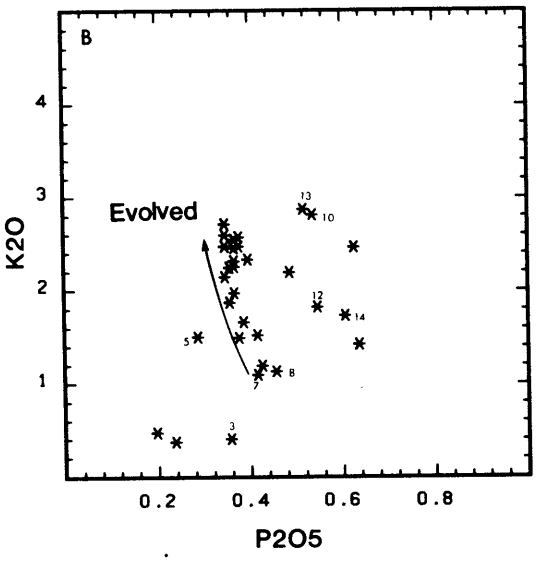
B
4
3
2
1
K2O
Evolved
13
10
12
14
5
8
7
3
0.2
0.4
0.6
0.8
P2O5

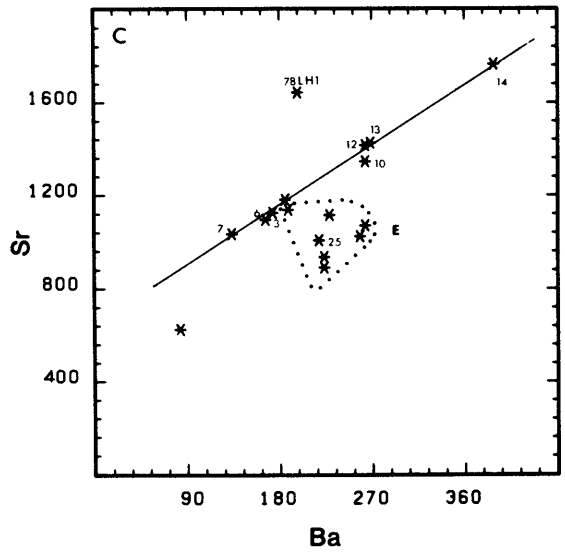
C
1600
1200
800
400
Sr
78LH1
14
13
12
10
7
9
3
25
E
90
180
270
360
Ba

in the primitive lavas, and intermediate concentrations in the evolved lavas. Therefore, the trend was not caused by partial melting. Fractionation of apatite in the evolved lavas would change the bulk distribution coefficient from <<1.0 to >1.0, and this explains the decoupling of trace elements and major elements. Apatite fractionation can also explain the negative correlation of the evolved lavas and the scattered positive correlation of the primitve lavas (labeled with an arrow) in the K_2O vs P_2O_5 diagram (Figure 2-6b). The correlations between Ba, and K_2O, Rb and Cs, is poor and this may reflect loss of alkalis by alteration, or fractionation within the Lihir suite, of phlogopite, biotite, amphibole or an undersaturated mineral, i.e. leucite, hauyne or sodalite.

Apart from 78LH1, which is enriched in Sr relative to Ba, there is an excellent correlation between Sr and Ba in the primitive lavas from Lihir (Figure 2-6c). The evolved lavas plot as a group with lower Sr and intermediate Ba concentrations and have fractionated an assemblage that has decreased Sr and Ba (DSr and DBa >1.0) if they are derived from the primitive lavas with highest trace element abundances, i.e., L14. If the evolved lavas are derived from parents which are similar to L7, then DBa <1.0 and DSr >1.0. The line drawn through the primitive lavas intersects the Sr axis at approximately 620 ppm, thus Sr is more compatible than Ba. The bulk DSr of approximately 0.45 was estimated from the slope of this array on a logSr-logBa plot.

The coherence of Sr and Ba, and the REE and P_2O_5 in the primitive lavas, suggests a cogenetic relationship for the primitive lavas. While mixing would result in a linear data array on this type of diagram, the sequence of the primitive samples along these lines is incorrect if the Sr isotopic compositions, trace element abundances or trace element ratios (Zr, Th, La/Yb) are examined. The primitive samples falling along the line that have been analyzed for isotopic composition have identical Nd and Pb isotopes. This suggests the Sr isotopic composition has changed without changes to the other isotopic systems or to trace elements.

Compatible elements

The ranges of Sc and Cr in the primitive Lihir lavas (Figure 2-7) require substantial crystal fractionation and cannot be explained by melting. Sc abundances are between 48 and 16 ppm and this range is substantially larger than is typical of primitive lavas from other arcs and oceanic environments (Thirwall and Graham 1984, Johnson et al. 1985, Leeman et al. 1980, Clague and Frey 1982). Studies of residual peridotites (Frey et al. 1985) show that Sc is moderately incompatible during melting of garnet lherzolites with a bulk DSc for this element of approximately 0.3; if a similar D is applicable to the generation of the Lihir lavas, positive correlations between Sc and other incompatible elements would be found in a suite of lavas generated by

Figure 2-7

Log-Log diagrams of selected trace elements against Ba. Lines show approximate crystal fractionation vectors for primitive and evolved groups. Lines are labeled with approximate bulk partition coefficients calculated from the gradients of the lines. Filled symbols are primitive lavas and open symbols evolved lavas. Additional data in some plots from Wallace et al. (1983).

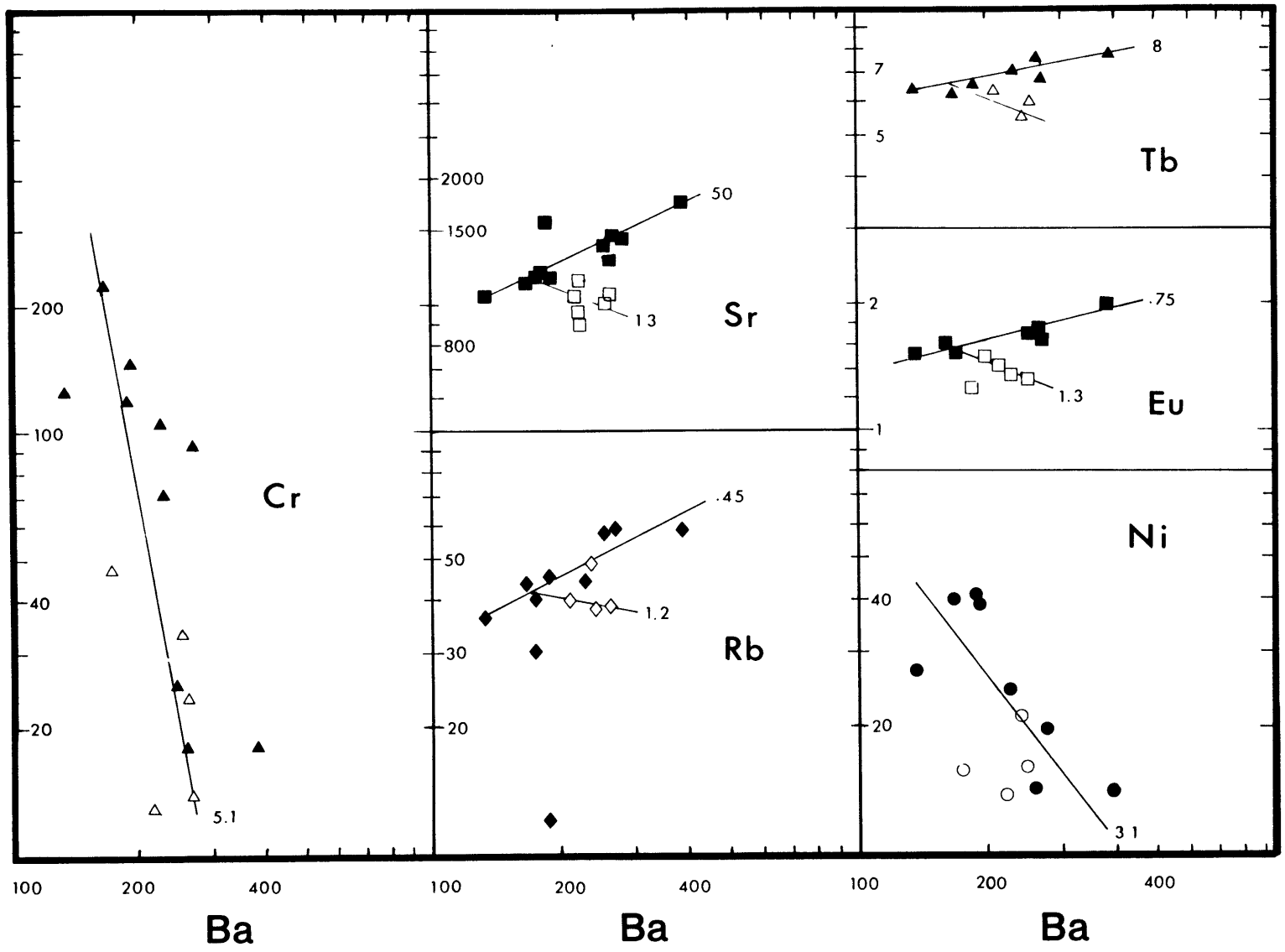
Cr
200
100
40
20
5.1
Sr
2000
1500
800
50
1.3
Tb
7
5
8
Eu
2
1
.75
1.3
Rb
50
30
20
.45
1.2
Ni
40
20
3.1
100
200
400
Ba

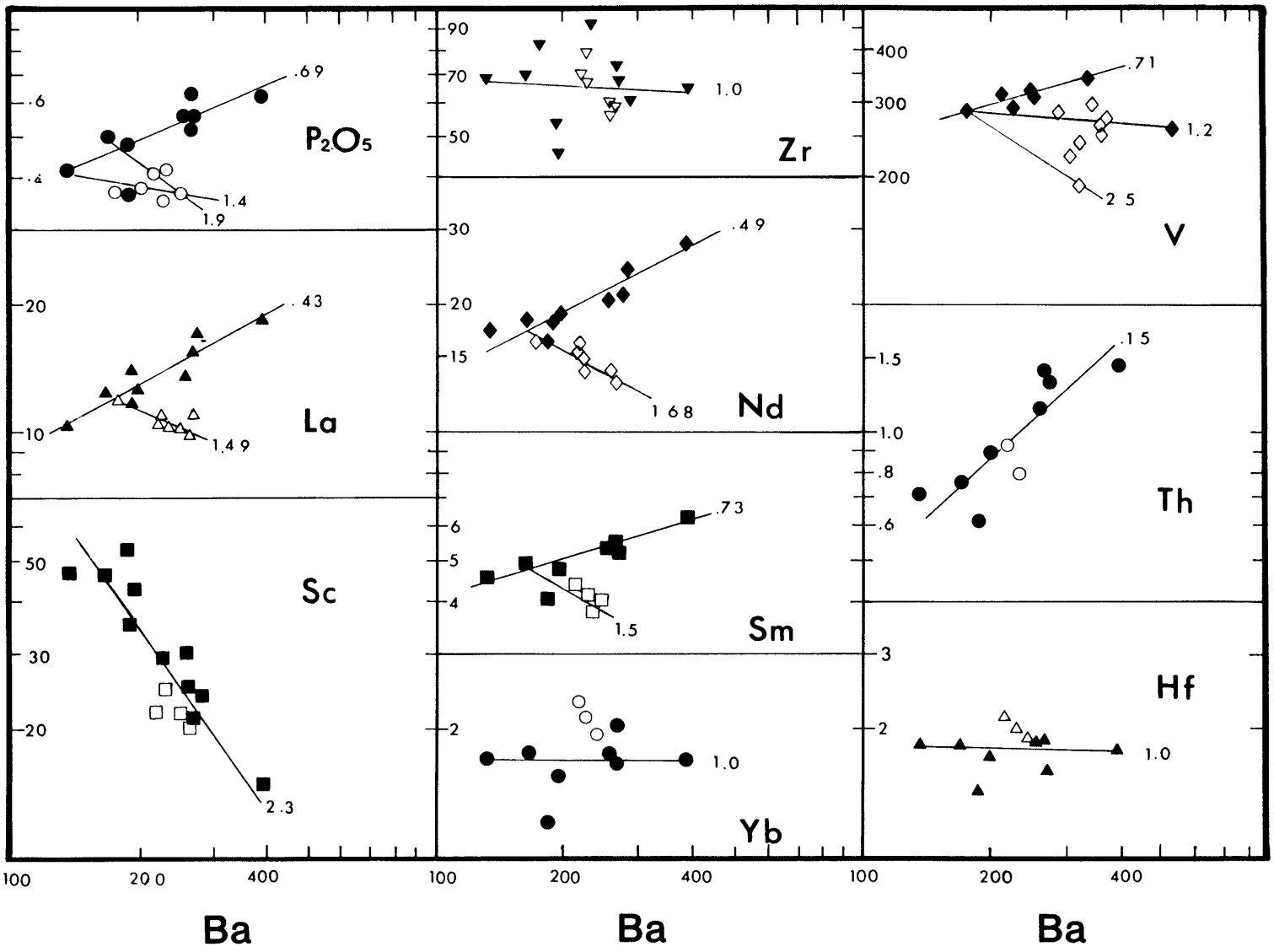
P2O5
.69
.6
.4
1.4
1.9
Zr
90
70
50
1.0
V
400
300
200
.71
1.2
2 5
La
20
10
.43
1.49
Nd
30
20
15
.49
1 68
Th
1.5
1.0
.8
.6
.15
Sc
50
30
20
2.3
Sm
6
5
4
.73
1.5
Hf
3
2
1.0
Yb
2
1.0
100
200
400
Ba

partial melting. This is opposite to what is observed, and the primitive Lihir lavas have undergone variable amounts of fractionation of an assemblage with a bulk D of approximately 2.3 for Sc, which is similar to the distribution coefficient range (2.0-6.0) calculated from ion microprobe studies of clinopyroxene in Feni lavas (Kennedy and Shimizu, unpublished data) and within the range for literature values for clinopyroxene and amphibole (Lemarchand et al. 1987, Ray et al. 1983).

Ni and Cr scatter more than Sc, but also decrease during differentiation, and Sr, La, Nd and V increase consistently with increasing Ba in the primitive samples. The evolved samples do not follow these trends and plot as a group with lower Sr, La, Nd, and V. Yb is higher in the evolved samples than in the primitive samples, which have relatively constant Yb, and this suggests a bulk DYb close to 1.0 during the early evolution of these lavas, and a bulk DYb <1.0 at a latter stage.

Trace element evolution of the Lihir lavas

Lavas from the Tabar-Feni islands contain phenocrysts of olivine, clinopyroxene, plagioclase, Ti-magnetite, amphibole, biotite, apatite, and hauyne-sodalite, and most elements normally considered incompatible, i.e., U, Th, P, LREE, Ba, Rb, Cs, and Nb are compatible in at least one of these phases. The isotopic data, as previously noted, suggests

that most of the observed trace element variation results from differentiation rather than compositional variation in the source material.

The isotopic differences in the primitive Lihir lavas are confined to $^{87}Sr/^{86}Sr$ for samples that have consistent trace element characteristics and identical Nd and Pb isotopes. Therefore, there may be some justification for ignoring the Sr isotope variation in this sample group. The trace element data has been plotted on the process discrimination diagrams of Minster and Allegre (1978) to test this hypothesis.

LogCC-logCH, logCM-logCH and CH-CC diagrams are used to identify fractional crystallization effects, and CH-CH, CH-CH/CH and CH/CM-CH plots to examine melting, mixing and crystal fractionation (CH = the concentration of the least compatible element, CC = the concentration of a compatible element, CM = the concentration of an element which is highly to moderately incompatible.

The validity of conclusions derived from these diagrams depends on the relative incompatibility of elements M and H and it is important to use the least compatible element as H. This is a problem with the Lihir lavas because none of the elements are highly incompatible throughout the entire evolution of the lavas (see Minster and Allegre (1978) for a discussion of these constraints). Ba is the least compatible element in the primitive Lihir lavas (Nb has been ignored because of poor analytical precision) having the largest

relative increase in abundance (135 to 390 ppm), a factor of 2.9 change in concentration. La, Cs and Th have smaller abundance ranges with respective factors of 1.8, 2.1 and 2.3, and this order of incompatiblity is different to that found in other undersaturated suites (Minster and Allegre 1978, Allegre et al. 1977, Sun and Hanson 1975b, Clague and Frey 1982).

Estimation of bulk partition coefficients

Two different linear trends exist in some log-log plots (Figure 2-7), especially for the LREE and MREE. Bulk distribution coefficients for both trends may be calculated from the slope of the data arrays. The log-log plots suggest the following order of compatibility during fractionation of the the primitive Lihir lavas, Cr>Ni>Sc>Yb=Hf=Zr>Sm=V=P>Sr=Nd>Rb=La>Th, and the values for the bulk partition coefficients are respectively 5.1, 3.1, 2.3, 1.0, 1.0, 1.0, .73, .71, .69, .50, .49, .45, .43, and .15. These are rough approximations for elements that scatter, for example V, Ni and P. The difference between many of these values is insignificant relative to the error associated with the calculated gradient and the order given may not be correct, however the magnitude of the bulk partition coefficients can only increase if DBa>0.0 and these values will be compared with the values calculated for the evolved lavas. The most significant feature of this data is

the consistently high bulk partition coefficients for elements that are typically incompatible (P, Rb, La, Th). Removal of a phase, such as apatite, with partition coefficients for most elements >> 1.0 is required if crystal fractionation is the only process affecting the trace elements. However, apatite fractionation cannot explain the high bulk D for Rb, and the only possibile explanations for this feature are fractionation of mica or alteration.

The calculated bulk Ds for the evolved fractionation trend are even larger than those calculated for the primitive trend and are >1.0 for some elements normally considered incompatible. There is no clear cut change in the bulk partition coefficients of compatible elements (Ni, Cr, Sc) between the evolved and primitive groups, as the variation in abundance of these elements is, like the major elements, controlled by fractionation of clinopyroxene and Ti-magnetite. The V, P_2O_5, Sr and Yb data for the evolved lavas is more scattered, and an estimated range for the bulk D is given, which is calculated from a range of possible gradients for the data arrays. The estimated order of compatibility is Cr>Ni>Sc>V>P>Nd>Sm>La>Sr>Rb>Yb, and the Ds calculated from the gradients of the data arrays (Figure 2-7) are 5.1, 3.1, 2.3, 1.2-2.5, 1.42-1.87, 1.68, 1.51, 1.49, 1.3, 1.2, .49-1.0. These values must be considered rough estimates, however they still provide insight into this phase of the evolution of the Lihir lavas. The calculated bulk Ds

are large and only the HREE, Hf, Nb, Ba and Th have bulk Ds <1.0, and the order of compatibility has changed.

Considering these high values, it is possible that Ba was not highly incompatible, and this would result in the overestimation of bulk Ds for compatible elements and underestimation for incompatible elements as the assumption that F=Co/Cl is invalid (Allegre et al. 1977). For this reason, the validity of the assumption of incompatibility for Ba must be addressed, especially considering the restricted variation (135-270 ppm) of this element and the large major element compositional variation in the evolved lavas relative to the primitive lavas. Whether DBa is > or < 1.0 during evolution of the evolved lavas depends on the concentration of Ba in the parental magma of these lavas.

The correlations between Ba and, Sr, P_2O_5 and the Nd, in the CH/CM-CH plots (Figure 2-8) can be used to examine the compatibilty of these elements during the two differentiation intervals. A curved data array on this type of diagram can occur if the bulk partition coefficient of one of the elements changes during fractionation, or if one element is compatible. A linear array with constant CH/CM ratio, and a positive intercept on the CH/CM axis, can be interpreted as crystal fractionation, with M and H incompatible or having identical Ds, or as partial melting. The Lihir data forms two linear data arrays that separate the samples into the previously described evolved and primitive groups. The primitive array has positive intercepts, indicating these

Figure 2-8

Ba/X vs Ba diagrams for selected trace elements. Lines are drawn through the primitive and evolved trends. Separation of these trends becomes difficult or impossible for the HREE, TH, and the alkalis K_2O and Rb.

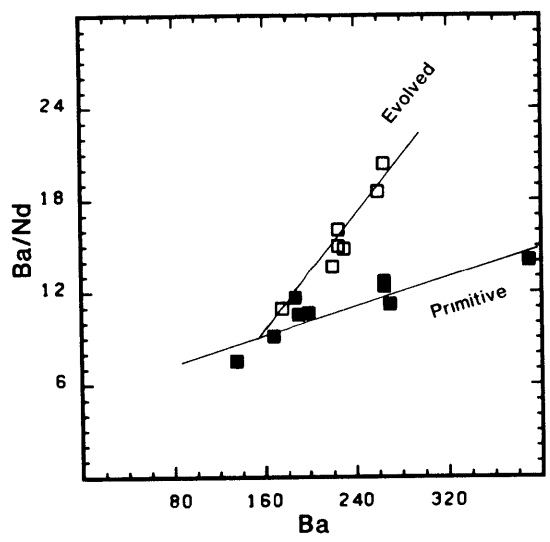
Ba/Nd
24
18
12
6
Evolved
Primitive
80
160
240
320
Ba

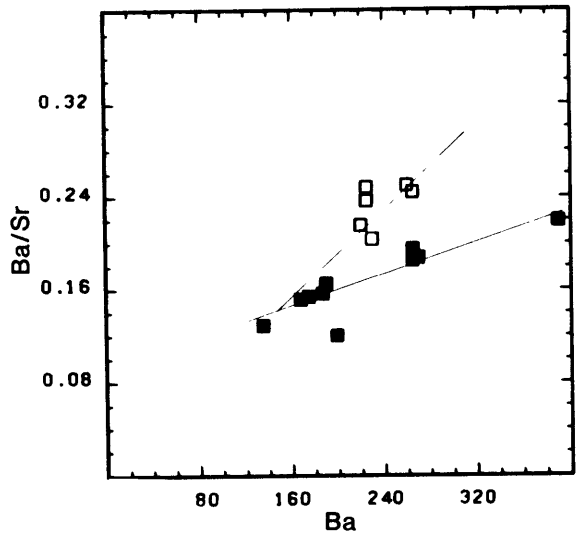
Ba/Sr
0.32
0.24
0.16
0.08
80
160
240
320
Ba

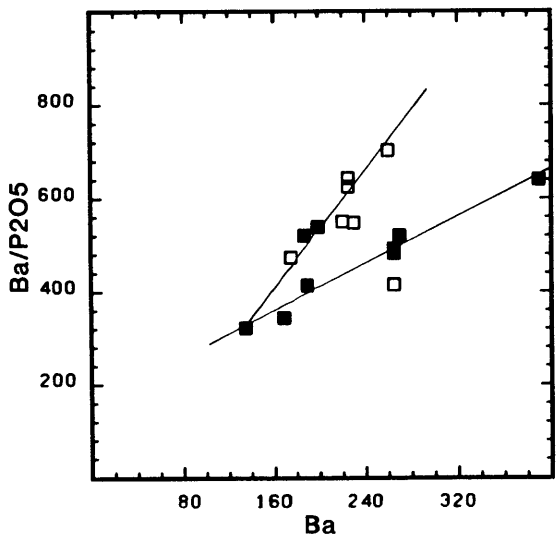
Ba/P2O5
800
600
400
200
80
160
240
320
Ba

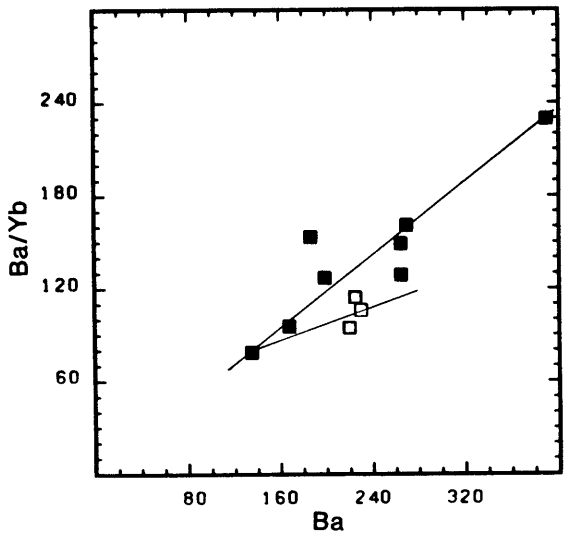
Ba/Yb
240
180
120
60
80
160
240
320
Ba

elements are more compatible than Ba, and smaller gradients than those of the evolved arrays which have intercepts close to or less than zero. This indicates a change in compatibility. The Yb data does not separate the samples into groups and forms a single array and this results from Yb having similar relative compatibility in both groups.

The previous sections have shown that two fractionation trends exist for the lavas from Lihir and that trace element abundances of the evolved lavas from Lihir are not strongly coupled to the major elements. The change in partitioning between the evolved and primitive groups requires either a change in the fractionating assemblage or a change in the process controlling the trace element evolution of the lavas, i.e., AFC or mixing, instead of crystal fractionation.

In the CH/CM-CH diagrams, the intersection of the primitive and evolved arrays provides an upper limit for the Ba content of the a magma that could be parental to both groups. L7, which has low Ba, and plots close to the intersection point, will be used as a hypothetical parent for both the evolved and primitive lavas in subsequents sections.

Estimation of F for the Lihir lavas

If Ba is assumed to have a bulk distribution coefficient of close to zero, the range of Ba in the lavas (135-390 ppm) can be used to estimate F, the amount of liquid remaining after fractionation, using F=Cl/Co (Shaw 1970). Calculated F

values are between 0.34 and 0.48 depending on the initial Ba concentration of the primary liquid, and this gives a minimum of 50% crystallization. This is a relatively large amount of fractionation within a group of primitive lavas which show minor changes in SiO_2, Al_2O_3, TiO_2, FeO* and CaO, and is similar to lavas from Iceland (Wood 1978). There is however no guarantee that DBa=0.0 and the calculated amount of fractionation may be less than the true value. If an accessory phase with high partition coefficient is part of the fractionating assemblage, F values calculated from trace element abundances may be vastly different to the true F.

If Na_2O, which increases by almost a factor of two in the lavas, is considered incompatible, approximately 50% fractionation has occurred. The amount of fractionation can also be estimated by comparing the major element compositions of the lavas and 1 atmosphere experiments. This method provides a reasonable estimate provided the fractionating assemblage contains small proportions of amphibole as removal of this phase does not change the liquid composition greatly (Grove and Kinzler 1986). The estimate derived from the experiments is approximately 45% crystallization between L7 and L25.

Estimation of F for the primitive lavas depends entirely upon the trace element data, as the restricted range of major element compositions prevents comparison with the experiments. If L7 and L14 are assumed to be parental and derivative lavas, the bulk partition coefficients from the

log-log plots, and the concentrations within these samples, can be substituted into the Rayleigh fractionation equation and F values calculated. Only those elements with good correlations were used to calculate F and the respective values for La, Nd, Sm, P_2O_5, Th, Cr and Sc are, 0.37, 0.45, 0.34, 0.30, 0.42, 0.35, 0.64 and 0.41. The lowest calculated F gives an upper limit of 0.11 for DBa and most of the values are close to 0.35, the value for F if DBa=0.0. The consistency of these F values suggests a single fractionation process in the primitive lavas.

Since estimates of the amount of residual liquids have been made, it is now possible to test hypothetical fractionation assemblages by the construction of quantitative models.

Crystal fractionation models

The Rayleigh equations for surface equilibrium have been used in the crystal fractionation models, as these equations are more realistic, considering the abundant zoned phenocrysts in the Lihir lavas. Trace element partition coefficients depend on temperature, pressure, melt composition, and the attainment of equilibrium. Trace element partition coefficients derived from phenocryst-matrix studies in alkalic lavas show substantial ranges for most elements, in most phases, even within the same suite of lavas (Villemant et al. 1981, Dostal et al. 1983, Worner et al. 1983, Lemarchand et al. 1987, Francalanci et al. 1987).

Table 2.2 contains both an upper and lower values for each of the partition coefficients used in this section. Where only one value is given (e.g., olivine and hauyne), the partition coefficient is reasonably consistent in the literature, or is taken from ion microprobe studies of the Tabar-Feni lavas.

Trace element partition coefficients in undersaturated lavas are relatively independent of the melt composition until greater than 50% crystallization (Lemarchard et al. 1987), and for this reason, a single set of D values (either high or low) were used throughout each calculation. This may not be a realistic approach, given the evidence for rapid crystallization in the Lihir magmas, but is presently the only alternative. The evidence for rapid crystallization is, trapped melt and fluid inclusions within clinopyroxene, numerous apatite microphenocrysts in lavas with low P_2O_5 (<1.0%), and sector zoned clinopyroxenes in most samples. The assumption of constancy of phase proportions as a function of temperature in the fractionating assemblage was also adopted, as experiments on 78LH1 (Kennedy et al. 1987) show little change in phase proportions, and there is insufficient information on the abundance of phases in the lavas to justify a more complex model.

The primitive lavas from Lihir, L6, L7, L10 and 78LH1, and samples L9, L12 and L14 (which are equivalent to LH1/9, LH1/12 and LH1/14 of Wallace et al. (1983)), which have similar major element composition, except for K_2O and P_2O_5, have crossing REE patterns. This observation may be

Table 2.2

Equilibrium Mineral/Melt Partition Coefficients Used in Fractional Crystallization Calculations

Low									High							
	Cpx	Plag	Amp	Mica	Apat	Ti-mag	Oliv	Hauyne	Cpx	Plag	Amp	Mica	Apat	Ti-mag	Oliv	Hauyne
La	.12	.05	.17	.04	6.4	.03	.008	.18	.25	.25	.7	.045	14	.23	.008	.18
Ce	.15	.049	.26	.045	10	.032	.008	.17	.42	.16	1.6	.05	24	.3	.008	.17
Nd	.29	.046	.44	.029	17	.038	.005	.18	1.5	.10	3.1	.06	54	.45	.005	.18
Sm	.48	.043	.76	.026	19	.053	.005	.18	3.8	.09	4.9	.07	95	.6	.005	.18
Eu	.56	.043	.88	.022	20	.055	.005	.21	4.5	.085	6.0	.075	102	.8	.005	.21
Tb	.7	.04	.83	.028	17	.092	.005	.15	4.0	.06	5.5	.09	41	1	.005	.15
Dy	.68	.04	.78	.028	15	.1	.0075	.09	3.0	.05	4.5	.1	25	.6	.0075	.09
Yb	.6	.035	.59	.042	9	.12	.008	.03	1.5	.006	2.0	.12	9	.2	.008	.03
Lu	.56	.03	.51	.048	3.7	.14	.009	.02	.8	.001	1.8	.13	7	.3	.009	.02
K	.002	.1	.33	1.6*	.01	.001	.0002	.5	.01	.2	.4	10*	.01	.001	.0002	.5
Rb	.001	.03	.2	1.6	.01	.001	.0002	.05	.01	.1	.2	10	.01	.001	.0002	.05
Sr	.054	1.5	.1	.08	1.5	.001	.0002	4.0	.1	5.0	3.5	.08	3.0	.001	.0002	4.0
Ba	.0008	.1	.2	6.0	.01	.001	.0001	.05	.008	2.5	1.0	10.5	.01	.001	.0001	.05
P	.009	.01	.01	.01	100*	.001	.04	.01	.009	.01	.1	.01	100*	.001	.04	.01
Zr	.13	.003	.4	.1	.9	.1	.005	.001	.2	.003	1.3	.5	.9	3.6	.005	.001
Nb	.1	.001	.5	.33	.1	.5	.01	.01	.3	.001	1.5	.7	.1	1	.01	.01
Hf	.25	.003	.5	.08	.9	.08	.004	.04	.7	.003	1.3	1.0	.9	.37	.004	.04
Ta	.07	.0008	.2	.3	.1	.5	.03	.014	.25	.0008	1.5	.8	.1	1	.03	.014
U	.02	.001	.08	.38	1.0	.04	.00004	.02	.07	.009	.2	.15	1.0	.26	.00004	.02
Th	.01	.001	.03	.04	1.3	.001	.00001	.02	.06	.001	.5	.1	1.3	.19	.00001	.02
Pb	.01	.1	.034	.006	.4	.001	.0004	.03	.04	.2	.08	.006	.4	.1	.0004	.03
Cs	.0004	.01	.05	2.0	.01	.01	.0001	.01	.0004	.01	.05	2	.01	.01	.0001	.01
Sc	2.5	.01	2.0	1.8	.04	3.0	.08	.05	6.4	.03	6	4	.04	4.5	.08	.05
Cr	5.0	.01	.8	.18	.001	1.2	0.3	.001	10	.01	3	10	.001	30	1.0	.001
Ni	3.0	.01	1.6	.5	.011	.1	12	.001	4	.01	3	5	.011	.1	15	.001

*Approximate value as this element is present as structural component and not as a trace element

explained by crystal fractionation, dynamic partial melting (Langmuir et al. 1977), source heterogeneity, or the melting of a garnet lherzolite when garnet is a residual phase for only some of the melts. If these lavas have only fractionated olivine, then the differences in REE patterns must be inherited from the source. However, these lavas have fractionated clinopyroxene and possibly minor amphibole and apatite, and this may change the REE patterns. The trace element evolution of the primitive lavas can be represented by examining L7 and L14, two samples that are at the ends of the primitive lava fractionation trends.

It is possible to use matrix calculations to derive the proportions of the phases in the fractionating assemblage (Allegre et al. 1977, Villemant et al. 1981), assuming that crystal fractionation is responsible for the evolution of the lavas. The partition coefficient matrix used in thesecalculations must contain elements which have distinctly different relative partition coefficients, as this removes any possible singularity resulting from the similarity of the REE partition coefficient patterns of apatite, amphibole and clinopyroxene. A similar problem has been discussed for olivine, orthopyroxene and spinel in inverse problems of mantle melting (Allegre et al. 1977). The final solution of a near singular matrix may rely heavily on the abundances of a few elements and the calculated proportions may be unrealistic (Albarede and Tamagnan 1986). The choice of a fractionating assemblage for use in modeling is complicated

by the large number of phases present as phenocrysts and microphenocrysts in the Lihir lavas. L3 has a fairly simple assemblage and contains olivine, clinopyroxene, plagioclase, Ti-magnetite and analcime, while L12 and L14 contain these phases plus apatite, hauyne, leucite, and respectively amphibole and biotite (Wallace et al. 1983). The primitive lavas show a consistent increase in P_2O_5, and this trend is similar to the experimental glasses (Kennedy et al. 1987) that crystallized clinopyroxene, plagioclase and magnetite, but which did not crystallize apatite. The bulk partition coefficients from the log-log plots for the primitive lavas, and the partition coefficient for each element, in each phase, given in Table 2-2, have been used to derive the proportions of clinopyroxene, Ti-magnetite, olivine, plagioclase, amphibole, hauyne, apatite and biotite in the fractionating assemblage. As noted before, the bulk Ds are at best reasonable estimates; however, the constraints obtained from the major element data and 1 atmosphere experiments can be used to examine the validity of the solution and the fit for each element can also be used to gain insight into the fractionation process.

The results of the constrained least squares calculation of the proportion of phases in the crystallizing assemblage for the primitive and evolved groups are given in Table 2-3. Figures 2-9a and 2-9b, show the ratio of the calculated bulk D for the best solution with positive or zero proportions for all phases, and the bulk partition coefficients derived from

Figure 2-9

Relative differences between bulk partition coefficients calculated by constrained least squares using the partition coefficients in Table 2-2 and bulk partition coefficients derived from Log-Log diagrams. a) Results of models 1 (▲) and 2 (●), Table 2-3, for primitive lavas. b) Results for models 4 (■) and 5 (◆), Table 2-3, for the evolved lavas.

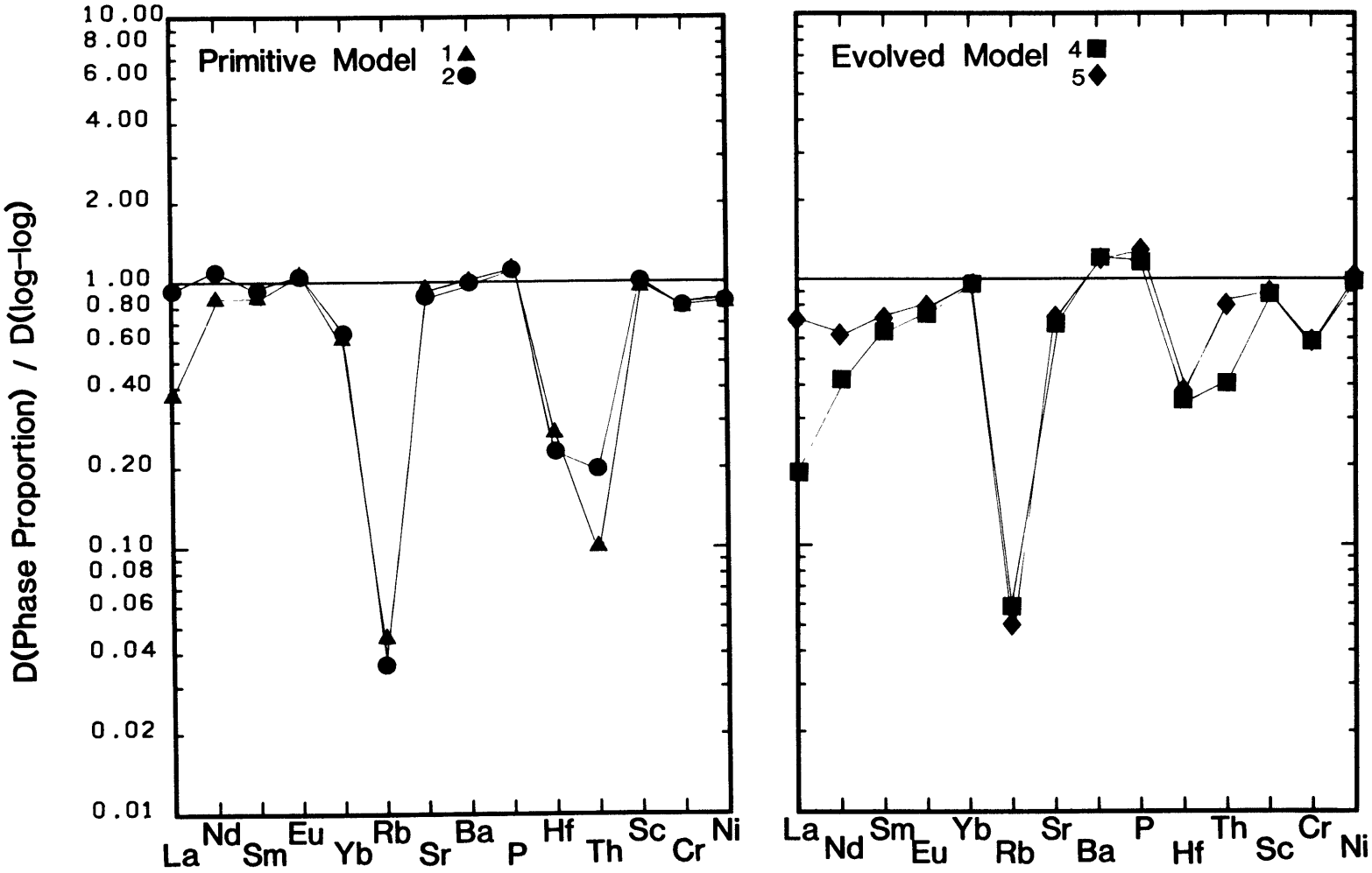
D(Phase Proportion) / D(log-log)
10.00
8.00
6.00
4.00
2.00
1.00
0.80
0.60
0.40
0.20
0.10
0.08
0.06
0.04
0.02
0.01
Primitive Model 1▲ 2●
La Nd Sm Eu Yb Rb Sr Ba P Hf Th Sc Cr Ni
Evolved Model 4■ 5◆
La Nd Sm Eu Yb Rb Sr Ba P Hf Th Sc Cr Ni

the log-log plots. Three models were calculated for both the primitive and evolved fractionation trends. Models 1 and 4 were calculated with the low value set of partition coefficients given in table 2 and models 3 and 6 with the high set. Models 2 and 5 use an apparent set of partition coefficients for apatite and this is discussed below.

The proportion of clinopyroxene, amphibole and apatite predicted by models 1, 2, 4 and 5, and given in Table 2-3, are reasonably consistent with the mineralogy predicted by the major element chemistry and 1 atmosphere experiments (Table 1-1). This is especially true for models 1 and 2, although the amount of hauyne is higher than the abundance of this phase in the lavas. The high partition coefficient models, 3 and 6, predict unreasonably high proportions of olivine (40 and 18%), Ti-magnetite (28 and 14%), and hauyne (21 and 46%) in the fractionating assemblages. These models produce very poor fits to the bulk Ds, and the low set of partition coefficients are more applicable to the Lihir lavas provided no other phase is involved, and that crystal fractionation is the correct process.

The calculated bulk Ds for the primitive data shows a reasonable fit, considering the scatter of the data on log-log plots, to the compatible elements (Cr, Ni and Sc), some of the REE (Nd, Sm and Eu), Sr, Ba and P_2O_5. The models produce poor fits to Th, Yb, Rb and Hf, and this may, in part result from the large amount of scatter in the data for these elements, resulting in an incorrect gradient in the log-log

plots. There is a large discrepancy between the value of the bulk D calculated from model 1 and 4 for La and the value from the data arrays, even though the gradient in the log-log plot is well defined. A better fit is obtained for the LREE and most other elements that are incompatible in clinopyroxene when apparent partition coefficients are used for apatite (Table 2.3).

The best model for the evolved lavas shows little similarity to the values derived from the log-log plots and Ds are consistently lower. This probably reflects the larger errors associated with the calculation of the gradients, the difficulty of choosing the correct partition coefficients, and the possibility of Ba not being completely incompatible.

Apparent partition coefficients

There are few fractionation processes (Cann 1982, DePaolo 1981) that result in bulk partition coefficients for incompatible elements, calculated using abundances within the lavas that are larger than would be calculated from phenocryst-matrix studies in the same lavas. The use of apparent partition coefficients for apatite (given in Table 2.3), improves the fit for the LREE in both the primitive and evolved models. Apparent partition coefficients are hard to justify given the relative constancy of literature partition coefficients for this phase (Watson and Green 1981, Fujimaki 1986). Recent work on Hawaiian undersaturated lavas has

Table 2.3

Matrix Calculation of Phase Proportions in Fractionating Assemblage

Bulk Partition Coefficients

	Primitive*	Model 1	Model 2	Model 3	Evolved*	Model 4	Model 5	Model 6	Apparent$^{\Delta}$ Kd
La	.43	.16	.4	.18	1.49	.28	1.04	.32	38.6
Nd	.49	.42	.53	.49	1.68	.71	1.04	1.0	31
Sm	.73	.63	.67	.90	1.51	.96	1.08	1.9	24
Eu	.69	.72	.74	1.05	1.41	1.07	1.12	2.2	22
Yb	1.00	.62	.63	.25	0.49-1.0	.73	.73	.47	9
Rb	.55	.025	.02	.02	1.2	.07	.06	.02	.1
Sr	.50	.47	.45	.86	1.2-1.8	.82	.87	2.0	5
†Ba	.01	.01	.01	.01	0.05	.06	.06	.05	.02
P	.69	.77	.77	.32	1.42-1.87	2.2	2.4	.93	100$^{\Phi}$
Hf	1.00	.27	.23	.19	0.9	.32	.34	.25	1.8
Th	.2	.02	.04	.07	0.1	.04	.08	.08	3.0
Sc	2.3	2.2	2.3	2.0	2.3	2.0	2.0	2.0	.04
Cr	5.1	4.09	4.1	10.8	5.1	3.0	3.0	6.6	.001
Ni	3.1	2.59	2.6	6.4	3.1	2.2	2.3	3.6	.011

Calculated Phase Proportions

Model	Oliv	Cpx	Amp	Mica	Apat	Plag	Ti-mag	Hauyne
1	-	79.9	12.0	-	.76	.07	.001	7.5
2	-	80.1	12.4	-	.76	-	-	6.3
3	39.6	10.3	-	.03	.3	-	28.0	21.47
4	-	53.7	33.5	-	2.2	-	-	10.4
5	.9	56.1	30.0	-	2.3	-	-	10.6
6	18.1	17.1	4.1	-	.9	-	14.0	46.0

* Values derived from log-log plots
† Assumed bulk partition coefficient
$^{\Phi}$ Approximate value as this element is an essential structural component
$^{\Delta}$ Apatite partition coefficients required by models

identified the presence of rhabdophane, an accessory phase which contains very high concentrations of the LREE, and is capable of fractionating the REE (Fodor et al. 1987). This phase also has similar relative abundances for Y (i.e., the HREE) and cannot produce a decrease in the LREE without a similar decrease in the HREE. The presence of small amounts of a phase, such as allanite, monazite, chevkinite or sphene (Gromet and Silver 1983, Michael 1983, Cameron 1984, Cameron and Cameron 1986) in the fractionating assemblage in the Lihir lavas could easily produce the observed decrease in the LREE, and in some of the above instances, a concomitant increase in the HREE was noted. These phases normally occur only in siliceous lavas, and fractionation of these phases would destroy the correlation between Ba and Th. With the exception of sphene which only occurs in the qtz-trachytes, these phases have not been identified in the Tabar-Feni lavas. Cameron and Cameron (1986) have also separated magnetite with very high partition coefficients because of the presence of inclusions of accessory phases, and Ti-magnetite is a ubiquitous phase in the Lihir lavas. Some arguments can be put forward for use of apparent partition coefficients, and these are discussed below.

Kinetic effects can increase the partition coefficients for incompatible elements during fractionation (Albarede and Bottinga 1972, Haskin and Korotev 1977, Henderson and Williams 1979) and apatites found in cumulates are markedly enriched in LREE close to the boundary between this phase and

augite (Suzuki 1981). Kinetic disequilibrium during crystallization of the various phases in the Tabar-Feni lavas is highly likely given: 1) the trapping of melt within growing clinopyroxenes, 2) the presence of numerous apatite microphenocrysts in lavas with low P_2O_5, 3) the large sizes of complexly zoned clinopyroxene phenocrysts (up to 2.5 cm in length), 4) the presence of sector zoned clinopyroxene in most samples, and 5) high concentrations of Sr and Ba in plagioclase (Heming 1979) with values up to 1.6% and 0.2%. This may explain the failure of simple fractionation models that use literature e.g. equilibrium partition coefficients and the Rayleigh fractionation equations (Shimizu 1981, 1983). The partition coefficients for both compatible and incompatible elements may increase due to interface kinetics. The amount of change is dependent on the conditions of crystallization, diffusion rates, phenocryst growth rates, temperature, and melt composition (Shimizu 1981, Watson 1985, Sawka et al. 1984). The difference between the apparent and equilibrium partition coefficient is greatest for highly incompatible elements. For the Lihir trace element data the greatest discrepancy between modeled and observed concentrations is in these elements.

If the ubiquitous apatite microphenocrysts, that are included within clinopyroxene phenocrysts, grow in the boundary layer adjacent to the surface of the growing clinopyroxene, the melt that the apatite is growing within is enriched in elements that are excluded from the

clinopyroxene, and the apatite that is removed, will have higher apparent partition coefficients. The difference between this apatite apparent partition coefficient and the equilibrium partition coefficient depends upon the rate of crystallization, the diffusion rate for the element concerned in the melt and crystallizing phases, and the partition coefficient of this element in clinopyroxene.

Apatite fractionation has been identified in undersaturated lavas (Hofmann et al. 1987, Lanphere and Frey 1987, Sun and Hanson 1975) and can result in substantial changes in the REE abundances and incompatible element ratios. The complexing of lanthanide elements by P_2O_5 in aluminosilicate melts has been suggested by Jones and Burnett (1987) and the strong effect of P_2O_5 concentration on trace element partitioning (Hess 1980) supports the possibility of apparent partition coefficients for apatite grown in a boundary layer. Until trace element analysis is completed on apatite separated from the Lihir lavas, the trace element fractionation models are unproven, and other more complex models, such as AFC, must be tested.

Assimilation and mixing

The above crystal fractionation models are unsuccessful in describing the trace element evolution of the Lihir lavas unless apparent Ds are used for apatite and before these models are accepted, alternative processes must be

considered. Alternatives are: 1) complex crystallization processes, such as open system and boundary layer crystallization (O'Hara and Matthews 1981, Haskin and Korotev 1977, Langmuir 1988), 2) AFC (Neumann et al. 1954, DePaolo 1981), or 3) mixing (Langmuir et al. 1978). Some of these can be eliminated, as predicted geochemical features are not observed. For example, open system crystallization produces steady state magma compositions with fairly constant major element chemistry if the volumes of erupted and crystallized material in each cycle is small relative to the volume of the magma chamber that is being replenished by primitive magmas. Under these circumstances, the incompatible and highly incompatible elements are rapidly enriched in the lavas, and the ratios of these elements change drastically with time. These characteristics are not shown by the Lihir lavas whichhave limited enrichment of incompatible elements, essentially constant ratios, i.e., Sm/Nd, and a range of major element compositions. Boundary layer crystallization is difficult to constrain without information of the cumulate portion of the magmatic system, and will not be discussed. AFC and mixing are usually identified by a relationship between the degree of evolution of the lavas, trace elements, and isotopes, and this is not apparent in the Lihir data. The poor constraints of models which use an often unknown endmember, prevents the complete elimination of either as an alternative fractionation mechanism, however there is little evidence to substantiate their existence, and some general

arguments can be made against each. If the evolved lavas are to be explained by mixing, then the endmember that is being mixed with the primitive lava must produce major element changes similar to crystal fractionation, and at the same time, dilute the incompatible elements, while increasing the Ba concentration.

The identification of mixing and AFC processes when there is no isotopic differences between the endmembers is difficult, and this is especially true when the fractionating assemblage changes and the bulk Ds change, or if the composition of the assimilant changes (DePaolo 1981, Powell 1984). There is no observable change in bulk Ds in the primitive lavas on log-log plots and both the evolved and primitive lavas lie along linear trends in CH/CM-CH plots. Bulk assimilation, assimilation of wallrock melts and mantle during magma ascent, diffusive interaction with crust or mantle, multiple parent, and multiple assimilant models (DePaolo 1981, Patchett 1980, Marsh and Kantha 1978, Watson 1982, Navon and Stolper 1987, Reagan et al. 1987) are poorly constrained, especially considering the possibility of temporal variation in assimilant and magma (Hofmann and Feigenson 1983). The AFC equations require estimates of bulk Ds and R, the ratio of the masses of assimilants, and crystals fractionating from the magma; these parameters are assumed constant. The simplest method of constraining parameters in any AFC model is to test assimilants of known composition, which is the method adopted here. Potential

assimilants in the Lihir magmatic system are, mantle materials, oceanic crustal materials, cumulates, and lavas.

The assimilation of crustal materials by undersaturated magmas has been advocated by Rutter (1987). However, undersaturated lavas have high calculated ascent rates (Spera 1987), and this, and the refractory nature of peridotite, may preclude interaction of these magmas with mantle peridotite during ascent. If the magma does interact with N-type MORB mantle, the resultant magma is likely to have lower $^{87}Sr/^{86}Sr$ and higher $^{143}Nd/^{144}Nd$ than the original melt, if the original melt derived its isotopic signature from a mantle region that had been produced by prior subduction events. The Sr/Nd of MORB is less than the Sr/Nd of the primary uncontaminated magma and assimilation would result in a greater variation in $^{143}Nd/^{144}Nd$ than $^{87}Sr/^{86}Sr$, which is opposite to what is observed.

Crustal assimilants, assuming the crust beneath Lihir contains no continental derived materials, are probably similar to the various units within an ophiolite. Residual harzburgites, lherzolites and dunites can be ignored because of low concentrations and refractory composition (Prinzhoffer and Allegre 1985) and this reduces the possible contaminants to gabbros, sheeted dykes, pillow basalts and sediments. Assimilation of large amounts of these materials would produce unusual major element compositions and is not consistent with the constancy of the Nd and Pb isotopes. A small amount of assimilation would be difficult to detect

since the abundances of Nd and Pb are low in non sedimentary oceanic crustal materials (McCulloch et al. 1981, Jacobsen and Wasserburg 1979, Chen and Pallister 1981).

The Lihir lavas have high Sr (640-1800 ppm), even in the most primitive lavas. Therefore, varying $^{87}Sr/^{86}Sr$ by contamination requires a contaminant that is similarly enriched in Sr, or has extreme isotopic composition. The Sr isotopes of the Lihir lavas do not show any well defined trends. However, the isotopic composition and Rb/Sr ratio are easily altered by variable degrees of melting, crystal fractionation effects, assimilation, seawater contamination and alteration. Thus, the heterogeneity $^{87}Sr/^{86}Sr$ (Table 2.1) could result from contamination, however, this requires special circumstances, as the isotopic composition must change without a drastic change in the Sr abundance. The primitive lavas that are isotopically homogeneous in Pb and Nd, but heterogeneous in Sr isotopes, show excellent correlations between Sr and other moderately incompatible elements (Figure 2-6 La, Ba, Nd). The range of $^{87}Sr/^{86}Sr$ (0.703822-0.704241) is relatively small and could be explained by contamination with a component, with isotopic composition similar to seawater (0.70905) and a high Sr concentration, or with a lower Sr concentration and higher $^{87}Sr/^{86}Sr$. $^{87}Sr/^{86}Sr$ ratios > 1.0 have been measured in celadonites (Hart and Staudigel 1986), however the Sr concentration is too low for this material to disturb the isotopic signature of the Lihir lavas. Similarly, seawater which contains approximately 8

ppm (von Drach et al. 1986), is an unlikely contaminant, as the 1000-1800 ppm of Sr in the magmas would require a very large proportion of seawater in a simple two component mixture. Strontium is highly mobile and is concentrated in calcareous materials in oceanic environments with concentrations averaging 500-600 ppm and ranging between 300 and 2000 ppm in calcites, aragonites and dolomites (Veizer 1983). Contamination during ascent through the altered oceanic crust or assimilation of reef materials would increase the $^{87}Sr/^{86}Sr$ ratio. Addition of calcareous materials with concentrations between 600 and 2000 ppm, and the isotopic composition of seawater, would require 4-12% of this component in the mixture, which would result in a 2-6% increase in CaO. The Lihir lavas have high CaO, however there is no relationship between CaO and $^{87}Sr/^{86}Sr$.

The oceanic crust may, even in the unaltered parts, have an unusual isotopic signature since the Tabar-Feni islands are close to the Ontong-Java plateau, and if the data from Malaita (Bielski-Zyskind et al. 1984) is typical of this type of crust, then assimilation of oceanic crust may move the isotopic composition toward either a more or less radiogenic composition.

Cumulates produced by fractionation of previous melts and solidified magmas undoubtedly have created the Tabar-Feni islands and are traversed by the magmas during ascent. Magma chambers at shallow depth (<15 km) would have wallrocks composed of these materials, and if magma chambers develop at

the crust-mantle interface, which is commonly cited as an energetically favorable site for the pooling of magmas (Marsh and Kantha 1978, Walker et al. 1979), the wallrocks are likely to be cumulates, oceanic crust and mantle. The early cumulates from the Lihir lavas are probably olivine-rich, contain clinopyroxene and possibly amphibole. Just how much effect assimilation of these cumulates would have, depends on the proportions of clinopyroxene and amphibole, the only phases containing significant amounts of trace elements other than the transition elements. Assimilation of cumulate materials cannot produce the complete range in isotopic composition unless the lavas that produced the cumulates have never been sampled. Melts from unaltered cumulates, provided there is no residual plagioclase, may have sufficiently high Sr concentration to change the $^{87}Sr/^{86}Sr$ of a melt during assimilation. Contamination with trachytic material, given its low abundances of many trace elements, may decrease the concentration of these elements in the contaminated lavas while the high Na_2O, K_2O, Ba and Sr buffer these elements at levels similar to the parental melt. These qtz-trachytes have isotopic compositions close to the most radiogenic compositions found in the Tabar-Feni islands (Perfit and McCulloch 1982) however, as argued above, this type of assimilation cannot generate the entire range of $^{87}Sr/^{86}Sr$ ratios.

In conclusion, assimilation of alteration products from the oceanic crust or carbonates can explain the observed variation in $^{87}Sr/^{86}Sr$. The other alternative is, minor source heterogeneities, and presently there are no constraints that can adequately separate these alternatives.

The effects of assimilation on the evolved suite is less clearly defined, and the possibility of AFC controlling the evolution of this group is tested using the equations of Neumann et al. (1954), assuming sample L7 is parental, L25 derivative, and the compositions of the possible contaminants are known. The transition from L7 to L14 has also been modeled, and the results for each of the models are shown in Figure 2-9, where solution curves of R (mass ratio of assimilant/crystal fractionate) against F for each element, are given. Fixed concentrations in the uncontaminated melt, the contaminated melt and the assimilant were used in the calculations. F is a measure of the amount of crystallization and is the ratio of the (original mass of the magma minus the mass crystallized/ original mass of magma). This definition is different to the F of DePaolo (1981), where F is the fraction of liquid remaining including assimilated materials. The F of DePaolo (1981) can have values greater than 1.0 when R> 1.0 while the one used here (Neumann et al. 1954) is constrained to a value < 1.0. Once these parameters are fixed, it is possible to rearrange the AFC equation to describe a relationship between F and R. A common intersection point for all of the curves within a plot

would define a unique solution for R and F. The two assimilants tested are the qtz-trachyte F17, which is taken as the composition of a crustal melt, and a cumulate assemblage consisting of clinopyroxene, olivine and Ti-magnetite, that was calculated as an average cumulate generated by 5% Rayleigh fractionation from L7, using the partition coefficients in Table 2.2, and the trace element concentrations in these assimilants are given in Table 2.4, along with the bulk Ds for the trace elements used in the calculations.

Errors bounds have not been plotted on each of the R-F curves in the diagrams as propagation of errors in the partition coefficients, concentrations in the assimilant, uncontaminated and contaminated magmas was not attempted. The greatest uncertaintities are associated with the concentration of the unknown, the assimilant, and with the bulk partition coefficient when accessory phases are involved. Under these circumstances an acceptable intersection point between two curves would become an area in F and R. Although the lack of error propagation detracts from the accurate definition of a unique solution in terms of F and R, a common intersection point should still be identifiable, and this is the best that can be realistically hoped for, given the freedom of the parameters of the model. More complex models exist (Reagan et al. 1987) however the available data from Lihir is too poorly constrained to

Table 2.4

Trace Element Concentrations of Assimilants and Partition Coefficients Used in AFC Models

	Assimilant 1 Qtz-trachyte	Assimilant 2 cumulate	Partition coefficients L7-L14	Partition coefficients L7-L25
Ba	443	0.098	0.01	0.10
Th	1.3	0.0058	0.20	0.10
La	4.01	1.071	0.43	1.49
Nd	4.1	4.3	0.49	1.68
Sr	2361	46.5	0.50	1.30
Rb	48.2	0.05	0.55	1.20
P	0.11%	0.006	0.69	1.9
V	90	256	0.71	1.2
Sn	0.87	1.87	0.73	1.51
Hf	1.8	0.37	1.00	0.9
Yb	0.37	0.84	1.00	0.6
Sc	21	98	2.30	2.3
Ni	8	105	3.10	3.1
Cr	4.9	512	5.10	5.1
Eu	0.27	0.70	0.69	1.41

Partition coefficients taken from log-log plots
Qtz-trachyte is data from F17
Cumulate concentrations calculated for 5% Rayleigh fractionation of L7 with phase proportions cpx:oliv:Ti-mag, 80:15:5.

justify expansion of the proposed models to include additional components.

Results of AFC models

The result of the AFC models for the evolution of L7 to L25 and L7 to L14 is shown in Figure 2-10. The AFC model for L7-L25 (Figure 2-10a) which uses a trachytic assimilant, does not show a unique intersection point, as the solution curves for the transition elements Ni, Cr and Sc, the HREE, Sr and Rb produce a large number of widely dispersed single intersection points. Only two possible multiple intersection points exist in this diagram, occurring at an R value of approximately 2.0 and at F values of 0.85 and 0.96. These values are inconsistent with the major element data, which gives F of 0.45-0.55. The sub-parallel nature of V, Ba and Th, and Eu, Nd, Sm, P and La, reflects the lower abundance of these elements in the contaminated magma relative to the uncontaminated magma and bulk distribution coefficients less than 1.0. Under these circumstances a large amount of assimilation is required to balance the increase produced by differentiation. The AFC model of L7 to L25 (Figure 2-10b) with a cumulate assimilant, which would be rich in Ni, Cr, Sc and V, and depleted in all other elements, produces two separate groups of solution curves. The first includes Eu, Sm, Nd, La, Sr and P, and gives unrealistically high F and R values, however in this model the curves do not define any

Figure 2-10

R vs F diagrams for AFC models. Labeled curves are calculated solution curves for each element. Uncontaminated lava, contaminated lava and assimilant for each model are as follows: a) L7, L25 and trachyte b) L7, L14 and trachyte c) L7, L25 and cumulate, and d) L7, L14 and cumulate. Cumulate has phase proportions Oliv 0.15, Cpx 0.8, Ti-Mag 0.05.

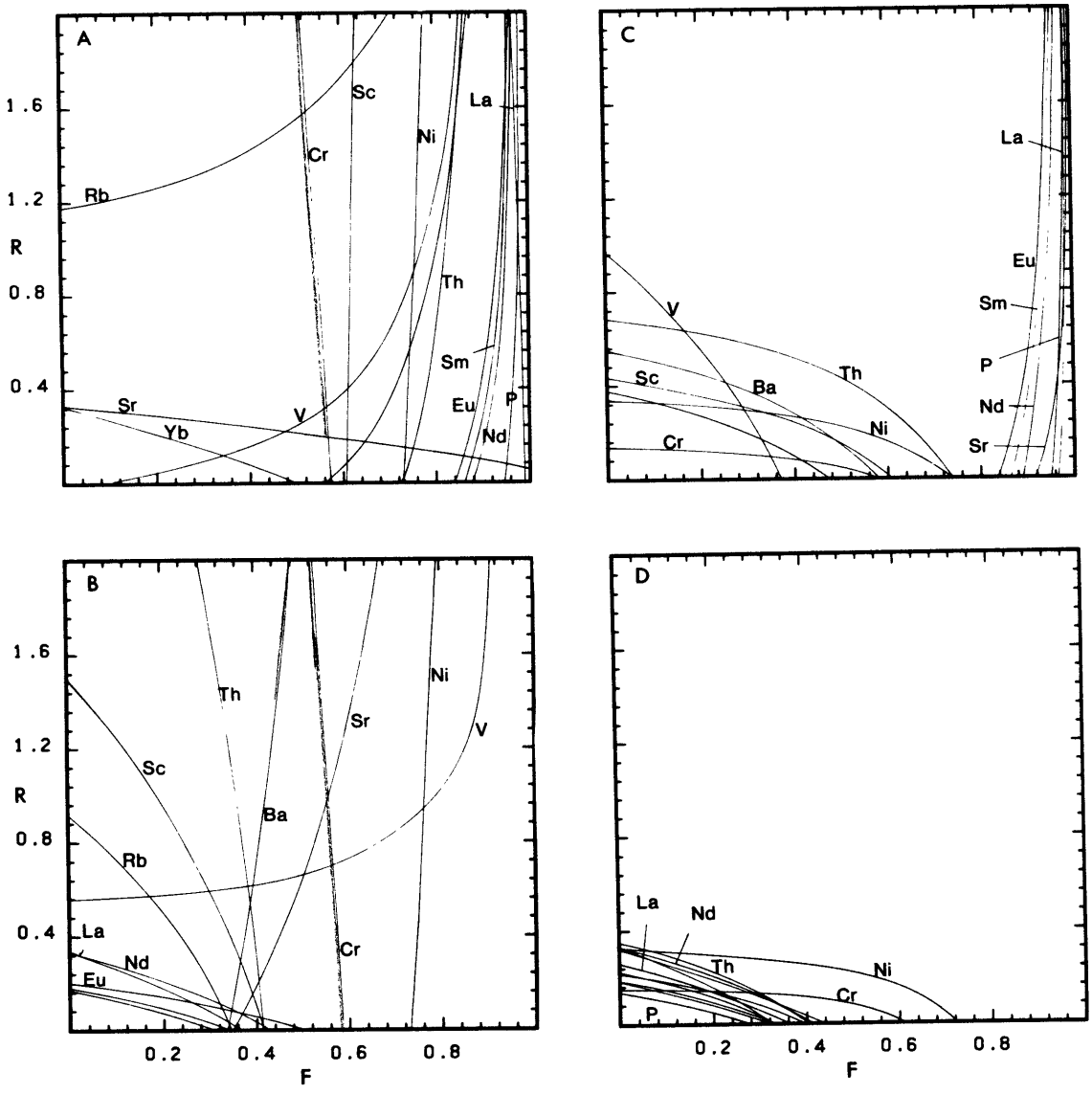
A
1.6
1.2
R
0.8
0.4
Rb
Sr
Yb
V
Cr
Sc
Ni
Th
La
Sm
Eu
P
Nd
C
La
Eu
Sm
P
Nd
Sr
V
Sc
Ba
Th
Ni
Cr
B
1.6
1.2
R
0.8
0.4
Th
Sc
Rb
La
Nd
Eu
Ba
Sr
Ni
V
Cr
0.2
0.4
0.6
0.8
F
D
La
Nd
Th
Ni
Cr
P
0.2
0.4
0.6
0.8
F

multiple intersection points. The second group of curves, for Ba, Th and the transition elements V, Cr, Ni and Sc, do not show a unique intersection point but do suggest more realistic amounts of fractionation and lower values for R. Neither of these models successfully explain the generation of the evolved lavas from the primitive lavas, and if anything, these models are less successful than the earlier crystal fractionation models.

AFC models for the transition L7 to L14 in the primitive lavas are shown in Figures 2-10c and 2-10d. The F value predicted by both models, if there is no assimilation, is approximately 0.3-0.4, and this is slightly lower than would be predicted if the major element data is modeled by crystal fractionation, and this slight discrepancy could be explained by amphibole fractionation. As mentioned above, the Ni and Cr curves are displaced to higher F values as a result of the low abundance of these elements in L7, and the use of higher Ni and Cr concentrations for the parental magma results in greater internal consistency for the models. The curves in Figure 2-10d are restricted to low F and R, and most of these curves are almost parallel. This reduces the number of intersections and the accuracy of locating any intersection points, and this results from the low abundances of most elements in the fractionating assemblage, and the similar abundances of the transition elements in the assimilant and fractionating assemblage. The low R values predicted by

these models support the fractionation models presented earlier.

Accessory phases with high partition coefficients can control the trace element evolution of a suite of lavas and this makes accurate trace element modeling difficult, especially if AFC processes are invoked. At best, the models presented here give some insight into what the effects of assimilation of trachytic (feldspathic) or cumulates might be, and rule out the assimilation of trachytic material (sensu stricto), but provide little conclusive information about the possibility of AFC.

Nd isotopic constraints on the timing of enrichment and depletion events in the Lihir source

The Nd systematics of mantle materials have been used to obtain a maximum age on the event which changed the parent/daughter ratio (Zindler et al. 1984, Roden and Murthy 1985, Roden et al. 1984). This is done by assuming that Sm and Nd behave coherently and the Sm/Nd ratio decreases during metasomatism and melting, and using the evolution of the MORB reservior to constrain the maximum $^{143}Nd/^{144}Nd$ at the time of metasomatism. The relative constancy of the Sm/Nd ratio during melting, at least for >10% partial melting (Hawkesworth 1982, Zindler et al. 1984) means this ratio can be used to assess the degree of depletion of the mantle

source region, and can in some instances, constrain the partial melting percentages.

The Lihir lavas have Nd and Sr isotopic compositions consistent with a time integrated evolution in a depleted reservior, yet the majority of the lavas are enriched, with Sm/Nd less than, and Rb/Sr greater than chondritic. This could result from small degrees of melting of a previously depleted source (Hawkesworth 1982) or from the influx of metasomatic fluids (Menzies et al. 1987 and references therein) followed by higher degrees of partial melting. The arc mantle is undoubtedly metasomatized by fluids liberated from the subducting slab, and both metasomatism and small degrees of partial melting may be involved in the generation of the Lihir lavas.

The presence of garnet in the mantle source region of lavas from Lihir, or the other Tabar-Feni islands, would constrain the possible variation of the Sm/Nd ratio during partial melting and the depth of melting. Lavas generated in equilibrium with garnet are expected to have high and variable La/Yb ratios and almost constant HREE concentrations (Gast 1968, Sun and Hanson 1975, Clague and Frey 1982, Hofmann and Feigenson 1983). There is no evidence for the presence of garnet as a residual phase during generation of the Tabar-Feni lavas, since the HREE and LREE of the primitive lavas have similar relative variations, and the La/Yb ratio is relatively constant. The variation in HREE abundances can be attributed to different degrees of partial

melting in the absence of garnet or to different HREE abundances in the mantle source regions that contain garnet. The latter explanation is supported by the Sr isotopic differences of the primitive lavas which have different HREE contents, however (Lu/Yb)c.n. >1.0 in all of the primitive lavas suggests that garnet is not a residual phase, which is consistent with the data for other arcs (White and Patchett 1984, Johnson et al. 1985, Arculus and Johnson 1981).

The relative constancy of the Sm/Nd ratio (Figure 2-11b) also argues against small degrees of partial melting since this ratio would remain fixed only if the degree of melting was constant or there are no residual phases capable of fractionating these elements, which is unlikely considering the difference in degree of undersaturation of individual lavas from Lihir and the other Tabar-Feni islands. The Lihir lavas all fall within the general arc field and fall within the Woodlark Basin field (Figure 2-11a). These lavas have higher Sm/Nd than the Feni samples, and this is consistent with the lower alkali contents and degree of enrichment (lower La/Yb, alkalis and LILE). The Mariana Trough, New Georgia, and the Lesser Antilles (Figure 2-11a) show the effects of mixing, and the Pacific MORB and Woodlark Basin fields show the possible range of $^{143}Nd/^{144}Nd$ and Sm/Nd in melts derived from the MORB reservior. The Lesser Antilles field shows the effects of sediment-crust contamination of arc lavas, and New Georgia arc basalts form an array with

Figure 2-11

$^{143}Nd/^{144}Nd$ vs Sm/Nd for Lihir (△) and Feni (■) lavas. Vertical line is chondritic Sm/Nd. Also shown for reference is a 2 By isochron. Labeled fields are for arcs, ocean floor basalts, OIB from the Pacific, and the Lesser Antilles arc. The field in Figure 2-11b is for arc lavas from the Pacific region. Data is from references in Figure 2-2 and 2-3, and from Thirwall and Graham (1984), Gill (1984), Volpe et al. (1987), Staudigel et al. in press, and Zindler et al. (1984). The MORB field is from Zindler et al. (1984).

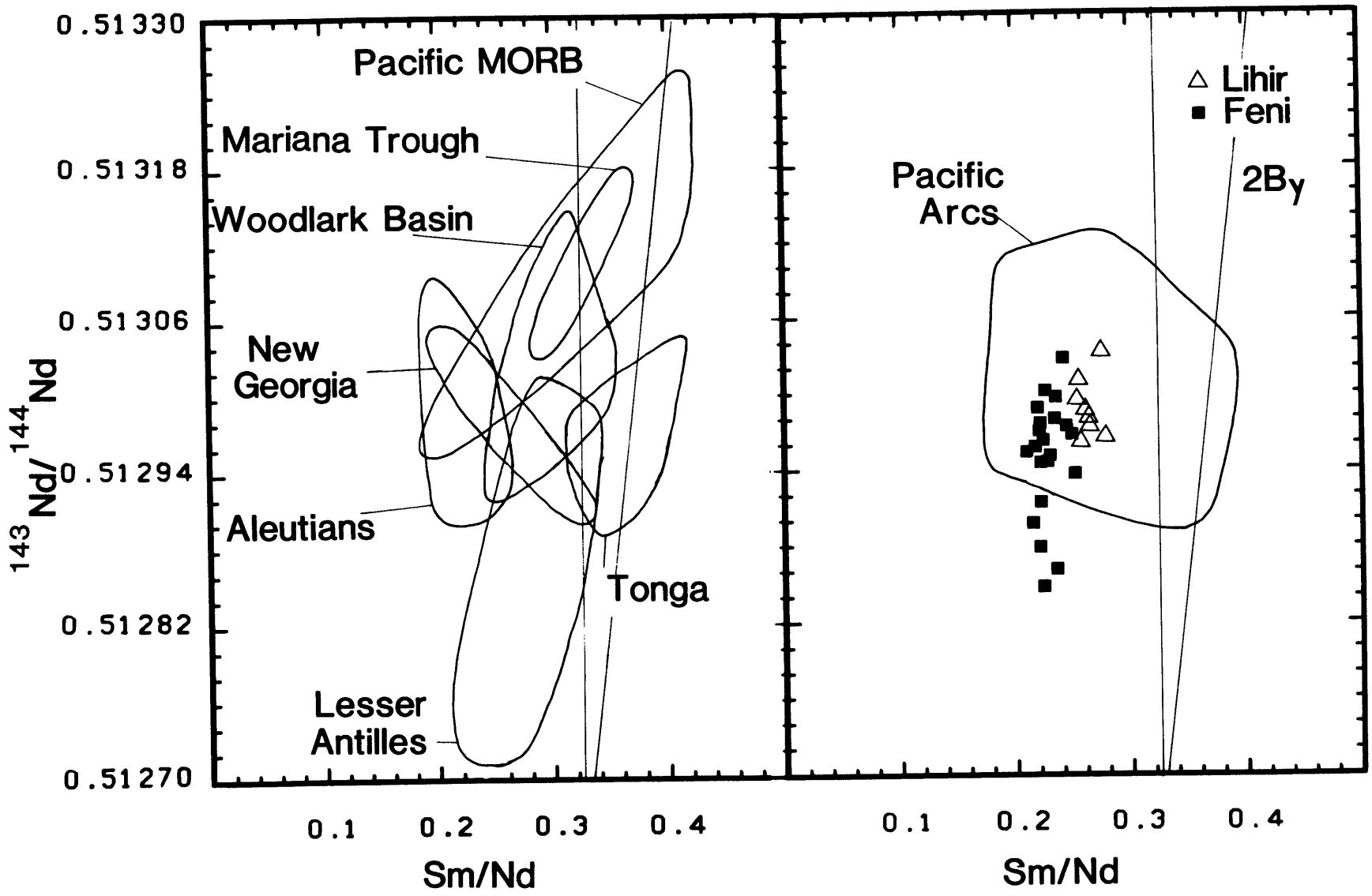
0.51330
0.51318
0.51306
0.51294
0.51282
0.51270
143Nd/144Nd
Pacific MORB
Mariana Trough
Woodlark Basin
New Georgia
Aleutians
Tonga
Lesser Antilles
0.1
0.2
0.3
0.4
Sm/Nd
Lihir
Feni
2By
Pacific Arcs
0.1
0.2
0.3
0.4
Sm/Nd

negative slope which could result from mixing of a depleted and enriched source in Sm/Nd, which both have $^{143}Nd/^{144}Nd$ greater than bulk earth.

Arc suites, with the exception of New Georgia, have small within arc Sm/Nd variations relative to the variation between arcs. The Sm/Nd differences between arcs probably reflects differences in the depletion or enrichment of the source. The position of each field relative to the chondritic Sm/Nd ratio of 0.325, a vertical line in each plot, can be used to compare the degree of depletion of the mantle source region. Melting, metasomatism and crystal fractionation normally decrease the Sm/Nd ratio of the melt and mixing produces a linear array between the endmembers. The Nd isotopic composition of all of the lavas shown are greater than bulk earth, here taken as 0.512647, and this indicates a time integrated depletion of the source reservior, and as the diagrams show, only the most depleted arc lavas have Sm/Nd consistent with derivation from a depleted source. The Tonga lavas have the highest Sm/Nd and have been derived from a mantle source which is more depleted in LREE than other arc lavas (Ewart and Hawkesworth 1987).

A variety of potential endmembers could be parental to the Lihir lavas given their $^{143}Nd/^{144}Nd$ ratios: mantle similar to the ultramafics from St. Paul's Rocks (Roden et al. 1984), a melt derived from an enriched MORB source, an OIB source (Morris and Hart 1983), or a PREMA type endmember (Zindler and Hart 1986). The possibility of a "common"

endmember, a polluted MORB source, which has a small range of isotopic composition and whose average isotopic composition is close to the intersection of the various arc fields would explain the limitation of arc lavas to $^{143}Nd/^{144}Nd$ <0.51310 and $^{87}Sr/^{86}Sr$ >0.7030 (von Drach et al. 1986, Davidson 1987).

The difference in Sm/Nd between the Lihir and Feni samples cannot be attributed to melting or fractionation as there is limited Sm/Nd variation, with the exception of the qtz-trachytes or clinopyroxene cumulates, in lavas with varying degrees of enrichment. Since some of the primitive lavas from Lihir and Feni have almost identical major element composition, if minor differences in the alkalis and P_2O_5 are ignored, the difference in Sm/Nd and hence the degree of enrichment, is a source characteristic and not the result of differences in partial melting. The relative constancy of the Sm/Nd ratio is best explained by moderate percentages of partial melting of previously enriched sources which were enriched to different degrees.

Conclusions

The undersaturated basalts and tephrites from Lihir have trace element and isotopic characteristics that are typical of arcs of the Western Pacific. Although enriched in LILE, in comparison to other arcs, the Lihir lavas are not as enriched as lavas from other islands in the Tabar-Feni

chain. Pb isotopes are homogeneous, Nd isotopes show minor variations, and the small amount of heterogeneity in Sr isotopes can be explained by the introduction of small amounts of a contaminant, such as aragonite or any Sr-rich contaminant derived from seawater. The limited range in isotopic composition is consistent with a cogenetic origin for this suite and the major and trace element data separates the lavas into two evolutionary groups.

Fractionation within these two sequences produces different rates of enrichment/depletion for elements normally considered incompatible, i.e., the LREE, Rb, Th and P. The bulk partition coefficients, calculated from log-log diagrams, for these elements are high, ranging between 0.15 and 0.70 in the primitive lavas and between 1.2 and 1.5 in the evolved lavas. This results in crossing REE patterns, primitive lavas with higher abundances of incompatible elements than evolved lavas. Crystal fractionation models are more successful than AFC models at duplicating the trace element data trends, although poor fits are obtained for La, Th and Rb if literature or measured partition coefficients are used for all phases. This discrepancy is probably the result of interface kinetics changing the partition coefficients in apatite microphenocrysts which nucleate at the crystal-liquid interface of rapidly growing clinopyroxene phenocrysts and are then trapped within the phenocryst. The trace element data for the primitive Lihir lavas can be

explained by fractionation of clinopyroxene, amphibole, magnetite, plagioclase and minor apatite, provided arbitrarily high partition coefficients are used for apatite. The predicted proportions of the phases in this assemblage are similar to those of the lavas with the exception of plagioclase, which is less prevalent in the lavas. However the abundance of plagioclase in cumulate nodules (Table 3.2 and Wallace et al. 1983) is similar to the abundances calculated in these models. Values for the fractionation of residual liquid (F) after crystal fractionation in the primitive group, calculated from incompatible element abundances and bulk partition coefficients, are close to 0.35, the value calculated from Ba, the most incompatible element. These values are lower than would be expected given the limited major element compositional range of these lavas. The evolved magmas can be modeled, albeit poorly, by fractionation of an assemblage with a higher proportion of amphibole to clinopyroxene and slightly higher proportions of apatite and hauyne. Correlations between trace elements in CH/CM vs CH diagrams show that the parent for the evolved lavas has similar composition to the primitive lava L7, and that the crossing REE patterns result from different fractionating assemblages and not different parental melts. The degree of enrichment, as measured by the abundance of elements normally considered incompatible, of lavas from the two fractionation sequences, depends on the abundance and fractionation of apatite, and

this may reflect variations in the relative cooling rates of the magmas.

AFC models for the generation of the evolved lavas are not successful when the assimilants used are similar to the trachytic lavas, which are found on the different islands, or to olivine, clinopyroxene and Ti-magnetite cumulates. AFC models for the primitive lavas indicate little or no assimilation. Further studies of trace element partitioning are required to improve the crystal fractionation models, as are studies of accessory phases that contain the LREE.

The primitive Lihir lavas, which are less enriched in alkalis, LILE and LREE than lavas from the other three island groups in the Tabar-Feni chain, are derived from a less enriched mantle source, rather than by larger partial melting percentages of a similar source. This results from variations in the intensity of the metasomatic process that produced the enrichment of LILE in a previously depleted mantle along the island chain. The similarity of the Sm/Nd ratios of these LILE enriched, undersaturated lavas with tholeiitic and calc-alkaline arc lavas suggests there has been much less enrichment of the REE than LILE during this metasomatic process.

CHAPTER 3

THE PETROLOGY OF THE FENI LAVAS

Introduction

SiO_2 undersaturated rocks occur in oceanic and continental arcs. These rocks are found in the Aleutians, Lesser Antilles, New Hebrides, Sunda, Halmahera, Kuriles, Aegean, Turkey and Eolian arc regions (Delong et al. 1979, Thirwall and Matthews 1984, Barsdell et al. 1982, Varne and Foden 1986, Morris et al. 1982, Bailey et al. 1987, Keller 1980, De Fino et al. 1986). Undersaturated arc lavas are found in two localities in Papua New Guinea (Rabaul; Heming and Rankin 1979, and the Tabar-Feni islands; Wallace et al. 1983).

The Feni islands, which are the southernmost island group in the Tabar-Feni chain, are closest to the presently active subduction zones beneath East New Britain and Bougainville, PNG. Earthquakes at very shallow (<30 km) and great depths (>400 km) have been located below these islands. The deeper earthquakes are associated with the present subduction of the Solomon Sea plate, and the shallow ones with movement on faults associated with tensional tectonics.

All samples in Table 3.1 were obtained from Ambitle island in the Feni group. Ambitle has an area of approximately 90 km^2 and is a single stratovolcano with a small eroded caldera. Older mafic and intermediate lava flows are overlain by a thin mantle of trachytic tephra, and

Table 3.1

Major Elements Feni Islands

	F1	F6	F14	F16	F21	F27	F30	F31	F34	F35	F2	F3
Group	1	1	1	1	1	1	1	1	1	1	2	2
SiO_2	51.56	51.85	55.39	56.70	57.86	51.88	51.45	51.66	55.48	55.01	52.31	51.00
TiO_2	0.69	0.64	0.58	0.66	0.57	0.65	0.66	0.66	0.58	0.74	0.74	0.77
Al_2O_3	16.62	16.65	16.56	18.20	18.32	16.96	16.28	16.73	16.48	18.26	18.97	18.16
Fe_2O_3	7.39	7.35	7.62	6.03	5.86	7.28	7.44	7.23	7.62	6.87	7.93	8.95
MnO	0.19	0.16	0.16	0.11	0.11	0.15	0.16	0.15	0.15	0.13	0.21	0.20
MgO	7.61	7.52	4.20	2.61	2.80	7.00	7.74	6.99	4.22	2.83	3.10	3.72
CaO	6.78	6.71	7.37	4.95	5.12	6.70	6.91	6.70	7.06	5.74	7.26	8.11
Na_2O	5.52	5.42	5.15	6.84	5.70	5.96	5.80	6.08	5.42	6.58	5.13	4.86
K_2O	3.39	3.39	2.68	3.50	3.30	3.16	3.27	3.49	2.62	3.41	3.91	3.63
P_2O_5	0.25	0.31	0.29	0.40	0.36	0.26	0.29	0.31	0.37	0.43	0.44	0.60
H_2O	0.34	0.62	0.40	0.10	0.65	0.22	0.42	0.36	0.27	0.25	1.00	0.50
CO_2	0.1	0.2	0.4	-	0.2	-	0.24	0.38	0.06	-	0.1	0.1
Fe^{2+}/Fe^{3+}	1.30	-	.831	-	-	1.14	1.06	.985	.763	.639	.823	-

	F4	F5	F7	F9	F10	F11	F15	F17	F18	F19	F20	F25
Group	2	2	2	2	2	2	2	2	2	2	2	2
SiO_2	48.52	51.13	52.47	49.81	53.35	48.16	55.20	65.68	50.23	55.57	50.82	50.89
TiO_2	0.83	0.83	0.69	0.81	0.75	0.77	0.71	0.33	0.93	0.58	0.71	0.80
Al_2O_3	17.27	17.41	19.18	16.77	19.01	15.11	18.52	17.83	15.01	16.58	18.71	15.43
Fe_2O_3	10.22	10.02	8.14	10.64	8.17	9.99	6.63	2.70	11.21	7.62	8.09	9.86
MnO	0.20	0.21	0.19	0.21	0.17	0.20	0.13	0.03	0.22	0.14	0.19	0.19
MgO	4.84	4.18	3.21	4.66	3.44	8.96	2.80	0.73	5.73	4.33	3.28	5.91
CaO	10.77	9.00	7.67	9.52	6.60	10.07	5.64	0.96	11.23	7.15	8.03	10.10
Na_2O	3.96	4.32	5.06	3.24	3.42	3.39	6.46	8.07	3.12	5.07	4.88	3.44
K_2O	2.63	2.32	2.91	3.64	4.55	2.70	3.46	3.56	1.90	2.67	4.74	2.99
P_2O_5	0.75	0.57	0.48	0.71	0.54	0.66	0.45	0.11	0.42	0.29	0.55	0.39
H_2O	3.70	1.21	1.10	1.30	1.40	2.50	0.20	0.20	1.60	0.30	1.40	1.00
CO_2	0.7	0.1	0.1	0.3	0.1	0.3	-	0.4	0.4	0.4	0.9	0.4
Fe^{2+}/Fe^{3+}	-	-	-	-	-	-	.664	.559	1.04	.866	-	1.31

Major element data by XRF analysis, except for K_2O which was obtained by isotope dilution for all samples except F22, 28-30, 32-38. Na_2O from INAA except for samples F2, 4, 9, 10, 21-24, 28-38. Fe^{2+}/Fe^{3+} after Heming (1979) and Wallace et al. (1983). Major element data normalized to 100% anhydrous H_2O and CO_2 by CHN analyzer at W.H.O.I. and from Wallace et al. (1983)

Table 3.1

Major Elements Feni Islands (cont'd.)

	F26	F37	F38	F12	F22	F23	F24	F28	F29	F32	F33	F36
Group	2	2	2	3	3	3	3	3	3	3	3	3
SiO_2	48.47	54.85	56.12	47.02	48.02	48.88	48.09	47.42	46.74	46.11	47.77	49.91
TiO_2	0.85	0.73	0.62	0.73	0.64	0.57	0.62	0.75	0.79	0.94	0.86	0.80
Al_2O_3	16.84	18.61	19.47	9.10	9.93	8.17	8.94	10.60	12.15	14.10	15.90	18.95
Fe_2O_3	10.95	6.76	5.66	10.60	10.48	9.47	10.05	11.23	11.41	12.59	10.39	7.81
MnO	0.22	0.15	0.13	0.19	0.19	0.16	0.18	0.20	0.21	0.23	0.20	0.19
MgO	5.26	2.75	2.12	14.42	10.89	12.14	11.02	9.23	8.24	6.06	5.17	3.11
CaO	10.30	5.81	5.25	12.95	15.34	17.23	17.07	14.89	14.29	12.09	10.16	7.25
Na_2O	3.50	6.37	6.51	2.50	3.32	2.39	2.89	2.90	3.55	4.08	5.26	6.92
K_2O	3.11	3.51	3.72	1.93	0.77	0.67	0.77	2.19	2.09	3.10	3.70	4.40
P_2O_5	0.51	0.46	0.40	0.56	0.42	0.32	0.37	0.59	0.53	0.71	0.58	0.66
H_2O	1.20	0.59	0.46	0.80	2.10	1.90	2.10	1.54	1.29	0.42	0.47	0.55
CO_2	0.3	0.05	0.26	0.2	0.7	0.4	1.0	0.05	0.05	0.13	0.27	0.09
Fe^{2+}/Fe^{3+}	1.06	.770	.656	-	-	-	-	.972	.958	1.39	.912	.779

the cauldera contains a trachyte cumulodome (Wallace et al. 1983).

There are few detailed studies of undersaturated arc lavas that examine the conditions under which the magmas evolved, i.e., pressure, temperature, fO_2 and fH_2O, or the phase proportions during crystallization. Identification of parental magmas is often difficult in undersaturated lavas (Maaloe et al. 1986) and the major element data and mineral chemistry of the Feni lavas in this chapter is used to identify parental magmas and to understand the evolution of the Feni volcanics. The wide spectrum of lava compositions (Table 3.1), derived from a variety of parental magmas, can be used to develop an understanding of how crystal fractionation and mixing control the evolution of undersaturated water-rich arc magmas.

Major element chemistry of the Feni lavas

The Feni rocks have many characteristics that are typical of calc-alkaline and tholeiitic island arc basalt (IAB). Low TiO_2 and MgO, and similar Al_2O_3 contents to MORB, is typical of IAB (Perfit et al. 1980). The K_2O/Na_2O ratio of the Feni lavas is similar to, or higher than most arcs, with the exception of the K-rich volcanics from Italy and some Indonesian islands. The high Na content of the phonolitic tephrites (Table 3.1 and Figure 3-1) is rare in arc

Figure 3-1

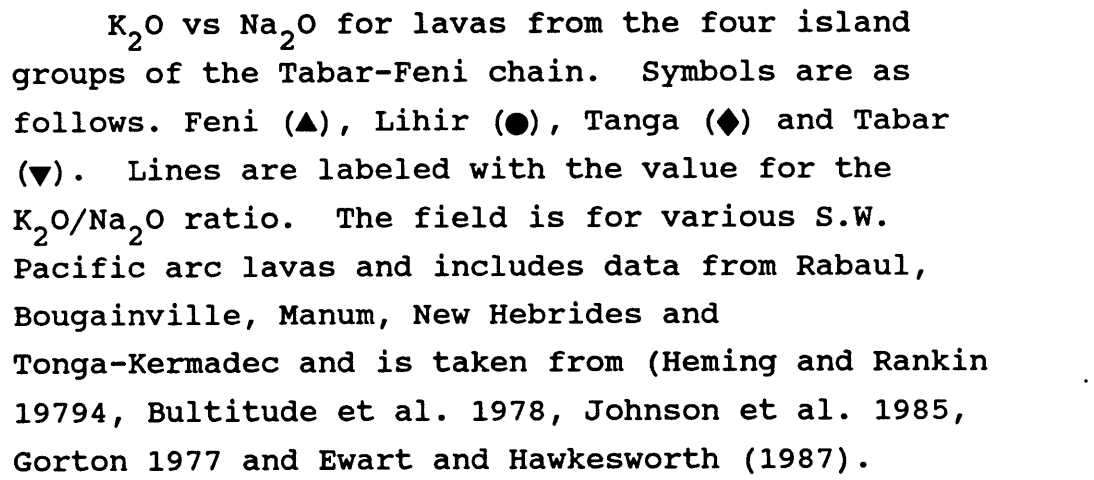

K_2O vs Na_2O for lavas from the four island groups of the Tabar-Feni chain. Symbols are as follows. Feni (▲), Lihir (●), Tanga (♦) and Tabar (▼). Lines are labeled with the value for the K_2O/Na_2O ratio. The field is for various S.W. Pacific arc lavas and includes data from Rabaul, Bougainville, Manum, New Hebrides and Tonga-Kermadec and is taken from (Heming and Rankin 19794, Bultitude et al. 1978, Johnson et al. 1985, Gorton 1977 and Ewart and Hawkesworth (1987).

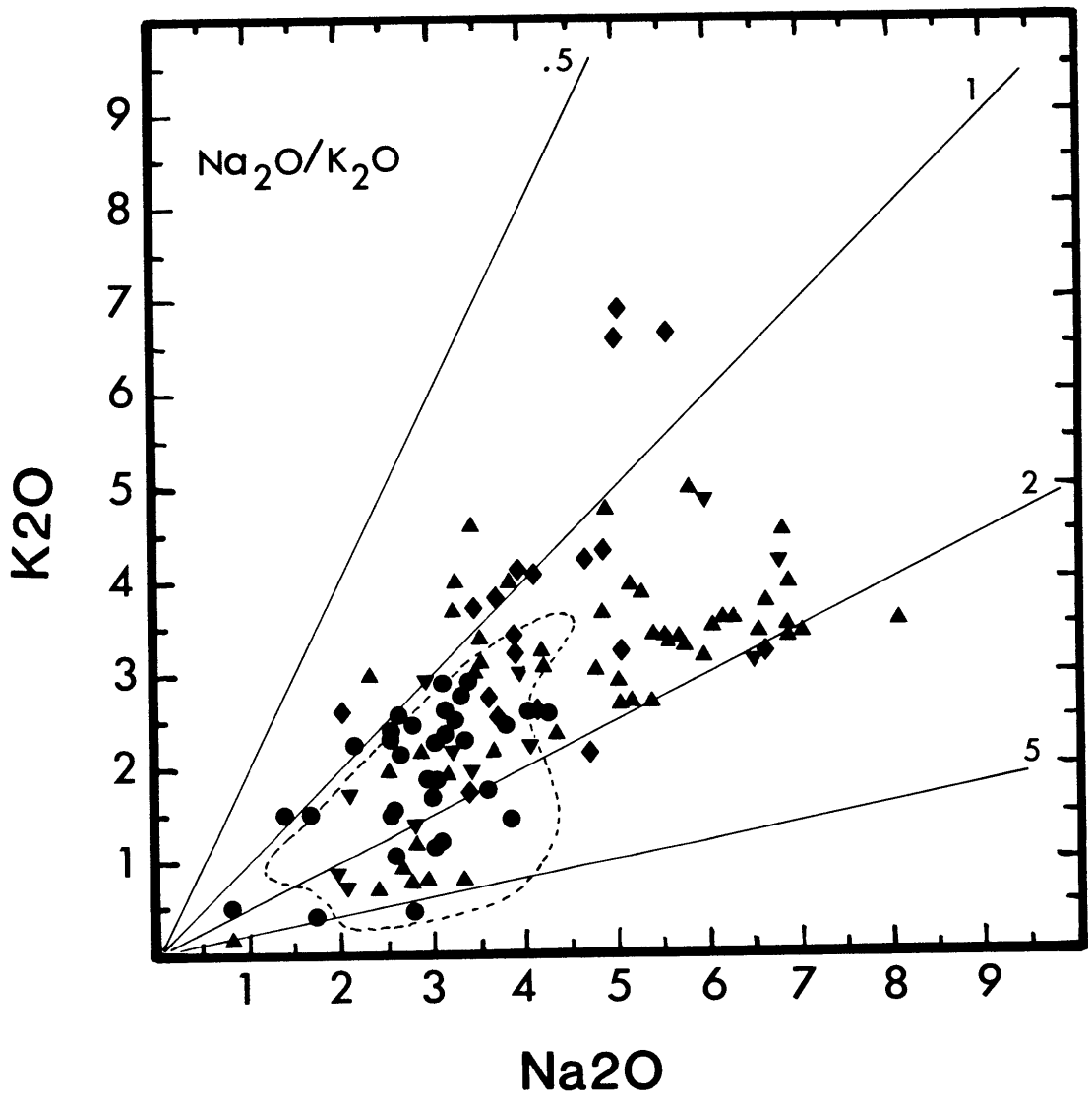
.5
1
2
5
Na_2O/K_2O
K2O
Na2O
1
2
3
4
5
6
7
8
9

volcanics. This figure shows the high alkali content of lavas from the Feni islands, the wide range in K_2O/Na_2O of the Tabar-Feni lavas in comparison to other S.W. Pacific arc suites, and the lower alkali contents of the Lihir lavas. Phonolitic tephrites, which are abundant in the Feni islands, have very high Na_2O (5.1-6.2%) and consequently a low K_2O/Na_2O ratio. Samples which have $Na_2O/K_2O > 3$ are mainly mafic phenocryst-rich lavas that usually have altered groundmass, and may have lost K_2O.

The AFM diagram (Figure 3-2) has traditionally been used to examine the degree of iron enrichment in various rock series and this plot is used to separate arc rocks into tholeiitic and calc-alkaline (Irvine and Baragar 1978). The Feni lavas have moderate iron enrichment, with only a few samples plotting in the tholeiitic field of Irvine and Baragar (1978). These lavas do not show the degree of iron enrichment that is typical of New Britain arc volcanics (Figure 4 of Johnson et al. 1978).

The AFM diagram separates the Feni samples into two groups. The phonolitic tephrites (F1, F6, F27, F30) are the parental magmas for one trend, which start at relatively low Fe and Mg, and high alkali proportions. Throughout the text F1 has been used as a representative parental lava for this group. This suite of lavas, which are referred to as group 1 throughout the text, show a relative enrichment in iron between F1 and F14 (which are both labeled on this figure) followed by the usual decrease that is apparent for all of

Figure 3-2

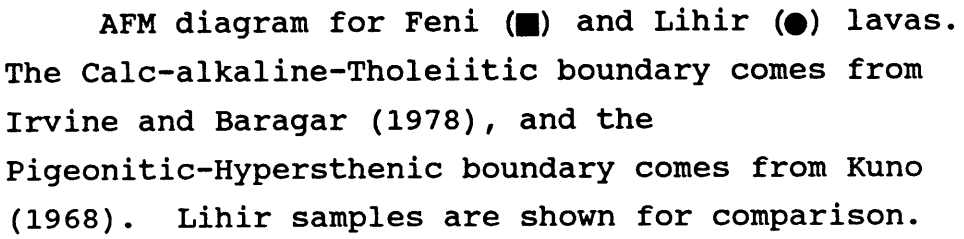

AFM diagram for Feni (■) and Lihir (●) lavas. The Calc-alkaline-Tholeiitic boundary comes from Irvine and Baragar (1978), and the Pigeonitic-Hypersthenic boundary comes from Kuno (1968). Lihir samples are shown for comparison.

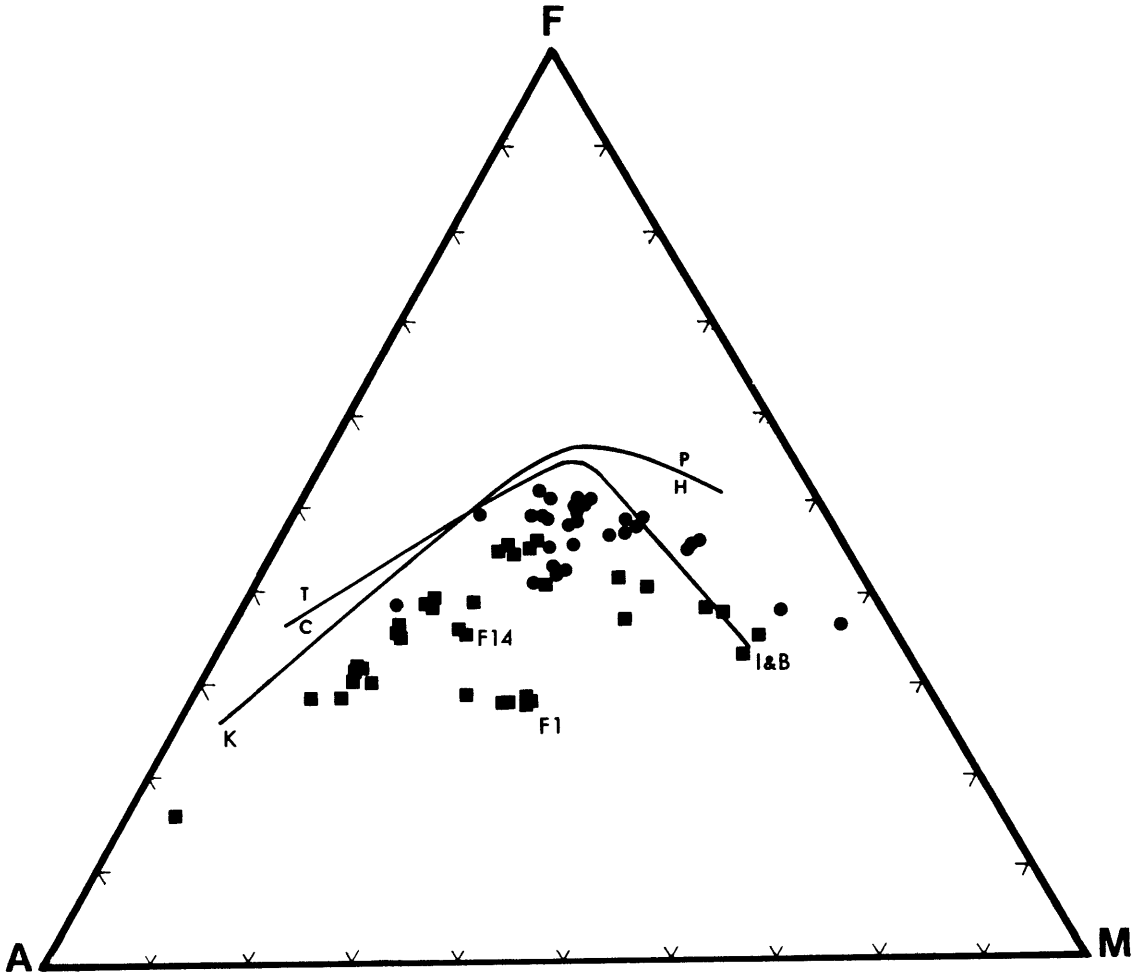
F
A
M
P
H
T
C
K
F14
F1
I&B

the Feni lavas. F14, F19 and F34 have been included in the group 1 lavas because of similarities in major elements, high Na_2O and SiO_2, and low P_2O_5, Fe_2O_3* and Al_2O_3, and trace elements, low REE, and high Ba and Nb (Table 4.1).

Parental lavas in the Feni islands

The identification of primary or parental lavas is essential for understanding: the generation of lavas, the degree of heterogeneity of the source, and delineating evolutionary sequences. Primitive lavas can be identified by using Mg/(Mg+Fe) values, Ni abundances, phenocryst compositions and modes. Parental lavas must have for major element, trace element and isotopic similarities to the evolved lavas. The phonolitic tephrites, F1, F6, F30, which have high Ni (184-220 ppm) and Mg' = Mg/(Mg+Fe) of .69-.70 are the the primitive lavas of the low Fe, high Na group in the AFM diagram. Fe^{3+} is taken as 10% of total Fe for Mg' calculation. These samples are parental and plot at the start of fractionation trends in Figure 3-6. F11 and F12 have Ni and Mg' values of, 167 and 264 ppm, and, .66 and .75. Jaques and Green (1980) produced melts of peridotite with Mg' values between .69 and .86; the primitive Feni lavas fall within this range and are close to being primary melt.

The high Ni and Mg' could result from accumulation of olivine. The modal percentages of olivine in F1 and F11 are low (<5%) and it is unlikely they are olivine accumulates.

F12 contains 12% olivine, however it is unlikely to have accumulated olivine. Olivines, in each of these three lavas, were analyzed for Ni concentration and it is possible to calculate an approximate DNi in olivine, from the Ni of the phenocryst cores and the whole rock Ni. Calculated values of DNi are respectively, 14, 11 and 9. These values are lower than or equal to the expected partition coefficient and are not suggestive of olivine accumulation. The Feni samples have been separated into groups 1, 2 and 3 in Table 3.1. F11 and F12, the primitive samples from groups 2 and 3, which are closest to being primary melts, have compositions that are close to the expected parental magmas for these two evolutionary sequences, and will be taken respectively, as the parents for group 2 and 3. The parental lava for group 1 is taken to be F1, although F6 or F27 or F30 would serve equally as well.

The differences in major element chemistry between these possible parental magmas are shown in Table 3.1. The group 1 (phonolitic tephrites) have high Na_2O, K_2O, SiO_2, and low Al_2O_3, TiO_2 and P_2O_5 compared to the group 2 and 3 lavas. The group 3 samples, have higher Fe_2O_3, CaO, Mg/Fe, TiO_2 and lower Al_2O_3 and SiO_2 than the group 1 and 2 volcanics. The high CaO/Al_2O_3 of F22-F28, in the group 3 samples, results from cpx accumulation. F12, which has the highest Ni of this group, has low modal abundance of cpx (Table 3.2) and high modal abundance of olivine (12%). Fractionation of olivine and cpx from this sample would produce an melt similar to the ankaramites. The high Fe samples in the AFM diagram, can

Table 3.2

Modal Percentages of Phenocrysts

		Oliv	Cpx	Plag	Amp	Ti-mag	Feldspthd	Biotite	Apat	Phen	Gm
F1		3.4	2.6	4.7	0.8	0.8	2.1 H	-	tr	14.4	85.6
F2		-	4.7	14.0	4.7	2.2	-	0.5	tr	26.1	73.9
F3		-	6.2	9.9	6.4	2.0	1.0 H	.03	tr	25.5	74.5
F5		-	9.8	12.2	6.7	2.4	2.1 H	-	tr	33.2	66.8
F7		-	8.6	13.1	1.4	1.1	0.9 H	-	tr	25.1	74.9
F11		5.2	10.8	<.01	-	1.8	1.3 A	-	tr	19.1	80.9
F12		12.4	1.6	<.01	-	-	-	-	-	14.0	86.0
†F13	L1	-	18.5	45.5	25.9	7.1	-	-	.3	97.3	-
	L2	-	39.8	46.8	3.1	10.2	-	-	.1	100	-
	Av.	-	29.8	49.9	11.6	8.6	-	-	-	99.9	-
F14		0.9	10.1	14.4	tr	2.5	-	-	tr	27.9	72.1
F15		-	3.3	12.6	2.1	1.1	1.4 H	-	tr	20.5	79.5
*		-	39.7	7.8	1.3	3.7	2.4 H	-	tr	54.9	45.1
F20		-	-	1.5	2.4	-	-	-	tr	3.9	96.1
F26		-	17.7	7.4	-	3.2	-	-	tr	28.3	71.7

† Layered cumulate nodule, L1 & L2 amphibole and clinopyroxene rich layers
Average calculated from thickness of layers

* Glomeroporphyritic patch
Number of points counted varied between 1600 and 2400

be separated into two groups which have different parental magmas and which have subtle differences in major element evolution. Groups 1, 2 and 3 lavas have different La/Yb (Table 4.1), REE patterns (Figure 4-2), trace element abundances (Table 4.1, Figure 4-1) and isotopic composition (Table 4.2). Thus, the three parental lavas cannot be related by crystal fractionation. The major element evolution of the Feni rocks will now be discussed in terms of the three evolutionary sequences.

Prior to examination of the different evolutionary paths of the three groups, the mineralogy of the Feni lavas is examined to aid in discussion of subtle differences between groups.

Mineral chemistry

Undersaturated rocks often contain a variety of minerals, and the Feni samples are typical in this respect. Phenocrysts of clinopyroxene, plagioclase, olivine, Ti-magnetite, amphibole and biotite commonly occur with a feldspathoid (hauyne, sodalite, leucite), rare analcime, alkali feldspar in the groundmass, and accessory apatite, sphene and sulphides. The diversity of the mineralogy and the phenocryst-rich nature of these lavas is apparent from Table 3.2, which gives phenocryst phase proportions obtained by point counting 12 samples from Feni. Representative analyses of the phases present in 12 samples that cover the

complete range of major element compositions are given in Table 3.3, and Table 3.4 summarizes the compositional variation of the phases within these samples.

The mineralogy, phase compositions and phase proportions vary widely in the Feni lavas (Tables 3.2, 3 and 3.4), for example, F20 is almost completely aphyric with rare amphibole and plagioclase phenocrysts while F26 and F14 are both phenocryst-rich samples having respectively 28.3% and 27.9% phenocrysts. In F26, abundant euhedral sector zoned clinopyroxene and scattered microphenocrysts of plagioclase are set in a groundmass of plagioclase laths which have been resorbed, clinopyroxene and Ti-magnetite. In F14, euhedral phenocrysts of plagioclase, hauyne, clinopyroxene, olivine, Ti-magnetite and rare amphibole, which is breaking down to a fine grained aggregate containing Ti-magnetite, clinopyroxene and feldspar are set in a groundmass of plagioclase, clinopyroxene, hauyne and Ti-magnetite.

Clinopyroxene

Most of the Tabar-Feni rocks contain abundant clinopyroxene phenocrysts and the composition of clinopyroxenes from a variety of lavas and one cumulate nodule are shown in Figure 3-3, along with olivines, amphiboles and biotites. The clinopyroxenes are restricted in composition in these lavas which is typical of high-K suites in orogenic settings (Ewart 1982). Salite is the

Table 3.3

Representative Clinopyroxene Analyses

	F1 Core	F1 Rim	F14 Core	F17 Core	F17 Rim	F17 *Core	F17 *Rim	F12 Core	F12 Rim	F22 Core	F22 Rim
SiO_2	52.61	51.14	52.16	52.95	52.25	53.16	53.04	52.83	49.38	52.62	48.01
TiO_2	0.21	0.50	0.38	0.15	0.25	0.48	0.18	0.26	0.81	0.20	0.85
Al_2O_3	1.49	2.16	1.92	1.21	1.15	0.41	0.26	1.35	4.53	1.49	5.25
FeO	3.61	8.92	6.15	4.07	10.02	19.61	21.13	3.98	7.60	3.77	8.69
MnO	0.06	0.50	0.14	0.20	0.33	0.41	0.29	0.07	0.20	0.10	0.14
MgO	17.01	12.76	15.83	15.97	12.68	7.05	6.16	17.28	13.69	16.68	13.1
CaO	24.11	23.39	23.12	24.09	20.92	10.29	9.11	23.63	22.79	24.04	22.51
Na_2O	0.27	1.02	0.38	0.45	1.99	7.88	8.42	0.26	0.55	0.19	0.51
Cr_2O_3	0.52	0.00	0.00	0.28	0.00	0.00	0.00	0.16	0.00	0.15	0.04
Total	99.90	100.40	99.99	99.36	99.59	99.28	98.60	99.83	99.56	99.23	99.10
cat	4.031	4.055	4.034	4.023	4.066	4.199	4.215	4.030	4.044	4.022	4.054
oxy	5.953	5.918	5.950	5.965	5.902	5.715	5.692	5.955	5.935	5.967	5.919
Mg/Mg+Fe	0.893	0.718	0.821	0.874	0.692	0.390	0.342	0.885	0.762	0.887	0.729
Wo%	47.6	48.6	46.3	48.7	45.1	29.1	26.7	46.5	47.7	47.9	47.3
En%	46.8	36.9	44.1	44.9	38.0	27.7	25.1	47.4	39.9	46.2	38.4
Fs%	5.6	14.5	9.6	6.4	16.9	43.2	48.3	6.1	12.4	5.9	14.3
AlVI	0.0	.04	.01	.01	.03	-	-	0.0	.05	.01	.06

	F13	F11 Core	F11 Rim	F26 Core	F26 Rim	F5 Core	F5 Rim	F7 Core	F7 Rim	F3 Core
SiO_2	48.67	51.63	48.24	50.73	48.17	52.23	45.21	51.35	49.74	48.72
TiO_2	0.76	0.42	0.85	0.62	0.72	0.38	1.45	0.58	0.55	0.84
Al_2O_3	4.99	2.72	5.49	3.78	6.02	1.82	7.86	2.34	3.33	5.69
FeO	7.12	4.58	7.87	6.96	8.46	6.43	9.50	7.41	8.21	7.33
MnO	0.24	0.08	0.20	0.23	0.29	0.41	0.05	0.39	0.32	0.12
MgO	13.55	15.83	13.01	14.39	12.80	15.43	12.05	13.69	13.11	13.50
CaO	23.59	23.60	23.42	22.89	23.11	22.72	22.95	23.55	23.23	23.65
Na_2O	0.67	0.27	0.56	0.49	0.53	0.64	0.39	0.88	0.79	0.47
Cr_2O_3	0.00	0.60	0.00	0.00	0.00	0.00	0.05	0.00	0.00	0.00
Total	99.58	99.72	99.64	100.10	100.10	100.06	99.60	100.20	99.27	100.30
cat	4.063	4.023	4.057	4.033	4.056	4.037	4.074	4.048	4.056	4.052
oxy	5.910	5.965	5.916	5.950	5.916	5.944	5.891	5.929	5.917	5.923
Mg/Mg+Fe	0.773	0.860	0.746	0.786	0.729	0.810	0.693	0.767	0.739	0.766
Wo%	49.2	48.0	49.1	47.3	48.6	46.2	48.7	48.7	48.5	49.1
En%	39.3	44.8	38.0	41.4	37.5	43.6	35.6	39.4	38.1	39.0
Fs%	11.5	7.3	12.9	11.2	13.9	10.2	15.7	12.0	13.4	11.9
AlVI	.05	.03	.06	.05	.08	.01	.07	.02	.03	.07

* Aegirine, All Fe normally Fe_2O_3

Table 3.3

Representative Plagioclase Analyses

	F1 Core	F1 Core	F1 Rim	F14 Core	F14 Core	F14 GM	F17 Core	F12 GM	F13 Core	F13 Rim
SiO_2	58.31	58.30	64.35	59.39	56.46	65.34	68.59	57.74	47.80	48.18
Al_2O_3	25.93	26.9	20.81	24.88	26.73	20.30	19.76	27.12	33.26	33.04
FeO	0.26	0.43	0.29	0.52	0.53	0.66	0.36	0.59	0.50	0.45
MgO	0.00	0.00	0.00	0.06	0.04	0.00	0.00	0.05	0.01	0.00
CaO	7.89	7.30	1.94	6.71	9.09	1.75	0.40	6.71	16.27	15.90
Na_2O	6.72	6.82	7.06	7.09	5.85	8.35	8.96	5.81	2.14	2.11
K_2O	0.71	0.73	4.98	0.80	0.47	3.46	2.79	1.05	0.13	0.13
Total	99.81	99.58	99.43	99.44	99.16	99.86	100.87	99.07	100.11	99.81
cat	5.007	5.006	5.003	5.001	4.996	5.010	4.970	4.961	5.007	4.993
oxy	7.988	7.990	7.994	7.998	8.006	7.983	8.052	8.062	7.988	8.010
An%	37.8	35.6	9.40	32.8	44.9	8.40	2.00	36.3	80.2	80.0
Ab%	58.2	60.2	61.9	62.6	52.3	72.0	81.3	56.9	19.0	19.3
Or%	4.10	4.20	28.7	4.60	2.80	19.6	16.7	6.80	0.80	0.80

	F26 Core	F26 GM	F3 Core	F3 Rim	F5 Core	F5 Rim	F7 Core	F7 Rim	F7 GM	F7 Core
SiO_2	49.35	56.21	51.46	59.68	53.90	56.02	49.32	57.18	61.79	47.02
Al_2O_3	31.96	26.74	30.21	25.11	28.81	27.44	31.44	26.34	23.36	32.97
FeO	0.55	0.51	0.56	0.48	0.45	0.52	0.58	0.50	0.52	0.57
MgO	0.08	0.04	0.08	0.04	0.03	0.05	0.09	0.08	0.04	0.06
CaO	14.70	8.80	13.54	6.90	10.87	9.28	14.85	8.54	4.14	16.78
Na_2O	2.84	6.07	3.86	7.31	4.85	5.68	2.71	6.09	7.55	1.94
K_2O	0.13	0.58	0.27	0.69	0.46	0.47	0.18	0.69	2.58	0.08
Total	99.60	98.95	99.98	100.2	99.37	99.47	99.17	99.42	99.98	99.42
cat	5.001	5.010	5.018	5.003	5.001	4.996	4.998	5.000	5.019	5.012
oxy	8.000	7.982	7.970	7.994	7.997	8.001	8.002	8.000	7.970	7.979
An%	73.5	43.0	65.0	31.9	53.8	46.1	74.4	41.9	19.9	82.3
Ab%	25.7	53.6	33.5	64.0	43.4	51.1	24.6	54.1	65.4	17.2
Or%	0.80	3.40	1.50	4.00	2.70	2.80	1.00	4.00	14.7	0.50

Table 3.3

Representative Amphibole Analyses

	F1 Core	F1 Rim	F3 Core	F3 Rim	F5 Core	F5 Rim	F7 Core	F7 Rim	F13 Core	F13 Rim
SiO_2	40.22	40.06	39.70	38.66	39.50	39.79	40.11	39.74	39.98	39.75
TiO_2	2.63	2.48	2.43	2.60	2.20	2.34	2.69	2.41	2.67	2.85
Al_2O_3	12.93	13.67	13.84	15.69	14.06	13.70	13.59	14.00	13.38	13.46
FeO	11.24	10.33	11.39	11.08	11.89	11.06	11.72	11.76	10.66	10.57
MnO	0.21	0.12	0.17	0.21	0.17	0.14	0.25	0.09	0.25	0.18
MgO	14.4	14.64	13.83	12.82	13.95	14.44	13.66	13.56	14.15	14.03
CaO	12.10	12.67	12.10	11.82	12.34	12.52	12.24	12.81	12.26	12.11
Na_2O	2.73	2.90	2.45	2.29	2.40	2.46	2.57	2.51	2.98	3.01
K_2O	1.22	1.17	1.34	1.35	1.46	1.47	1.51	1.41	1.18	1.15
P_2O_5	0.06	0.07	0.04	0.05	0.06	0.07	0.08	0.08	0.00	0.00
Cr_2O_3	0.08	0.08	0.00	0.00	0.03	0.05	0.04	0.03	0.00	0.03
Total	97.82	98.21	97.29	96.58	98.06	98.04	98.46	98.41	97.48	97.13
Mg/Mg+Fe	0.695	0.716	0.683	0.6783	0.676	0.699	0.675	0.672	0.703	0.703
*cat	16.095	16.136	16.058	15.975	16.120	16.119	16.074	16.098	16.121	16.109
*oxy	21.432	21.378	21.481	21.594	21.399	21.400	21.461	21.428	21.399	21.415
+ Fe^{3+}/Fe^{2+}	0.432	0.365	0.439	0.346	0.631	0.539	0.286	-	-	-

+ After Spear and Kimball (1984) using Average Fe^{3+}
- Fe^{3+}/Fe^{2+} not calculated due to non-stoichiometry of amphibole analysis
* Calculated assuming cat 15, oxy 23

Representative Olivine Analyses

	F1 Core	F1 Rim	F14 Core	F14 Rim	F11 Core	F11 Rim	F12 Core	F12 Rim	F22	F23
SiO_2	40.69	39.14	38.61	38.08	41.73	41.24	41.66	39.09	40.35	40.06
TiO_2	0.04	0.04	0.05	0.05	0.05	0.03	0.00	0.00	0.00	0.02
Al_2O_3	0.04	0.04	0.04	0.05	0.04	0.08	0.00	0.02	0.04	0.03
FeO	7.27	17.99	20.06	21.92	7.66	9.56	8.30	19.50	13.11	14.42
MnO	0.13	0.75	0.91	1.20	0.14	0.26	0.17	0.66	0.29	0.29
MgO	51.37	42.54	39.68	37.97	51.31	48.92	50.66	40.92	45.98	45.11
CaO	0.08	0.36	0.16	0.21	0.09	0.36	0.15	0.43	0.49	0.52
Cr_2O_3	0.06	0.02	0.00	0.00	0.06	0.06	0.08	0.01	0.00	0.05
NiO	0.33	0.05	0.00	0.03	0.22	0.09	0.33	0.11	0.08	0.07
Total	100.00	100.93	99.52	99.52	101.30	100.60	101.03	100.73	100.33	100.56
cat	3.009	3.007	2.997	2.999	2.998	2.994	2.996	3.001	2.997	3.000
oxy	3.987	3.990	4.003	4.000	4.002	4.008	4.004	3.998	4.003	4.000
Fo	93	81	78	76	92	90	92	79	86	85

Table 3.3

Representative Ti-magnetite Analyses

	F1 Core	F1 Rim	F14	F11	F22 gm	F23†	F26 Core	F26 Rim	F26 Core	F3
SiO_2	0.21	0.14	0.11	0.05	0.13	0.07	0.10	0.25	0.28	0.23
TiO_2	6.98	7.16	6.29	5.72	3.74	4.18	6.22	9.25	8.67	5.14
Al_2O_3	2.73	2.47	2.19	5.96	5.97	5.70	7.36	2.45	2.39	4.90
*FeO	41.00	41.07	41.52	47.55	45.28	46.98	39.24	43.81	43.10	40.33
Fe_2O_3	45.53	45.33	46.51	34.99	38.38	38.10	44.63	42.67	43.27	45.89
MnO	0.99	0.96	0.89	1.01	0.41	0.70	0.83	1.16	1.03	0.94
MgO	2.62	2.53	2.62	3.00	4.77	3.82	2.57	0.51	0.55	2.30
CaO	0.06	0.06	0.00	0.00	0.09	0.04	0.02	0.01	0.74	0.05
Cr_2O_3	0.06	0.07	0.00	0.03	0.00	0.00	0.00	0.00	0.00	0.11
NiO	0.03	0.06	0.00	0.00	0.08	0.00	0.00	0.00	0.00	0.02
Total	100.20	99.84	100.14	98.30	98.83	99.59	100.98	100.10	100.03	99.91
Fe^{2+}/Fe^{3+}	1.001	1.007	0.992	1.510	1.311	1.371	0.977	1.141	1.107	0.977

† Inclusion within clinopyroxene
* Calculated from stoichiometry

Representative Ti-magnetite Analyses

	F5	F7 Core	F7 Rim
SiO_2	0.05	0.09	0.13
TiO_2	5.21	5.12	6.12
Al_2O_3	6.36	4.78	3.84
*FeO	38.39	39.31	40.10
Fe_2O_3	46.61	46.93	45.85
MnO	0.69	0.97	0.98
MgO	3.79	3.30	2.79
CaO	0.00	0.02	0.05
Cr_2O_3	0.00	0.05	0.05
NiO	0.00	0.08	0.06
Total	101.11	100.65	99.97
Fe^{2+}/Fe^{3+}	0.915	0.931	0.972

Representative Biotite and Sphene Analyses

	F3 Rim	F3 Core	F17	F17 Sphene
SiO_2	36.81	36.62	39.16	29.41
TiO_2	3.85	3.85	2.58	37.15
Al_2O_3	14.94	15.09	14.25	0.38
FeO	13.09	13.1	14.41	1.33
MnO	0.24	0.29	0.13	0.10
MgO	16.56	16.54	17.78	0.00
CaO	0.00	0.02	0.05	27.95
Na_2O	0.69	0.80	0.70	0.07
K_2O	8.45	8.52	5.76	0.00
P_2O_5	0.06	0.02	0.00	0.15
Total	94.74	94.85	94.86	96.54
•cat	17.09	17.14	16.80	12.14
•oxy	22.46	22.39	22.86	19.76
Mg/Mg+Fe	0.692	0.692	0.687	-

•Biotite recalculated to 24 oxy 16 cat
Sphene recalculated to 20 oxy 12 cat

Table 3.3

Representative Feldspathoid Analyses

	F1 H/N/S	F1 H/N/S	F11 *	F11 *	F23 A	F23 A	F3 H/N/S	F7 H/N/S	F7 H/N/S
SiO_2	33.81	37.14	47.64	46.93	52.12	52.82	34.91	35.31	34.35
TiO_2	0.00	0.04	0.00	0.00	0.00	0.00	0.07	0.03	0.02
Al_2O_3	28.77	29.22	27.25	27.02	24.23	24.36	28.38	28.01	28.32
FeO	0.26	0.35	0.00	0.00	0.04	0.04	0.24	0.24	0.36
MnO	0.00	0.04	0.00	0.00	0.00	0.00	0.03	0.03	0.00
MgO	0.00	0.04	0.00	0.00	0.00	0.00	0.07	0.07	0.03
CaO	3.28	5.45	9.50	9.60	0.88	0.85	7.60	7.40	7.65
Na_2O	18.43	11.75	0.29	0.27	11.98	12.07	10.07	12.86	11.31
K_2O	0.64	0.80	6.60	6.76	0.00	0.00	0.63	5.12	5.11
P_2O_5	0.14	0.08	0.00	0.00	0.00	0.00	0.14	0.09	0.05
Total	85.33	84.90	91.33	90.63	89.25	90.13	82.19	89.25	87.19

*$(CaKNa)_{1.2}(Al_2Si_3)O_{9.6}$ approximates structure of natrolite

A Analcite

H/N Hauyne/Nosean solid solution

usual composition, and diopside and augite are also sometimes present (Figure 3-3). Aegirine occurs within the qtz-trachytes.

Zoning patterns in clinopyroxene range between fairly regular growth at essentially constant composition, and highly complex growth patterns where sector zoned clinopyroxenes also have Fe- and Mg-rich oscillatory zones. This complexity is typical of clinopyroxene in undersaturated rocks (Barton et al. 1982, Duda and Schminke 1985) and is more common in the more evolved Feni samples. Clinopyroxene in the group 3 ankaramitic lavas, such as F22-24, has limited compositional variation (Table 3.4). These cpx, which are up to 1.5 cm in length, appear to have grown slowly under more stable conditions in these water-rich magmas. Many of these cpx have higher SiO_2 and lower TiO_2 than clinopyroxenes from related samples that are more evolved.

Clinopyroxenes with the greatest compositional zoning (Wo,En,Fs 47.6, 46.8, 5.6 to 48.6, 36.9, 14.5) are found in samples with high alkali contents and relatively low water contents (F1, F5, F12). In general, cpx rims have higher Fe, Na, Al, Ti and Ca, and the main compositional changes are in the ($CaTiAl_2O_6$-$NaFeSi_2O_6$-$CaAl_2SiO_6$) components and this is typical of undersaturated lavas (Baldridge et al. 1981). Groundmass clinopyroxenes show a continuation of this compositional trend, and invariably have lower Mg/Fe and higher Al, Fe, Ca and Ti. This can be attributed to the lower activity of SiO_2 in undersaturated magmas (Baldridge et

Table 3.4

Phenocryst Compositional Ranges

	Olivine	Clinopyroxene			Amphibole	Biotite	Plagioclase	
	Fo	Mg/Mg+Fe	AlVI†	Fe^{3+}/Fe^{2+}*	Mg/Mg+Fe	Mg/Mg+Fe	An	Fe/Mg Lava
Group 1								
F1	93-78	.89-.69	.01-.02	.74-1.01	.72-.70		62-38	0.49
F14	77-74	.85-.78	.01-.02	.54-.74			62-29	0.92
Group 2								
F11	92-89	.87-.71	.02-.07	.45-.97			87-60	0.50
F26		.79-.73	.04-.08	.73-.96	.70-.65		74-63	1.05
F5		.81-.69	.01-.08	.67-1.03	.73-.64	.70-.69	82-48	1.04
F3		.77-.74	.07	.56-.92	.70-.65		90-59	1.21
F7		.77-.68	.02-.03	.79-.86	.70-.65		75-46	1.28
Group 3								
F12	92-77	.89-.74	0-.02	.45-1.06				0.37
F22	86-84	.89-.71	.02	.24-.93				0.49
F23	85-84	.89-.86	.01	.74-1.32				0.39
Qtz Trachyte								
F17		.87-.69	~0	.64-.83	.67-.62 .32-.30	.69-.68	Kf only	1.87
Cumulate Nodule								
F13		.79-.77	.05-.07	.63-1.12	.70-.69		81-78	

† AlVI from phenocryst cores using method of Lindsley and Andersen (1983)
* Fe^{3}/Fe^{2} after Papike et al. (1974)

Figure 3-3

A Mg-Ca-Fe ternary diagram showing compositions of clinopyroxenes, amphiboles and biotites. Olivine compositions are shown as Fo % where applicable. Data is from group 1 (F1, F14), group 2 (F11, F26, F3, F7), group 3 (F12, F23), a quartz-trachyte (F17), and a plag+cpx+amp+Ti-mag bearing cumulate nodule (F13). Symbols are as follows: Cpx (+), Amp (○), Oliv (×) and Biot (□).

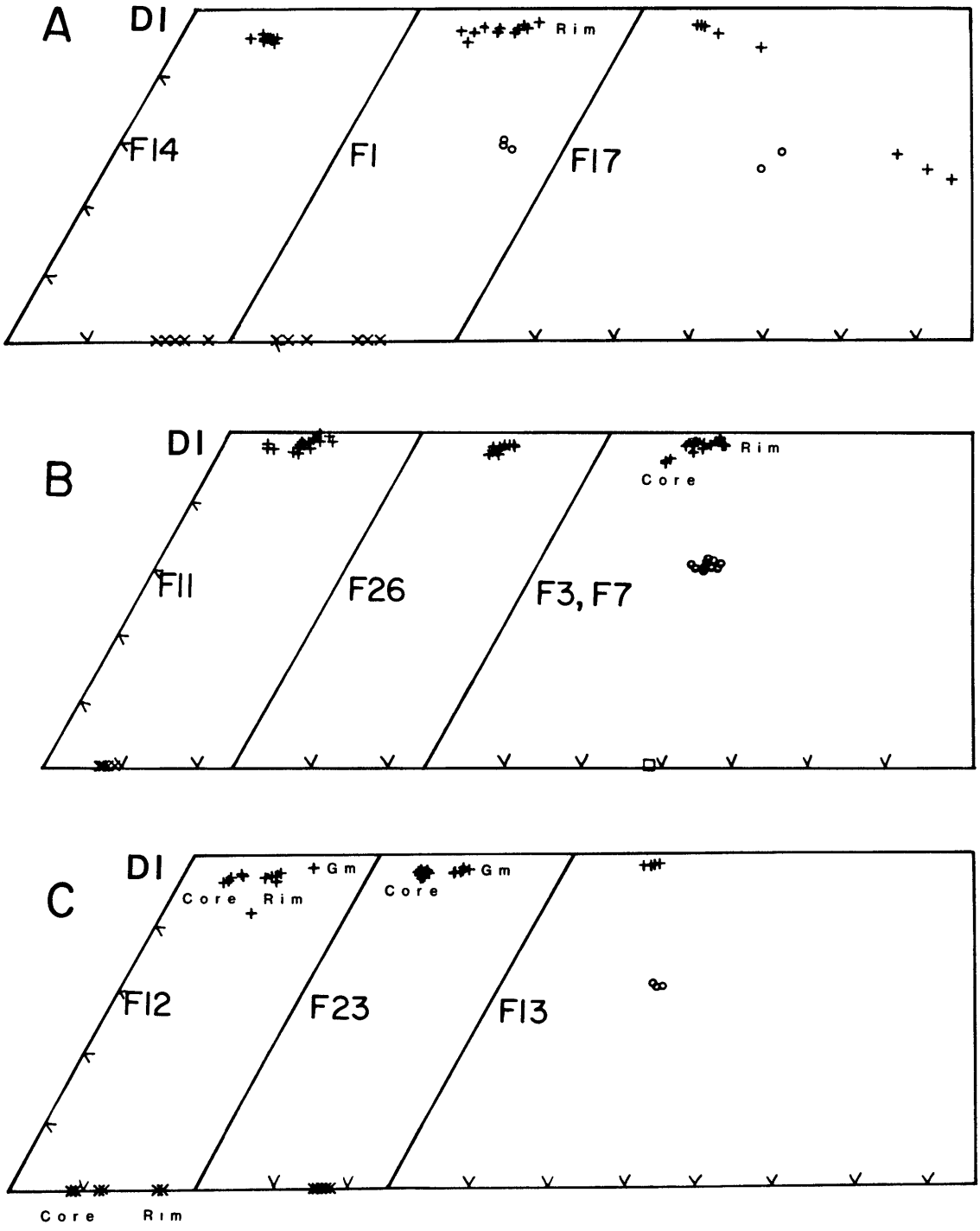
A
DI
Rim
F14
F1
F17
B
DI
Rim
Core
F11
F26
F3, F7
C
DI
Gm
Core
Rim
Gm
Core
F12
F23
F13
Core
Rim

al. 1981). This is different to the trend shown by cpx in saturated arc lavas (Johnson et al. 1985) and in the qtz-trachytes (Figure 3-3).

Olivine

Olivine occurs as euhedral phenocrysts and microphenocrysts in the mafic lavas. Olivine with extremely variable forsterite contents, Fo 93 to Fo 49, (Table 3-4, Heming 1979, and Wallace et al. 1983) occurs in some rocks and even within single phenocrysts, while in other samples the olivines are extremely homogeneous. Magnesian olivines are present in the group 1 phonolitic tephrites (F1, F6, F27), in the group 2 potassic trachybasalt (F11), and in group 3 potassic basalt (F12) (Table 3.4). Olivine phenocrysts are compositionally uniform within many of the Tabar-Feni lavas that have higher analysed water contents, i.e., F11, F22 and F23 (Table 3.4), and show greater compositional zoning in those rocks with lower H_2O, for example F1 and F12. Olivines of the cpx-rich samples have lower Fo contents and are more restricted in composition. The olivine microphenocrysts of F14 have limited compositional variation (Fo 77-73).

Feldspar

Plagioclase phenocrysts are abundant in the Tabar-Feni lavas, with the exception of rare aphyric lavas, ankaramites and some basalts (F20, F23, F24, F11). Phenocrysts are usually twinned, show oscillatory zoning, and a large compositional range within most samples from groups 2 and 3 (Figure 3-4). The group 1 lavas have plagioclase with lower An contents (62-38). A variety of plagioclase crystal morphologies are present in most lavas. Large phenocrysts often have An-rich (>An 70) cores or zones that are corroded. Other phenocrysts show complex oscillatory zoning, twinning. Groundmass and phenocryst laths often show resorbed rims. The plagioclase phenocrysts of the Feni rocks range in composition between An 90 and An 29 (Table 3.4) and are often more calcic than would be predicted from anhydrous experiments (Kennedy et al. 1987, see chapter 1), which is typical of arc volcanics (Perfit et al. 1980, Green 1980, Johnson et al. 1985). Anorthitic plagioclase phenocrysts (An 80-90) occur as resorbed cores in some evolved samples (F3, F7). This can be interpreted as disequilibrium between melt and phenocrysts, and could result from mixing (Sakuyama 1981) or variations in H_2O content (Ewart 1982). Both phenocryst and groundmass plagioclase contain significant amounts of the minor components Fe, Sr and Ba (Wallace et al. 1983, Heming 1979, and Table 3-3) resulting from the enriched nature of the magmas, and the highly oxidizing conditions during rapid

Figure 3-4

a) Plagioclase phenocrysts and groundmass compositions for group 2 and 3 lavas.

b) Plagioclase phenocrysts and groundmass compositions for group 1 lavas and the qtz-trachyte F17.

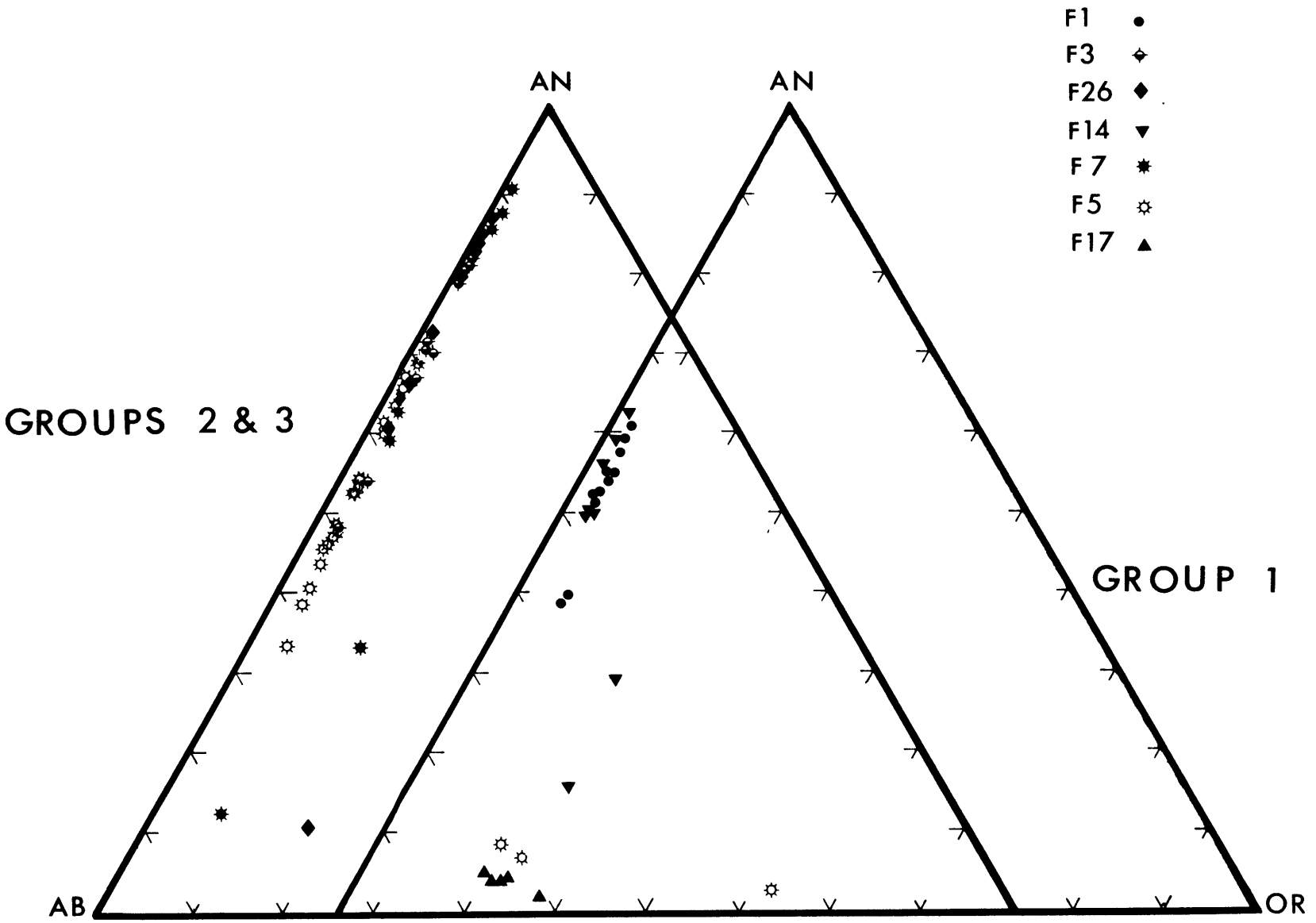
F1
F3
F26
F14
F7
F5
F17
AN
AN
GROUPS 2 & 3
GROUP 1
AB
OR

crystallization. FeO contents of plagioclase phenocrysts reach approximately 1% in rare instances while SrO contents are consistently between 0.3 and 1.3%. BaO contents are usually between 0.15 and 0.2% (Heming 1979). Alkali feldspar is confined to the groundmass as interstitual material, even in the trachytic lavas which contain phenocrysts of albite to anorthoclase (Heming 1979 and Wallace et al. 1983). Reverse zoning was found in some samples and the groundmass feldspars were consistently more albitic than rim compositions.

Amphibole and Mica

Amphibole, which is usually magnesiohastingsite or pargasite, is abundant in rocks and cumulate nodules that have high alkali contents. Tschermakitic hornblende is present in some rocks (Wallace et al. 1983). Amphibole is associated with olivine only in the phonolitic tephrites. It often encloses cpx, plag, Ti-magnetite and apatite and normally reacts to form an aggregate of oxides, cpx and feldspar or is rimmed by biotite. The compositional range is restricted (Figure 3-3 and Table 3.4) with Fe increasing from core to rim and the overall composition varying only slightly in response to variations in the Fe/Mg ratio of the host rock (Tables 3.3 and 3.4). All micas analyzed were biotite and there is very limited compositional variation (Table 3.4), although phlogopite has been identified in some cumulate nodules (Wallace et al. 1983).

Ti-magnetite

Phenocrysts and groundmass Ti-magnetite are common in the Feni lavas. This phase occurs only as a groundmass mineral in a few samples (F12, F22, F23). The Ti-magnetites of the Feni lavas contain Al, Mg, Cr as minor constituents and have relatively low Al. Variations in calculated Fe^{3+}/Fe^{2+} ratios are relatively minor and do not reflect the bulk composition of the lava. Ulvospinel contents increase from core to rim while Mg and Al decrease, and these minor elements tend to vary systematically with the Mg/Fe ratio of the rocks. No ilmenite is present in these lavas, due to the low TiO_2 contents.

Feldspathoids and accessory minerals

The principal feldsphathoid occuring as a phenocryst in the Feni samples is a hauyne-nosean-sodalite solid solution. Large variations in CaO and Na_2O occur within and between individual phenocrysts (Table 3-3 and Arculus et al. 1981). This feldspathoid, which for the sake of brevity is referred to as hauyne throughout the text, also occurs throughout the groundmass of many of the lavas. The CaO/Na_2O ratio of hauyne varies sympathetically with the CaO/Na_2O ratio of the magma. Analcime, leucite and sodalite also occur (Wallace et al. 1983). Sulphides (chalcopyrite, pyrrhotite) are found as

inclusions within plagioclase and magnetite, and as part of the groundmass assemblage in the some lavas (Heming 1979, Wallace et al. 1983 and EDS analysis). Apatite is common in all but the most mafic lavas, generally occuring as microphenocrysts within clinopyroxene phenocrysts and occasionally in the groudmass. Sphene occurs in the qtz-trachyte as rare phenocrysts. A single phenocryst of natrolite was analyzed in F11.

Fe/Mg partitioning

The large compositional range of most phases, and the phenocryst-rich nature of many of the lavas, makes accurate measurement of major element partitioning between the minerals and melt difficult. Information on partitioning of Mg/Fe can be obtained by examining: the core compositions of phenocrysts in lavas that do not show disequilibrium textures that may be evidence for mixing, samples that have restricted compositional ranges for the different phases, or samples which are nearly aphyric. Equilibrium partitioning of Fe and Mg between clinopyroxene and melt, and olivine and melt, are known from experiments. Comparison of the distribution of Fe and Mg in phenocrysts from the Feni lavas with those from experiments should shed some light on the assumption of equilibrium partitioning both in the experiments and lavas. Figure 3-5 shows Mg/(Mg+Fe) of clinopyroxene plotted against the same ratio for olivine for experiments of saturated and

Figure 3-5

Mg/Mg+Fe of olivine-clinopyroxene pairs from Feni lavas and from experimental studies of alkalic compositions. Curves are calculated assuming constant Fe/Mg partioning between olivine and melt, and clinopyroxene and melt. Tie lines connect core and rim pairs from Feni lavas. Symbols for experimental data are as follows: (▼) fO_2 Ni-NiO, (▲) fO_2 QFM, (◆) experiments on 78LH1, chapter 1. The data sources are from Mahood and Baker (1985), Sack et al. (1987), and Baker and Eggler (1987).

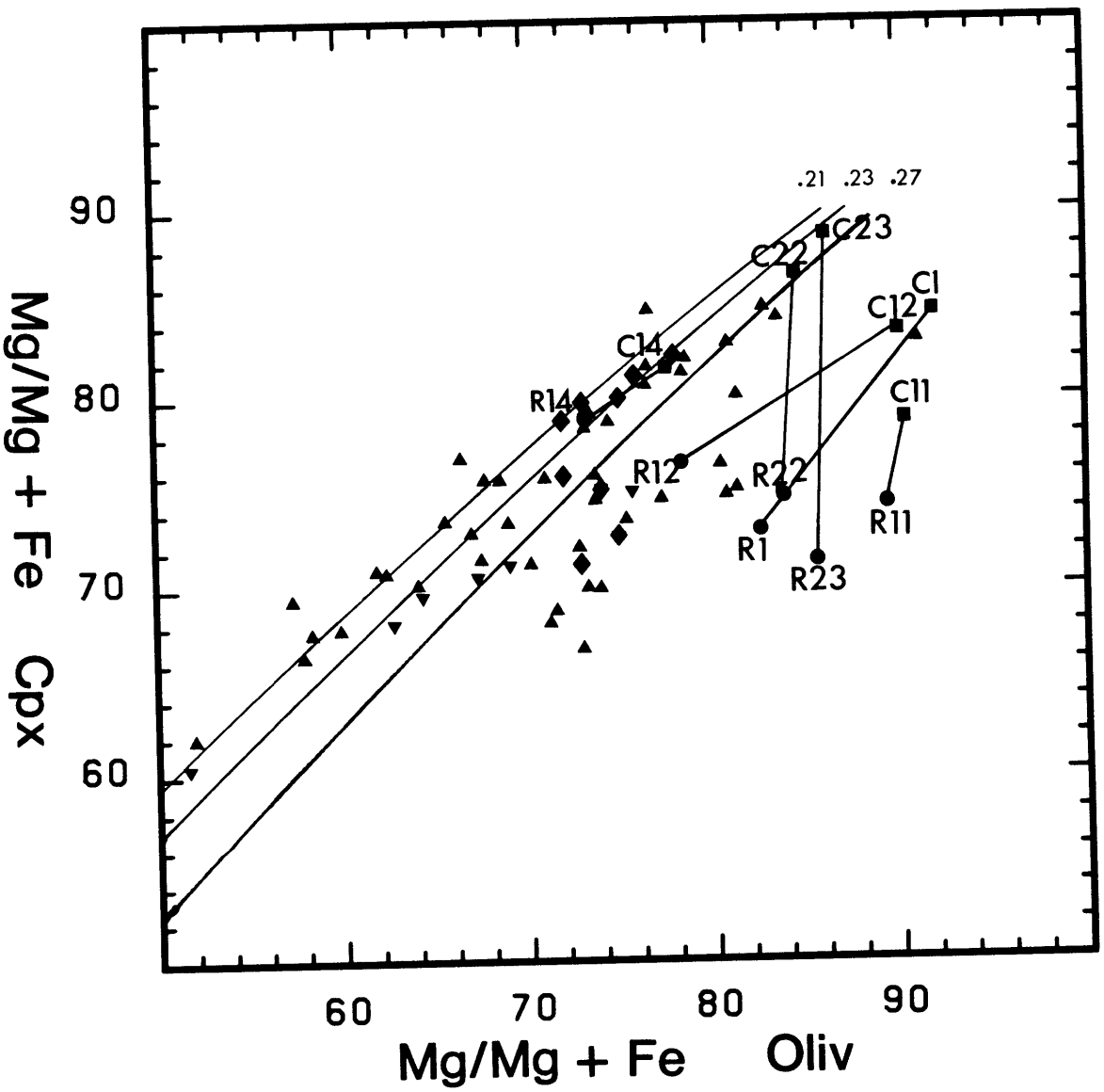
.21 .23 .27
C23
C22
C1
C12
C14
C11
R14
R12
R22
R11
R1
R23
90
80
70
60
Mg/Mg + Fe Cpx
60
70
80
90
Mg/Mg + Fe Oliv

undersaturated lavas and for the Feni samples containing both olivine and clinopyroxene. Assuming a constant Fe/Mg partition coefficient ((Fe/Mg)oliv/(Fe/Mg)melt) of 0.3, curves for constant values of this partition coefficient in clinopyroxene, are plotted on this diagram. The experimental data scatters considerably, but appears to have an upper limit that corresponds to a Fe/Mg partition coefficient of approximately 0.21. This scatter can be attributed to disequilibrium between clinopyroxene and the melt, changes in T, P, chemistry. The plotting position is also dependent on the fO_2, as clinopyroxene can incorporate Fe^{3+} into its structure and olivine cannot. This is observable in the experimental results from chapter 1. The three averaged clinopyroxene compositions from the Ni-NiO experiments have the lowest Mg/(Mg+Fe) due to the incorporation of Fe^{3+}. The QFM experiments have consistent partitioning of Mg/Fe between melt and cpx, and cpx and olivine (Figure 1-3). The data from the Feni samples which contain both olivine and clinopyroxene, plots in general, to the right of the experimental data, which is mostly QFM, and can be interpreted as disequilibrium changes in P, T, composition or high fO_2. Considering the high calculated Fe^{3+} contents of cpx (Table 3.4) in the lavas, the latter alternative is the most likely. The only sample that has rim and core pairs that are close to the upper limit and suggestive of QFM conditions is F14. Samples F11, F22 and F23 have high water contents, and the olivines in these samples are very

restricted in composition in comparison to those in samples with lower H_2O, F1, F12 and F14. The tie lines between core and rim pairs do not parallel equilibrium crystallization curves except for F1 and F14. This reflects differing rates of re-equilibration between cpx and melt and olivine and melt. The greatest discrepancy in partitioning between rim and core pairs are in the cumulate ankaramites F22 and F23. The Fe/Mg partitioning of clinopyroxene suggests high fO_2 during crystallization. The differences in compositional zoning in olivines, between samples with higher H_2O contents and lavas with lower water contents (Figure 3-5) suggests a closer approach to equilibrium crystallization in water-rich melts. Slower cooling rates in melts with lower liquidus temperatures and less variation in fO_2 are possible explanations.

The ankaramites F22 and F23 contain clinopyroxene phenocrysts with highly magnesian cores, which, coupled with the core compositions of olivines, plot between the curves calculated for Fe/Mg partition coefficients of 0.23 and 0.27, suggesting that these large phenocrysts may have grown at lower fO_2 than cpx-oliv pairs from the other lavas. These samples have CaO > 15%, CaO/Al_2O_3 approximately equal to 2, and have between 30 and 40% phenocrysts in the mode. They are undoubtedly cumulates.

Major element fractionation trends of the Feni lavas

The mafic and alkalic phases are well separated in Al_2O_3 and MgO contents and this can be seen in the Al_2O_3 vs MgO diagram (Figure 3-6a) which shows an excellent negative correlation between these elements. The slope of this data array can best be explained by fractionation or accumulation of clinopyroxene and olivine with the former phase being predominant. The Fe_2O_3* (total Fe as Fe_2O_3) vs MgO diagram allows the separation of the Feni samples into two distinct groups. The low Fe_2O_3* group with high MgO are the group 1 phonolitic tephrites. The parental lavas F1, F11 and F12, are labeled in this figure and in each of the element-element plots. A hypothetical evolutionary sequence of lavas derived from each parent is also sketched. Each of these evolutionary trend starts at a different levels of iron enrichment, CaO, Al_2O_3 and MgO. The amount of iron enrichment achieved prior to the onset of Ti-magnetite fractionation is different in each trend.

The importance of clinopyroxene in the evolution of the Tabar-Feni rocks and the different evolutionary paths identified above can be seen on the Al_2O_3/CaO vs MgO and CaO vs MgO diagrams. The parental lavas are displaced to higher MgO values from the general trend in these figures. In both diagrams one well defined fractionation trend can be seen, and a number of separate parental, high MgO lavas. The exact direction of the early fractionation trends is difficult to

Figure 3-6

Element vs MgO diagrams for Feni lavas. Hypothetical fractionation trends are drawn for parental compositions (F11 and F12) for group 1, 2 and 3. Ni data from chapter 4 and fractionation curves in Ni vs MgO diagram are calculated by iterative subtraction using the partitioning equation of Hart and Davis (1978). Symbols as follows: Group 1 (+), Group 2 (□) and Group 3 (×). Additional data to those listed in Table 3.1 are from (Wallace et al. 1983). A dashed line shows accumulation of cpx. The evolution of group 1 is a mixing trend and not a crystal fractionation trend. Group 2 samples fractionate with the following sequence of assemblages: 1) oliv, 2) cpx+Ti-mag, 3) cpx+plag+Ti-mag, and 4) cpx+plag+amp+Ti-mag. Group 3 samples fractionate with the following sequence of assemblages: 1) oliv, 2) cpx, 3) cpx+plag+Ti-mag, and 4) cpx+plag+amp+Ti-mag.

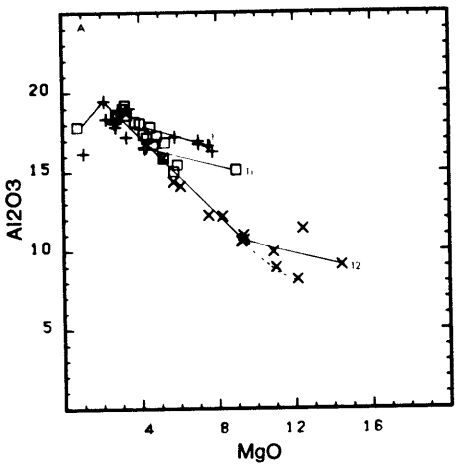
A
Al2O3
MgO

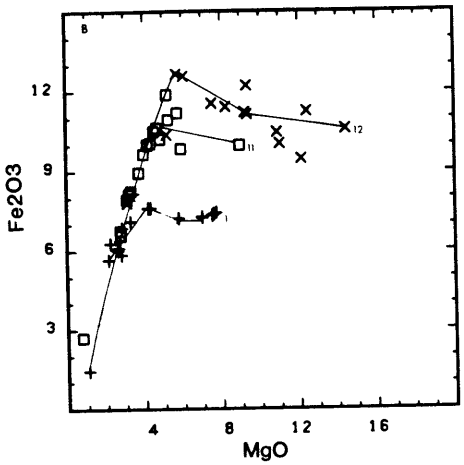
B
Fe2O3
MgO

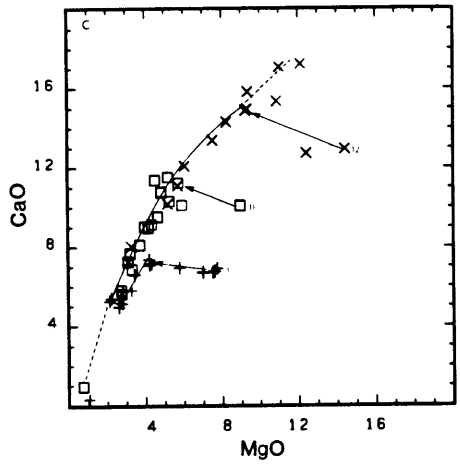
C
CaO
MgO

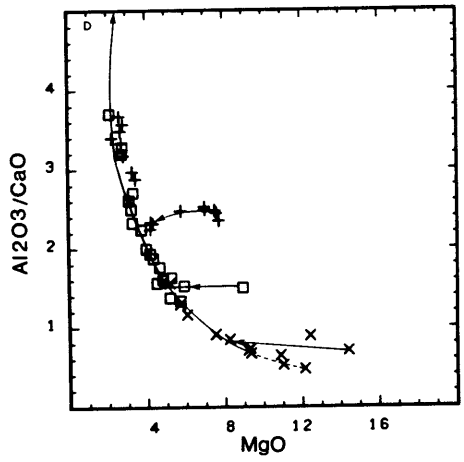
D
Al2O3/CaO
MgO

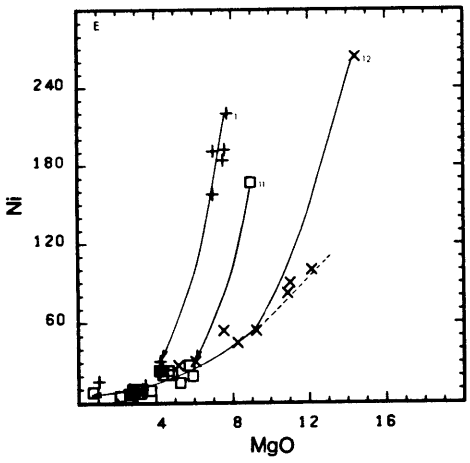
E
Ni
MgO

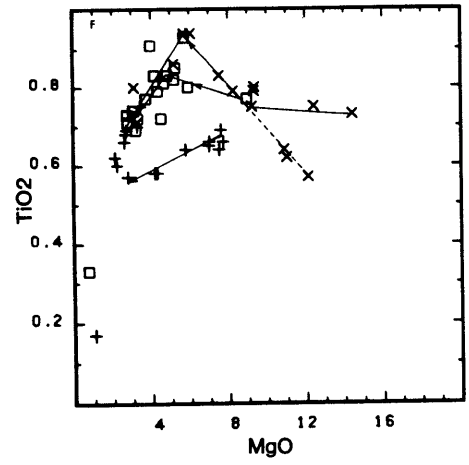
F
TiO2
MgO

discern because of the absence of intermediate composition samples between the parental magmas and the main trend. Samples F22, F23, and F24, which form an extension of the main trend are rich in large (up to 1.5 cm in length) clinopyroxene phenocrysts. These lavas have probably accumulated clinopyroxene. The clinopyroxene has lower Na, Ti and higher SiO_2 than clinopyroxenes found in other lavas, and additional studies are required before some of these ankaramites can be proven to be cumulates.

The separation of samples into groups is impossible using these types of plot if a lava has fractionated sufficiently and plots on the common evolutionary surface. The parental lavas are the only lavas with high Ni contents (Figure 3-6e) and the low Ni of most samples is common in arc suites (Ewart 1982). The Ni abundances of F11 (167 ppm) and F12 (264 ppm) are slightly lower than expected if these lavas were derived by equilibrium melting of lherzolitic mantle (Hart and Davis 1978). These lavas have undergone less than 8% olivine fractionation, assuming they have only fractionated olivine, based on the Ni content of primary lavas (Hart and Davis 1978). The parental tephritic phonolites have sufficiently high Ni contents (>190 ppm) to be primary mantle melts.

TiO_2 vs MgO (Figure 3-6f) shows similar features to the Fe_2O_3* vs MgO plot, but with different relative levels of enrichment prior to the onset of Ti-magnetite fractionation. The group 2 and 3 samples have similar evolutionary paths,

with olivine fractionation followed by olivine±clinopyroxene±Ti-magnetite. The group 3 lavas reach a higher TiO_2 content prior to the appearence of Ti-magnetite as a crystallizing phase, and this is consistent with the higher Fe enrichment of these samples.

The evolutionary paths for the different groups shown in the above figures are more clearly separated when P_2O_5, Al_2O_3, MgO, K_2O, Na_2O and CaO are plotted against SiO_2 (Figure 3-7). The increased separation results from the range of SiO_2 contents of magnetite, olivine, amphibole, clinopyroxene and plagioclase. The rough overall trends with increasing silica content are consistent with fractionation of the more mafic phases found in these porphyritic rocks. Hypothetical evolutionary paths for the three parental lavas are shown on these figures to help clarify the evolution of each group.

The initial rapid decrease in CaO and MgO, gradual decrease in TiO_2, and rapid increase in Na_2O, reflect the dominant role of clinopyroxene and the subordinate roles of olivine, Ti-magnetite and plagioclase. The dominance of clinopyroxene in alkalic lavas has been previously noted (Maaloe et al. 1986). In the group 1 lavas, clinopyroxene crystallizes in similar proportions to plagioclase and olivine, whereas in the group 2 and 3 lavas, clinopyroxene is far more abundant (F26, Table 3.2). The appearence of clinopyroxene within the fractionation assemblage occurs at different points in the evolution of the different groups.

Figure 3-7

Element vs SiO_2 diagrams for Feni lavas. Hypothetical fractionation curves and symbols as in Figure 3-6.

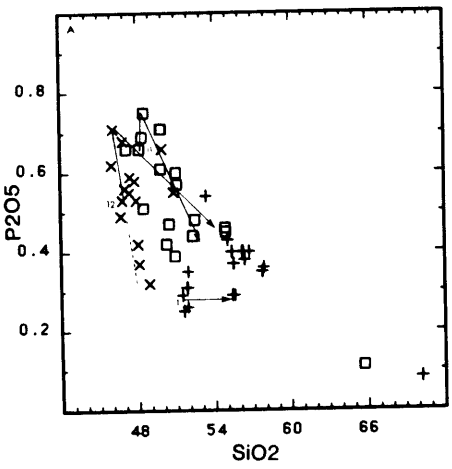
A
P2O5
0.8
0.6
0.4
0.2
48
54
60
66
SiO2

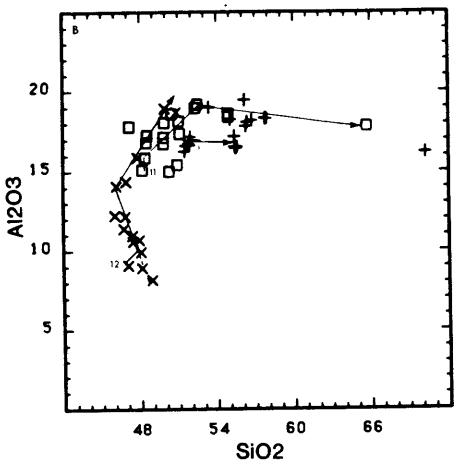
B
Al2O3
20
15
10
5
48
54
60
66
SiO2

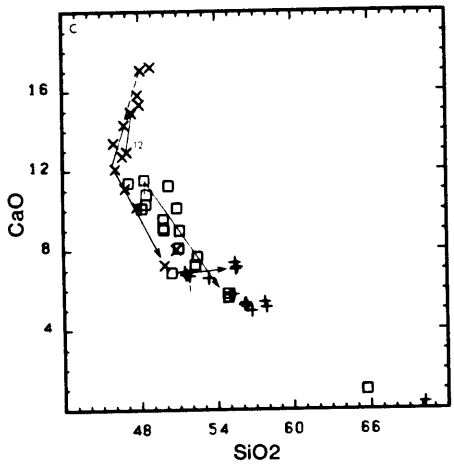
C
CaO
16
12
8
4
48
54
60
66
SiO2

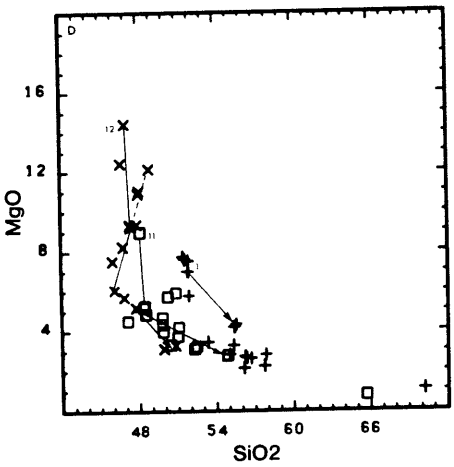
D
MgO
16
12
8
4
48
54
60
66
SiO2

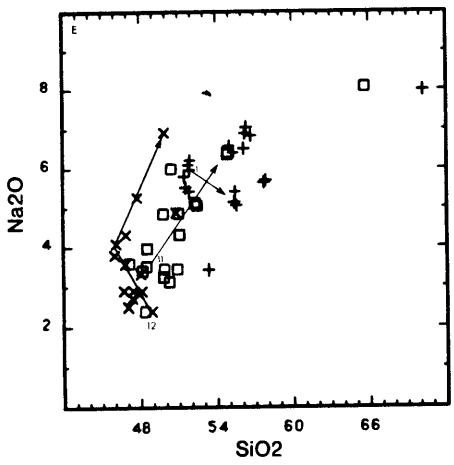
E
Na2O
8
6
4
2
48
54
60
66
SiO2

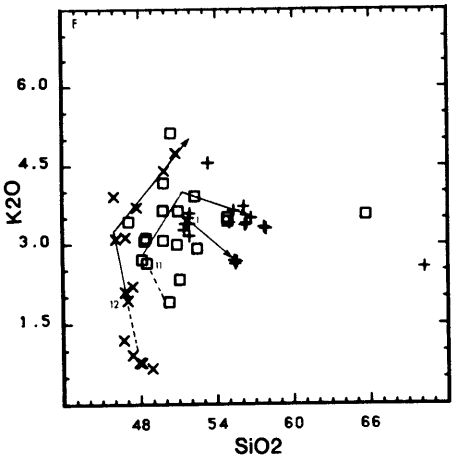
F
K2O
6.0
4.5
3.0
1.5
48
54
60
66
SiO2

Clinopyroxene fractionation is coincident with Ti-magnetite fractionation in group 2 lavas, but occurs prior to Ti-magnetite fractionation in group 3.

The gradual decrease in P_2O_5 with increasing SiO_2 results from two factors, variation in the P_2O_5 content of the parental magmas, and fractionation of apatite as inclusions within clinopyroxene in the mafic lavas. Since apatite is the only phase capable of fractionating P_2O_5, this plot can be used to examine the P_2O_5 concentration required for saturation in these lavas. The P_2O_5 content of the lavas associated with F12, which does not contain apatite in the mode, increases to reach a maximum of 0.75% and then decreases once apatite saturation occurs. F11 contains apatite in the mode and P_2O_5 decreases consistently amongst this group of lavas. The group 1 lavas (F1 to F14) show very little change in P_2O_5 contents.

Aluminum is relatively constant within each group except for the most primitive lavas and ankaramites. The phonolitic tephrites (group 1) have consistently lower Al_2O_3 (16-17%) than the other groups (18%) at similar SiO_2 contents. Al_2O_3 increases while SiO_2 initially decreases in group 3 lavas until Ti-magnetite and apatite start to fractionate, then Al_2O_3 and SiO_2 increase together until plagioclase joins clinopyroxene, magnetite, and apatite in the fractionating assemblage and the Al_2O_3 content then remains essentially constant. The appearance of amphibole and biotite as fractionating phases, depends on the alkali content of the

magma (Cawthorn et al. 1973), the water content and the pressure of crystallization (Holloway and Burnham 1972), and in general, these phases start crystallizing at a similar point to, or just after plagioclase. F11 contains olivine, Ti-magnetite and clinopyroxene phenocrysts; fractionation of this assemblage causes an increase in both SiO_2 and Al_2O_3 until fractionation of plagioclase begins.

Similar evolutionary paths are shown for the different groups on the TiO_2 vs SiO_2 diagram (not shown) as the P_2O_5 vs SiO_2 diagram and the crystallization of apatite is coupled to the crystallization of Ti-magnetite. These phases crystallize prior to plagioclase, amphibole and biotite in the group 2 and 3 lavas. The appearance of Ti-magnetite coincides with the disappearance of olivine, a coincidence that has been noted before (Grove and Baker 1984).

Normally arc rocks show a well defined positive correlation between K_2O and SiO_2 (Gill 1981) and in some instances show two well defined correlations (Gorton 1977, Whitford and Nicholls 1976). A lack of correlation, or a negative one, is usually interpreted as the result of crystal fractionation involving amphibole or biotite (Whitford and Nicholls 1976, Cawthorn et al. 1973). Although volatile contents in the rocks do not correlate negatively with K_2O contents, some rocks do show alteration of both phenocrysts and groundmass materials and this effect may be responsible for the some of the scatter. If the lavas are separated into

groups, then the scattered data on this plot separates into easily understandable fractionation sequences that are consistent with the mineralogy of the samples and previous plots. This separation is also helpful in explaining the Feni data on the CaO and Na_2O plots. The group 1 lavas show a very minor increase in CaO and a decrease in K_2O and Na_2O between F1 and F14. The only phase capable of reducing the K_2O content of the Feni samples is biotite, and this phase is not present in the group 1 lavas. This eliminates crystal fractionation of the phases present in the lavas as a process controlling the evolution of this group.

The major element evolution of the group 2 and 3 samples results from crystal fractionation/accumulation of the phases present in the rocks in the approximate proportions given by the modal abundances. The group 3 samples F22-24 have 30 to 40% clinopyroxene phenocrysts, with some euhedral crystals reaching 1.5 cm in length in some lavas. Similarly, the group 2 samples F18 and F25 appear to have accumulated some clinopyroxene.

Mixing between primitive and evolved magmas would produce linear mixing trends on oxide-oxide plots (Gill 1981); there is no evidence for this in the data from the Feni lavas. If this type of mixing did occur, then it would be easily identifiable on plots such as the Ni and Al_2O_3/CaO vs MgO. Mixing between primary melts or between different evolved lavas is difficult to detect from major element data and will also be addressed in chapter 4.

The CaO, Al_2O_3, MgO, K_2O and Na_2O vs SiO_2 plots show the evolution of the group 3 samples to be non-linear and composed of three segments which correspond to a different fractionating assemblage. The evidence against mixing controlling the major element composition of the group 2 lavas is limited and relies principally on the change of fractionation direction shown by these samples on Al_2O_3 and K_2O vs SiO_2 diagrams. Samples from this group are more widely scattered in all of the major element plots, and in most instances their evolution could be described by mixing.

Mixing effects

Textural and mineralogical evidence of mixing exists in a number of the Feni samples (F2, F3, F5, F7, F10, F14), in the form of resorbed plagioclase phenocryst cores, wide ranges in phenocryst core compositions within single samples (An 90-An 40), resorption of clinopyroxene phenocrysts, overgrowth of fluid inclusion-rich cores of clinopyroxenes by inclusion free clinopyroxene with higher Mg/Fe, reverse zoning and complex zoning of trace elements in phenocrysts (Kennedy and Shimizu unpublished data). Disequilibrium textures occur in many samples, but the importance of mixing in individual lavas and within each group can be debated. Most of the samples from group 2 show some evidence for mixing and this is especially true for the evolved lavas. The group 1 lavas (F14 and F19) have textural evidence for

mixing.

The fractionation vector between F1, and F14 and F19, in element-element plots is difficult to reconcile with any simple crystal fractionation process. The difficulty with deriving samples F14, F19, F35 from the more primitive samples F1, F6, F27 in the group 1 rocks can be assessed in two ways: 1) least squares calculation of the addition/subtraction of phases present in the lavas which are considered parental, and 2) by consideration of the major element data discussed above.

Least squares calculations with the additional constraint of closure, which is required by constant sum data (Reid et al. 1973), has been used to produce the data shown in Table 3.5. Although a reasonable mathematical fit can be obtained using the mineral compositions of phenocrysts in the rocks, none of the solutions presented are geologically reasonable considering the proportions of phases present in the lavas (Table 3.2). The mass balance suggests a fractionating assemblage that is 44% hauyne. The phenocryst phases present in F1 are olivine, clinopyroxene, plagioclase, hauyne, amphibole, Ti-magnetite and minor apatite. This diversity of phases should produce a good mathematical fit to a mass balance relationship. The solutions with a reduced number of phases are also geologically unreasonable, with the removal of olivine, amphibole and hauyne, and the addition of clinopyroxene, plagioclase and magnetite producing the best fit. This is suggestive of assimilation combined with

Table 3.5

Matrix calculation of phase proportions for fractional crystallization of F1 to F14

Rock and Mineral Compositions

	SiO_2	TiO_2	Al_2O_3	FeO	MnO	MgO	CaO	Na_2O	K_2O	P_2O_5
F1	51.94	0.70	16.74	6.70	0.19	7.67	6.83	5.56	3.42	0.25
F14	55.82	0.58	16.69	6.91	0.16	4.23	7.43	5.19	2.70	0.29
Ti-mag	0.15	7.50	2.58	85.4	1.0	2.65	0.06	0.0	0.0	0.0
Cpx core	52.61	0.21	1.49	3.61	0.06	17.01	24.11	.27	0.0	0.0
Cpx rim	51.14	0.50	2.16	8.92	0.50	12.76	23.39	1.02	0.0	0.0
Plag core	56.46	0.0	26.73	0.53	0.0	0.0	9.09	5.85	0.47	0.0
Oliv core	40.69	0.04	0.04	7.27	0.13	51.37	0.08	0.0	0.0	0.0
Oliv rim	39.14	0.04	0.04	17.99	0.75	42.54	0.36	0.0	0.0	0.0
Amp	40.06	2.48	13.67	10.33	0.12	14.64	12.67	2.9	1.17	0.07
Hauyne	33.81	0.0	28.77	0.26	0.0	0.0	3.28	18.43	0.64	0.14
Apatite	.039	0.05	0.0	0.85	0.14	0.41	53.04	0.37	0.01	40.3
Standard Deviations										
	.04	.02	.03	.03	.01	.06	.03	.06	.02	.002
Calculated Composition										
F1	52.38	0.61	16.71	7.00	0.17	6.25	7.11	5.91	2.31	.25

Calculated Proportions

F1	Ti-Mag	Cpx core	Cpx rim	Plag core	Oliv core	Oliv rim	Amp	Hauyne	Apat	F14
χ^2=0.3	*0.0	.00002	.0043	.0004	.0043	.041	.054	.083	~0	.813

*Proportions constrained to be positive and sum to 1.0

crystal fractionation, however the major element differences between F1 and F14 requires removal of clinopyroxene and the proportions of components are inconsistent with the assemblages of the lavas. A similar conclusion can be derived from the Al_2O_3 and MgO differences of F1 and F14. F14 has lower Na_2O, K_2O and TiO_2, and higher SiO_2, Fe_2O_3* and CaO than F1 (Table 3.1) but identical Al_2O_3. This requires that the removal of olivine, clinopyroxene and amphibole, or some combination of these phases, be exactly balanced by the addition of a plagioclase, k-feldspar and feldspathoids assemblage. Without an extremely fortuitous balance of the proportion of phases (which is nothing like the present mode of either rock) it would be impossible to derive F14 from F1 by crystal fractionation.

In conclusion, it can be stated that mixing is an important process in the evolution of some of the moderately evolved group 1 lavas (F14, F19, F34). Mixing cannot be identified in the group 3 lavas with the available major element data.

Projections

The evolution of the Feni lavas can be followed by examining the distribution of the rocks from the different groups when projected into the pseudoquarternary system oliv-diop-plag-neph (Sack et al. 1987). This projection scheme is based on anhydrous, 1 atm, QFM experiments and it

is not truly applicable to the Tabar-Feni magmas which have a wide range of water contents, variable fO_2 and crystallize amphibole, biotite and water-rich feldspathoids. However, this is the best available projection scheme for undersaturated rocks and valuable information can be obtained by a general analysis of the projection of the Feni rocks.

The projection scheme works well for most samples, although the plotting position is sensitive to both the sodium content and Fe^{2+}/Fe^{3+} ratio, for example, the highly evolved plagioclase-rich rocks F10 and F21 plot in the high pressure region on the oliv-diop-neph plot. The measured Fe^{3+}/Fe^{2+} has been used where possible for all projections. If Fe^{3+}/Fe^{2+} was not known, Fe^{3+}/Fe^{2+} was taken as 0.15. The 1 atm olivine+clinopyroxene+plagioclase saturated experimental glasses from experiments on a Lihir lava (78LH1) form well defined trends towards the nepheline apex, with decreasing temperature on the oliv-diop-neph projection and towards plagioclase on the oliv-plag-diop projection. This projected saturation surface parallels the multiple saturation surface of the experiments of Mahood and Baker (1986) on sample 38, an undersaturated lava from Pantelleria, but is offset to higher olivine proportions as a result of the higher MgO content of 78LH1 and slightly higher fO_2. Experiments at fO_2 close to the Ni-NiO buffer have higher Fe^{3+}/Fe^{2+} and calculated olivine proportions, and their positions in this projection can be used to infer that the trend shown by the QFM fO_2 experiments is simply translated

toward the olivine apex at higher oxygen fugacities.

The three projected oliv+cpx+plag multiple saturation surfaces discussed in the previous paragraph show systematic differences from the saturation surface of Sack et al. (1987), however this is to be expected as bulk compositional differences in MORB experiments (Walker et al. 1979, Grove and Bryan 1983, and Tormey et al. 1987) produce both displacement and crossing of the oliv-cpx-plag multiple saturation surfaces in the oliv-plag-cpx-qtz pseudoquarternary of Walker et al. (1979).

Prior to examination of the Feni samples using the Sack et al. (1987) projection scheme, it is informative to examine some other undersaturated suites from continental, oceanic and arc settings. The suites plotted in Figure 3-8 are the Alligator Lake (AL) volcanics (Eiche et al. 1987), the Honolulu volcanic series (HVS) (Clague and Frey 1982) and the M and C series lavas from Grenada (Thirwall and Graham 1984). The AL and HVS were chosen because they contain a large number of primary magmas that are isotopically homogeneous and thus constrain melt generation fields for undersaturated lavas. The AL samples represent magmas generated at different depths (Eiche et al. 1987) and these samples should define the effects of pressure on the primary magma projection positions while the HVS should show the effect of changing degree of melting.

On the oliv-diop-neph projection the AL samples generated at different pressures plot as a small tightly

Figure 3-8

Olivine-Plagioclase-Diopside (a) and Olivine-Diopside-Nepheline (b) projections of the pseudo-quarternary projection scheme of Sack et al. (1987). Hypothetical fractionation trends based on the 1 atm experiments of Sack et al. (1987) (S), and Kennedy et al. (1987) (K) are shown in (a). The 1 atm, QFM and Ni-NiO, olivine + high Ca pyroxene + plagioclase multiple saturation surfaces of Sack et al. (1987) (S), Mahood and Baker (1986) (M&B), and Kennedy et al. (1987) (K), are shown in (b) along with the fields for undersaturated lavas. Fields are for the (M) and (C) series lavas from the Lesser Antilles, the Honolulu Volcanic Series (HVS) and the Alligator Lake Complex (AL) (Arculus 1976, Thirwall and Graham 1984, Clague and Frey 1982, Eiche et al. 1987).

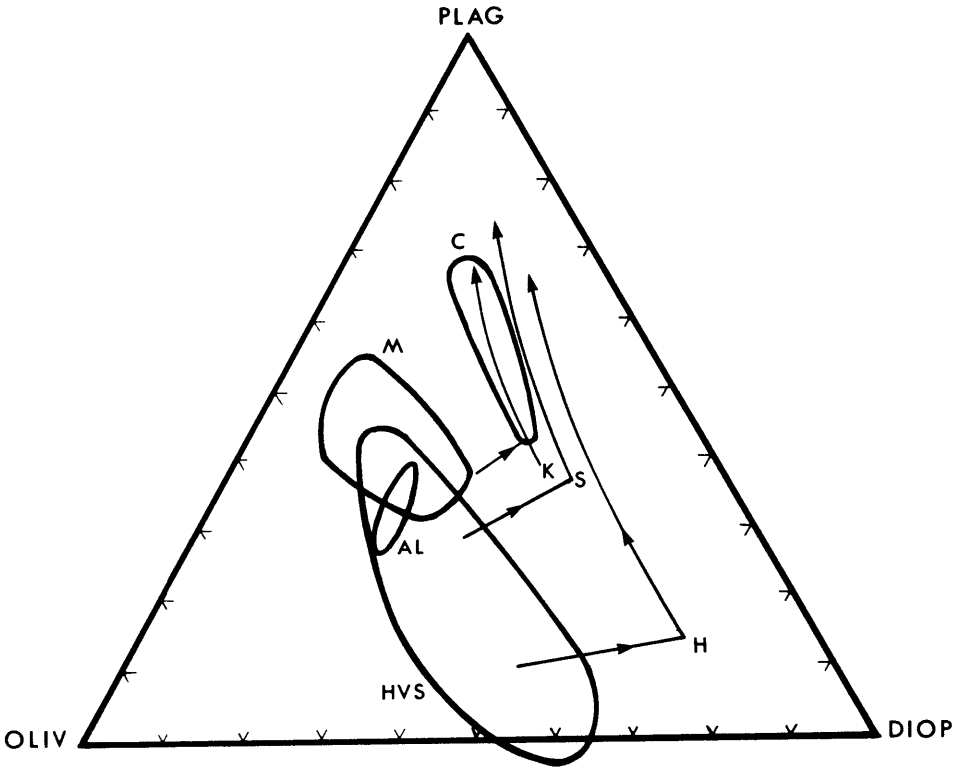
PLAG
C
M
K
S
AL
H
HVS
OLIV
DIOP

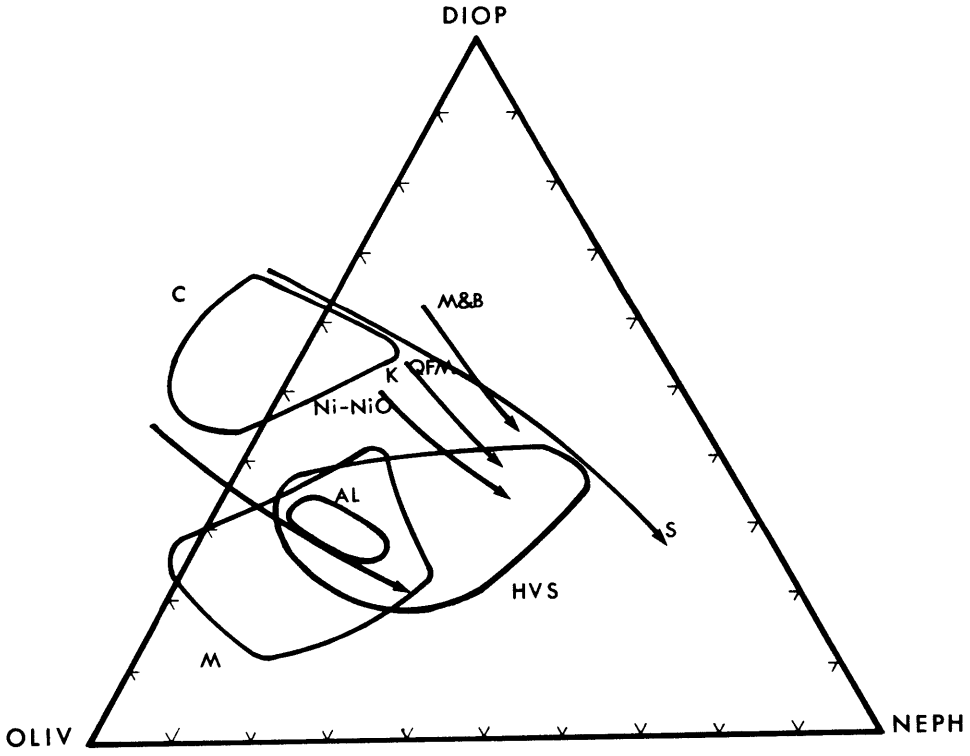
DIOP
C
M&B
K
QFM
Ni-NiO
AL
S
HVS
M
OLIV
NEPH

clustered group close to the high pressure oliv-opx-cpx multiple saturation surface suggested by Sack et al. (1987). In contrast, the HVS samples define a band between the high pressure and low pressure multiple saturation surface, with the nephelinites and melilitites plotting closest to the 1 atm boundary. The M-series from Grenada, which are the samples used to model mantle melting by Minster and Allegre (1978), scatter widely about the high pressure surface, while the C-series, which show the low Ni contents characteristic of arc lavas, plot as a group close to the QFM 1 atm boundary near the oliv-diop edge of the projection and have undergone substantial olivine fractionation prior to reaching multiple saturation at low pressure.

When these different series are projected onto the oliv-plag-diop face of the pseudoquarternary system, they fall into two distinct groups. The AL, HVS and M-series lavas define an elongate field representing primary mantle melts and the C-series lavas fall along the 1 atm multiple saturation surface. The AL and M-series lavas form fairly small fields in comparison to the HVS field, and it is apparent that variations in the degree of melting produce drastic changes in the bulk composition of the generated magma, relative to the effect produced by differences in pressure. Several hypothetical fractionation paths are shown on this projection. The olivine fractionation lines connecting the M- and C-series Grenada volcanics only shows a general evolutionary trend, as these two series cannot be

related by simple crystal fractionation (Thirwall and Graham 1984).

The group 1 Feni samples do not define a single trend and plot as two distinct groups in the oliv-diop-neph projection (Figure 3-9a). The primitive sample (F1) falls in between the low pressure multiple saturation curves and the primary melt field, close to the HVS field. The unusual major element composition of these phonolitic tephrites is not matched by any of the previously discussed primary melts (AL, HVS, M) and these melts are considered primary, even though they are outside this field.

The evolution of the group 1 samples in the oliv-plag-diop projection (Figure 3-9b) is initially towards the plagioclase-diopside edge and away from olivine, and this results in a constantly decreasing oliv/cpx ratio on projection through plagioclase. The plotting positions then move towards the olivine-plagioclase edge and these more evolved samples plot with larger projected olivine proportions. As the compositions approach plagioclase, the amount of calculated nepheline decreases and the relative proportions of clinopyroxene and olivine increase, since the decrease in calculated proportions of these phases is less than the decrease in nepheline. The plotting position is sensitive to relatively small variations in bulk composition for evolved samples, especially phenocryst-rich lavas that have variable Fe^{3+}/Fe^{2+}.

The oliv-diop-neph projection is better at showing the

Figure 3-9

Group 1, 2 and 3 samples from the Feni islands projected into the Olivine-Plagioclase-Diopside and Olivine-Diopside-Nepheline projections of Figure 3-8. Fields and multiple saturation surfaces as for Figure 3-8. Fields for amphibole (A) and biotite (B) as analyzed in the Feni lavas. Hypothetical fractionation trends are shown for each group. In addition, evolved samples and qtz-trachytes are shown on the group 1 and 2 diagrams. Parental samples F1, F11 and F12 are labeled.

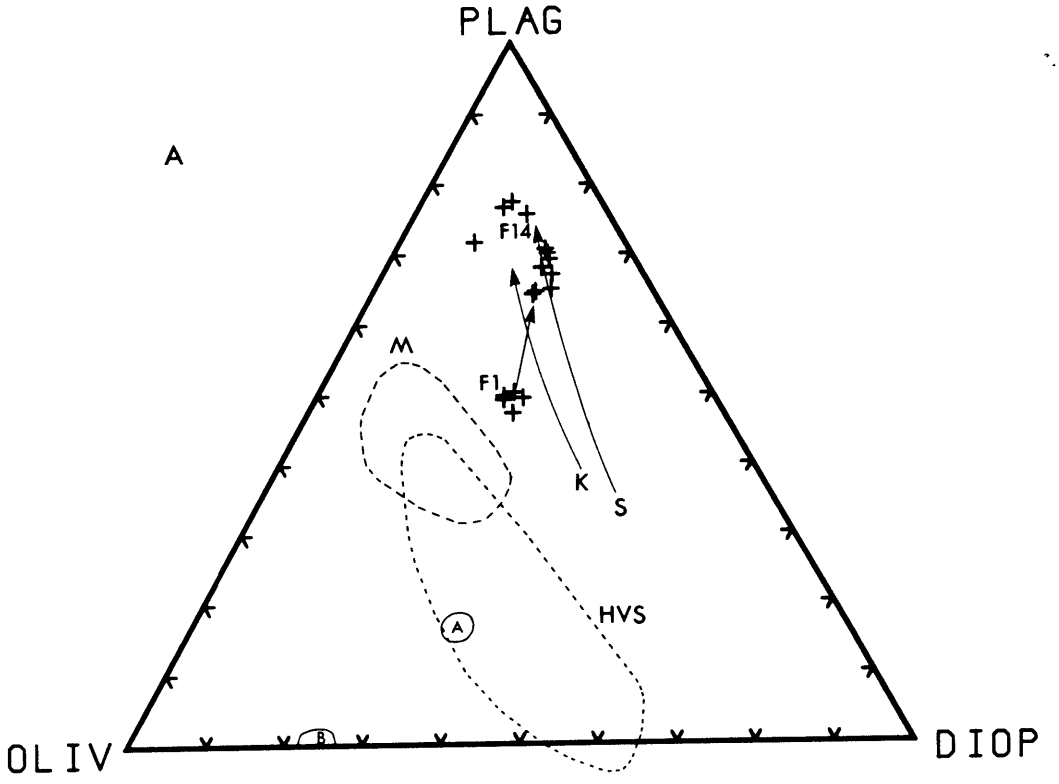
PLAG
A
F14
M
F1
K
S
HVS
A
B
OLIV
DIOP

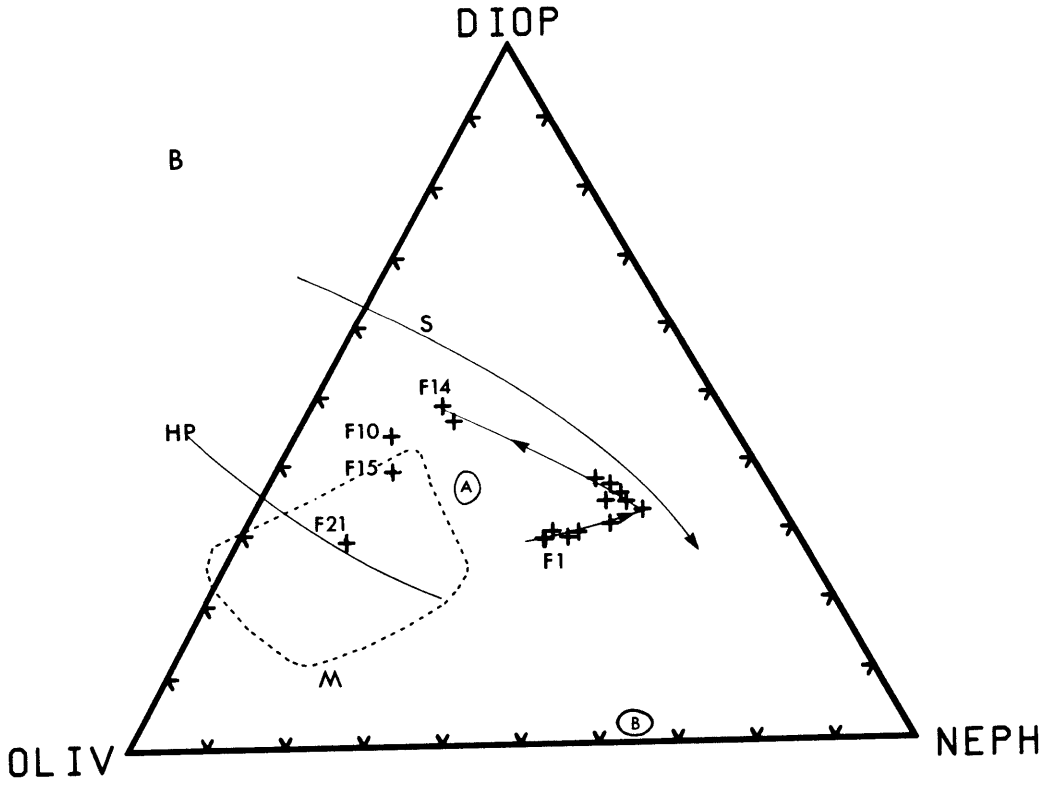
DIOP
B
S
F14
HP
F10
F15
A
F21
F1
M
B
OLIV
NEPH

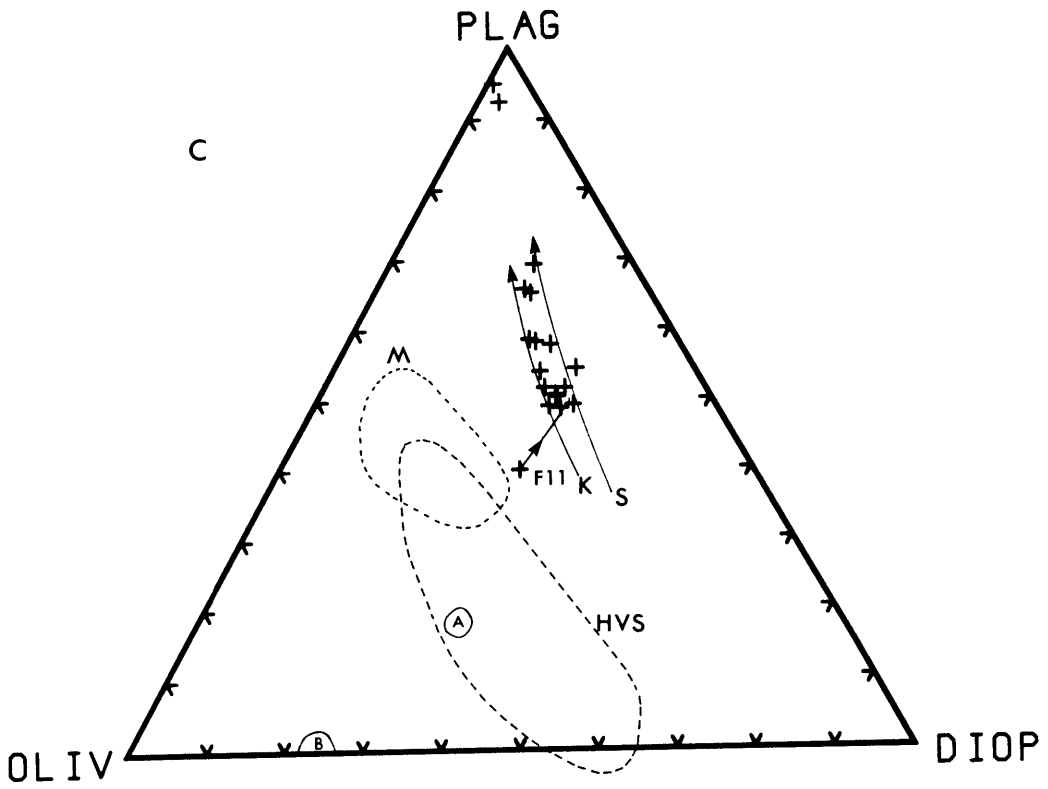
PLAG
C
M
F11
K
S
A
HVS
B
OLIV
DIOP

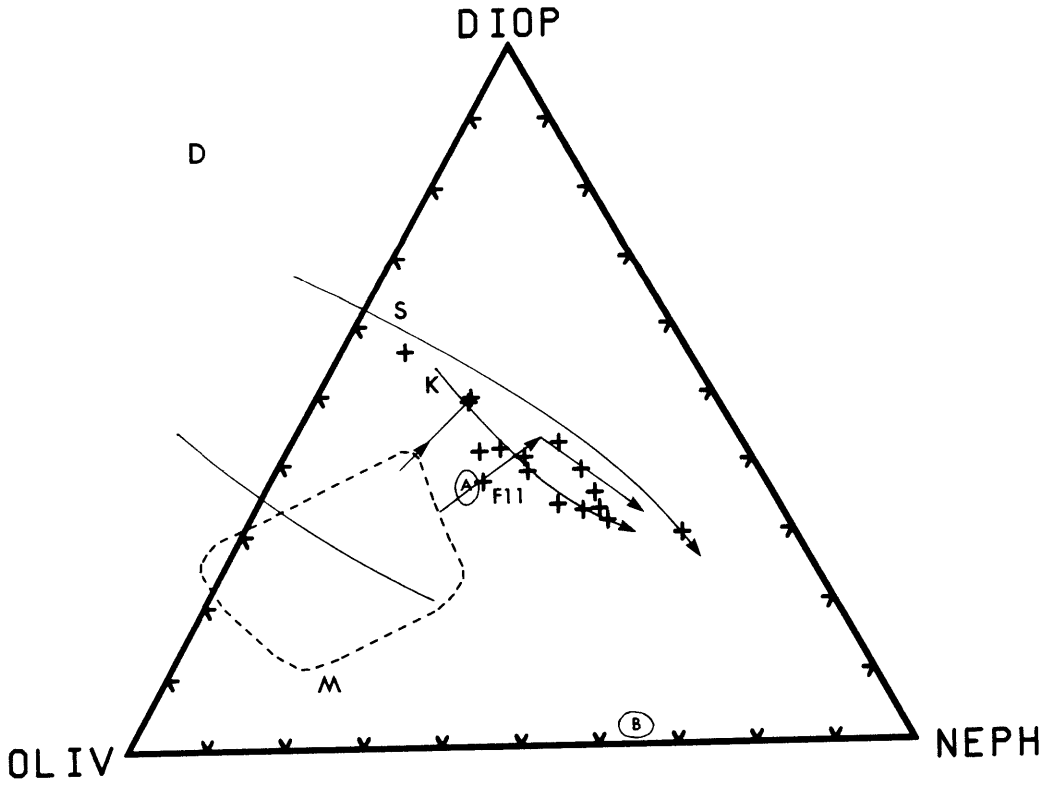
DIOP
D
S
K
A
F11
M
B
OLIV
NEPH

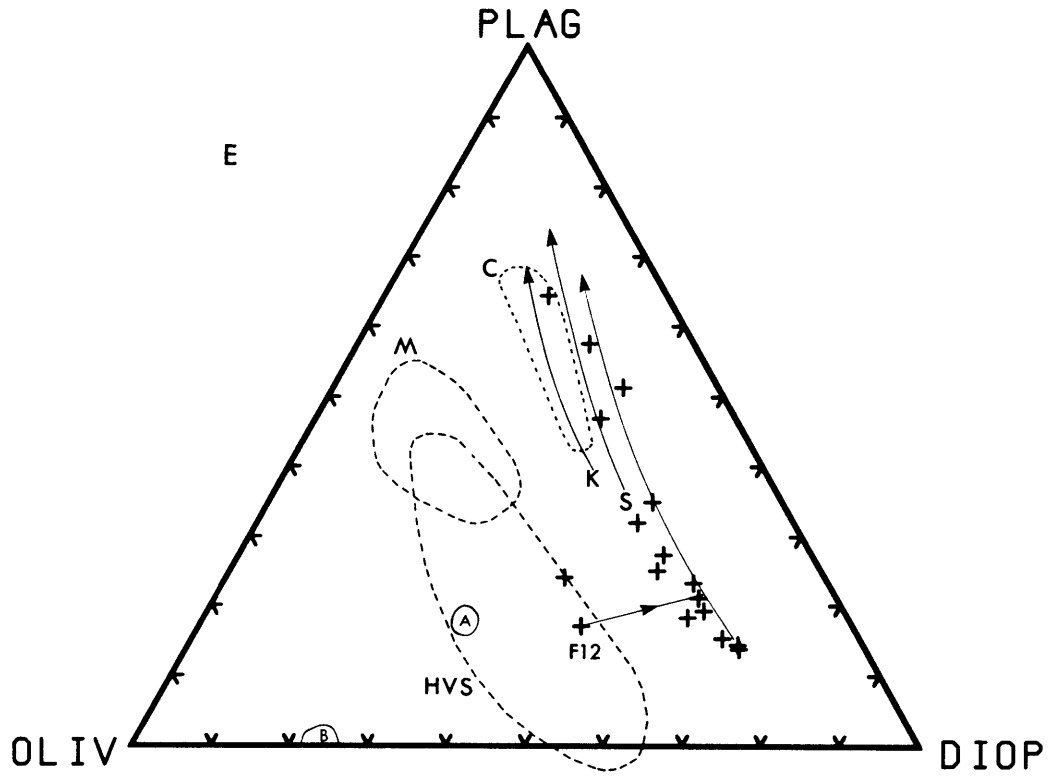
PLAG
E
C
M
K
S
F12
A
HVS
B
OL IV
DIOP

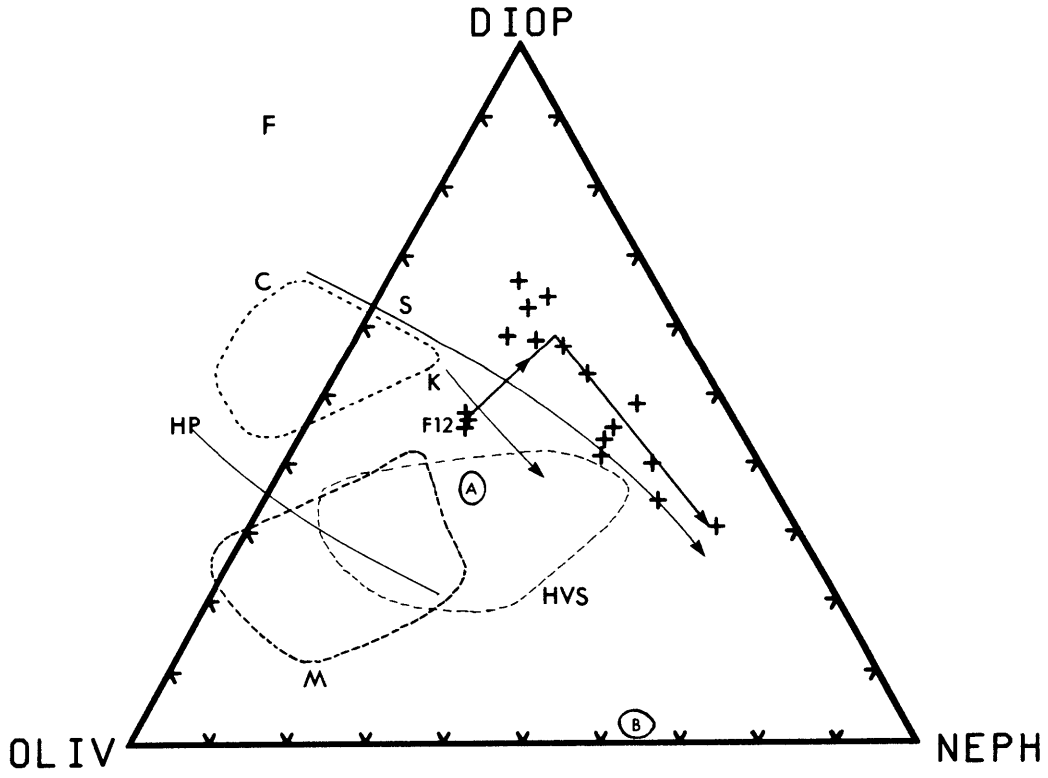
DIOP
F
C
S
K
F12
HP
A
HVS
M
B
OL IV
NEPH

evolution of the group 1 samples, the difference between groups 2 and 3, and the breakdown of the projection scheme for highly evolved samples. In this projection, the primitive to moderately evolved group 1 samples plot as a linear array that trends away from olivine and at right angles to the 1 atm, QFM and Ni-NiO multiple saturation surfaces previously described. F14 and F19 which appear to be part of this evolutionary sequence on oxide-oxide plots, project to lower nepheline and higher diopside contents, in a less evolved, higher temperature region of the projection. The drastic difference between F1 and F14 reflects an increase in SiO_2 content due to magnetite fractionation and mixing as previously discussed. The most evolved Feni lavas have also been included in this plot and these tephritic phonolites and trachyandesites (F10, 15, 21) plot close to the olivine apex in the high pressure region of the oliv-diop-neph projection, as a result of their highly evolved plagioclase-rich compositions.

The dominance of clinopyroxene during fractionation of the Feni lavas is best seen using the oliv-plag-diop projection (Figures 3-9a and 9e). The rocks from groups 2 and 3 form fairly well defined sub-linear trends which are parallel to one another and close to the plagioclase-diopside edge of the ternary. The fractionation vector described by these trends is almost directly away from the clinopyroxene apex, as would be expected if the fractionating assemblage was dominantly clinopyroxene. Samples F11 and F12 are offset

toward the olivine apex from these trends, and fall in or close to the field of primary mantle melts. The fractionation sequences that start from these samples are the same ones that were shown on the oxide-oxide plots and pass through the same sequence of points. The general evolution of both groups is olivine crystallization and removal until the melt reaches the above mentioned multiple saturation surface and then along this surface toward plagioclase, and then, for the highly evolved feldspar-rich samples the fractionation trend is toward the olivine-plagioclase edge, close to plagioclase.

The group 2 and 3 samples show similar fractionation trends in different regions of the oliv-diop-neph projection. The inferred multiple saturation surface for the group 3 samples is much closer to the diopside-nepheline edge of the triangle than any of the experimental surfaces, and the inferred multiple saturation surface for the group 2 lavas is on the Ni-NiO multiple saturation surface of 78LH1 and the extension of this surface toward the nepheline apex and the reaction point described by Sack et al. (1987). Thus, the 3 groups plot in different regions in the projections. The plotting positions of the evolved samples from group 2 are not consistent with the simple fractionation curve drawn on the oliv-diop-neph projection. They do not plot in a down temperature sequence based on their MgO and CaO contents, and this may result from mixing or from increased fractionation of Ti-magnetite moving the evolved

lavas to less undersaturated compositions and reversing the direction of fractionation on this plot. Some of the group 2 lavas may be: 1) mixtures of a primary lava similar to F12 and a moderately evolved magma from groups 2 or 3, 2) a mixture of a moderately evolved lava and one of the evolved lavas that plot towards the oliv-diop edge, or 3) samples initially evolved by fractionation towards a nepheline rich composition and later away from nepheline. The first alternative can be eliminated as the element-element diagrams have shown that mixing between evolved and primitive magmas has not occured.

The different positions of the multiple saturation surfaces of groups 2 and 3 could be interpreted as the effect of: 1) variation in the pressure at which fractionation occurs, 2) expansion and contraction of the primary phase volumes of olivine, clinopyroxene and plagioclase with changes in the partial pressure of H_2O and CO_2, and 3) differences in fO_2 during crystallization.

With increasing water content or pressure, clinopyroxene stability is enhanced and the appearance of plagioclase is suppressed (Graham 1980, Spulber and Rutherford 1983). In general higher pressure reduces the primary phase volume of olivine (Stolper 1980, Takahashi and Kushiro 1983), however an increase in H_2O has the opposite effect (Kushiro 1972b). most of the Feni lavas with H_2O <1.5% have CaO/Al_2O_3 <1.1 (Figure 3-11); the possiblity of the observed difference in the projections resulting from differences in water

Figure 3-10

Fe^{2+}/Fe^{3+} vs MgO for the Feni lavas with a fitted regression line. Data from Heming (1979) and Wallace et al. (1983).

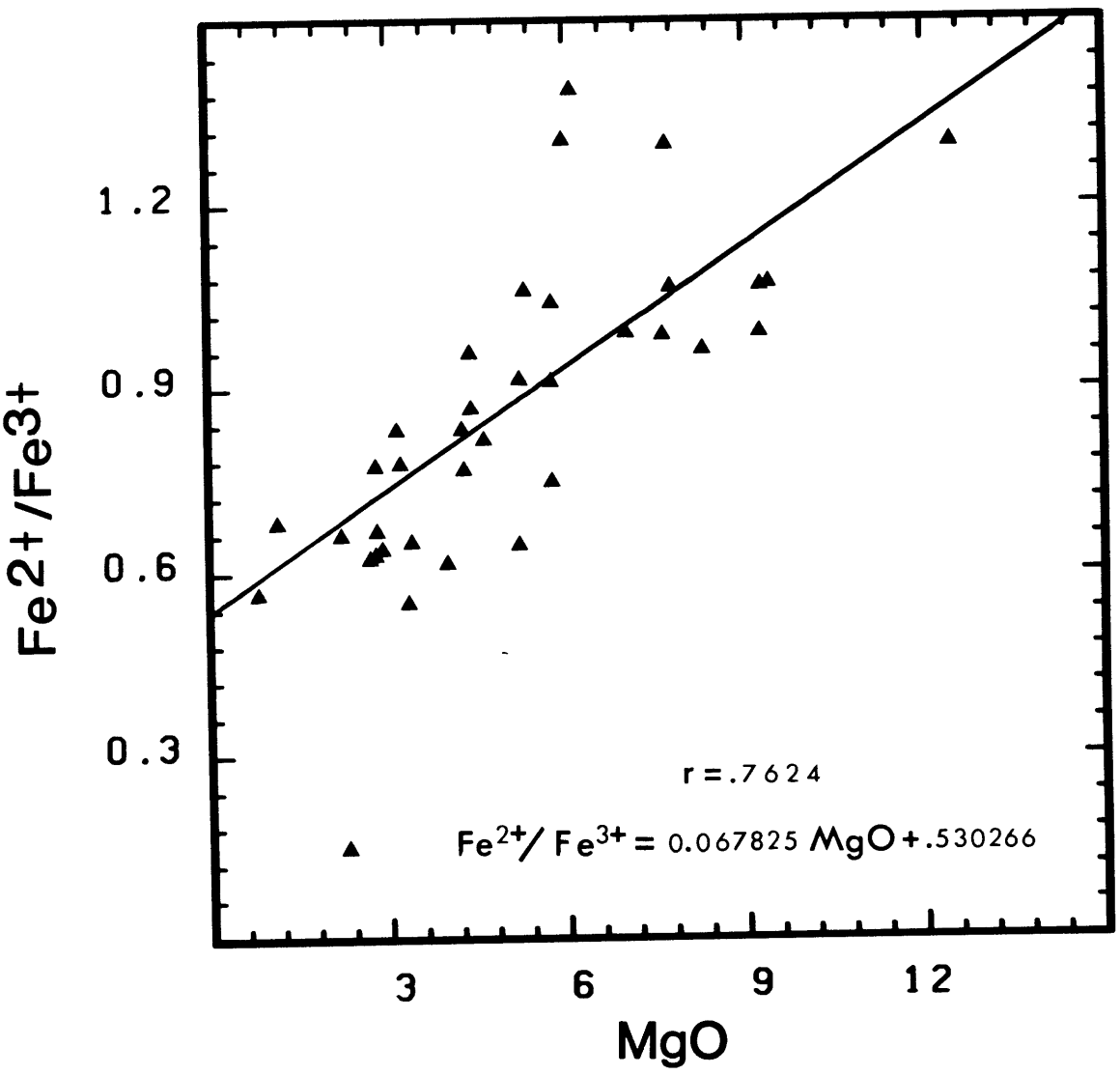
1.2
0.9
0.6
0.3
Fe2+/Fe3+
r=.7624
Fe2+/Fe3+ = 0.067825 MgO+.530266
3
6
9
12
MgO

contents can be examined using this plot. Although the more calcic group 3 lavas have high water contents, the group 2 lavas show similar enrichment of H2O. The two groups are not separated using this criteria. Enrichment could result from changes in H_2O contents upon eruption, or by alteration after eruption, and cannot be used to disprove this possibility. Since the multiple saturation surface for the group 3 lavas projects on the diopside side of the QFM data and it is unlikely that highly reducing conditions would exist in these arc lavas during crystallization, the position of this saturation surface reflects the higher CaO of group 3.

Spinel (Ti-magnetite) is a liquidus or near liquidus phase in undersaturated lavas if fO_2 is high (>Ni-NiO), and this is a major influence on the development of the iron enrichment trends characteristic of some suites (Humphries 1980, Grove and Kinzler 1986). Differences in fO_2 between the groups is undoubtedly responsible for some of the separation of the multiple saturation surfaces. The group 2 lavas have higher modal abundances of Ti-magnetite than the group 3 lavas which contain little or none of this phase (Table 3.2). The group 3 lavas attain the maximum enrichment of Fe_2O_3* and TiO_2 of any of the Feni lavas, and in general have higher Fe^{2+}/Fe^{3+} ratios, both measured (Figure 3-10) and calculated from olivine melt equilibria. Olivines in the mafic group 2 lavas are more magnesian than those in the group 3 lavas. All of these facts are consistent with the

group 2 lavas crystallizing at higher fO_2.

Different proportions of phases in the fractionating assemblage would also change the residual liquid compositions (Grove and Baker 1984). The group 3 lavas all plot in the diopside field of Sack et al. 1987 in the oliv-diop-neph projection and this could be explained by accumulation of clinopyroxene. This hypothesis is supported by the abundance of clinopyroxene in the lavas. Undoubtedly some of the samples which plot closest to the diopside apex have accumulated some cpx. However, F12, which has a major element composition that would make it an ideal parent for this group, has less than 2% cpx and 12% oliv phenocrysts. If olivine is the only phase crystallizing from this melt, it would evolve to an ankaramitic composition.

Constraints on the conditions of fractionation in the Feni lavas

The 3 groups of lavas appear to have evolved under different conditions, and this will be examined in closer detail in this section. Pressure, fO_2 and H_2O contents control the order of appearance of olivine, plagioclase, spinel, clinopyroxene and amphibole in undersaturated lavas and the resultant fractionation trends. At 1 atm pressure, and fO_2 less than Ni-NiO, the first phase on the liquidus in systems with low H_2O (<1%) is usually olivine for alkali basalts and basanites (Graham 1980, and Mahood and Baker

1986, Maaloe et al. 1986, Sack et al. 1987). However, if the sample has high Al_2O_3 or CaO content, the first phase on the liquidus may become respectively plagioclase (Baker and Eggler 1983) or clinopyroxene (Graham 1980). Undersaturated rocks also normally contain CO_2, Cl, F, and S, and each of these has an effect on the stabilty of olivine, plagioclase, clinopyroxene, amphibole, phlogopite, and which feldspathoid crystallizes in an undersaturated lava.

Pressure of crystallization

A number of general constraints can be placed on the likely pressure of crystallization of magmas from the different groups. The existence of amphibole and biotite in some lavas is suggestive of higher pressures in H2O-rich melts, although the presence of amphibole in 1 atm experiments (Mahood and Baker 1986) may limit the applicability of this statement for undersaturated rocks with high F contents that may stabilize Fluor-amphiboles (Troll and Gilbert 1974). The amphiboles from Feni were not analyzed for F, so this possibility cannot be ruled out. However, as discussed below, there is additional evidence for crystallization pressures greater than 1 atm.

Clinopyroxenes in the Mahood and Baker (1986) experiments on undersaturated lavas have average Al^{VI} of 0.023 for 1 atm experiments and 0.13 in the 8 kbar experiments; this is typical of clinopyroxenes at elevated

pressures (Thompson 1974, Tormey et al. 1987). Cpx from the Feni lavas have low to moderate Al^{VI} for the Mg-rich cores of cpx phenocrysts, and the highest values (.05-.08) occuring in cpx-rich basalts and ankaramites. This could result from: 1) crystallization at slightly higher pressures, 2) differences in melt chemistry, 3) water depolymerizing the melt and affecting the activity of Al^{VI} or 4) kinetic effects during growth of the clinopyroxene. In this instance, it is believed to be a pressure effect, as samples with both low and high water contents have high Al^{VI} (F3, F11), samples with extremely homogeneous phenocryst composition (F11, F22) have consistent but different Al^{VI} contents and samples with different compositions show a variety of Al^{VI} contents (Tables 3-3 and 3-4). The plagioclase, clinopyroxene and amphibole cumulate nodule F13 contains clinopyroxenes with Al^{VI} contents of 0.05-0.065, this is within the abovementioned range and consistent with moderate pressure crystallization.

The variation in Al^{VI} contents between samples can be explained by polybaric crystal fractionation in this suite of samples at pressures less than 8 kbar and probably between 5 kbar and 1 atm. Although the differences are small, the group 2 clinopyroxenes usually have higher AL^{VI} than those from groups 1 and 3 (Table 3.4). This is permissive of the interpretation that crystallization occured at higher pressures or under different conditions. The higher proportions of cpx in the initial fractionating assemblages

for the group 2 samples is consistent with crystallization at pressures greater than 1 atm.

Temperature

The application of geothermometers is difficult under most circumstances and even more difficult for undersaturated lavas like those from the Tabar-Feni islands. These lavas do not have coexisting ilmenite and magnetite, or clinopyroxene and orthopyroxene, and this eliminates the use of some of the more reliable geothermometers, for example Spencer and Lindsley (1981) or Lindsley and Andersen (1983). These lavas have variable water contents, pressure, fO_2 dis-equilibrium textures, as well as complex zoning, and this presents additional difficulties to those that exist normally in geothermometry, i.e., the attainment of equilibrium and calibration.

The usefulness of geothermometry is further reduced by, calibration on anhydrous, low fO_2, low pressure, experimental systems and the high fO_2 of crystallization of the water-rich Feni lavas. Temperatures derived from phenocrysts are difficult to interpret and the choice of a melt composition is impossible in phenocryst-rich lavas. Temperatures were calculated with the geothermometers of Nielson and Dungan (1983) as a simple test of the application of geothermometry to undersaturated arc lavas. These geothermometers are based on a melt structural model similar to that introduced by

Bottinga and Weill (1972) and the results are given in Table 3.6. These thermometers were used as they produced more consistent results when applied to the experiments on sample 78LH1 from Lihir, and the experiments of Mahood and Baker (1986) and Sack et al. (1987).

As expected, the results are poor. Some of the problems observable in the data are: 1) higher temperatures for more evolved lavas than the primitive lavas in group 1, 2) temperatures up to 1400°C from plagioclase in evolved lavas, 3) higher temperatures for plagioclase laths than the earlier crystallizing clinopyroxene, 4) many of the calculated temperatures are higher than the temperature for anhydrous 1 atm experiments of similar composition (see chapter 1), and 5) calculated temperatures for amphibole bearing lavas (F1, F2, F3, F5) are, apart from one or two instances, higher than the upper stability limit (approx. 1050°C) for hydroxy amphibole at 2 kb (Wendlandt and Eggler 1980).

Oxygen fugacity

The Tabar-Feni rocks, like most arc rocks, have relatively high fO_2 (Ewart 1981, Johnson et al. 1985). Olivine is more magnesian than would be predicted using an Fe^{2+}/Mg partition coefficient of 0.3, unless there is a high Fe^{3+}/Fe^{2+} ratio present in the melt during crystallization. The high calculated Fe^{3+}/Fe^{2+} ratios in amphibole (Wallace et al. 1983) and clinopyroxene (Table 3.4) indicate high

Table 3.6

	Calculated Temperatures (C°)			
	Olivine	Plagioclase	Clinopyroxene	Ti-magnetite
Group 1				
F1	1230-1280	1060-1120	1000-1080	1120
F14	1160-1175	1160-1400	1043-1111	
Group 2				
F11	1177-1187		990-1070	1162-1163
F26		1098-1160	1023-1065	1065-1132
F3		1114-1200	1020-1058	1074-1090
F5		1145-1174	1030-1125	1162-1165
F7		1114-1200	860-900	1070-1083
Group 3				
F12	1082-1391	969-980 gm	920-1060	970-1060 gm
F22	1282	960-1040		
F23	1245-1250	960-1050		

Fe^{3+}/Fe^{2+} during crystallization. Measured Fe^{3+}/Fe^{2+} values of greater than 1.0 in the lavas, a lack of iron enrichment in the lavas, and the early appearance of Ti-magnetite as a phenocryst phase, all indicate high oxygen fugacity during crystallization. None of the Feni lavas have developed a Eu anomaly (Figure 4-2) and this is further indication of a high fO_2 during crystallization (Drake and Weill 1975).

The primary Fe^{3+}/Fe^{2+} ratio for the individual Feni lavas cannot be accurately assessed, as this ratio changes during crystallization or ascent of the magma (Christie et al. 1986, Carmichael and Ghiorso 1986) or during post eruptive equilibration in a water rich magma (Gill 1981) or by alteration (Feigenson et al. 1983, Chen and Frey 1985). This ratio is also dependent on the bulk composition of the magma (Mysen et al. 1984, Dickenson and Hess 1985), the oxidation rate of ferrous iron to ferric iron (Candela 1986), the pressure of crystallization (Mysen and Virgo 1985) and the possibility of assimilation of materials with different Fe^{3+}/Fe^{2+} ratios. Minor changes in this ratio may result from disassociation of H_2O (Foley et al. 1986), degassing and introduction of fluids into the magma chamber (Luhr and Carmichael 1985, Taylor et al. 1983).

Some late stage variation in the Fe^{3+}/Fe^{2+} ratio of the Feni lavas is expected to result from the above processes, however the high fO_2 cannot be denied. A high Fe^{3+}/Fe^{2+} ratio is often found in freshly erupted arc lavas with low water contents (Johnson et al. 1985). The Fe^{2+}/Fe^{3+} ratio

Figure 3-11

H_2O vs CaO/Al_2O_3 for the Feni lavas.
Additinal data as for Figure 3-10. Symbols are:
(●) Feni lavas, (▲) all other islands.

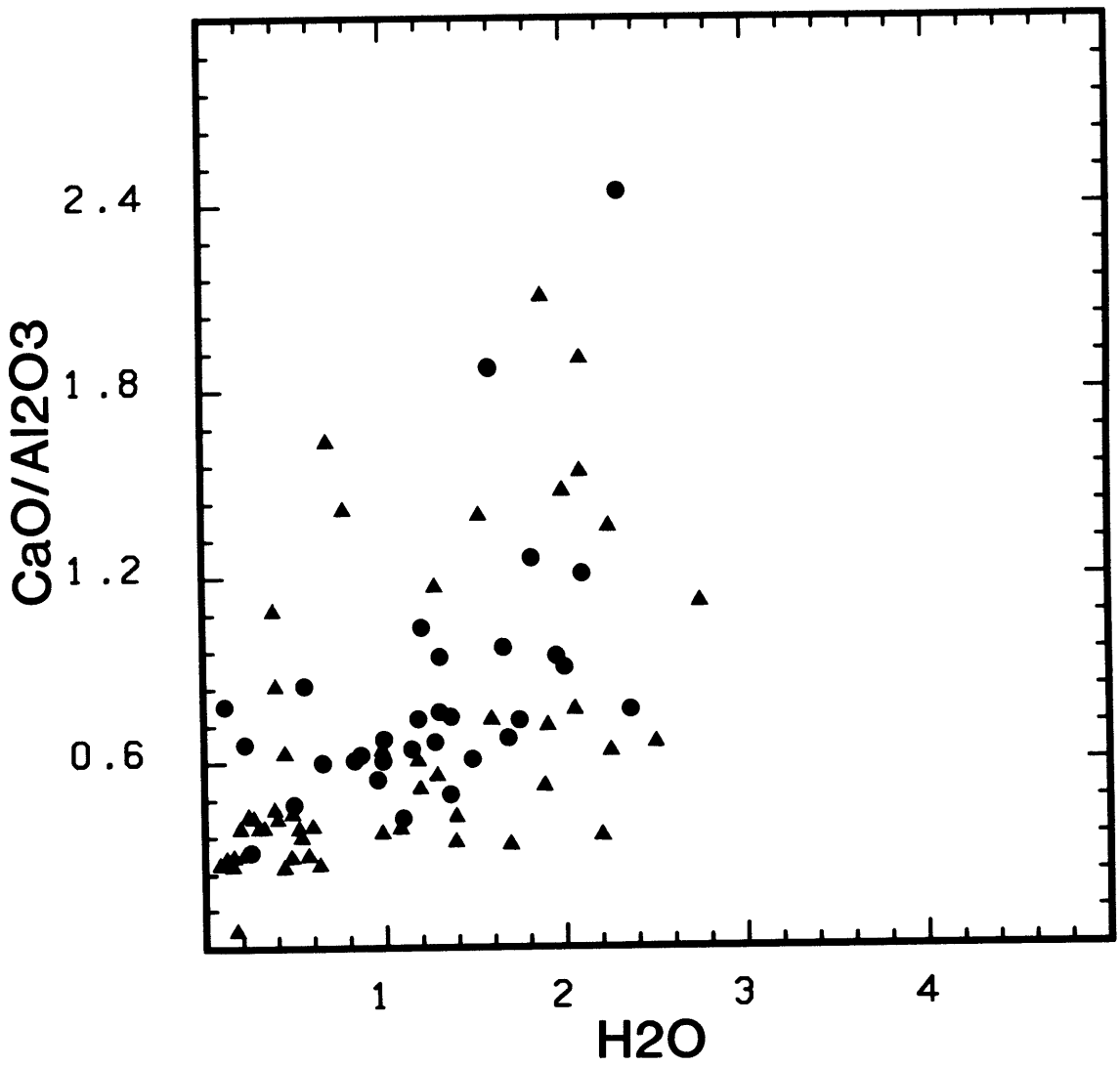
2.4
1.8
1.2
0.6
CaO/Al2O3
1
2
3
4
H2O

correlates well with MgO content of the lavas (Figure 3-10) suggesting that this ratio changes in response to fractionation of Ti-magnetite (Byers et al. 1984) and has not been severely disrupted or has been offset by a relatively constant amount by some form of buffering mechanism (Christie et al. 1986) during post eruptive re-equilibration or alteration. An estimate of the fO_2 range for samples from the different groups can be obtained by: 1) using Fe^{3+}/Fe^{2+} measured, or 2) the Fe^{3+}/Fe^{2+} ratio derived from the Fe^{2+}/Mg Kd for olivine phenocrysts, and an estimate of the temperature (Kilinic et al. 1983). Estimation of the Fe^{3+}/Fe^{2+} using olivine relies upon the assumption of constant Fe^{2+}/Mg partitioning, and this is true for olivine (Jones 1984, Takahashi and Kushiro 1983). The value used here (0.3) is the same as the value obtained in experiments on 78LH1 and is identical to the average value obtained in other experiments on undersaturated lavas (Mahood and Baker 1986, Sack et al. 1987). The calculated Fe^{3+}/Fe^{2+} is subject to large uncertaintities due to error magnification and variation of the partition coefficient between 0.29 and 0.31 produces an uncertaintity of approximately 30% in the calculated ratio. Therefore, these values must be considered a rough estimates. The calculated Fe_2O_3/FeO ratios of samples F1 and F11 are respectively 0.9 and 1.2, whereas for F12 the value is 0.3. The $\log fO_2$ values calculated for the above samples fall between -8 and -9 for an assumed

temperature of 1150 °C and are between the Ni-NiO and H-M buffer curves and typical of arc magmas (Luhr and Carmichael 1985, Arculus and Wills 1980).

The Feni lavas have high sulphur contents (Heming 1979, Wallace et al. 1983) and this can result in a buffering of the fO_2 of the magma (Carmichael and Ghiorso 1986). The solubility of S in a basaltic melt changes rapidly with minor changes in fO_2 and reaches a minimum at oxygen fugacities close to the Ni-NiO buffer (Katsura and Nagashima 1974). This minimum is associated with a change in the speciation of sulphur in the melt from sulphide to sulphate as the oxygen fugacity increases and passes the minimum, and this change in solubility can result in the crystallization of either sulphides or sulphates, depending on which side of the minimum the magmas is crystallizing. The Feni lavas contain either sulphates (hauyne) or sulphides (pyrite, pyrrhotite) and often both, suggesting crystallization occurs at oxygen fugacities close to the solubility minimum. The presence of hauyne rather than nepheline or sodalite as the predominant feldspathoid requires high sulphur contents and oxygen fugacities, at or above the Ni-NiO buffer. Below this oxygen fugacity sulphur occurs primarily as sulphides (Carmichael and Ghiorso 1986).

Although the principal conclusion of this section is the difficulty of accurately assessing fO_2 in hydrous undersaturated lavas, there is evidence for high and variable fO_2 in the Tabar-Feni suite, and some evidence for differing fO_2 in the different groups.

H_2O contents of the Feni lavas

Most of the Feni samples have high measured H_2O contents (Table 3.1). Values range between 0.1% in some trachytic lavas and 3.7% in F4, a sample which contains vesicles filled with calcite and zeolite. The basalts and ankaramites have higher values than the other lavas and usually have about 2% H_2O. The group 1 lavas have consistently lower H_2O (Table 3.1), but higher Cl and S (Heming 1979). H_2O correlates positively with the CaO/Al_2O_3 ratio (Figure 3-11) and there are a number of possible explanations for this relationship between composition and H_2O content: 1) the water content is related to the degree of melting during generation in the mantle, 2) the observed decrease is produced by fractionation of amphibole, 3) outgassing during crystallization within a magma reservoir reduces the water content, and 4) post-eruptive addition of H_2O has preferentially affected the cpx-rich samples. The higher water content of the calcic lavas from group 3 (F28, F29) would result in an expansion of the olivine phase volume and this could allow the production of cpx-rich lavas.

The cpx-rich samples have higher LREE/HREE (chapter 4) as would be expected if they were the result of smaller degrees of partial melting, however they are isotopically distinct and the variations cannot be simply related to different degrees of melting of the same source. The proportion of hydrous phases crystallizing is too small to explain the decrease in H_2O and fractionation of a hydrous phase can be eliminated as an explanation. The greater degree of alteration of the cpx-rich samples is probably a crystallization effect because the water in these rocks is not structurally bound in minerals, as it is in the amphibole and biotite bearing samples.

Conclusions

There is a wide diversity of magma compositions in the Feni islands and at least 3 parental magmas are present. These magmas have evolved under different pressure, fO_2 and perhaps pH_2O. The different fractionation assemblages induced by the specific conditions of crystallization and compositional difference between the parental magmas result in three distinct evolutionary paths. The group 1 lavas, the phonolitic tephrites, initially evolve by crystal fractionation of an oliv+plag+amp+Ti-mag assemblage, however mixing is required to produce the more evolved lavas (F14, F19) of this group.

The principal differences between group 2 and 3 are the amount of olivine fractionation prior to crystallization of clinopyroxene and the later appearance of Ti-magnetite and apatite in the group 3 lavas. Fractionation of large amounts of olivine from the calcic parental magmas of group 3 results in residual melts that are ankaramitic. Lower fO_2 results in more iron enrichment and the later appearance of Ti-magnetite in this group. A larger amount of clinopyroxene in the mantle melt producing group 3 is required by the higher CaO/Al_2O_3 and these magmas differentiate at low pressure <2 kb, and lower fO_2, perhaps under more H_2O-rich conditions.

The group 2 lavas have evolved under higher fO_2 and these magmas do not reach the same level of iron enrichment prior to Ti-magnetite fractionation. Slightly higher pressures during crystallization result in earlier appearance of clinopyroxene in the group 2 magmas. These two groups may have undergone assimilation and/or magma mixing, however these processes are difficult to distinguish from the effects of differentiation, which appears to be the dominant process. In the instances where mixing can be identified, it appears to be confined to mixing of moderately evolved lavas in the group 2 samples.

The different groups follow distinct evolutionary paths when projected onto the oliv-diop-neph and oliv-plag-diop faces of the pseudoquarternary of Sack et al. (1987) and this projection scheme provides excellent separation of the different groups until high plagioclase proportions, at which

point the projection is no longer applicable. The group 2 lavas have clinopyroxene phenocrysts that have higher Al^{VI} contents and also contain abundant amphibole in the evolved samples, and the position of the multiple saturation series for this suite is closer to the olivine apex in the oliv-diop-neph projection as would be expected if the lavas crystallized at pressures > 1 atm, with fO_2 between the Ni-NiO and H-M buffers. The multiple saturation surface for the group 3 samples is on the low fO_2 side of the Sack et al. (1987) surface and this results from the calcic composition of the lavas, lower fO_2 and perhaps higher H_2O.

The general fractionation sequence followed is oliv, cpx+oliv, cpx+Ti-mag+apa+oliv, cpx+plag+Ti-mag+apat+amp. Groups 2 and 3 start at different points along this sequence and the amount of fractionation of each assemblage is different. The compositions of the Feni lavas is consistent with a polybaric fractionation under high oxygen fugacities (Ni-NiO to H-M), of olivine at moderate to high pressure, followed by differentiation of different cpx-rich assemblages within the crust, at pressures between 1 atm and 5 kb. The H_2O content and Fe^{2+}/Fe^{3+} decrease during evolution probably as a result of degassing and fractionation of Ti-magnetite. The above conclusions are consistent with the major element chemistry, mineral chemistry, modal abundance of phases, and some trace element data. The relationship between these models and the trace element and isotope data will be examined further in the next chapter.

CHAPTER 4

CRYSTAL FRACTIONATION, MAGMA MIXING AND ASSIMILATION IN THE FENI LAVAS

Introduction

The complexity of arc lavas in isotopes, trace and major elements has produced numerous highly complex, multiple component, multiple process models (Kay 1980, Morris and Hart 1983, Hickey et al. 1986, Gill 1984, Myers and Marsh 1987). The decoupling of trace elements and major elements, and of isotopes and trace elements is common in arc settings (Gill 1981) and is one of the main stumbling blocks in the development of successful and unique models. Crystal fractionation at different pressures and under different pH_2O and fO_2 (Grove and Baker 1984) is also responsible for variations in major element and trace element chemistry. In many ways "arc processes" are synonymous with mixing and it is difficult to find recent references that do not invoke this process. The sequence and timing of crystal fractionation, mixing and assimilation is of critical importance to understanding the evolution of any complex suite of arc lavas. Recent attempts at separating the effects of these processes in complex magmatic systems have produced equivocal results, especially when quantification of endmember compositions has been attempted (McBirney et al. 1987, Reagan et al. 1987, Wyers and Barton 1987). The principal difficulties faced by these investigators were, the identification of criteria or parameters that clearly distinguish between processes, assessing the importance of each process and understanding the timing of each.

The Feni lavas are highly complex, with three evolutionary groups which have evolved by crystal fractionation, and possibly magma mixing and/or assimilation. Variation of fO_2, pH_2O, pressure of fractionation, parental composition and fractionating assemblages has produced different major element and trace element compositions in these lavas. In this chapter the trace element and isotopic data (tables 4.1 and 4.2), petrologic information and quantitative models are used in an attempt to identify criteria that clearly separate these processes. The grouping of samples used in the previous chapter is continued in this chapter, and the validity of these groups with reference to trace elements and isotopes is also assessed.

The apparent decoupling of major and trace elements, and the difficulty of modeling the LREE in the Lihir lavas, which was attributed to apatite fractionation in chapter 2, also occurs in the Feni lavas and is also discussed. The following section discusses the trace element characteristics of the magmas that can be attributed to mantle melting, as this provides a geochemical basis for comparison of the effects of crystal fractionation, magma mixing, and assimilation.

The trace element geochemistry of the Feni lavas

The Feni lavas, like those of the other islands, are enriched in Pb, Sr, K, Rb and Cs, depleted in Nb, Ta, Hf, Zr and Ti, and have variable enrichment of Ba and P relative to the REE. These enrichments and depletions are characteristic of arc lava and are observable in Figure 4-1, which shows the trace elements normalized to BSE (Table 4.7) for Feni samples plotted in order of incompatibility. Sr abundances range between 1000 and 2700 ppm, with most samples having 1400-2000 ppm, and this level of enrichment is typical of other alkali and alkali earth elements (Table 4.1). K_2O, which is usually enriched, varies between 0.75% in ankaramitic lavas like F23 and 4.7% in the tephritic phonolite F20. Th, which is normally enriched in arc lavas (Hickey et al. 1986), is depleted in the Feni lavas. These enrichments are larger than those normally found in calc-alkaline and tholeiitic arc volcanics (Gill 1981). The incompatible (I) diagram patterns of the group 1, 2 and 3 lavas of chapter 3 provide an opportunity to identify differences in trace element abundances between these groups. The primitive group 1 lavas, F1, F6, and F27, are enriched in Cs, Ba, Th, Pb, K and Nb and depleted in the other elements relative to the primitive group 2 lavas. F12, the adopted parental lava for the group 3 samples in chapter 3 is even further depleted in trace elements, with the exception of P, the MREE and Sc. The calcic group 2 lavas, F18, F25 and F26 are depleted in most trace elements, with

Table 4.1

Trace Elements Feni Islands

	F1	F6	F14	F16	F19	F21	F27	F30	F31	F34	F35	F2
Group	1	1	1	1	1	1	1	1	1	1	1	2
Rb	55.6	56.6	49.8	60.2	47.7	66.5	52.3	54.5	53.8	48	61	72.9
Sr	1462	1462	1715	1739	1660	1485	1545	1451	1444	1635	1830	2056
Ba	394	428	410	433	405	412	407	387	387	400	440	317.5
Cs	1.84	1.77	0.78	1.37	0.687	0.663	2.02	1.85	1.85	0.000	0.000	1.28
V	228	221	151	191	149	165	224	227	225	204	217	240
Cr	349	360	55	2.20	50.8	4	283	342	292	47.0	11.0	2.9
Co	45.3	29.4	34.8	14.8	36.7	0.00	0.00	36	38	26	0.00	0.00
Ni	192	184	23	10	26	7	158	220	191	31	5	10
Sc	13.1	13.1	15.9	9.40	15.9	0.00	12.2	12	11	14	9	16
Zn	65	63	49	36	48	63	64	69	67	63	51	61
Ga	0.00	0.00	0.00	0.00	14.00	0.00	0.00	21.5	21.5	18.5	22.5	0.00
Y	15	15	15	0.00	0.00	0.00	16	13	13	14	12	22
Zr	95 0	92	92	123	93	113	87	76	78	88	90	118
Nb	6.1	5.8	4.3	4.8	4.6	4.6	6.2	4.5	5.0	3.5	4.0	3.8
Hf	2.1	2.1	2.4	2.5	2.4	0.00	2.2	0.00	0.00	0.00	2.3	0.00
Ta	0.7	0.4	0.4	0.2	0.4	0.00	0.7	0.00	0.00	0.00	0.00	0.00
U	1.3	1.5	1.1	2.1	0.8	0.00	1.2	0.00	0.00	0.00	1.2	0.00
Th	2.3	2.1	1.0	1.4	1.2	0.00	2.5	0.00	0.00	0.00	1.6	0.00
Pb	13.5	14.2	0.0	0.0	11.3	0.0	14.2	0.0	0.0	0.0	14	0.00
La	14.6	14.8	13.8	12.7	13.1	25	15.2	14	15	13	14.4	18
Ce	31	30.5	29.4	28.4	30.7	23	31.1	29	31	32	31.5	39
Nd	16.03	16.7	17.0	14.9	17.4	0.00	16.5	15.0	14	16	18.1	23.8
Sm	3.58	3.75	3.83	3.33	3.90	3.26	3.56	3.55	0.00	0.00	3.70	5.20
Eu	1.13	1.11	1.18	1.03	1.20	0.00	1.15	0.00	0.00	0.00	1.13	0.00
Tb	0.44	0.44	0.55	0.34	0.45	0.00	0.47	0.00	0.00	0.00	0.41	0.00
Yb	1.2	1.2	1.4	1.0	1.2	0.00	1.2	0.00	0.00	0.00	1.0	0.00
Lu	0.18	0.20	0.21	0.15	0.20	0.00	0.18	0.00	0.00	0.00	0.00	0.00

Rb, Sr, Ba, Cs, Sm, Nd, analyzed by isotope dilution for samples F1-21, 23-27.
REE, U, Th, Cr, Co, Hf, Sc by INAA for samples F1,3,5,6,7,11-20, 25-27.
All other trace elements by XRF at Amherst using techniques of Rhodes (1983).
Data for F28-38 from Wallace et al. (1983). Pb by isotope dilution in F1,3,5,6,7,11, 19,25,26,27.

Table 4.1

Trace Elements Feni Islands (cont'd.)

	F3	F4	F5	F7	F9	F10	F11	F15	F17	F18	F20	F25
Group	2	2	2	2	2	2	2	2	2	2	2	2
Rb	67.1	66.3	61.9	53.4	55.8	77.6	56.9	56.2	48.2	15.0	64.7	54.7
Sr	1826	2713	1838	1712	1921	2195	1768	1861	2361	1405	2457	1608
Ba	260	244	271	286	290	470	246	421	443	187	332	235
Cs	0.985	1.31	1.13	1.44	1.25	0.854	1.17	1.35	1.09	27.5	4.13	0.758
V	286	337	294	249	314	272	312	229	90	303	297	229
Cr	6.50	17	23.4	5.00	17	6	423	2.00	4.90	36.0	2.30	36.8
Co	25.90	0.00	28.7	31.7	0.00	0.00	44.5	30.9	22.1	47.0	27.4	37.1
Ni	9	21	24.00	7	24	13	167	10	8	28	10	20
Sc	14.4	0.00	17.9	11.2	0.00	0.00	18.8	10.1	2.03	29.1	10.9	27.7
Zn	82	96	74	77	85	80	79	46	21	89	76	62
Ga	0.00	0.00	0.00	0.00	0.00	0.00	0.00	0.00	0.00	0.00	0.00	0.00
Y	18	0.00	0.00	18	0.00	0.00	0.00	0.00	9.00	19.00	0.00	0.00
Zr	99	110	106	87	96	128	87	114	111	76	117	85
Nb	2.8	4.1	2.8	3.2	2.4	4.6	3.7	4.5	3.3	3.1	5.1	3.2
Hf	2.2	0.00	2.1	2.2	0.00	0.00	2	2.4	1.8	2.0	2.6	2.1
Ta	0.2	0.00	1.4	0.4	0.00	0.00	0.4	0.5	0.4	0.3	0.4	0.3
U	0.00	0.00	2.0	1.1	0.00	0.00	0.00	1.0	1.5	0.7	0.00	1.0
Th	1.7	0.00	1.4	2.1	0.00	0.00	1.7	1.8	1.3	1.1	2.6	1.4
Pb	8.4	0.0	6.5	9.8	0.0	0.0	44.4	16.9	0.0	8.3	0.0	9.1
La	18.9	0.00	18.2	18.8	21	19.8	19.6	14.0	4.01	15.7	24.5	14.6
Ce	43.1	0.00	42.3	42	38	39	43.7	30.5	8.28	35.8	52.5	34.0
Nd	25.5	27.5	25.0	23.2	26.6	24.3	23.8	17.4	4.1	21.7	24.2	20.23
Sm	5.63	0.00	5.58	5.29	6.16	5.43	5.61	3.89	0.87	5.06	5.97	4.78
Eu	1.67	0.00	1.67	1.57	0.00	0.00	1.67	1.20	0.27	1.58	1.80	1.51
Tb	0.68	0.00	0.83	0.57	0.00	0.00	0.75	0.32	0.12	0.68	0.81	0.52
Yb	1.6	0.00	1.7	1.6	0.00	0.00	1.5	1.1	0.37	1.7	1.7	1.5
Lu	0.26	0.00	0.26	0.24	0.00	0.00	0.23	0.16	0.07	0.25	0.25	0.22

Table 4.1

Trace Elements Feni Islands (cont'd.)

	F26	F37	F38	F12	F22	F23	F24	F28	F29	F32	F33	F36
Group	2	2	2	3	3	3	3	3	3	3	3	3
Rb	36.2	53	57	57.5	0.00	24.5	21.9	30.5	56	61	70	73
Sr	2026	1920	2016	1082	1207	919	972	1280	1570	1709	1622	2195
Ba	232	445	395	134	0.00	116	122	155	215	205	290	365
Cs	0.961	0.000	0.000	0.513	0.00	0.635	0.832	0.000	0.660	0.770	1.43	0.000
V	305	224	202	275	265	235	246	281	289	376	327	319
Cr	9.90	10.0	3.00	748	145	216.00	196	147	84	16.0	21.0	3.00
Co	40.9	0.00	15	53.4	0.00	0.00	0.00	0.00	0.00	48	38	26
Ni	15	6	5	264	82	100	90	54	45	31	28	8
Sc	19.5	7	8	39.9	0.00	0.00	0.00	34	24	26	19	9
Zn	75	51	55	85	83	65	64	87	84	109	88	86
Ga	0.00	22.0	22.5	0.00	0.00	0.00	0.00	15.0	15.5	18.5	20.5	24.5
Y	18	12	13	14	0.00	0.00	0.00	12	15	19	17	18
Zr	76	91	93	68	63	49	64	76	66	76	78	103
Nb	1.9	4.0	4.0	1.8	2.1	1.8	1.4	2	2	2.5	3.0	5.0
Hf	2.0	2.1	3.0	1.7	0.00	0.00	0.00	0.00	1.7	2.3	2.1	0.00
Ta	0.3	0.00	0.00	0.2	0.00	0.00	0.00	0.00	0.00	0.00	0.00	0.00
U	0.00	1.2	1.3	0.0	0.00	0.00	0.00	0.00	0.8	1.0	1.3	0.00
Th	1.6	1.6	2.1	1.0	0.00	0.00	0.00	0.00	1.3	1.7	2.2	0.00
Pb	8.2	14	12	6.6	0.0	0.0	0.0	0.0	16	10.	14	0.0
La	18.6	15.6	19.8	15.3	0.00	16	13	19	20.6	20.3	22.9	22
Ce	40.8	35.4	43.9	36.2	0.00	30	26	44	50.1	50.0	56.1	54
Nd	25.5	18.8	21.0	22.8	0.00	14.8	16.4	24	30.6	30.6	28.2	26
Sm	5.81	3.91	4.34	5.57	0.00	3.74	4.11	0.00	6.65	7.26	6.17	0.00
Eu	1.77	1.19	1.29	1.63	0.00	0.00	0.00	0.00	1.93	2.12	1.78	0.00
Tb	0.69	0.46	0.51	0.52	0.00	0.00	0.00	0.00	0.65	0.80	0.66	0.00
Yb	1.6	1.0	1.3	1.1	0.00	0.00	0.00	0.00	1.2	1.4	1.4	0.00
Lu	0.24	0.18	0.00	0.19	0.00	0.00	0.00	0.00	0.00	0.00	0.00	0.00

Table 4.2

Isotopic composition of Feni lavas

	$^{87}Sr/^{86}Sr$	$^{143}Nd/^{144}Nd$	$^{206}Pb/^{304}Pb$	$^{207}Pb/^{204}Pb$	$^{208}Pb/^{204}Pb$
F1	0.704061±25	0.512875±19	18.614	15.553	38.357
	0.704077±30	0.512887±18			
F2	0.703799±30	0.512960±19	18.659	15.551	38.346
F3	0.703565±28	0.512989±22	18.681	15.554	38.355
	0.703542±25				
F4	0.703906±25	0.512979±17	18.695	15.546	38.345
F5	0.703631±27		18.676	15.563	38.376
F6	0.704061±25	0.512849±20	18.624	15.548	38.330
F7	0.703755±23	0.512947±16	18.653	15.540	38.309
F9	0.703794±28	0.512952±23	18.703	15.556	38.382
F10	0.703964±27	0.512973±15	18.672	15.561	38.377
F11	0.703914±25	0.512981±16	18.690	15.548	38.351
F12	0.703669±22	0.512984±16	18.679	15.540	38.305
		0.512987±25			
F14	0.703955±30	0.512965±15	18.682	15.547	38.347
F15	0.703936±28	0.512949±40	18.660	15.552	38.362
		0.512948±20	18.663	15.554	38.372
F16	0.704030±28	0.512915±18	18.662	15.561	38.389
F17	0.704033±26	0.512956±25	18.662	15.550	38.350
F18	0.703809±29	0.513015±25	18.700	15.537	38.413
	0.703820±30	0.512981±14			
F19	0.703882±25	0.512978±25	18.692	15.561	38.398
			18.694	15.563	38.402
F20	0.703999±20	0.512976±18	18.663	15.533	38.300
		0.512975±18			
F21	0.703906±25	0.512950±20	18.684	15.566	38.410
F23	0.703877±25	0.512926±30	18.712	15.559	38.393
		0.512949±20	18.716	15.564	38.408
F24	0.703861±23	0.512970±17	18.699	15.555	38.366
		0.512983±16			
F25	0.703822±30	0.512998±15	18.694	15.539	38.352
			18.702	15.551	38.368
F26	0.703752±25	0.513009±19	18.706	15.536	38.317
		0.512997±14			
F27	0.704051±26	0.512909±25	18.624	15.551	38.341
	0.704055±30	0.512889±21	18.627	15.554	38.375
F30	0.704067±30	0.512863±25	18.626	15.562	38.375
F31			18.636	15.561	38.379
F32	0.703784±32		18.720	15.557	38.387
F33	0.703962±25		18.651	15.551	38.346

$^{87}Sr/^{86}Sr$ and $^{143}Nd/^{144}Nd$ error given are 2σ on the mean and are for the last 2 significant digits

In run statistics are better than .015% amu^{-1} and reproducibility is better thank 0.05% amu^{-1} for Pb isotopes corrected for machine fractionation using average from multiple analyses of NBS 981. NBS 981 value taken as average of Todt et al. (1983) and Hamelin et al. (1985).

the exception of Sr, the MREE and Sc, relative to the other group 2 samples. The evolved group 1 samples, F14 and F19, are depleted in Cs, Th and Nb, but otherwise have very similar abundances of most other elements to the parental lavas.

The REE enrichment of the Feni lavas is less than that in undersaturated continental rift (De Mulder et al. 1986) or Mediterranean arc lavas (De Fino et al. 1986, Pecerillo et al. 1984). This appears to be consistent with the low REE abundance of lavas from the New Britain and Bougainville regions (Heming and Rankin 1979, Arculus and Johnson 1981, Bultitude et al. 1978). In general, lavas from this region of the S.W. Pacific are depleted in REE; similar depletion in REE abundances in the Tonga-Kermadec volcanics have been interpreted as a reflection of a depleted arc mantle (Ewart and Hawkesworth 1987). Nb, Ta, Hf and Zr have similar abundance levels to lavas from other arcs in this region (Johnson and Arculus 1978, Marcelot et al. 1983, Ewart and Hawkesworth 1987, Johnson et al. 1985, Perfit et al. 1987, Gill 1984).

The parental lavas from chapter 3 have different REE characteristics. The group 1 phonolitic tephrite F1 has lower REE abundances than the potassic trachyandesite F11 (group 2) and the potassic basalt F12 (group 3), Figure 4-2d. This difference cannot be attributed to differences in olivine or clinopyroxene contents, as F11 and F12 have higher modal proportions of these phases and higher

La/Yb. The group three samples have higher La/Yb than the group 1 and 2 lavas, and they have a pronounced curvature to their REE patterns. F1 has higher La/Sm, Nb, Ba, Th and Cs and lower Sr and P_2O_5, which is inconsistent with the lower REE of this lava, resulting from accumulation of plagioclase or any other phase. F11 and F12 have different REE patterns with the former being enriched and having a relatively straight REE pattern, and the latter enriched in Nd, Sm and Eu relative to the other REE (Figure 4-2). The greater curvature of the REE pattern in the region of Nd, Sm, and Eu, which gives a pronounced hump to the pattern of the calcic lavas (F3, F7, F12, F18, F25 and F26) is difficult to explain, as no phase is capable of enriching these REE or depleting both La, Ce and the HREE. A combination of phases has limited success in enriching only these elements. The group 1 lavas (Figure 4-2a) have lower REE abundances than group 2 (Figure 4-2b) and group 3 (Figure 4-2c). The group 1 lavas have relatively constant Ba, 354-450 ppm, when compared with the lavas from the other groups, 116-470 ppm, and higher Th and Nb, and lower Sr at a similar MgO content.

Feni samples are LREE enriched with (La/Yb)c.n.> 7.0 in all samples (Figure 4-2), and this is typical of undersaturated lavas. Some lavas (F1, F6, F11, F14, F20 and F27) have relatively straight REE patterns, while other lavas (F7, F15 and F16) show a relative depletion in Tb and the HREE. A third group (F3, F12, F18, F25 and F26) are enriched in Nd, Sm and Eu and have concave downwards curvature in the

Figure 4-1

Incompatible element (Spidergram) diagram with the Feni samples normalized to the BSE values (Table 4.7). Order of incompatibility after Wood et al. (1979). a) Group 1, b) and c) Group 2 and Group 3. Selected samples have been numbered.

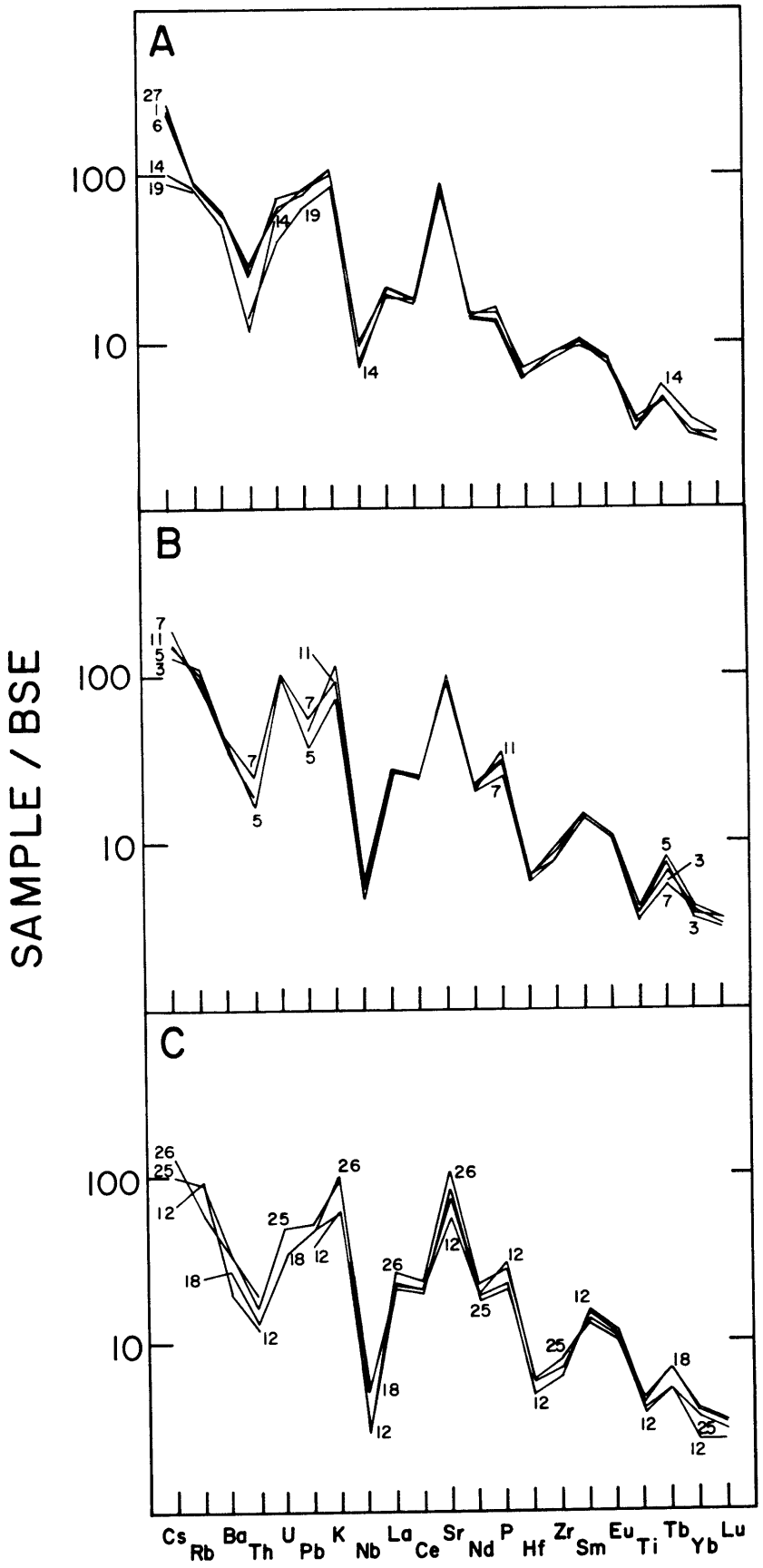
A
B
C
100
10
SAMPLE / BSE
Cs Rb Ba Th U Pb K Nb La Ce Sr Nd P Hf Zr Sm Eu Ti Tb Yb Lu

LREE-MREE. The REE abundances of the lavas decrease with increasing degree of differentiation, and the lowest REE concentrations occurs in the qtz-trachyte F17 (Table 4.1 and Figure 4-2). As the lavas become more "plagioclase-rich", the REE contents decrease, however none of the lavas have europium or cerium anomalies, which are common in some arcs (White and Patchett 1984, White and Dupre 1986). F14, an evolved group 1 lava, has similar REE patterns to the primitive group 1 lavas, F1, F6 and F27, although this lava is slightly enriched in the HREE.

The HREE and LREE show similar relative variation in abundance in the Feni samples and this is unusual in undersaturated lavas, which normally show relatively constant HREE abundances and large variation in the LREE concentrations (Sun and Hanson 1975a,b, Minster and Allegre 1978, Shimizu and Arculus 1975, Clague and Frey 1982).

Isotopic composition of Feni lavas

The Feni lavas have isotopic compositions typical of intraoceanic arcs, with $^{87}Sr/^{86}Sr$, $^{143}Nd/^{144}Nd$ and $^{206}Pb/^{204}Pb$ that fall respectively between 0.70355-0.70407, 0.51285-0.51303, and 18.612-18.712. $^{207}Pb/^{204}Pb$ and $^{208}Pb/^{204}Pb$ are essentially identical within errors in all of the Tabar-Feni lavas and have respective ranges of 15.553-15.564 and 38.300-38.413. The group 1, 2 and 3 primitive lavas, F1, F11 and F12, are isotopically distinct in Sr and

Figure 4-2

Chondrite normalized rare earth element patterns for the Feni lavas. Chondritic values are from Haskin (1981). A) Group 1, B) Group 2, C) Group 3, D) Parental lavas F1, F11 and F12. Additional data from Wallace et al. (1983).

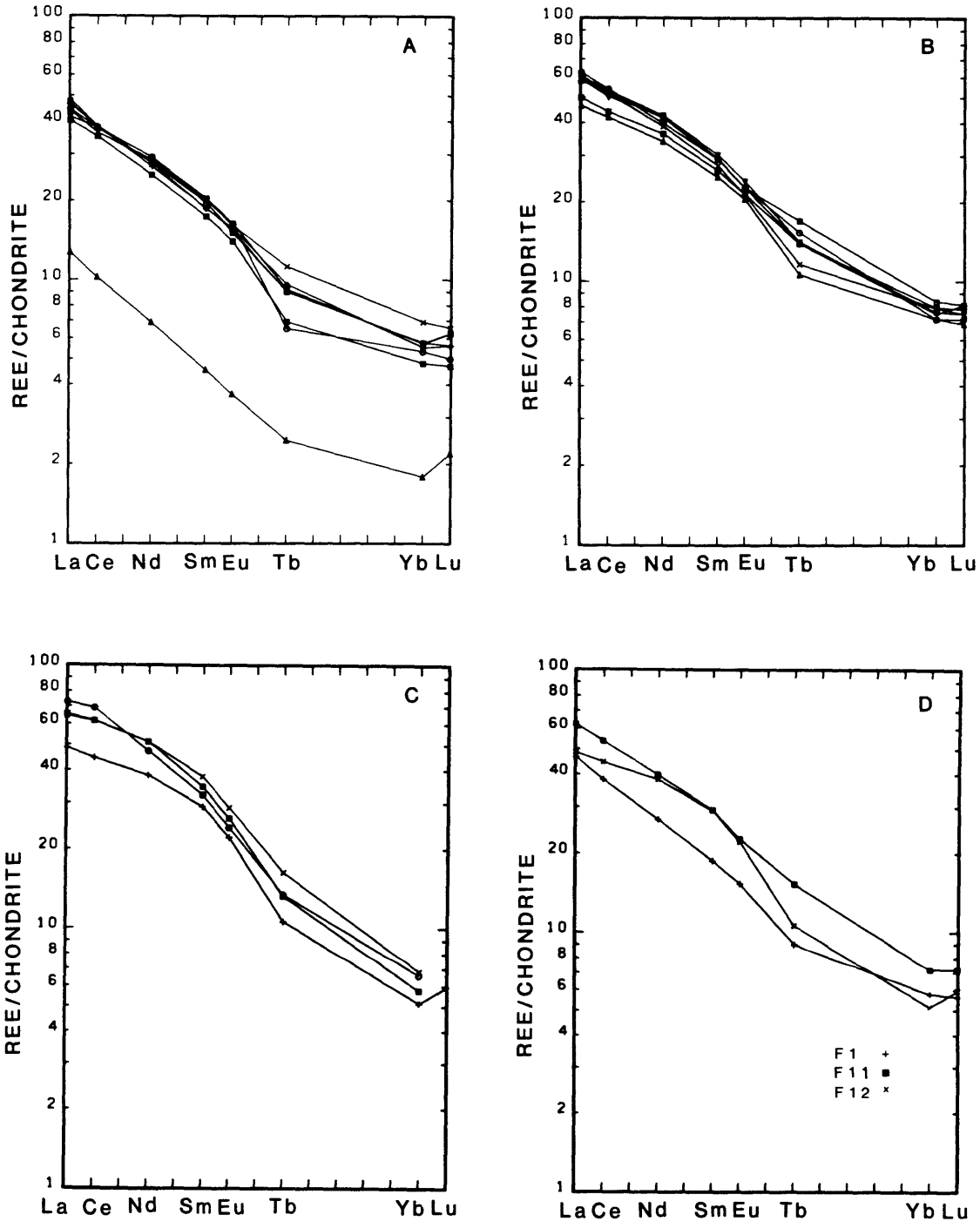
A
B
C
D
REE/CHONDRITE
100
80
60
40
20
10
8
6
4
2
1
La Ce Nd Sm Eu Tb Yb Lu
F1 +
F11 ■
F12 ×

Table 4.7

Normalizing Values BSE (ppm)

Cs	Rb	Ba	Th	U	Pb	K	Nb	Ta	La	Ce
.00773	.6182	6.99	.0869	.0208	.1786	262	.62	.0359	.604	1.577

Sr	Nd	P	Hf	Zr	Sm	Eu	Ti	Tb	Yb	Lu	Sc	Y
19.6	1.17	86	.29	11	.381	.143	1170	.0908	.407	.0627	17	3.94

Sr, Nd, U from Hart and Zindler (1986). Rb from bulk earth $^{87}Rb/^{86}Sr$ of .089. Cs, Ba from Cs/Ba and Rb/Ba of Hofmann and White (1983). Th and Pb from U/Pb and Th/U ratio of BSE, Kwon and Tilton (1987). Nb and K from Nb/U and K/U ratio of BSE, Hofmann (1986), Jochum et al. (1983). Ta from Nb/Ta, Jochum et al. (1986). La, Ce, Eu, Tb, Yb and Lu from chondritic ratios Anders and Ebihara (1982). Zr from Jagoutz et al. (1979). Hf from bulk earth $^{176}Lu/^{177}Hf$ of .029633, Patchett et al. (1981). P_2O_5 from P_2O_5/Ce ratio Sun and Hanson (1975) and Clague and Frey (1982). Y = 2.5 x chondritic value of Jochum et al. (1986). Ti from TiO_2/P_2O_5 ratio, Sun (1987).

Nd (Table 4.2 and Figure 4-10). F11 and F12 have similar Pb isotopic compositions which are close to the upper limit of $^{206}Pb/^{204}Pb$ values measured. F12 has low $^{87}Sr/^{86}Sr$ and high $^{143}Nd/^{144}Nd$ (Table 4.2). F1 and the other phonolitic tephrites have the lowest $^{206}Pb/^{204}Pb$, $^{143}Nd/^{144}Nd$ and highest $^{87}Sr/^{86}Sr$ of the Feni lavas, and F11 has intermediate isotopic composition in all three systems.

Although the three primitive lavas discussed above cover the observed major element compositional range of erupted melts that are close to primary, the isotopic compositions of these samples do not encompass all of the isotopic variation present in the Feni lavas. F3 and F5, two alkali basalts with slightly lower MgO, have lower $^{87}Sr/^{86}Sr$ and the trachybasalt, F26, and tephrite, F32, have higher $^{206}Pb/^{204}Pb$. This suggests that there is minor isotopic heterogeneity amongst the parental magmas for groups 2 and 3. The primitive phonolitic tephrites of group 1, F1, F6 and F27, have a narrow range in Sr isotopic composition (0.704053-0.704069) and greater variation in Nd and Pb istopes.

Crystal fractionation in the Feni lavas

The effects of differentiation must be known before any separation of processes is possible and this section examines crystal fractionation in the Feni suite. The importance of each of the minerals, clinopyroxene, olivine, plagioclase, Ti-magnetite, amphibole, biotite, apatite and the

feldspathoids has already been covered in the previous chapter and this can be expanded upon with the trace element data.

The compatible trace elements Cr, Ni and Sc are all positively correlated and decrease with crystal fractionation of olivine, clinopyroxene, amphibole and Ti-magnetite. Low Ni (<40 ppm) in most of the Feni samples, and the absence of olivine phenocrysts, attests to the early fractionation of olivine from these lavas. The importance of clinopyroxene in the evolution of the Feni samples has been stressed in the previous chapter. The high Cr and CaO content (748 ppm and 13%) of F12, a relatively aphyric lava with less than 2% clinopyroxene phenocrysts, reflects a melt rich in a clinopyroxene component.

The major element data provide the best criteria for assessing the importance of amphibole, as removal of amphibole produces similar changes in the REE as removal of clinopyroxene ± apatite. An amphibole-rich assemblage, especially one containing Ti-magnetite, would result in rapid SiO_2 enrichment without drastically changing the Al_2O_3/CaO ratio. Fractionation of plagioclase, which has high Al_2O_3/CaO, and/or clinopyroxene, which has low Al_2O_3/CaO, can change this ratio. The Feni lavas do not show rapid SiO_2 enrichment and the Al_2O_3/CaO ratio increases constantly with differentiation within the Feni lavas as a result of a high clinopyroxene/plagioclase ratio during crystal fractionation (Figure 4-3a). The Sc vs Ba plot (Figure 4-3b) shows Sc to

Figure 4-3

a) Al_2O_3/CaO vs Ba for the Feni lavas. Symbols for major element groups of chapter 3 are: group 1 (+), group 2 (□) and group 3 (X). b) Sc vs Ba for Feni lavas. Calculated mixing lines are for mixing between F12 and F17, and F26 and a hypothetical evolved endmember with respective Ba and Sc abundances of 430 ppm and 6 ppm.

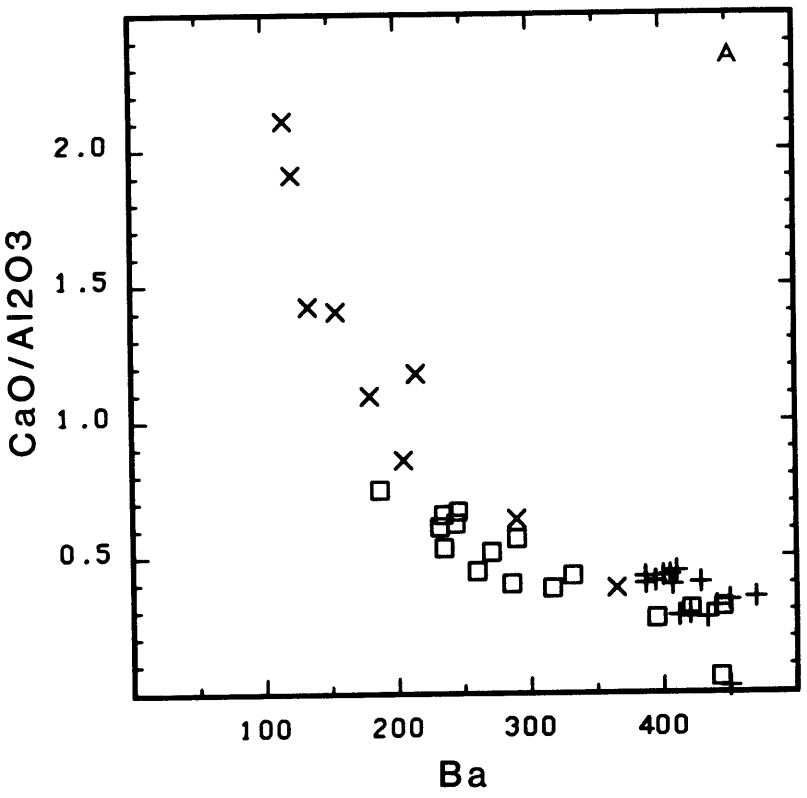
A
CaO/Al2O3
2.0
1.5
1.0
0.5
100
200
300
400
Ba

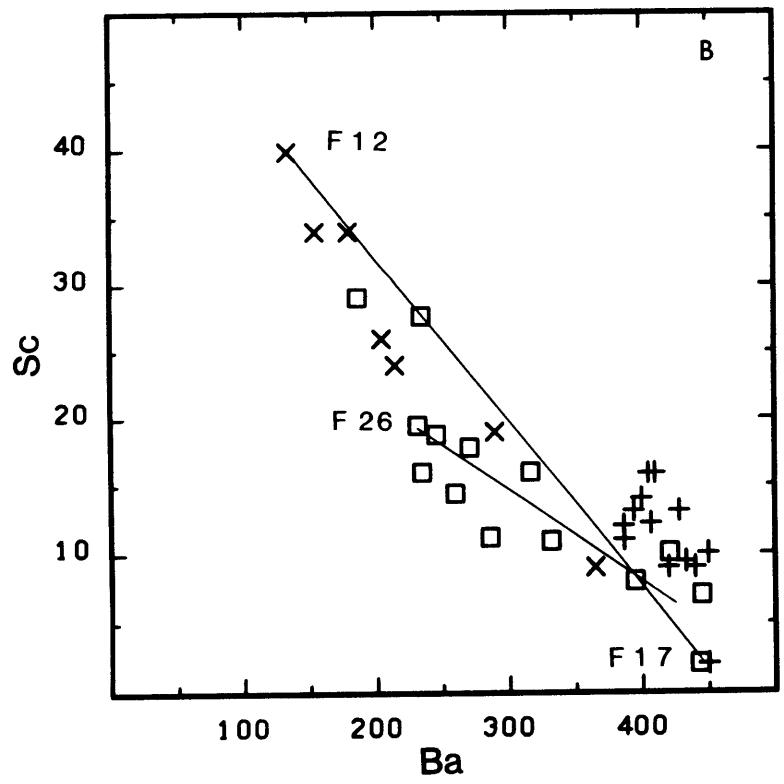
B
F12
F26
F17
Sc
40
30
20
10
100
200
300
400
Ba

be highly compatible in the group 2 and 3 lavas, but to have relatively constant abundance in the group 1 lavas. In the group 1 lavas the parental magmas have low Sc (<15) and high Ni (>190 ppm), and may have fractionated clinopyroxene at high pressure, as has been suggested for the generation of phonolites and alkali basalts (Duda and Schmincke 1985, Maaloe et al. 1986, Frey et al. 1988).

The REE are positively correlated with each other and the correlations are strongest between Nd, Sm and Eu, and between the LREE and MREE or, the LREE and HREE. Examples of these correlations are shown in Figure 4-4, and what appears to be a relatively straightforward relationship is in fact complex, as the lowest REE contents are found in the ankaramites F23 and F24, and the qtz-trachyte F17, while lavas with high Mg/(Mg+Fe), F1, F6, F11 and F12, have intermediate abundances. Evolved samples can be enriched (F10, F20) or depleted (F14, F16, F17) and this complexity is found for all of the REE. The REE and P_2O_5 are positively correlated (Figure 4-5) and the strongest correlations are for Nd, Sm and Eu. The phonolitic tephrites of group 1 have low REE and P_2O_5 abundances which do not change to any degree during the evolution of this group.

This is best explained by P_2O_5 and the REE being incompatible for part of the evolution of the Feni lavas. The abundance of apatite once it starts crystallizing, controls the concentration of the REE. Amphibole has a similar effect on the REE and undoubtedly results in further

Figure 4-4

a) Sm vs Nd and b) La vs Nd for the Feni lavas. Symbols as for previous figures.

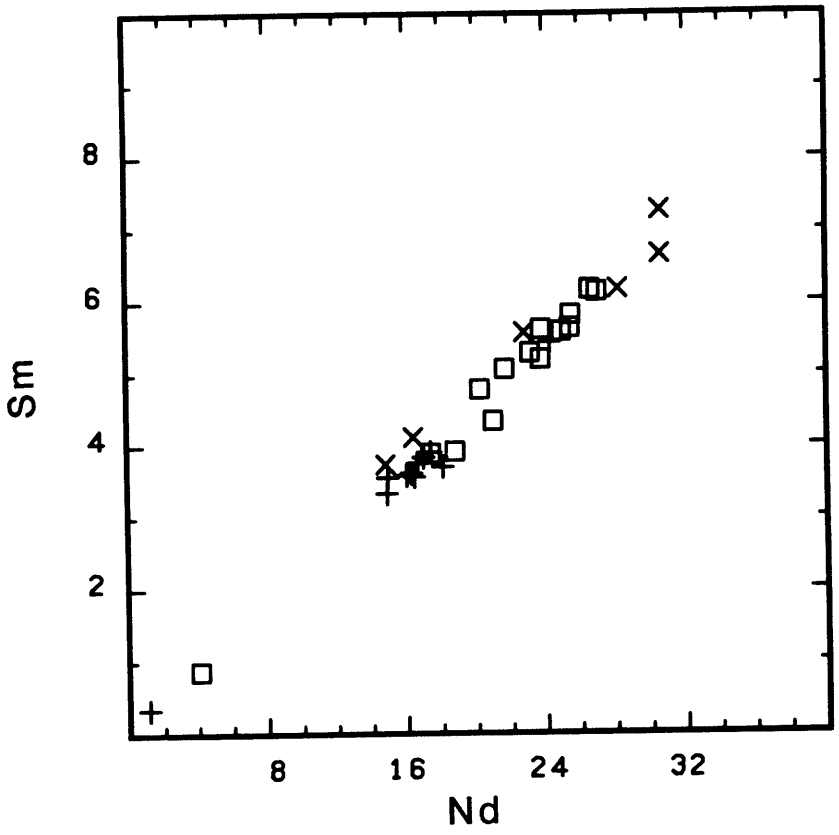
Sm
8
6
4
2
8
16
24
32
Nd

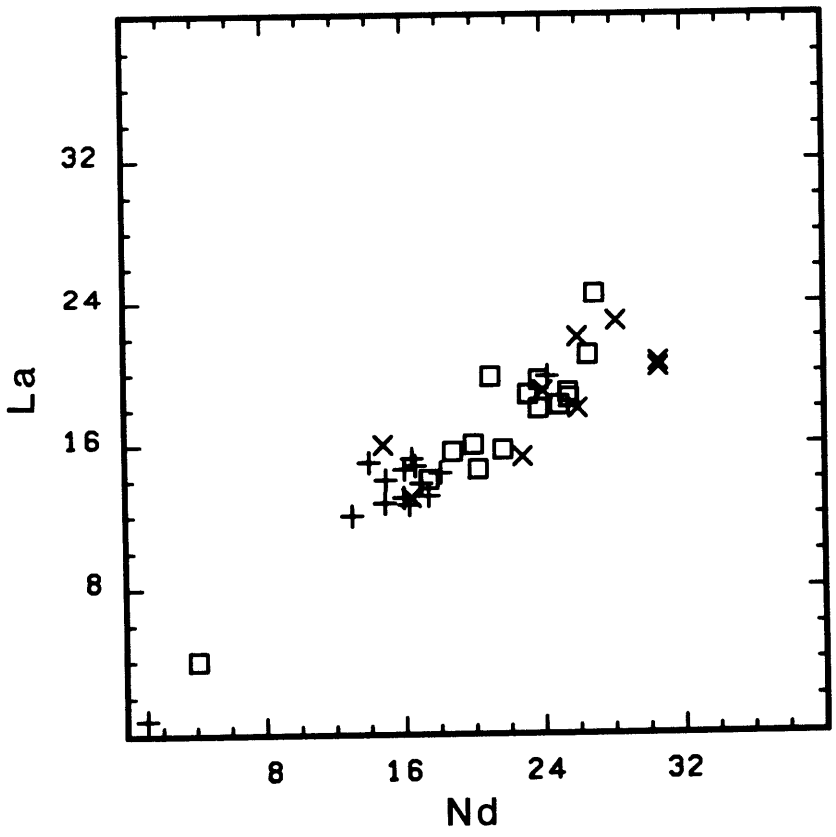
La
32
24
16
8
8
16
24
32
Nd

depletion of the REE when amphibole becomes a fractionating phase, at a later point in the crystallization history of these lavas. The group 2 and 3 major element chemistry groups of chapter 3 are not clearly separated in these plots.

The major element data presented in chapter 3 supports the hypothesis that apatite fractionation controls the concentration of the REE in the Feni lavas. P_2O_5 increases as SiO_2 decreases during the early differentiation of the group 3 lavas until magnetite and apatite saturation occurs, and then P_2O_5 and the REE decrease as the SiO_2 of the melt increases. The concentration at which apatite saturation occurs is between 0.6% and 0.8% P_2O_5, which is lower than expected from experiments on low SiO_2 compositions (Harrison and Watson 1984).

Two groupings are observable in the Ba vs P_2O_5 plot (Figure 4-5) and the high Ba, low P_2O_5 lavas are mostly group 1 phonolitic tephrites. Some of the evolved samples from groups 2 and 3 have reached apatite saturation and then fractionated sufficient apatite to decrease P_2O_5 as Ba increases. The two samples with lowest P_2O_5 and high Ba are both qtz-trachytes. K2O, Th and Nb show similar poor correlations with P_2O_5, and this is typical of Zr, Hf and other alkali elements when plotted against the REE or P_2O_5.

Both TiO_2 and V are positively correlated with P_2O_5 and co-precipitation of apatite and Ti-magnetite explains the observed correlation. Minor fO_2 variation can produce

Figure 4-5

Selected trace elements vs P_2O_5 for the Feni lavas. Symbols as for Figure 4-3.

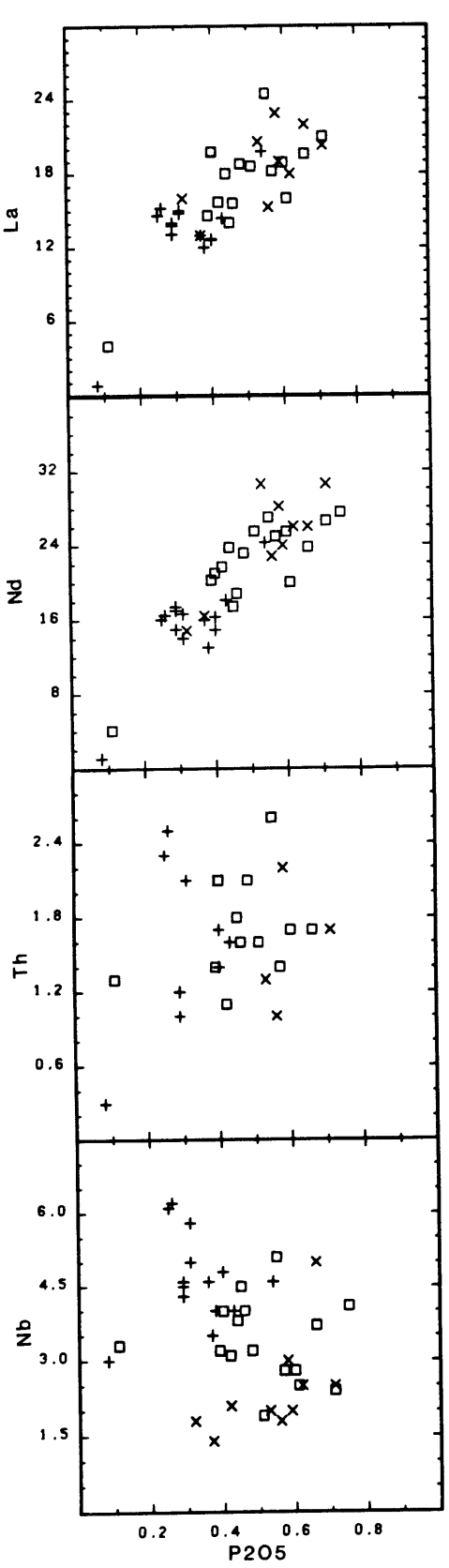
La
Nd
Th
Nb
P2O5

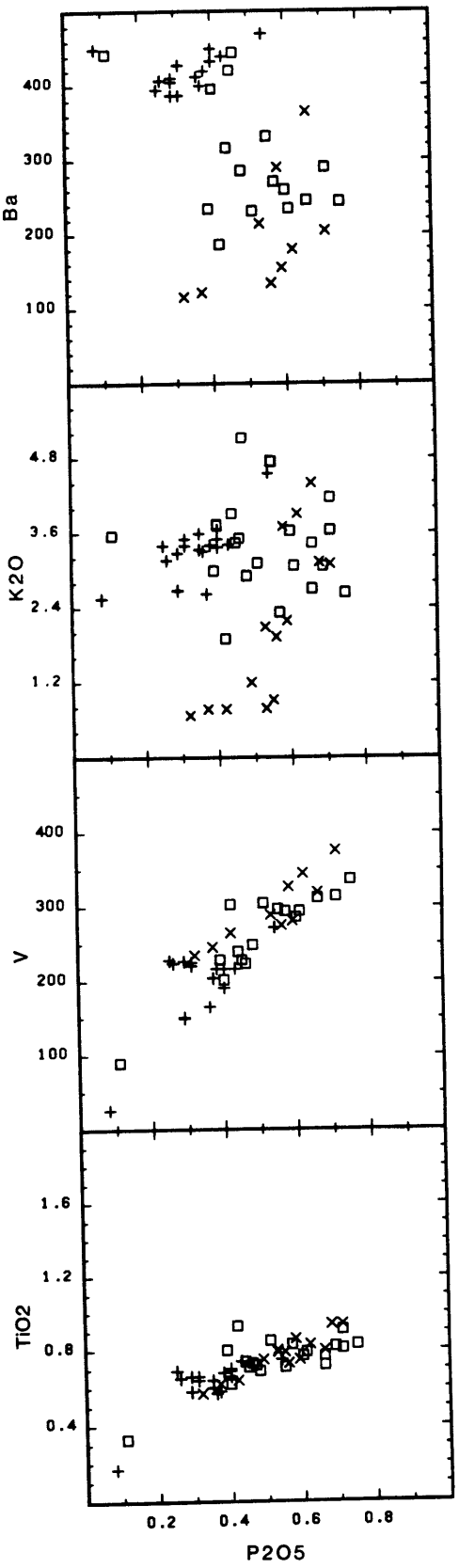
Ba
K2O
V
TiO2
P2O5

drastic changes in the partitioning of Ti, V and Cr (Irving 1978). TiO_2 is depleted (<1.0%) in Feni lavas and does not show any well defined relationship to the other HFSE as this element occurs at the percent levels in Ti-magnetite, amphibole, clinopyroxene and biotite. The proportion of Ti-magnetite in the fractionating assemblage is controlled by the fO_2 and the lack of any well defined relationships reflects variable fO_2 during fractionation.

The alkali and alkali earth elements behave as a reasonably coherent group and show positive correlations within the group, although there is considerable variation within samples with similar major element chemistry, especially K_2O. Ba concentrations increase by a factor of 3.3 between the alkali basalts and the tephritic phonolites and qtz-trachytes, and this element separates the lavas into two groups and shows a regular increase with differentiation. Rb, on the other hand is remarkably constant within most of these lavas and is within the concentration range, 45 to 73 ppm. Samples falling outside of this range have usually accumulated cpx, for example F18 and F22-F24. At present there is no explanation for the constancy of Rb in the Feni lavas. Cs shows a much larger relative variation than Rb, from 0.5 ppm in F12 to 4.0 ppm in F20, and in one sample, F18, the Cs concentration is 27.5 ppm. This sample has groundmass alteration. The mobility of the alkalis during alteration and crystallization is well documented (Hart 1971), and this process could also explain

the exceptionally low K_2O of this lava and the poor correlations amongst these elements.

Sr varies coherently with Ba in the group 2 and 3 lavas and the plotting position of any sample along the curved array of data points (Figure 4-6) can be explained by fractionation of parental magmas with compositions similar to F11 and F12, or by minor accumulation of clinopyroxene, for example F18, F23 and F24. The curvature of this array at higher concentrations of Ba and Sr results from an increase in the bulk partition coefficient for Sr once plagioclase fractionation begins.

The group 2 and 3 lavas are difficult to separate in the above diagrams partly because of the scatter and the similarity of fractionating phases and parental compositions.

The above discussions identify olivine, clinopyroxene, Ti-magnetite and apatite as the phases controlling trace element concentrations prior to eruption. Plagioclase and amphibole fractionation is not important in the primitive lavas, and only becomes important in the more evolved lavas. The trace element data and correlations discussed above are only partly explained by differentiation of the phases present in the lavas. The evolution of the group 1 lavas cannot be adequately explained by crystal fractionation of the phases present in the parental lavas (see chapter 3) as many elements which have low calculated bulk partition coefficients have a narrow range of abundances. Superimposed on the fractionation effects are mixing effects.

Figure 4-6

Sr vs Ba for the Feni samples. Symbols as before.

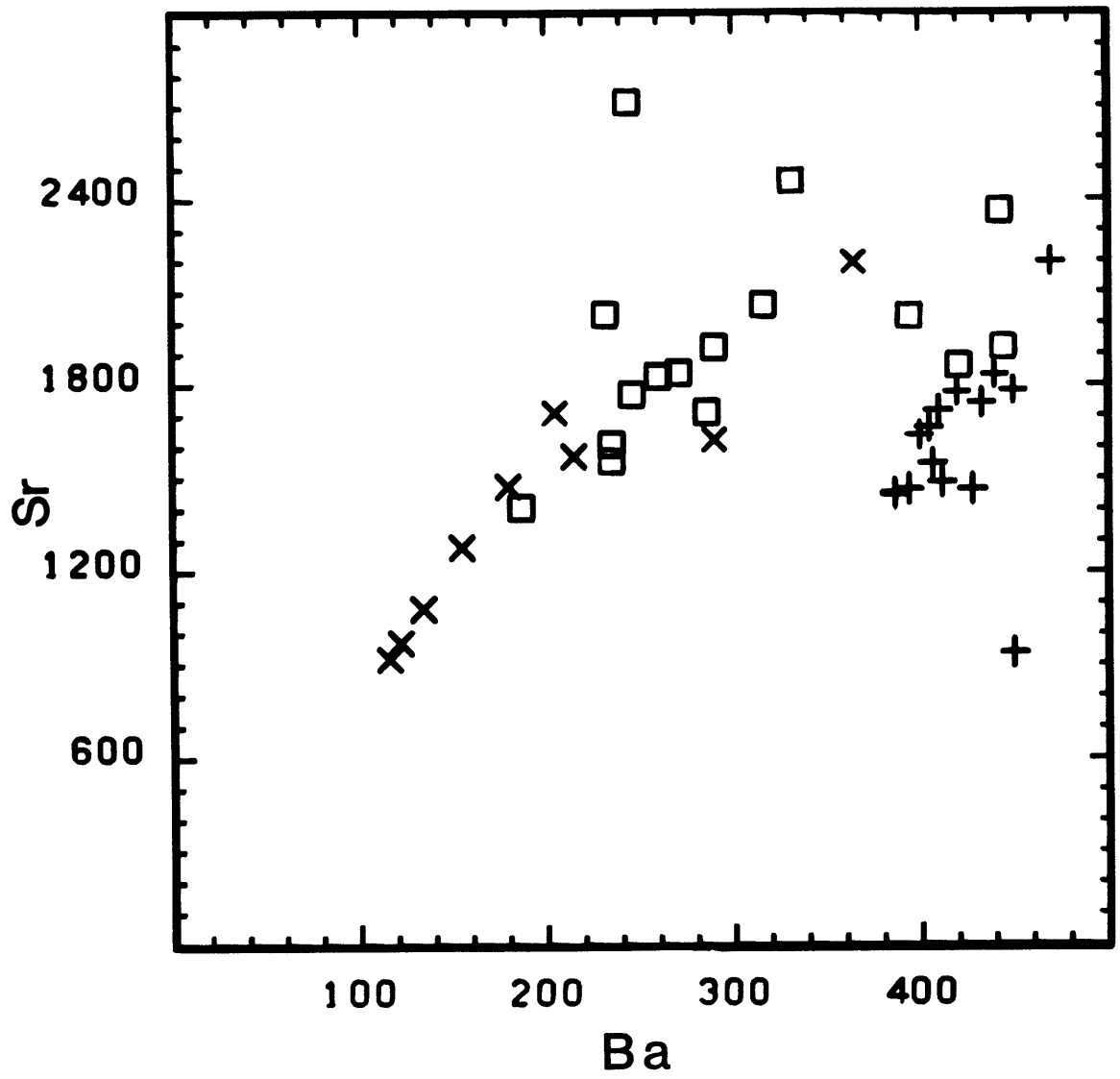
2400
1800
1200
600
Sr
100
200
300
400
Ba

Criteria for identifying and separating magma mixing and assimilation

Mixing in arcs covers a wide spectrum of magmatic and non-magmatic processes, and a variety of sources (Bacon 1986, Vogel et al. 1986, Koyaguchi 1986). Mixing may occur by: 1) mixing prior to melt generation, which includes, bulk mixing of mantle materials and metasomatism by fluids or melts, 2) mixing after generation by, magma mixing within the mantle, mixing within a magma chamber, assimilation of crust, mantle or cumulates, or, 3) combinations of the above processes. Where isotopes and major element chemistry have shown some covariance (DePaolo and Johnson 1979, Thirwall and Graham 1984, Myer and Sinha 1985, James 1982) the data is typically modeled as magma mixing or assimilation.

Trace element abundances are changed by differentiation, and this makes them difficult to use for the identification of mixed magmas. Compatible vs incompatible element plots, either in rectilinear or log form (Gill 1981, Allegre et al. 1977) are the simplest way of using trace element abundances to identify mixed magmas. In a rectilinear type of plot, simple binary mixing will produce linear data arrays, while crystal fractionation will produce curved arrays. In a log-log plot, crystal fractionation produces a linear array, and mixing a curved array. Given the usual statistical scatter in most arc data bases, this approach can only

identify mixing between evolved and primitive samples. Mixing between two evolved magmas, or between two primitive magmas cannot be identified. For example, the Feni data, which plots as a linear array on a logBa vs logSc diagram (not shown) plots as a smooth curve in Figure 4-3. There is however, sufficient scatter to prevent the elimination of mixing between evolved tephritic phonolites and alkali basalts. Mixing between the most primitive lavas and the trachytes can definitely be eliminated and the curvature of the data array suggests that mixing does not control the Sc and Ba abundances of these lavas.

Trace element ratios formed from incompatible elements, are relatively unchanged by differentiation and are changed by assimilation or mixing. The choice of an incompatible element ratio for the Feni lavas is complicated by fractionation of apatite, which changes ratios that are normally unaffected by differentiation.

Assimilated materials in arcs range from ophiolitic units (Arculus et al. 1983, Kelemen and Ghiorso 1986) to continental crust (Thirwall and Graham 1984, Leeman and Hawkesworth 1986) and everything in between. Assimilation is here taken to be, digestion of included materials (McBirney 1980), incorporation of wallrock melts (Patchett 1980), and diffusional interaction with the surrounding wallrocks (Watson 1982). When this process is accompanied by crystal fractionation, the two processes can be related by a constant (R, the ratio of mass assimilated to mass crystallized). It

is described by the assimilation combined with fractional crystallization (AFC) equations of DePaolo (1981). The rate of assimilation can decrease with time and temperature (Huppert and Sparks 1985, Devey and Cox 1987, Thirwall et al. 1983) and although this assimilation is undoubtedly accompanied by crystallization it will be labeled simply as assimilation, to prevent confusion with AFC.

The basic premise behind any method that separates processes, is that if two or more processes occur, it is possible to identify a least one variable for each process which is influenced only by that process. The identification of a relationship between two or more such variables implies a simultaneous occurrence of both processes. Plots of elements and ratios which are only changed by mixing, i.e., isotope ratios and incompatible element ratios, against elements or ratios that are continuously changed by differentiation, i.e., Sc, Ni, Mg', Al_2O_3/CaO are normally used for this purpose. The choice of variables depends on the composition of the mixing endmembers and fractionating assemblage. If mixing is between two primitive lavas and the mixtures undergo differentiation, there should be no relationship between the isotopic or incompatible element ratios, and ratios or elements that measure differentiation. If however there is a relationship between some index of differentiation and, isotopes and/or incompatible element ratios, mixing must be by AFC or by magma mixing of evolved and, primitive or relatively primitive lavas.

Petrographic evidence for mixing

It is difficult to find mineralogic criteria that adequately separate magma mixing from assimilation. Almost every conceivable phenocryst zoning pattern or disequilibrium texture can be explained by either of these processes or simply by changing conditions of crystallization within a magma chamber. The presence of disequilibrium mineral assemblages composed of minerals that rapidly equilibrate with the host melt or inclusions of crystallized liquids of different composition (Vogel et al. 1986), may be interpreted as magma mixing.

A variety of disequilibrium texture and zoning patterns exist in the Feni lavas. In the calcic group 2 lavas, clinopyroxene often shows multiple growth zones and sector zoning. Magnesium-rich zones in these clinopyroxenes often contain inclusions of plagioclase, olivine and Ti-magnetite, and occasionally glass and fluid inclusions. In F14, clinopyroxene phenocrysts sometimes have Fe-, Na-, fluid inclusion-rich cores that are overgrown by magnesian clinopyroxene. These overgrowths are normally zoned to a Fe-rich rim which has similar composition to groundmass clinopyroxene. The Fe-rich cores of these clinopyroxenes are enriched in Sr and depleted in Sc and V relative to both the magnesic overgrowths and rim compositions (Kennedy and Shimizu unpublished data).

Figure 4-7

An-Ab-Or compositions of complex growth textures in plagioclase. a) shows An 68 core overgrown by An 50-55 outer zone in F5 plagioclase. b) cyclic resorption and overgrowth of An 70 core by An 35-55 oscillatory zones in F26 plagioclase. Inserts show compositional variation along the microprobe traverse from core to rim. The arrows show the positions of the end of one growth cycle and the start of resorption. These arrows also mark the position of included groundmass Ti-mag,cpx and K-feld.

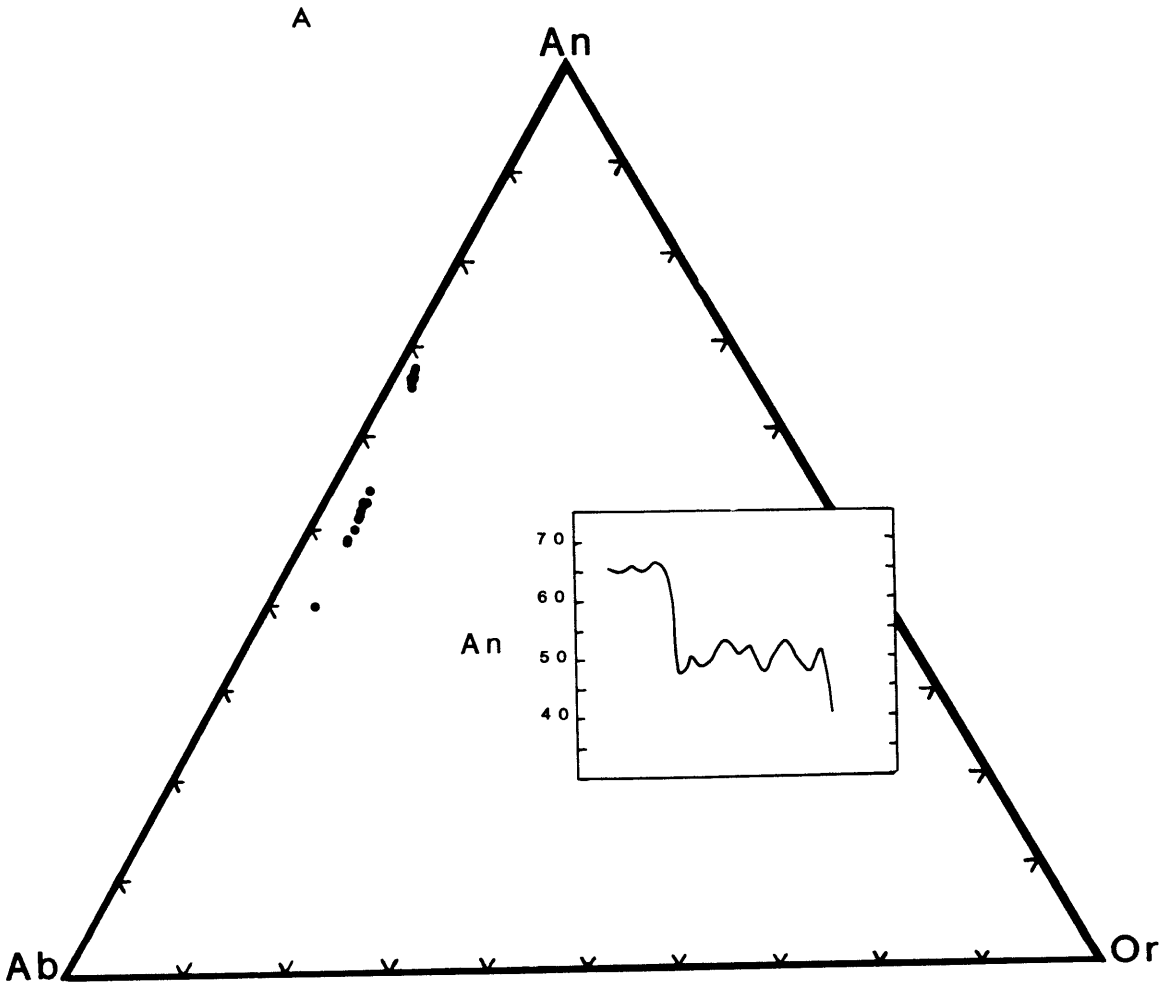
A
An
Ab
Or
An
70
60
50
40

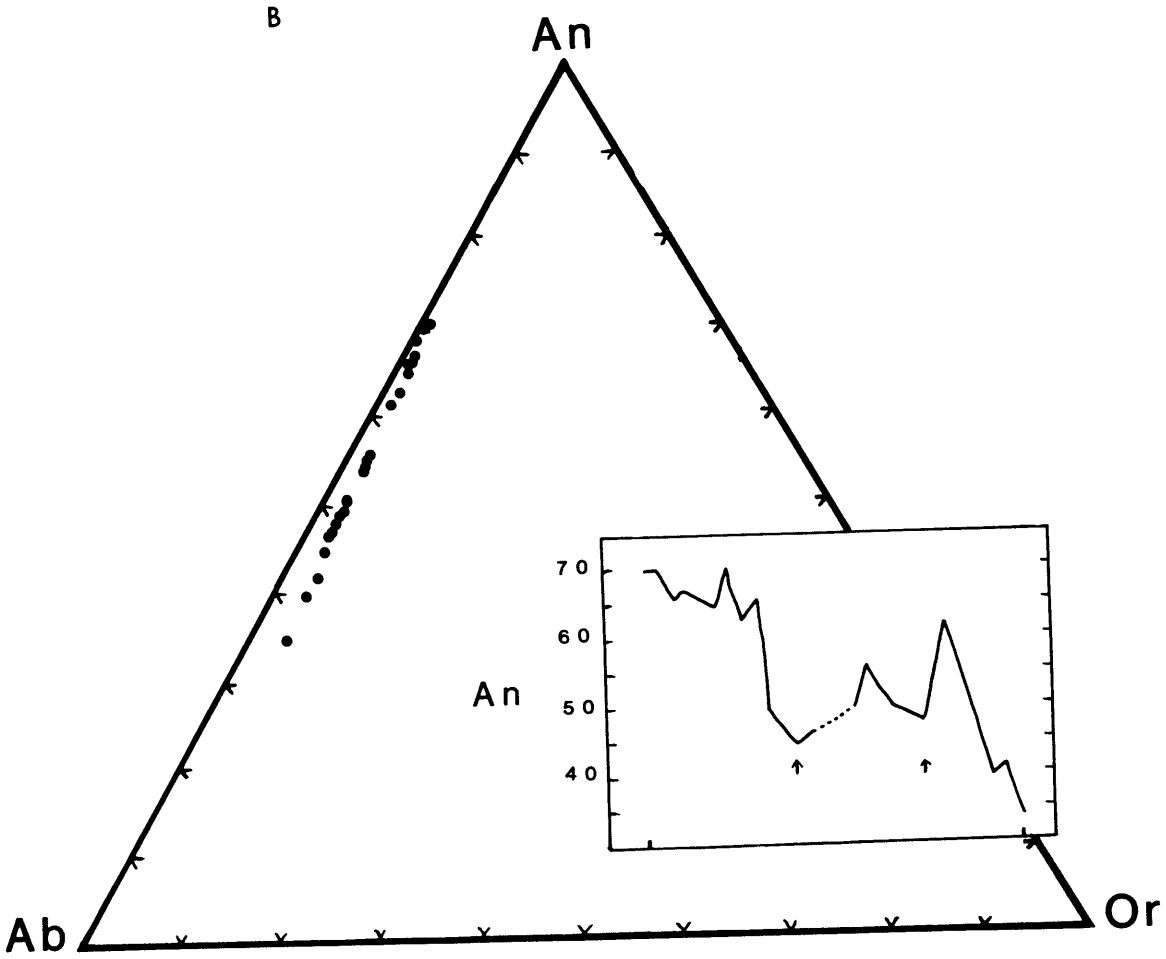
B
An
Ab
Or
An
70
60
50
40

Plagioclase often occurs as phenocrysts which have anorthitic cores (An 70) that are undergoing resorption and which are overgrown by a much more albitic composition (An 40-50). Plagioclase sometimes show multiple cycles of dissolution and trapping of groundmass K-feldspar, clinopyroxene and Ti-magnetite inclusions, followed by overgrowth with a more calcic plagioclase composition (Figure 4-7).

Trace element evidence for mixing

Comparison of elements which are incompatible in most phases and which are not affected by alteration, or crystal fractionation of apatite, clinopyroxene, amphibole or plagioclase and which have different abundances in the parental magmas from each group (F1, F11, F12) should separate the lavas. Nb and Th abundances are useful for examining the co-magmatic nature of the undersaturated lavas from Feni. Samples from group 1 form a linear trend that is well separated from the primitive group 3 samples on a plot of Nb vs Th (Figure 4-8). The group 1 samples have higher Nb and evolve to lower Th and Nb while the calcic group 3 samples evolve to higher Th and Nb. The group 2 samples fall between these two trends and can be interpreted as: 1) fractionation of a parental magma with intermediate Nb and Th that produces a parallel trend to that of the group 3 samples, 2) mixing between the group 1 and 3 samples to

Figure 4-8

Nb vs Th for the Feni samples. Symbols are: group 1 (+), group 2 (□) and group 3 (X). Three possible evolutionary models for generating the present data distribution are shown in the diagrams at right and are discussed in the text. Model 1: group 2 lavas produced by mixing between group 1 and 3 lavas. Model 2: Three distinct parental magmas and fractionation trends. Model 3: group 2 parental magmas generated by mixing of group 1 and 3 parental magmas, followed by separate fractionation processes. Parental lavas from chapter 3 labeled.

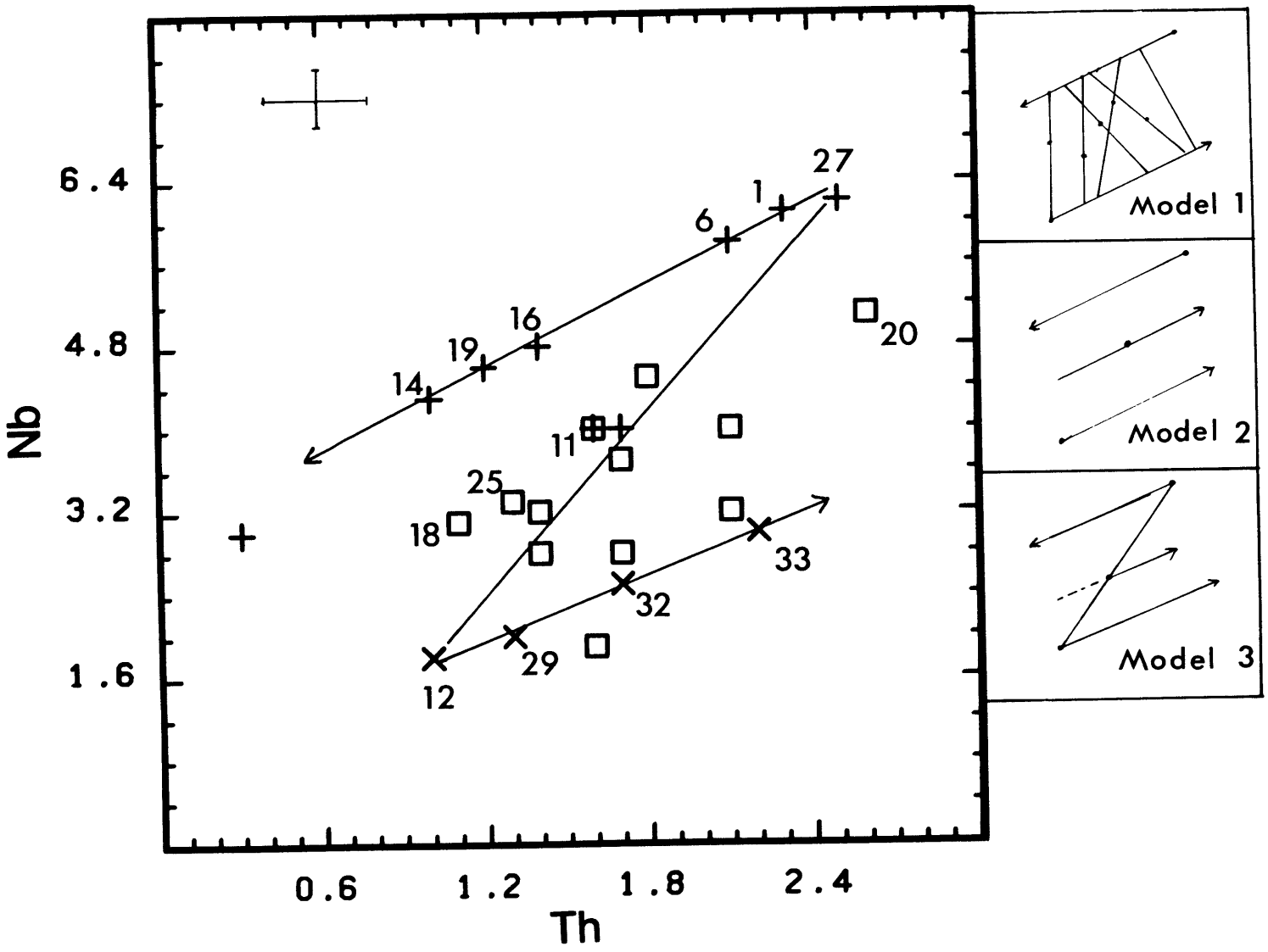
Nb
6.4
4.8
3.2
1.6
0.6
1.2
1.8
2.4
Th
27
1
6
16
19
14
11
20
25
18
33
32
29
12
Model 1
Model 2
Model 3

produce a spectrum of mixtures that are the group 2 lavas, or 3) mixing of the primary magmas of groups 1 and 3 to produce a parental magma for group 2, followed by fractionation of this mixture to form a parallel array of data. Each of these cases are shown as a small diagram attached to the right side of Figure 4-8. The consistent trend to higher Nb and Th, with increasing degree of differentiation in the group 2 and 3 samples, is consistent with the changes expected during crystal fractionation, as Th and Nb have low calculated bulk partition coefficients. The evolution of the group 1 samples with their decreasing Th and Nb cannot be explained by crystal fractionation of the observed phenocryst assemblages, and must have resulted from magma mixing, AFC or some other process.

The application of trace elements to mixing problems in the Feni lavas is complicated by the similarity of the group 2 and 3 lavas in trace element characteristics, both ratios and abundances. As a result, most ratio-ratio plots suggest mixing between two possible endmembers. La, Th and Ba are normally incompatible elements during differentiation. Ratios formed from these elements are usually constant during fractionation. For example, in Figure 4-9 the shortest curve labeled with F (amount of residual liquid) values (0.2, 0.1, 0.05) is a Rayleigh fractionation curve based on an assemblage (cpx:plag:oliv:Ti-mag:amp:hauyne; .4:.4:.05:.05:.05:.05). This curve is similar to any that would be calculated for assemblages containing only

Figure 4-9

La/Th vs Ba/La for Feni lavas. The three curves showing tick-marks are for Rayleigh crystal fractionation as discussed in the text. Curve A is for an assemblage that does not contain apatite. Curves B and C are for an assemblage containing 2% apatite. DLa is taken as 6.4 for curve B and 14 for curve C. Symbols as before. Mixing between F12 and F6 shown as dashed line. The arrow indicates the La/Th of the qtz-trachyte which has Ba/La of 110.

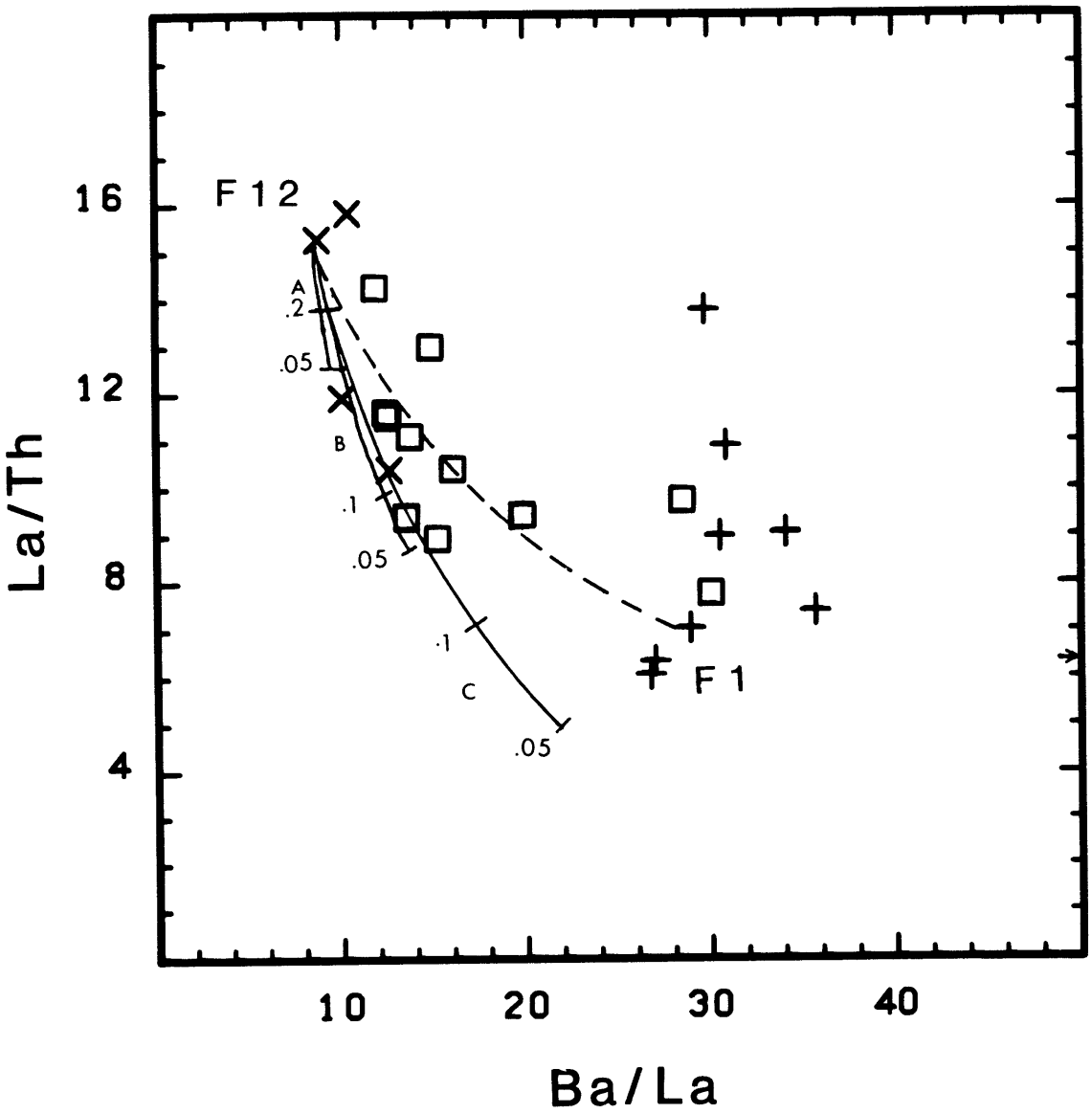
16
12
8
4
La/Th
10
20
30
40
Ba/La
F12
F1
A
.2
.05
B
.1
.05
.1
C
.05

clinopyroxene, olivine, plagioclase, amphibole, Ti-magnetite, and hauyne, since La, Th and Ba are incompatible in these minerals. As this curve shows, the spread of the data cannot be explained by crystal fractionation of any assemblage that doesn't contain apatite. Also shown are: 1) two Rayleigh fractionation curves for an assemblage that contains 2% apatite and 38% plagioclase, but with different DLa in apatite, and 2) a calculated mixing curve between F12 and F6. The two fractionation curves for apatite bearing assemblages have similar features to the Feni data but require far too much fractionation ($F<0.2$), when compared to the major element difference between the lavas, to represent realistic models for the generation of the data. The group 2 and 3 samples fall along the above mentioned mixing curve and could easily be explained by mixing or AFC combined with minor fractionation of apatite. The group 1 samples scatter on this plot but trend away from the group 2 and 3 samples and toward higher La/Th, with little change in the Ba/La ratio. Ratio-ratio plots can be interpreted in a variety of ways, and the most straightforward approach that results in the unambiguous identification of magma mixing or AFC is to examine the isotopic data. Mixing is easy to identify if the various components have different isotopic compositions, and this is the case for Feni lavas.

Isotopic evidence for mixing

Plots of the three combinations of $^{87}Sr/^{86}Sr$, $^{143}Nd/^{144}Nd$ and $^{206}Pb/^{204}Pb$ (Figure 4-10) show well defined mixing arrays. Plots involving $^{87}Sr/^{86}Sr$ require a minimum of three components while the other plot requires only two components. This indicates that two of the endmember are identical in Pb and Nd isotopes. The group 1 phonolitic tephrites F1, F6 and F27 have the highest $^{87}Sr/^{86}Sr$ and lowest $^{206}Pb/^{204}Pb$ and $^{143}Nd/^{144}Nd$ and plot at one end of the mixing array that contains most of the samples. F26, a group 2 alkali basalt, is at the other end of this array in the Sr-Pb isotope diagram. The group 2 lavas (F2, F3, F5, F7, F9) and F12 form a separate group in plots involving $^{87}Sr/^{86}Sr$, and these samples appear to form a second mixing array that has F3 as one endmember. The small number of samples forming this array and the scatter of these samples, prevents accurate definition of the other endmember of this mixing array, as a variety of mixing curves could be proposed that would account for the data. However, the intersection of this rough trend and the main array suggest that this unknown endmember must have $^{206}Pb/^{204}Pb < 18.681$, $^{143}Nd/^{144}Nd < 0.51299$ and $^{87}Sr/^{86}Sr > 0.7039$, and is probably similar to the group 1 lavas or an evolved lava with similar isotopic composition. The three previous sections provide evidence of mixed lavas in the Feni samples, and the following sections look at and separate magma mixing and AFC, to identify

Figure 4-10

a) $^{143}Nd/^{144}Nd$ vs $^{87}Sr/^{86}Sr$ for the Feni samples. Symbols as before. Mixing curves are shown as solid lines and AFC models as dashed lines. Labeled tick marks give mixing proportions for mixing models and F values for AFC models. AFC trajectories are for R=0.7. b) $^{143}Nd/^{144}Nd$ vs $^{206}Pb/^{204}Pb$ for the Feni samples. The symbols and the labeling of curves is the same as for Figure 4-10a. c) $^{87}Sr/^{86}Sr$ vs $^{206}Pb/^{204}Pb$ for the Feni lavas. Labeling of curves and symbols are the same as Figure 4-10a.

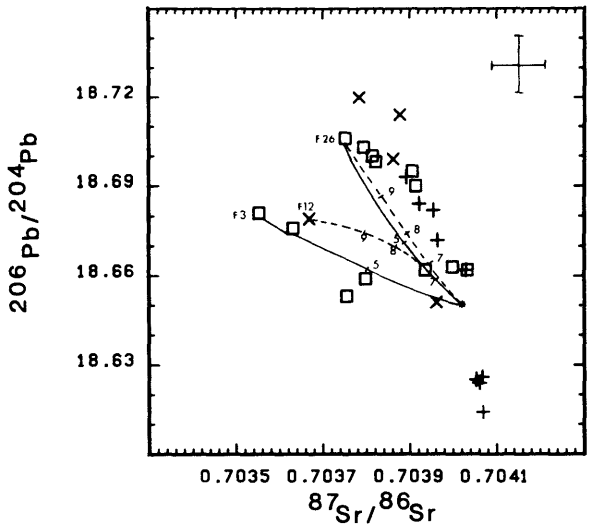
18.72
18.69
18.66
18.63
$^{206}Pb/^{204}Pb$
F26
F12
F3
0.7035 0.7037 0.7039 0.7041
$^{87}Sr/^{86}Sr$

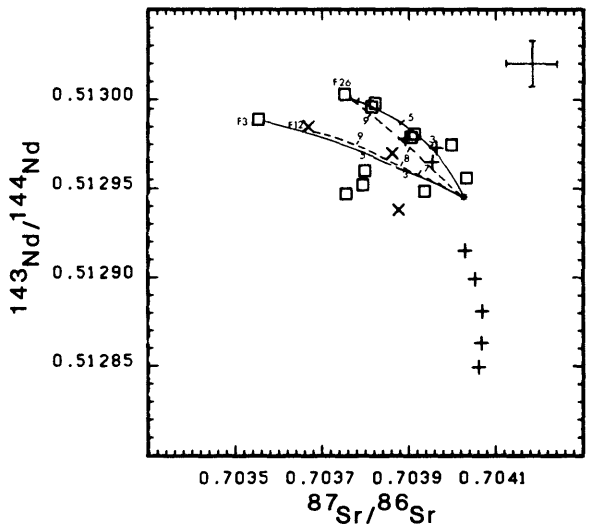
0.51300
0.51295
0.51290
0.51285
$^{143}Nd/^{144}Nd$
F26
F3
F12
0.7035 0.7037 0.7039 0.7041
$^{87}Sr/^{86}Sr$

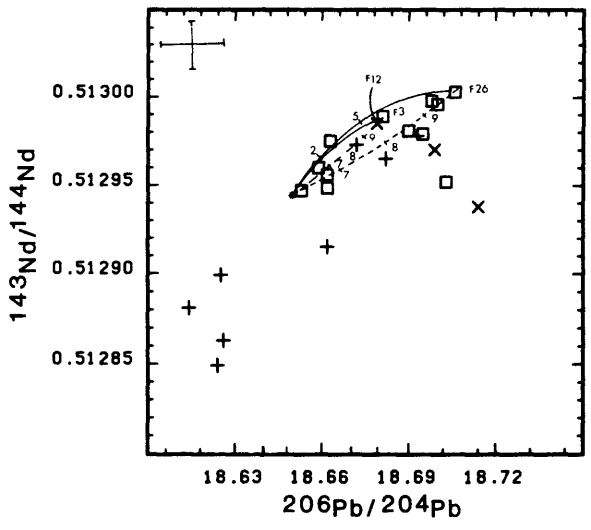
0.51300
0.51295
0.51290
0.51285
$^{143}Nd/^{144}Nd$
F12
F3
F26
18.63 18.66 18.69 18.72
$^{206}Pb/^{204}Pb$

endmembers, and to quantify these processes where possible.

Isotopic evidence for both assimilation and magma mixing

Since the three isotopic systems are coupled in the Feni lavas, the discussion of one system can be generalized to the three and this approach is taken in the following discussion of the correlations between isotopic composition and Nb and Th abundances. Neither the group 1 or group 3 lavas are isotopically homogeneous, although each group has a restricted range in comparison to the overall range. Samples F12, F29, F32, and F33 have increasing Th contents (Figure 4-8) and are used to define the group 3 evolutionary line. The $^{87}Sr/^{86}Sr$ ratio of F29 has not been measured, but the other samples have respective $^{87}Sr/^{86}Sr$ ratios of 0.703669, 0.703752, 0.703784 and 0.703962, while samples F27, F1, F6, F16, F19 and F14, which have continuously decreasing Th (Figure 4-8) and define the group 1 line, have respective values of 0.704053, 0.704069, 0.704061, 0.704030, 0.703892 and 0.703955. Most of the samples which have previously been referred to as group 2, and which fall between these two trends on the Nb and Th diagram, have $^{87}Sr/^{86}Sr$ ratios that fall between the ranges of the group 1 and 3 samples. For example, F18, F25, F11 and F20 which have increasing Th and have respective $^{87}Sr/^{86}Sr$ ratios of 0.703814, 0.703822, 0.703914, 0.703936 and 0.703999. Samples F3, F5 and F7,

which are part of a different mixing array in the isotope-isotope diagrams that contain $^{87}Sr/^{86}Sr$, plot close to the group 3 line but have lower $^{87}Sr/^{86}Sr$ at a similar Th content.

The group 1 samples have decreasing Nb, Th and $^{87}Sr/^{86}Sr$ and this is consistent with a mixing process. On the other hand the group 3 samples have increasing Nb, Th and $^{87}Sr/^{86}Sr$ and this can be explained by an AFC type process or mixing between moderately evolved alkali basalts, and, trachyandesites or tephritic phonolites. The samples which fall between these two arrays (Figure 4-8) show a similar trend to the group 3 samples with higher $^{87}Sr/^{86}Sr$ associated with higher Th and Nb. Th and $^{87}Sr/^{86}Sr$ are positively correlated in all of the groups, with the exception of F17, the qtz-trachyte which has lower Th and Nb than would be predicted from the measured $^{87}Sr/^{86}Sr$ value of 0.704033. Unfortunately the variation of isotopic compositions and Nb and Th abundances in the group 2 samples is consistent with any of the three evolutionary models presented in Figure 4-8.

Although the above trends and groups are consistent with the major element groups of chapter 3, there are discrepancies. F26 has lower Nb than other group 2 lavas and falls amongst the primitive group 3 lavas. It should also be noted that the isotopic data cannot be used to distinguish between group 2 and 3, as there is almost complete overlap between these groups.

Further separation of the above processes can be achieved by plotting the isotope ratios against a compatible element such as Sc, or an incompatible element, such as Ba, elements which decrease or increase continuously during differentiation. The $^{87}Sr/^{86}Sr$, $^{143}Nd/^{144}Nd$ and $^{206}Pb/^{204}Pb$ vs Sc diagrams (Figure 4-11) shows that what appears to be a single mixing array in the $^{206}Pb/^{204}Pb$ vs $^{143}Nd/^{144}Nd$ and two mixing arrays in the $^{143}Nd/^{144}Nd$ vs $^{87}Sr/^{86}Sr$ diagram, is in fact 3 mixing arrays. Isotopic composition does not change with crystal fractionation and crystal fractionation trends are linear and parallel to the trace element axis. In these plots, samples which have accumulated clinopyroxene plot at higher Sc or lower Ba. The $^{87}Sr/^{86}Sr$ vs Sc diagram shows the same separation as was observed in the $^{143}Nd/^{144}Nd$ and $^{206}Pb/^{204}Pb$, vs $^{87}Sr/^{86}Sr$ diagrams. The $^{143}Nd/^{144}Nd$ vs Sc diagram does not separate the group 2 and 3 lavas, but clearly separates the group 1 samples which show only minor variation in Sc and substantial changes in $^{143}Nd/^{144}Nd$. The increase in $^{87}Sr/^{86}Sr$ in the group 2 and 3 lavas between the more primitive lavas, F12, F11, F3, F5 and the evolved lavas, F15, F16, F17 could be interpreted as magma mixing between evolved and primitive magmas or AFC. In the $^{87}Sr/^{86}Sr$ vs Sc plot, it is tempting to attribute the variation in Sc abundances only to differentiation, as samples F2, F3, F5, F7, and F16 are more evolved than samples F12, F18, F25, F11, F32 and F1, which form an upper bound in Sc for the data. However, these more evolved samples clearly have lower

Figure 4-11

$^{87}Sr/^{86}Sr$, $^{143}Nd/^{144}Nd$ and $^{206}Pb/^{204}Pb$ plotted against Sc and Ba for the Feni lavas. Curves and symbols as for Figure 4-10.

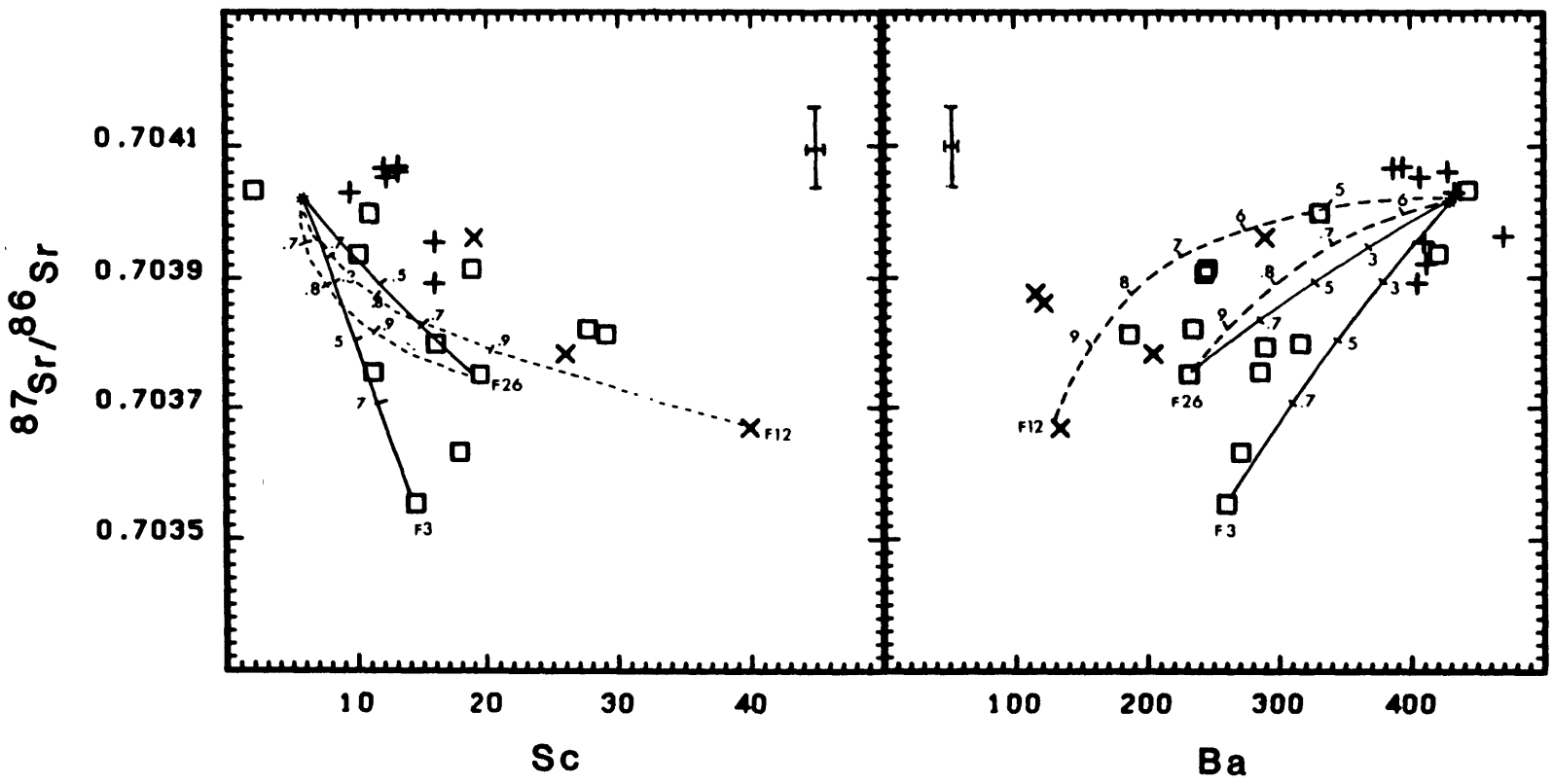
0.7041
0.7039
0.7037
0.7035
$^{87}Sr/^{86}Sr$
10
20
30
40
Sc
100
200
300
400
Ba
F3
F26
F12

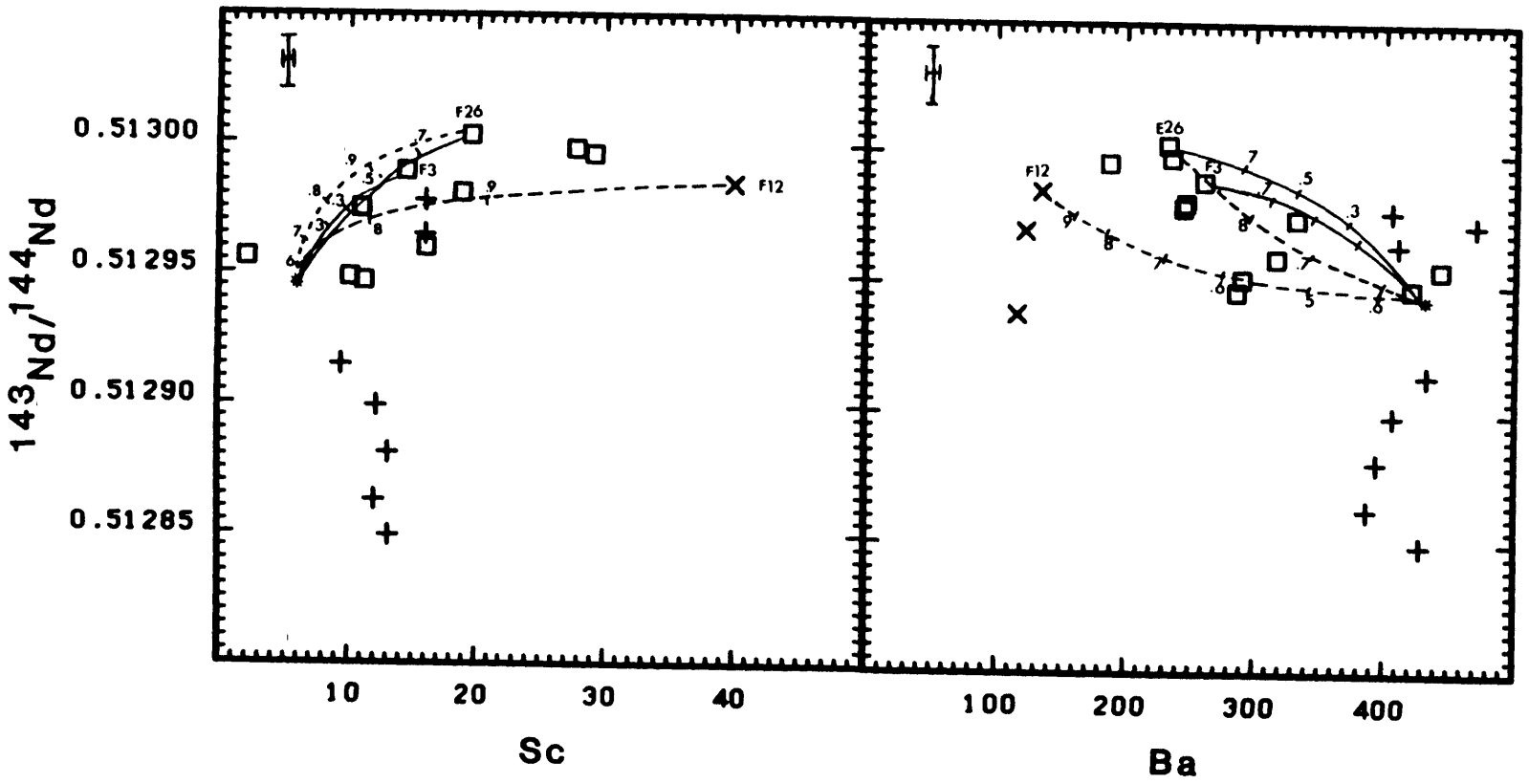
0.51300
0.51295
0.51290
0.51285
$^{143}Nd/^{144}Nd$
F26
F3
F12
10
20
30
40
Sc
E26
F12
F3
100
200
300
400
Ba

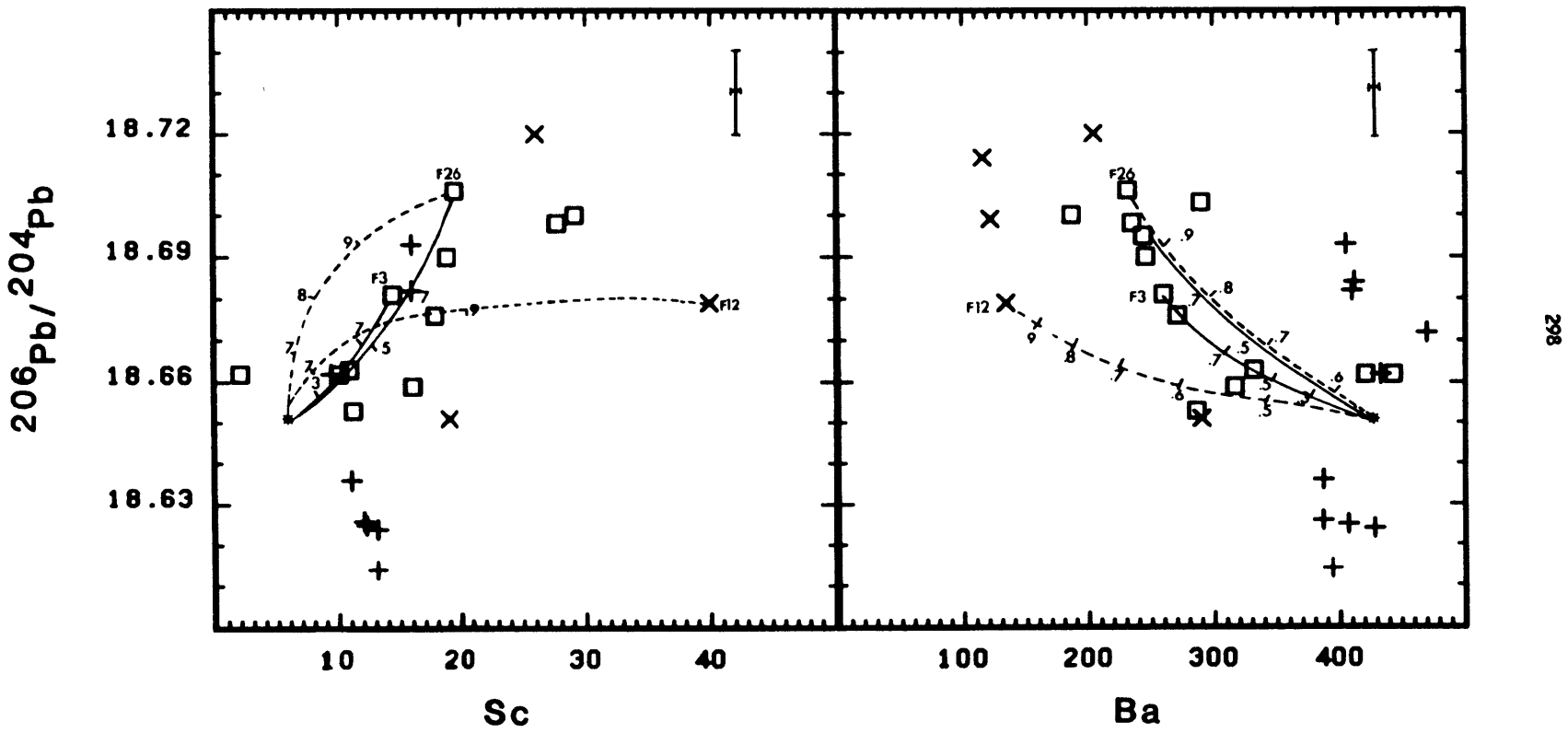
18.72
18.69
18.66
18.63
$^{206}Pb/^{204}Pb$
F26
F3
F12
10
20
30
40
Sc
100
200
300
400
Ba

$^{87}Sr/^{86}Sr$ than would be predicted from their $^{206}Pb/^{204}Pb$ and $^{143}Nd/^{144}Nd$ and are separate groups in Sr-Nd and Sr-Pb isotope diagrams. Within this group of lavas the more evolved samples, F2, F7 and F16, have higher $^{87}Sr/^{86}Sr$. This is true for all of the group 2 and 3 samples, with the more evolved lavas having higher $^{87}Sr/^{86}Sr$ than the primitive samples. The group 1 samples show the opposite trend. F14 and F19 have lower $^{87}Sr/^{86}Sr$ than the parental lavas of this group.

In the Sc vs $^{143}Nd/^{144}Nd$ diagram, the parental group 1 samples plot at low $^{143}Nd/^{144}Nd$ and relatively constant Sc. In contrast to the previous plot, the calcic group 2 and 3 samples show very limited $^{143}Nd/^{144}Nd$ variation while Sc decreases. The Sc vs $^{206}Pb/^{204}Pb$ diagram has features of both of the other diagrams. This isotopic ratio decreases between the primitive and evolved group 2 and 3 lavas. Group 1 samples have the lowest $^{206}Pb/^{204}Pb$, and they form a separate array to the group 2 and 3 lavas. F12 plots at higher Sc and slightly lower $^{206}Pb/^{204}Pb$ than the other primitive calcic lavas, and is anomalous in this diagram.

Ba vs $^{87}Sr/^{86}Sr$, $^{143}Nd/^{144}Nd$ and $^{206}Pb/^{204}Pb$ (Figure 4-11) show similar features to the Sc vs isotope diagrams, because Ba is another index of differentiation in the group 2 and 3 samples which is relatively constant in the group 1 lavas. A larger number of samples are plotted in these diagrams and two of the additional samples, the ankaramites F23 and F24, plot at low Ba due to the accumulation of

clinopyroxene. As expected, the $^{87}Sr/^{86}Sr$ diagram shows a good positive correlation. The low $^{87}Sr/^{86}Sr$ group (F2, F3, F5, F7 and F9) forms an upper bound on the data, and the calcic lavas form a lower bound. The Ba vs $^{143}Nd/^{144}Nd$ and $^{206}Pb/^{204}Pb$ diagrams are grossly similar as a result of the good correlation between these isotopes (Figure 4-10). Increasing Ba is accompanied by a slight decrease in $^{206}Pb/^{204}Pb$ and relatively constant $^{143}Nd/^{144}Nd$ in the group 2 and 3 lavas. These diagrams suggest that assimilation accompanies crystal fractionation in the group 2 and 3 lavas. The group 1 samples plot as a separate group in both diagrams. F14 and F19 are again displaced from the other group 1 samples, falling between the highly evolved (F15, F16 and F17) and moderately evolved group 2 and 3 samples. The evolved and primitive group 1 samples have very similar Ba and Sc (Table 4.1), and this would not be predicted given the phenocryst assemblages of these samples (chapter 3).

Isotopic and trace element constraints on magma mixing

The Sc-isotope and Ba-isotope diagrams show that the observed mixing arrays on isotope-isotope diagrams are composed of segments, with mixing between the principal endmembers and an intermediate component or components. F11, which is assumed to be a parental lava to some of the group 2 Feni lavas, and the evolved lavas (F15, F16 and F17), have isotopic compositions close to the midpoint between the

calcic alkali basalt endmember, F26, and the phonolitic tephritic endmembers (F1, F6 and F27) along the main data array in all the isotopic systems, and may represent such a component. The evolved samples plot close to the intersection of the data arrays in isotope-isotope and trace element-isotope diagrams, and mixing between a component similar to these lavas and F3, F5 and F26 could explain these arrays.

This possibility has been tested by calculating mixing curves between a hypothetical evolved endmember, with a composition given in Table 4.3, and F26 and F3, two alkali basalts with low Ni abundances and endmember isotopic composition. These two lavas were selected because they have major and trace element chemistry that is slightly more evolved than the most primitive Feni lavas, and this places them along the main fractionation sequence (Figure 4-3a). The calculated mixing curves which are drawn on the isotope-isotope diagrams could explain the distribution of data points in the $^{143}Nd/^{144}Nd$ vs $^{87}Sr/^{86}Sr$ and $^{206}Pb/^{204}Pb$ vs $^{143}Nd/^{144}Nd$ diagrams but fails to explain the distribution of data points in the $^{206}Pb/^{204}Pb$ vs $^{87}Sr/^{86}Sr$ diagram. The curvature of a mixing hyperbola is a function of r (Langmuir et al. 1978), a ratio constructed from the abundances of the two elements in both endmembers, and the predicted curvature can be changed by changing one or more of the concentrations. The changes in concentrations required to produce the correct curvature of a calculated mixing curve

Table 4.3

Magma Mixing Models

Evolved Endmember Composition

Sr	Nd	Pb	Sc	Ba	$^{87}Sr/^{86}Sr$	$^{143}Nd/^{144}Nd$	$^{206}Pb/^{204}Pb$
2100	11	15	6	430	0.70402	0.512945	18.650

Table 4.4

Partition Coefficients

	Cs	Rb	Ba	Th	Pb	K	Nb	La	Ce	Sr	Nd	P	Hf	Zr	Sm	Eu	Ti	Yb	Lu	Sc
cpx	.004	.001	.008	.011	.01	.002	.1	.16	.48	.054	1.5	.009	.7	.15	2.2	2.24	.3	2.67	2.82	4.5
plag	.01	.1	.25	.001	.1	.4	.01	.35	.16	2.5	.1	.01	.003	.003	.009	.085	.001	.05	.03	.03
amp	.04	.2	.02	.35	.08	.6	1.5	.7	1.6	3.5	3.1	.1	2.3	2.3	4.9	6.0	3.0	2.0	1.8	3.0
apat	.01	.01	.01	1.3	.4	.01	.1	5.0	10.0	3.0	18.0	100	.9	.9	16.0	15	.01	15	15	.04
Ti-mag	.01	.001	.001	.19	.1	.001	1.0	.03	.032	.001	.038	.001	.08	.1	.053	.055	6.0	.12	.14	3.0
oliv	.0001	.0002	.0001	.00001	.0004	.0002	.01	.008	.008	.0002	.005	.04	.004	.005	.005	.005	.01	.008	.009	.08
hauyne	.01	.15	.05	.02	.03	.5	.01	.059	.052	1.4	.048	.01	.04	.001	.048	.053	.01	.03	.02	.028

are difficult to envision in the primitive endmembers. If the hypothetical evolved endmember had lower Pb concentrations, mixing models would be successful. This however, would require a depletion of Pb during crystal fractionation; this is not observed in the Tabar-Feni islands.

The calculated mixing curves for F3 and F26 combined with the evolved endmember, are similar to the distribution of data points in the Sc vs isotope diagrams, and could be used to model the evolution of the evolved group 2 and 3 samples. These models also show similar fits to the data in the $^{206}Pb/^{204}Pb$ and $^{143}Nd/^{144}Nd$ vs Ba diagrams. The calculated mixing curve for F3 and the evolved endmember does not fit the data array produced by samples F2, F3, F5, F7 and F9 in the $^{87}Sr/^{86}Sr$ vs Ba diagram, having incorrect curvature. In general, simple two component mixing models are eliminated by the failure of the samples to lie along linear mixing curves in isotope vs the inverse of daughter element abundances, and the incorrect curvature of mixing arrays in the $^{87}Sr/^{86}Sr$ vs $^{206}Pb/^{204}Pb$ diagram. This type of model can explain the evidence cited earlier for a relationship between trace elements (Ba and Sc) and isotopes. More complex mixing models, which allow for crystal fractionation after mixing of slightly evolved alkali basalts and tephritic phonolites or trachyandesites, are difficult to support or rule out with the available data. The rest of this chapter presents AFC models for the

generation of the above mentioned mixing arrays amongst the group 2 and 3 samples and the generation of the evolved group 1 lavas. It is unlikely that these models will account for all or even most of the trace element and isotopic data given the complexity of the actual process. Even successful models are probably non-unique, given the number of parameters that are difficult to constrain. However, at least, these calculations will eliminate some models, provide constraints on the components involved in AFC models, give the author a better understanding of the limitations of this type of modeling and test if there are any clear distinctions between AFC and magma mixing models.

AFC models

One of the great difficulties in applying the AFC equations is the number of parameters that must be estimated. If the trace element concentration of an assimilant relative to the uncontaminated magma (Ca/Co) is to be estimated using equation 6a of DePaolo (1981), values for R, F, Co, Cm and D are required. Co and Cm are easy to estimate and can be taken as a primitive lava and an evolved lava. D, the bulk partition coefficient, can be estimated from the modal abundances of phases in the sequence of lavas, provided the assemblage composition is relatively constant and the fractionating assemblage is close to the modal abundance.

The concentrations of compatible, and especially highly compatible trace elements during AFC does not differ drastically from those predicted by the Rayleigh crystal fractionation equation for F values >0.5, and this is the only possible way to place some constraints on F. Provided there is no change of slope in the data array in log-log plots of a compatible and incompatible element, it may be possible to estimate F. This assumes that the bulk distribution coefficients (Table 4.4) of the two elements are significantly different. For the Feni samples, the two elements best suited to the estimation of F are Ba and Sc. Sc is compatible in the Feni lavas, and the calculated bulk distribution coefficient, derived from log Sc vs log Ba (not shown) for samples from groups 2 and 3, is approximately 2.65, assuming DBa=0.0. This value is quite robust as a value of DBa=0.1 gives a calculated DSc of 2.49. The calculated bulk distribution coefficient for the fractionating assemblage in Table 4.5 is almost identical to this value, and therefore the F estimate from the decrease in Sc concentrations is the same as the F estimate from Ba. The concentration of Ba in the parental and derivative lava, here taken to be F12 and F15, gives an F value of 0.31, assuming DBa=0.0. If Ca/Co for Ba is > 1.0, this estimate of F will be an underestimate and a value of 0.4 was used in the first F12 AFC model. The same approach gives F=0.55 for the evolution of F26 to F15. An estimate of F=0.55 for the generation of F19 from F1 was calculated from the decrease in

Ni between F1 and F19 assuming a bulk DNi of 4.4. Ni was used in this instance since Ba and Sc contents are similar in both of these lavas. An F value of 0.6 was used in a second AFC model using F12 as the uncontaminated magma.

The most difficult parameter to estimate in the AFC equations is R, and it is likely to be less than 1.0 (Kelemen 1986, Wyers and Barton 1987, DePaolo 1981, Singer and Kudo 1986). R probably decreases at shallow depths (Taylor 1980) and the Feni lavas have fractionated at shallow levels within the crust. Equation 7 of DePaolo (1981) shows that it is unlikely for the concentration of an incompatible element ($D<<1$) to decrease during AFC unless R is relatively large. Unfortunately as R approaches 1.0 the equation discussed above becomes invalid, as F is constant and equals 1.0. Also as R+D approaches 1.0, or as R approaches 1.0, a solution for Ca/Co can be found, for all elements. This was apparent at R values close to 0.9 in the models examined and simply reflects the physical model of a magma chamber that exists for an extremely long time with the addition of a component which acts as a dilutant. Even when R was equal to 0.8, this problem existed. The assimilant concentration approaches D X Cm if D is large and R is close to 1.0 and these models with large R values become impossible to interpret. For this reason R was constrained to have a value between 0.3 and 0.7 in the models.

Table 4.5

AFC Models

Parental Uncontaminated Magmas

F1, F12, F26

Derivative Magma Compositions

F1 model uses F19 as derivative magma

F12 & F26 models use a derivative magma with 1) isotopic composition

$^{87}Sr/^{86}Sr$ = 0.70402 $^{143}Nd/^{144}Nd$ = 0.512945 and $^{206}Pb/^{204}Pb$ = 18.650

2) Trace element abundances from F15 with the exception of Pb which was taken as 15 ppm.

Fractionating Assemblages

	Oliv	Cpx	Plag	Ti-mag	Amp	Apat	Hauy
F12 & F26	.05	.46	.255	.11	.09	.015	.02
F1	.23	.183	.32	.06	.06	.007	.14

Calculated Bulk Partition Coefficients

	Cs	Rb	Ba	Th	Pb	K	Nb	La	Ce	Sr	Nd	P	Hf	Zr	Sm	Eu	Ti	Yb	Lu	Sc
F12 & F26	.009	.047	.087	.078	.055	.167	.296	.310	.560	1.05	1.27	1.52	.553	.302	1.70	1.82	1.07	1.66	1.71	2.68
F1	.008	.066	.101	.044	.051	.236	.164	.227	.306	1.24	.607	.711	.271	.168	.789	.876	.555	.722	.731	1.17

F values

F12 0.40, 0.60

F26 0.55

F1 0.55

The values for the variables used in the models are given in Table 4.5 and the results are shown in Figure 4-12 and given in Table 4.6. The models that use F12 and F26 as the uncontaminated parental magmas, have a derivative magma that has a trace element composition similar to F15 and isotopic composition close to the intersection of the arrays in the isotope-isotope and isotope-trace element diagrams. The phonolitic tephrite model uses the group 1 lavas, F1 and F19, as the uncontaminated magma and the derivative magma.

In each diagram in Figure 4-12 there are three trace element abundance patterns that have been normalized to the parental composition: 1) the parental composition, which is the unit line, 2) the derivative composition, and 3) a composition that would result from Rayleigh crystal fractionation of the parental composition using the bulk partition coefficients and F values of Table 4.5. The phonolitic tephrite F14 is also plotted in Figure 4-12.

The proportions of olivine, clinopyroxene, plagioclase, amphibole, apatite, Ti-magnetite and hauyne, used to calculate D values, are based on the modal abundances of phenocrysts found in parental and derivative lavas, and in lavas of intermediate composition. The assimilant trace element concentrations were calculated for R values between 0.3 and 0.7, and these ranges are shown as a vertical bar for each element. The tick-marks along this bar are labeled with the R value.

Table 4.6

Calculated Isotopic Composition of Assimilant

	R	$^{87}Sr/^{86}Sr$	$^{143}Nd/^{144}Nd$	$^{206}Pb/^{204}Pb$
F12	.3	0.704248	0.512839	-
F=.4	.5	0.704123	0.512921	13.229
	.7	0.704044	0.512942	18.264
F26	.3	0.705718	-	17.620
F=.55	.5	0.704427	0.512821	17.897
	.7	0.704115	0.512926	18.193
F1	.3	0.703645	-	-
F=.55	.5	0.703774	0.513431	-
	.7	0.703852	0.513078	-
F12	.3	0.704346	-	18.581
F=.6	.5	0.704213	0.512853	18.584
	.7	0.704094	0.512928	18.592
F26	.3	0.708140	-	18.406
F=.65	.5	0.704727	0.512515	18.422
	.7	0.704196	0.512902	18.454

Figure 4-12

a) AFC model for evolution of F12 using F=0.4. Trace element abundances, of the uncontaminated parental magma (F12), the contaminated magma from Table 4.5, the calculated assimilant for R values between 0.3 and 0.7, and the abundances predicted for Rayleigh crystal fractionation. All abundances have been normalized to the parental magma. Vertical bars with tick marks are for the calculated assimilant and the tick-marks are labeled with the R value. Order of elements based on assummed order of incompatibilty during generation of MORB after Wood et al. (1979).
b) AFC model for evolution of F26 using F=0.55.
c) AFC model for evolution of F1 using F=0.55.
d) AFC model for evolution of F12 using F=0.6.

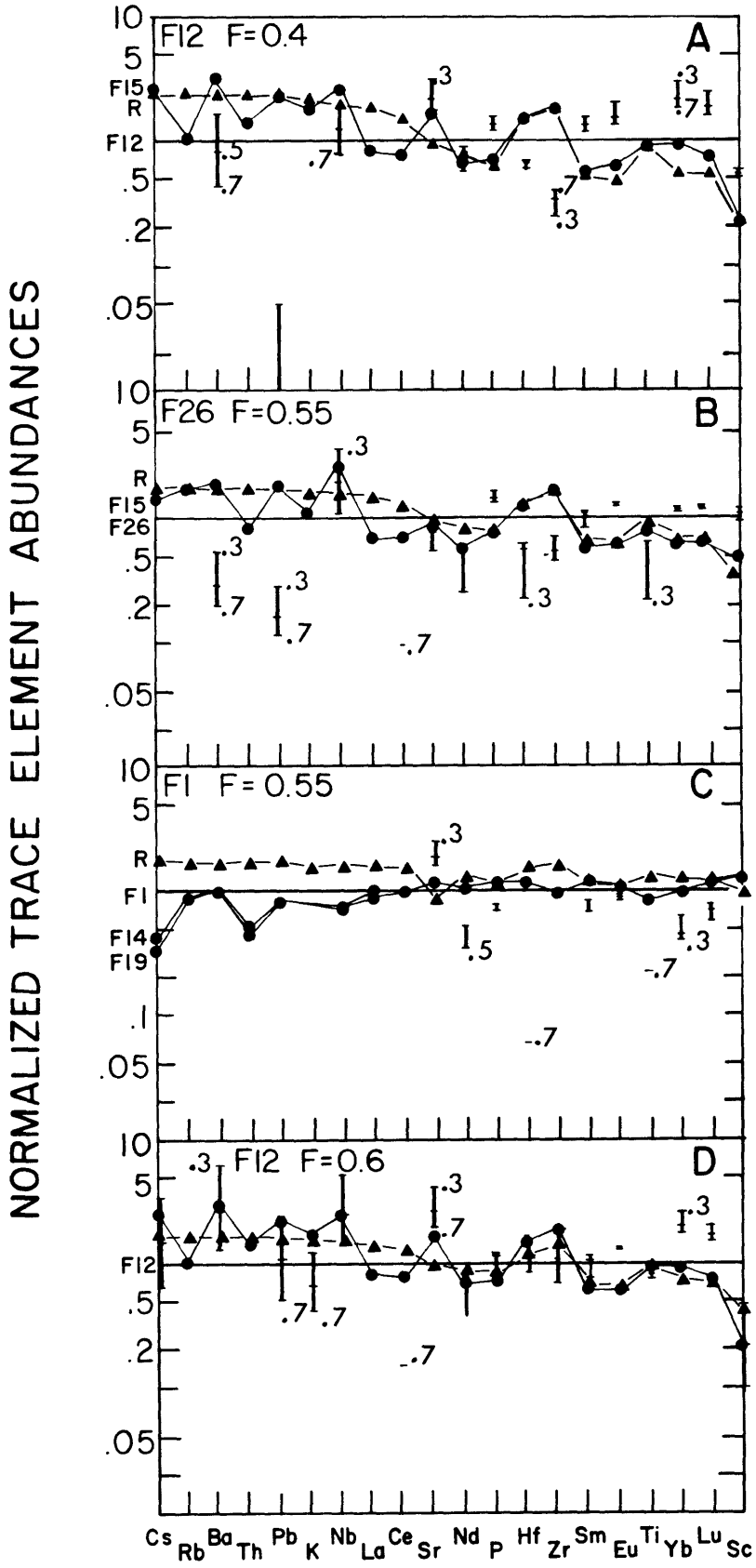
NORMALIZED TRACE ELEMENT ABUNDANCES
F12 F=0.4
A
F15
R
F12
F26 F=0.55
B
R
F15
F26
F1 F=0.55
C
R
F1
F14
F19
F12 F=0.6
D
F12
Cs Rb Ba Th Pb K Nb La Ce Sr Nd P Hf Zr Sm Eu Ti Yb Lu Sc

The Rb, Ba, Pb, Sr, P, Hf, Zr, Ti, Sc and the HREE abundance of F15 are almost identical to those predicted for Rayleigh crystal fractionation of F26. Cs, Pb, K, Nd, P, Hf, Zr, Sm, Ti and Sc are successfully modeled by Rayleigh crystal fractionation of F12. This is to be expected for some of these elements, because elements with bulk partition coefficients close to, or greater than 1.0, have similar predicted abundances for either process (DePaolo 1981), especially when F is large. Th, K, La, and Ce were significantly lower than predicted by the Rayleigh models while Ba and Nb abundances were higher than predicted in the models using F12 and F26 as parents. In both sets of models there were no solutions for Rb, Th, K and La within the adopted parameter limits, and the only solution for Ce was at R=0.7. The predicted assimilant was enriched in the HREE, Sc and P in both models and depleted in Hf, Zr and Pb. The calculated assimilant is depleted of Ba and Sr in the F26 model, while in the F12 model the assimilant is enriched in Sr and has similar or slightly lower Ba abundances and is depleted in Cs relative to the parental magma.

The trace element abundances of the group 1 lavas, F14 and F19, cannot be duplicated with any of the models. The Rayleigh crystal fractionation model predicts an increase in the concentrations of all elements except Sr and Sc. However, F19, which is closely related to F14, is depleted in many of these elements relative to F1. The AFC model is equally unsuccessful and no solutions were obtainable for

half of the elements examined, even at R values up to 0.85. The similarity between F1, and F14 and F19, is apparent in this diagram, especially for elements to the right of Nb. The isotopic differences between F14 and F19 are significant even though they have very similar major and trace element compositions (Figure 4.1, and Table 4.3.1) and this makes modeling difficult.

The isotopic compositions of the assimilants (Table 4.6) were calculated from the isotopic compositions of the uncontaminated and contaminated magma, and the calculated concentration of the assimilant. Where no solution exists, or the calculated isotopic composition is unrealistic, the model is unlikely to be correct. For example, if the model gives a $^{206}Pb/^{204}Pb$ of 13.229, it is safe to assume this model is incorrect. This isotope data also gives an indication of the sensitivity of the models to variation in R for the different isotopes. The models with lower F values are more sensitive to changes in R, as the equations predict, and the higher R value models predict assimilant isotopic compositions that are closer to those measured in the suite of lavas. Pb, the most incompatible daughter element of the three systems considered, gives the widest range in calculated isotopic compositions due to the lower calculated abundances of this element in the assimilant. Higher Pb abundances in the contaminated endmember results in assimilant isotopic compositions closer to the lavas and improves the stability of this value to changes in R.

The model shown in Figure 4-12d is for F=0.6, a higher F value than 0.4 which was used in the model shown in 12a, and all other parameters are the same. With higher F, it is possible to obtain solutions for more of the incompatible elements, as would be expected, and the concentrations of the assimilant are higher for elements with higher abundances than would be predicted by Rayleigh fractionation. This F value results in a poorer fit between the derivative magma abundances and the Rayleigh abundances for the more compatible elements. The abundances and isotopic composition of the assimilant are more realistic in this model, and this points to a fundamental problem with the application of AFC models; without excellent constraints on all of the input parameters, it is possible to generate an array of models that could work, especially for high F values.

The trajectories for the isotopic composition of a magma that is assimilating the calculated assimilants are shown on the isotope-isotope and isotope-trace element diagrams as dashed lines. The models shown are for R=0.7 and for the isotopic composition and assimilant abundances calculated from the F values given in Table 4.5. These trajectories are similar to the previously discussed mixing curves. The AFC model which uses F26 as the parental magma has an isotopic compositional trajectory which is closer to the sample data array in the Sr vs Pb isotope plot than the mixing model, although the fit is still poor. This model however has less success at duplicating the distribution of data than the

mixing model in the $^{143}Nd/^{144}Nd$ vs $^{87}Sr/^{86}Sr$ diagram. In the other isotope-isotope and isotope-trace element diagrams, there is no more success for the AFC models than for the mixing models discussed earlier.

Undoubtedly, the modeled solutions are dependent on the fractionating assemblage chosen, especially the proportion of apatite, and this can be used to explain the enrichment of the assimilant in the HREE and P in the AFC models, which have F12 and F26 as starting compositions. These models suggest an assimilant which is depleted in incompatible elements and enriched in compatible elements, as would be expected if assimilation of cumulates was taking place.

Even though the interpretation of the assimilant composition is open to debate, some important general conclusions can be obtained from these models. 1) The LREE, Rb, Th, and K are difficult to model with either Rayleigh crystal fractionation models or AFC models based on Ba and Sc abundances, and the bulk partition coefficients in Table 4.5. In this way, the Feni lavas are similar to the Lihir lavas, as these elements are difficult to model with currently accepted partition coefficients in both suites. 2) Unless R is greater than 0.7, and the assimilant is highly depleted in an incompatible element, there cannot be a decrease in concentration during assimilation accompanied by crystal fractionation. This argues against AFC and for magma mixing when highly incompatible element concentrations decrease between parent and derivative magmas. 3) The

solutions obtained are fairly robust to changes in R between 0.3 and 0.7, with only small variations in the composition of the calculated assimilant, especially when F is small. 4) A good fit to a Rayleigh crystal fractionation model for compatible elements cannot be used to argue against AFC and for fractional crystallization. 5) In many instances the AFC models are similar to magma mixing models, and there is no justification for choosing one over the other, if they both don't work.

Generation of evolved group 1 lavas

F14, F19 and F34 contain olivine, amphibole reacting to form a fine aggregate of cpx+Ti-magnetite+feldspar, sodic plagioclase and clinopyroxene with overgrown Fe-rich cores. If simple magma mixing is responsible for the disequilibrium textures, at least one of the endmembers must have been a primitive magma and at least one must have been more evolved than these lavas. The parental lavas for the three groups (F1, F11, F12) or the isotopic endmembers F26 and F3 can be taken as one endmember in this process. The evolved endmember must then fit a variety of compositional restraints enforced by the trace element and isotopic data of the chosen primitive endmember. F1 and F14 have almost identical Al_2O_3, CaO, and P_2O_5, and F14 has higher Sc than F1 and this requires an unusual evolved magma composition. Cs, Rb, Th, Nb, U, Pb, K and La, which are normally considered

incompatible, decrease between F1, and F14, F19 and F34. Ce, Ba, Zr and Hf abundances are similar in all of these lavas and most of the REE (Nd through Lu), and Sr are enriched in the evolved lavas relative to F1. Ni and Cr abundances are lower in F14, F19 and F34.

If mixing is invoked for the derivation of F14, F19 and F34, then one endmember cannot have a composition that is similar to <u>any</u> of the Feni lavas. Mixing between an evolved magma having similar composition to F16 and F17 (Tables 4.1 and 4.2), and a primitive magma similar to F11 or F12 could produce a mixed lava with major element composition similar to F14, however the isotopic and trace element data is impossible to explain with this model. This model requires an evolved endmember with high Nb and low Th (Figure 4-8) which would plot outside all analyzed lavas in this diagram. The La/Th vs Ba/La diagram (Figure 4-9) suggests an unknown endmember with high La/Th. This appears to be a dilution effect resulting from addition of a component that contains little or no Th as La also decreases between F1 and F14. This component may be a small degree partial melt which would be depleted in the HREE and Th and have high La/Th if apatite was residual. The qtz-trachytes, which may be crustal melts (Wallace et al. 1983) have many of the characteristics of such a component, being depleted in the REE and Th. However, these lavas have extremely high Ba/La and Sr/Nd. This is opposite to what is required by the constancy of Ba/La in the group 1 samples and curvature of the group 1 samples on a

$^{143}Nd/^{144}Nd$ vs $^{87}Sr/^{86}Sr$ diagram. To evolve from F1 to F14 or F19 requires drastic changes in $^{143}Nd/^{144}Nd$ while Nd abundances remain essentially constant.

From this discussion it can be concluded that simple binary mixing, between any of the analyzed lavas, cannot produce magmas with compositions like F14, F19 and F34. Derivation of these lavas from the parental lavas by crystal fractionation has previously been shown to be unfeasible by major element models (p 209) and trace element data (Figure 4-12c). The only remaining alternatives are mixing between a primitive Feni lava and an unknown magma/component of unusual composition.

Conclusions

The Feni volcanic lavas are complex, having evolved from at least 3 parental magma compositions by crystal fractionation, magma mixing and assimilation, either concurrently or as individual events. The trace element data is consistent with crystal fractionation of clinopyroxene, Ti-magnetite, plagioclase and apatite. Decreasing REE abundances in the lavas results from fractionation of an assemblage containing apatite. Evidence exists for multiple influxes of more primitive magmas in some of the alkali basalts (F3 and F5) and phonolitic tephrites (F14) in the form of cyclic overgrowths of more anorthitic plagioclase, overgrowth of Fe-rich clinopyroxenes by more magnesian clinopyroxene. The

group 3 lavas have higher La/Yb, higher REE abundance, and lower Nb than the group 2 samples. Apart from these differences, the trace element and isotopic composition of lavas from both groups are similar. The Sr, Pb and Nd isotopic data requires at least 3 isotopically distinct components to be involved in the generation of the Feni lavas. The group 2 and 3 lavas are more heterogeneous in Sr isotopes than the group 1 lavas, which have greater Nd isotopic variation.

AFC is suggested by increasing $^{87}Sr/^{86}Sr$ and decreasing, $^{143}Nd/^{144}Nd$ and $^{206}Pb/^{204}Pb$, coupled with decreasing Sc and increasing Ba. Quantitative magma mixing models and AFC models produce similar results, and are unsuccessful at explaining the observed abundance variations of elements with low calculated bulk partition coefficients and the curvature of some mixing arrays in isotope-isotope and isotope-trace element diagrams. It is difficult to disprove magma mixing, however the linearity of the logSc-logBa data and the good fit between the trace element abundances of the evolved lavas and predicted trace element abundances for Rayleigh fractionation models for compatible elements, suggests AFC is likely. The calculated assimilant is depleted in these elements and enriched in the HREE relative to the parental uncontaminated magma. Higher bulk partition coefficients for the incompatible elements would alleviate the difficulty of modeling these elements. AFC models with R values close to 0.7 allow abundances to be calculated for more elements and

have calculated assimilant isotopic compositions that are closer to the erupted lavas.

The group 1 lavas show large relative variations in Nd and Pb isotopes and only limited variation in $^{87}Sr/^{86}Sr$, and relatively constant Nd, Ba and Sc. Increasing La/Th at relatively constant Ba/La and high Nb/Th in the more evolved samples (F14, F19, and F34) of this group suggest an endmember that is not represented within the analyzed suite of lavas. These lavas have evolved by mixing between a primitive group 1 lava and another magma or component which is at present poorly constrained.

CHAPTER 5

THE GEOCHEMICAL CHARACTERISTICS OF THE MANTLE SOURCE OF THE TABAR-FENI LAVAS

Introduction

Previous chapters have dealt with the evolution of the Tabar-Feni lavas during fractionation, mixing and assimilation. Although these processes are complex, there is sufficient data for the Tabar-Feni islands to allow examination of the geochemistry of the mantle source regions, the mantle mineralogy, the possible components, (OIB, MORB, sediments/crust), and the enrichments of LILE and depletion of HFSE. The validity of "big picture" models must be assessed carefully as there are only a small number of primitive magmas from the Feni islands, a similar number from the Lihir islands, and each of the other island groups; most of these samples have lower Ni abundances than primary magmas (Hart and Davis 1978).

Tectonic setting

Undersaturated arc lavas are usually found in tectonically complex regions and sometimes show geochemical features that are gradational between arc and continental rift. These lavas are found behind extensional arcs on the boundaries of back arc basins (Gill 1981, 1984), where a linear feature, such as a transform fault, is subducted (De Long et al. 1979, Perfit et al. 1987), in regions undergoing rifting (Luhr and Carmichael 1985), and in

continental and oceanic arcs where contamination is common (Defino et al. 1986, Wyers and Barton 1987, Davidson 1987). Seismic data from New Ireland and the Tabar-Feni region (Weibenga 1973) shows no evidence for a slab beneath the Tabar-Feni islands, with all earthquakes located at shallow depths (<30 km) beneath the Tabar, Lihir and Tanga groups. Earthquakes beneath the Feni islands are <30 km or >300 km, with the the deeper ones resulting from plate subduction beneath East New Britain and Bougainville. The lack of deep seismicity, a volcanic hiatus of 25 my on New Ireland, and the development of basinal structures in the Tabar-Feni region (Exon and Tiffin 1982) all argue for a tensional rift environment being responsible for the undersaturated volcanism in the last few million years. The Tabar-Feni volcanics are not associated with a subducted plate, nor with fluids escaping from a subducting plate.

Characteristic element ratios in undersaturated arc lavas

The geochemical effects of mixing, assimilation and differentiation can be separated from inherited mantle characteristics by examination of ratios that are unaffected by the above processes. Trace elements and major element ratios that are relatively unaffected by fractionation of apatite and cpx, or data from primitive samples which have not crystallized apatite, can be used. In this chapter the samples from the Tabar-Feni islands have been divided into

primitive (MgO> 5.75%) and evolved so the effects of crystal fractionation can be examined and separated from source characteristics. The primitive samples have fractionated assemblages comprised of olivine and clinopyroxene. The evolved samples have, in addition, fractionated Ti-magnetite ±amphibole±plagioclase±apatite±hauyne.

Comparisons of the Tabar-Feni lavas with other arc lavas

The applicability of conclusions derived from the Tabar-Feni data to arcs in general, depends on whether these lavas have been derived from a "typical" arc mantle. Is the unusual major element chemistry an indication of an abnormal mantle source, a function of smaller melt fractions, different residual mantle mineralogy? The major element and trace element abundances, characteristic island arc basalt (IAB) ratios (Ba/La, Sr/Nd, Ba/Nb) and oceanic island basalt (OIB) ratios (P_2O_5/Ce, Nb/U, Pb/Ce), and isotopic ratios of Table 5.1 can be used to assess the "normality" of the mantle source of the Tabar-Feni lavas. This table contains data for five primitive Tabar-Feni lavas (F1-TG1), two other PNG suites (Bagana and Manam, Bultitude et al. 1978, Johnson et al. 1985), lavas from the Kermadec arc (Ewart and Hawkesworth 1987), from Aoba in the New Hebrides (Gorton 1977), and undersaturated arc lavas from Patmos, Greece (Wyers and Barton, 1987). Data for N-type MORB from the Woodlark Basin (Perfit et al. 1987) and alkali basalts from the Honolulu

Table 5.1 Major element trace element abundances and ratios, and isotopic ratios of lavas from the Tabar-Feni Islands and other arcs

	F1	F11	F12	L6	TG1	Bagana	Manam	Woodlark Basin	Kermadec	Aoba	Patmos	HVS[+]
SiO_2	51.51	48.18	47.18	47.24	47.81	55.21	52.44	50.23	49.5	48.3	50.27	45.1
MgO	7.60	8.96	14.47	7.47	6.21	3.78	7.34	7.82	6.24	13.7	6.83	8.20
Na_2O	5.82	3.39	2.51	2.15	3.55	3.83	2.41	2.85	1.73	2.06	3.24	3.25
K	28144	22415	16106	18513	29555	15340	5832	1127	2325	8999	22706	4898
Rb	55.6	56.9	57.5	43.5	70.4	24.1	9.4	1.0	5.6	17-7	107	7
Cs	1.84	1.17	0.513	0.850	1.25	.26		<.06				
Ba	394	246	134	168	290	253	167	4.5	94	332	1767	387
Sr	1469	1768	1082	1120	1749	799	568	111	237	587	1471	585
Nb	6.1	3.7	1.8	1.5	2.5	4	<1	1.7	0.53	1.31	18.0	24
Zr	95	87	68	70	71	80	26.9	99	29	45	220	110
Hf	2.1	2.0	1.7	1.8	1.9	2.2	0.78	1.9	1.1			2.65
Th	2.3	1.7	1 0	0.7	1.8	1.3		<.09	0.39	1.62	9.5	2.05
Pb	13.5	44.4	6.6		9.8	5.5		.48	1.56			4.0
U	1.3					.55		<.1	.167	0.51	3.77	1.62[♦]
La	14.6	19.6	15.3	12.2	18.2	11	4.3	2.90	2.38	11.74	70	21
Ce	31.0	43.7	36.2	28.4	49.1	24	9 7	10.2	6.7	26.5	114	44
Nd	16.0	23.8	22.8	18.4	24.4	13	6.2	10.1	5.8	15.1	52.16[*]	22
Sm	3.58	5.61	5.57	4.78	4.77	2.9	1.52	3.37	1.95	3.23	9.44	5.9
Yb	1.20	1.49	1.07	1.78	1.43	1.7	1.34	3.08	2.18	1.52	2.02	1.55
Lu	0.18	0.23	0.19	0.27			.211	0.520			.355	.245
Ba/La	27.0	12.6	8.76	13.8	15.9	23.0	39	15.5	39	28	25	18
Sr/Nd	91.2	74.3	47.5	60.9	71.7	61.5	92	11	41	39	28[*]	27
Ba/Th	171	145	134	240	161	195		>50	241	205	186	189
Ba/Nb	64.6	66.5	74.4	112	116	63	>170	2.6	177	253	987	16
P_2O_5/Ce	80.6	151	154	173	141	141	133	408	88	77	67	86
Ce/Pb	2.3	0.98	5.5	0.8-5.0[†]	1.9	4.4		26	3.4			11
Nb/U	47			2.5-4.0[†]	2.6	7.3		>17	2.3	3.2	4.77	15
Zr/Sm	26.5	15.5	12.2	14.6	14.9	27.6	17.7	29.4	13.3	13.9	23.3	19
La/Yb	12.2	13.2	17.2	6.7	12.7	6.5	3.2	.94	1.1	3.6	35	14
$^{87}Sr/^{86}Sr$	.704069	.703914	.703669	.703862	.703921	.7038	.7031-.7034	.7026-.7027	.7033-.7042		.70496	.70332
$^{143}Nd/^{144}Nd$	.512881	.512981	.512986	.512990	51292-.51303		.51295-.51303	.5130-.5131	.51297-.51305			.51302
$^{206}Pb/^{204}Pb$	18.614	18.690	18.679	18.74-18.76[†]	18.756		18.65-18.68		18.31-18.73			18.164
$^{207}Pb/^{204}Pb$	15.553	15.548	15.540	15.54-15.57[†]	15.555		15.55-15.54		15.54-15.59			15.466
$^{208}Pb/^{204}Pb$	38.357	38.330	38.305	38.33-38.44[†]	38.397		38.40-38.54		37.93-38.47			37.88
n						4	8	8	9	4	4	4

[*] Interpolated value or ratio using interpolated value; [†] Range from similar samples, sample not analysed or contaminated; [+] data from samples with SiO_2>44%; [♦] calculated from U/Th ratio of Honolulu Volcanic Series lavas, Tatsumoto (1978); Trace element data from previous chapters and Wallace et al. (1983), White and Patchett (1984), Perfit et al. (1987), Wyers and Barton (1987), Defino et al. (1986), Johnson et al. (1985), Ewart and Hawkesworth (1987), Bultitude et al. (1978), Gordon (1977), Oversby and Ewart (1972), Clague and Frey (1982).

Volcanic Series (HVS), Hawaii (Clague and Frey 1982) are given for comparison. The Tabar-Feni lavas are enriched in K, Ba, Sr, Cs, Th, Pb, the LREE and Na_2O, and have higher La/Yb than calc-alkaline basaltic andesites from Bagana volcano on Bougainville and tholeiitic basalts from, Manam, the Kermadec arc and Aoba. The Patmos ne-trachybasalts, and leucite bearing undersaturated arc lavas from Indonesia and Italy (Wheller et al. 1987, Pecerrilo et al. 1984, DeFino et al. 1986) are enriched in most trace elements relative to the Tabar-Feni samples. The level of trace element enrichment in the Tabar-Feni suite is not unusual for undersaturated arc lavas. The Nb, Zr and Hf abundances of the Tabar-Feni alkali basalts are similar to calc-alkaline and tholeiitic arc lavas and, similar to or lower than, N-type MORB from the Woodlark basin. The phonolitic tephrites have higher Th, Nb, Pb, Zr and Ba than the alkali basalts.

The similarity of the Tabar-Feni lavas to lavas from other arcs is best seen in similar, elevated Ba/La, Sr/Nd and Ba/Nb ratios accompanied by low Ce/Pb, Nb/U and Zr/Sm ratios. The primitive Tabar-Feni lavas have unusually high Pb (up to 44 ppm) and high Sr (up to 1900 ppm) when compared to other undersaturated arc lavas.

Morris and Hart (1983) have shown there is considerable overlap between OIB and IAB in K/Rb, K/Sr, K/Ba ratios and little or no overlap in K/Cs and Ba/La. Arc lavas normally have K/Cs <25000, K/Ba between 12 and 58, and Ba/La >15, while OIB have K/Cs have >30000, K/Ba <40 and Ba/La <15. The

two primitive samples F12 and F1 can be used as representative of the limits of compositions in the Tabar-Feni samples (Table 5.1). F12 and F1 have respective K/Cs, K/Ba and Ba/La of, 31000 and 15000, 120 and 71, and 8.8 and 27. Both of these lavas have extremely high arc K/Ba. The high K/Cs and low Ba/La of F12 suggests it is more "OIB" like than F1. This is opposite to what is suggested by HFSE depletions, as F12 has higher La/Nb. This inconsistency suggests differing relative enrichments of Ba, Cs, and K in the different mantle source regions. Positive correlations between Cs, K, and Nb (not shown) indicate these variations are not produced by alkali mobility during alteration.

Ce/Pb and Nb/U ratios are constant in oceanic basalts (Hofmann et al. 1986, Newsom et al. 1987) and have respective values of 25 and 47. The arc lavas of Table 5.1 have low Ce/Pb and Nb/U, with the exception of the phonolitic tephrites (F1) which has Nb/U identical to the oceanic value. U is enriched relative to Th during melting in intraoceanic arcs (Newman et al. 1984) and the low Ce/Pb and Nb/U reflect high Pb and U and low Nb in arc lavas.

Cs/Rb and Ba/Rb are constant in oceanic basalts (Hofmann and White 1983) with respective values of 1.25×10^{-2} and 11.3. The primitive Tabar-Feni lavas have respective ranges for these ratios of 0.9×10^{-2}-3×10^{-2}, and, 2-7. F12 has lower Cs/Rb and Ba/Rb and F1 has higher Cs/Rb and lower Ba/Rb than oceanic basalts. None of the Tabar-Feni lavas have both Cs/Rb and Ba/Rb values close to the oceanic values. In the

Tabar-Feni lavas there has been an enrichment of Rb, relative to Ba, and Cs relative to Rb in most of the lavas. The highest values for both ratios are found in the group 1 phonolitic tephrites and the lowest in the group 3 calcic alkali basalts. The group 3 samples have Cs/Rb close to the oceanic value but have higher Ba/Rb than the oceanic value.

The P_2O_5/Ce ratio, which is usually constant at 80±5 in undersaturated lavas from oceanic and continental environments (Sun and Hanson 1975a, Frey et al. 1978, Clague and Frey 1982), ranges from 80 in the group 1 tephritic phonolites from Feni to 170 in the calcic alkali basalts from Lihir. These values suggest the mantle source of the calcic alkali basalts has a relative enrichment of P_2O_5 over Ce. The source of the group 1 lavas from Feni have a P_2O_5/Ce ratio typical of OIB. Although the Tabar-Feni lavas have some unusual trace element abundances and ratios (high Pb, Sr, K/Ba, and low Th, Ce/Pb), and some lavas have OIB values for a few ratios (Nb/U, P_2O_5/Ce), they are undoubtedly derived from arc sources with the usual LILE enrichments and HFSE depletions.

Isotopic components in the Tabar-Feni lavas

The narrow range of Sr and Nd isotope ratios in uncontaminated arcs (Davidson 1987, von Drach et al. 1987, Stern and Ito 1983) argues for either efficient homogenization of components within the arc mantle or the

existence of a pervasive component (PREMA, Zindler and Hart 1986) that dominates the isotopic signature of lavas in arcs. The Tabar-Feni samples have limited variation in isotopic composition ($^{87}Sr/^{86}Sr$ 0.70356-0.70422, $^{143}Nd/^{144}Nd$ 0.51285-0.51302, and $^{206}Pb/^{204}Pb$ 18.61-18.76), are similar to other suites from this region of Papua New Guinea (DePaolo and Johnson 1979, Johnson et al. 1985), and to other oceanic arcs (Morris and Hart 1983, Myers and Marsh 1987, Meijer et al. 1976, McCulloch and Perfit 1981, Kay et al. 1986, Ewart and Hawkesworth 1987). These values are almost identical to the mean OIB isotopic compositions of Morris and Hart (1983). Isotopic data for samples from the Tabar and Tanga island groups which were not given in previous chapters are given in Table 5.2. This data shows lavas from these islands have similar isotopic composition to those found on Lihir. The Tabar-Feni samples plot to the right of a line connecting the most depleted Pacific MORB (highest $^{143}Nd/^{144}Nd$) and bulk earth (Figure 5-1a), and this is typical of arc lavas (Perfit et al. 1980, Hawkesworth 1982, von Drach et al. 1986).

The isotopic data for the Feni islands requires a minimum of 3 isotopic components (see chapter 4). The Tabar-Feni samples have isotopic compositions that are intermediate between the MORB and Samoa fields in Figure 5.1a. The Lihir, Tanga and Tabar samples have slightly higher $^{87}Sr/^{86}Sr$ than the Feni samples. There is some overlap with the field for Rabaul volcanics.

Table 5.2

Isotopic composition of Tanga and Tabar lavas

	$^{87}Sr/^{86}Sr$	$^{143}Nd/^{144}Nd$	$^{206}Pb/^{204}Pb$	$^{207}Pb/^{204}Pb$	$^{208}Pb/^{204}Pb$
Tanga					
TG1	0.703921±28		18.756	15.555	38.397
TG2	0.703927±28	0.513027±18	18.750	15.542	38.358
TG8	0.704264±30	0.512920±18	18.651	15.543	38.311
TG11	0.703977±30	0.512970±25			
Tabar					
TB1	0.703977±25	0.512941±18	18.750	15.540	38.324
TB2	0.703948±30	0.512969±18	18.746	15.551	38.381
TB3	0.703652±26	0.512980±23			
TB4	0.704174±28	0.512985±14			
TB5	0.704223±28	0.513000±15	18.762	15.550	38.359
	0.704239±28*				

* Acid washed

$^{87}Sr/^{86}Sr$ and $^{143}Nd/^{144}Nd$ error given are 2σ on the mean and are for the last 2 significant digits

In run statistics are better than .015% amu^{-1} and reproducibility is better thank 0.05% amu^{-1} for Pb isotopes corrected for machine fractionation using average from multiple analyses of NBS 981. NBS 981 value taken as average of Todt et al. (1983) and Hamelin et al. (1985).

Figure 5-1

a) $^{143}Nd/^{144}Nd$ vs $^{87}Sr/^{86}Sr$ for Tabar-Feni lavas. Symbols are as follows: (+) Feni, (X) Tabar, (○) Tanga, (□) Lihir (■) Rabaul, (◁) Bougainville. Data for the fields are taken from White et al. 1986, Wright and White 1986, McCulloch and Perfit 1981, von Drach et al. 1987, White and Patchett 1984, DePaolo and Johnson 1979, Palacz and Saunders 1986, Morris and Hart 1983, DePaolo and Wasserburg 1979. Bulk silicate earth is labeled as BE. The line connecting BE and the most depleted (i.e. highest $^{143}Nd/^{144}Nd$) Pacific MORB is discussed in the text.

b) $^{143}Nd/^{144}Nd$ vs $^{206}Pb/^{204}Pb$. Symbols and data for fields as for Figure 5-1a.

c) $^{207}Pb/^{204}Pb$ vs $^{206}Pb/^{204}Pb$. Symbols and data for fields as for figure 5-1a.

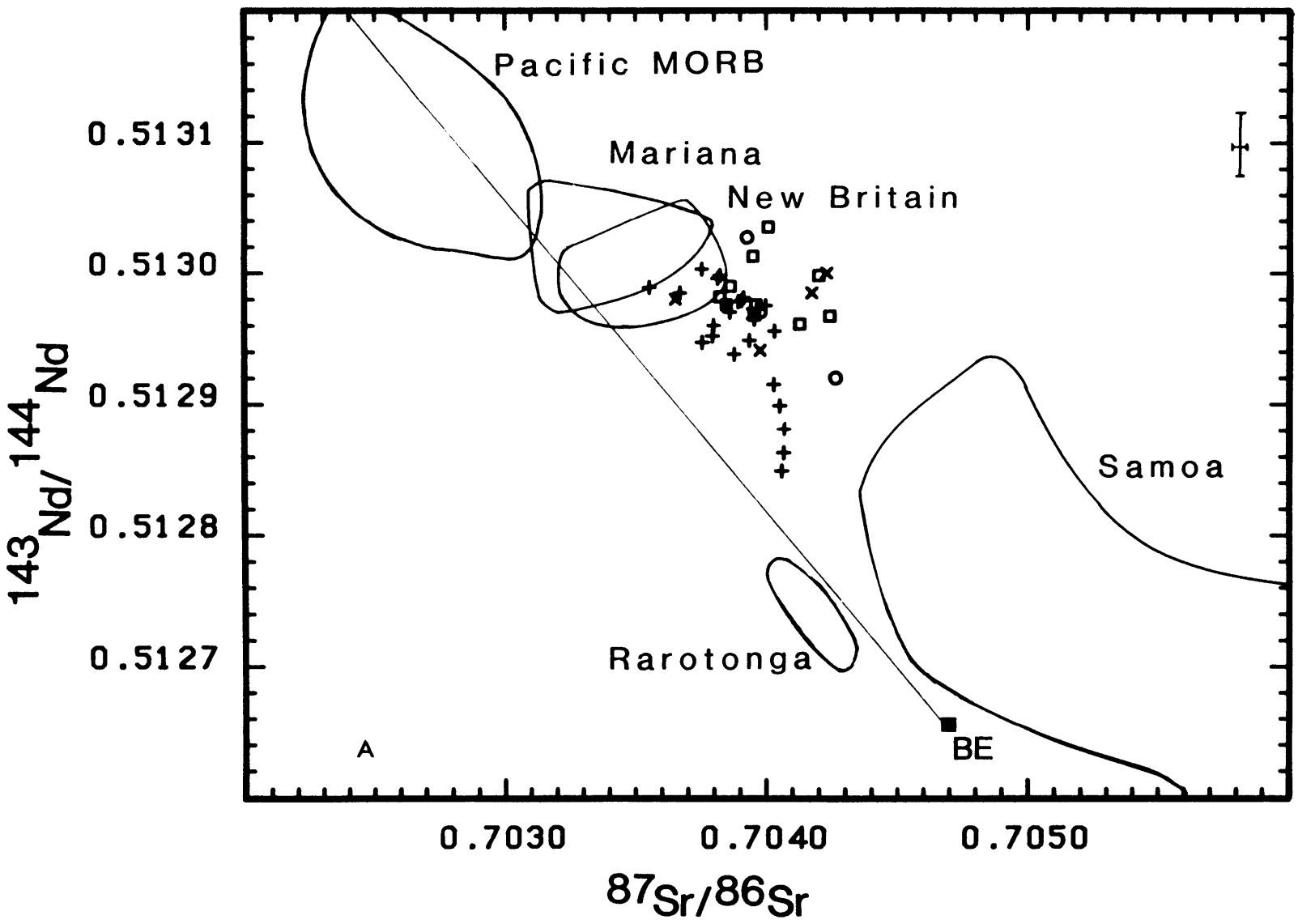
Pacific MORB
Mariana
New Britain
Samoa
Rarotonga
BE
A
0.5131
0.5130
0.5129
0.5128
0.5127
143Nd/144Nd
0.7030
0.7040
0.7050
87Sr/86Sr

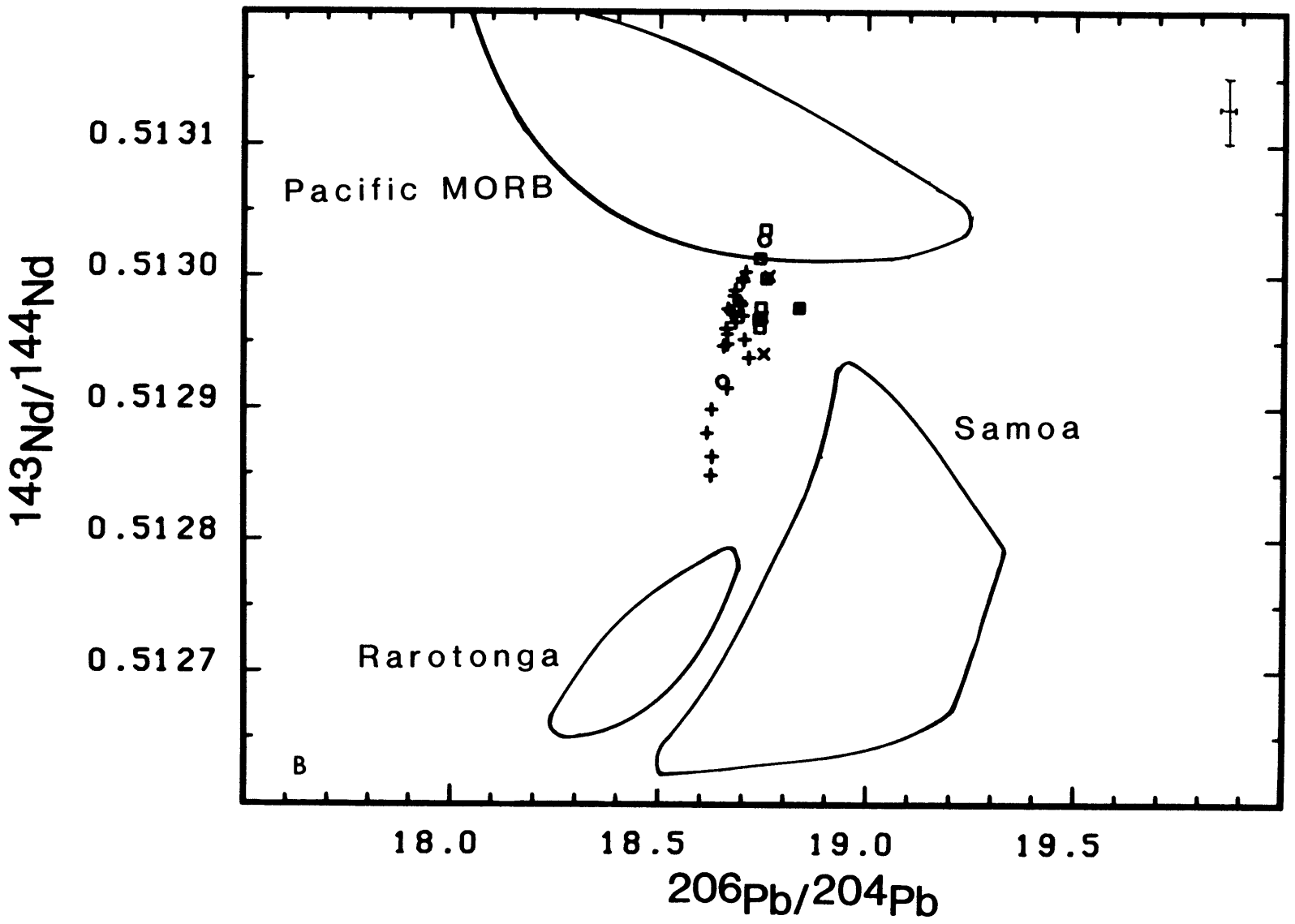
0.5131
0.5130
0.5129
0.5128
0.5127
143Nd/144Nd
Pacific MORB
Samoa
Rarotonga
B
18.0
18.5
19.0
19.5
206Pb/204Pb

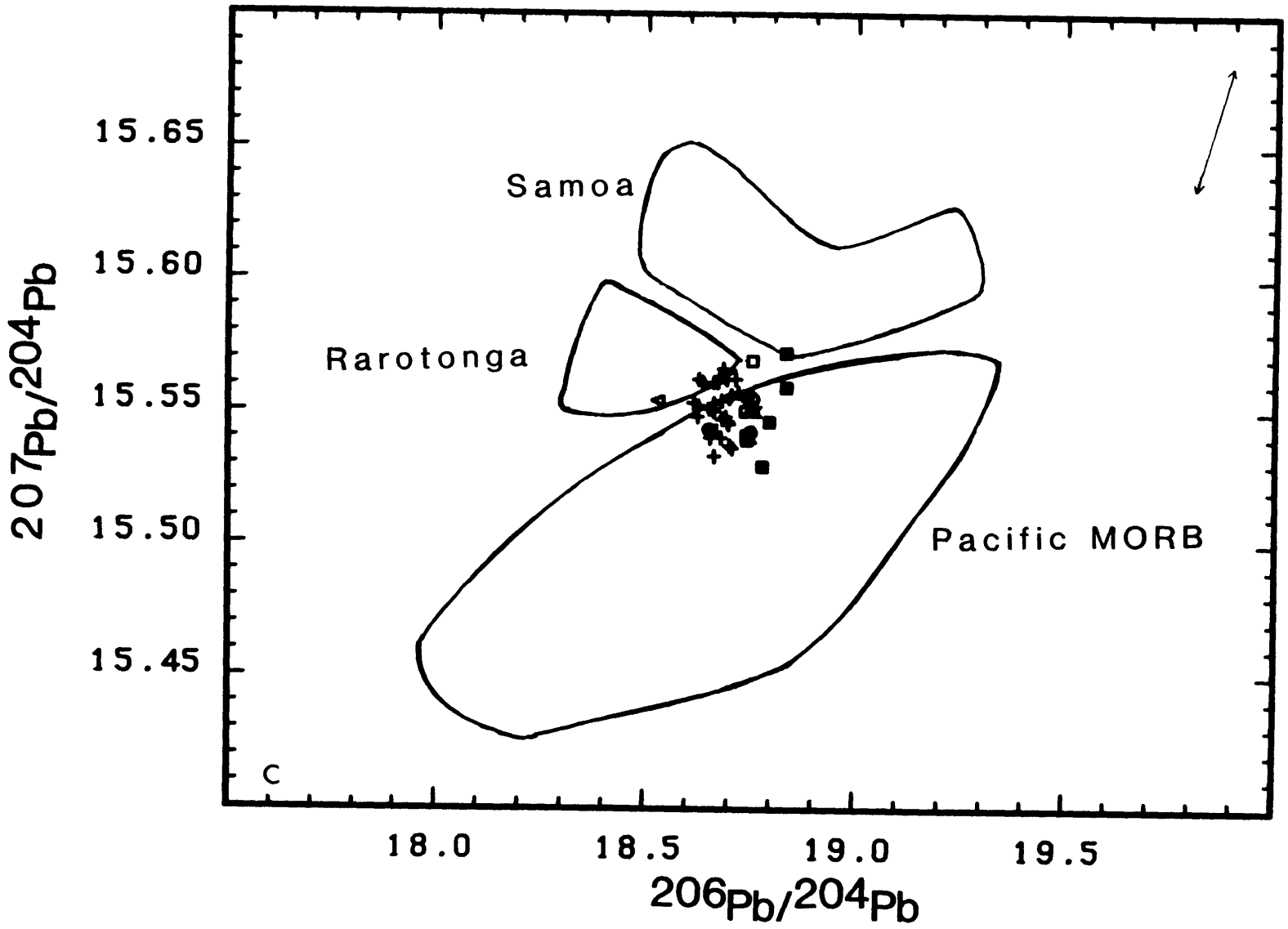
15.65
15.60
15.55
15.50
15.45
207Pb/204Pb
Samoa
Rarotonga
Pacific MORB
C
18.0
18.5
19.0
19.5
206Pb/204Pb

In Figure 5-1b the Tabar-Feni samples form a well defined array that extends downwards from the MORB field towards the Rarotonga and Samoa fields, suggesting both OIB and MORB components are involved in the genesis of the Tabar-Feni lavas. The isotopic composition of the mixing endmembers for the Tabar-Feni are similar to an EMII-type OIB (phonolitic tephrite) and to the PREMA components of Zindler and Hart (1986). The calcic alkali basalts have high $^{143}Nd/^{144}Nd$, $^{206}Pb/^{204}Pb$ and low $^{87}Sr/^{86}Sr$ and are close to an E-Type MORB composition in Figure 5-1a, and lie within the MORB field in Figures 5.1b and 5.1c. This endmember is difficult to assign to a specific component, as OIB, or a metasomatized MORB have the above characteristics. The data from the Tabar-Feni lavas support the model of Morris and Hart (1983) which calls for an OIB component in arcs.

The isotopic and trace element data and eruptive chronology of Fiji lavas (Gill 1984) are used to argue for a mantle source containing both OIB and MORB components. Lavas from Rarotonga (Palacz and Saunders 1987, Wright and White 1987), which have higher $^{208}Pb/^{204}Pb$ than the Tabar-Feni lavas, have $^{87}Sr/^{86}Sr$, $^{143}Nd/^{144}Nd$, $^{206}Pb/^{204}Pb$ and $^{207}Pb/^{204}Pb$ similar to the phonolotic tephrites. An OIB component similar to the Fiji or Rarotonga sources is probably present in the Tabar-Feni mantle. The higher $^{208}Pb/^{204}Pb$ of the Rarotonga lavas can be attributed to a long-term enrichment of Th in the source.

Data from the Lihir, Tabar and Tanga island groups

requires a component with higher $^{206}Pb/^{204}Pb$ than the two endmember Pb isotopic compositions identified in the Feni data (Figure 5-1c). The Pb data (Tables 2.1, 4.2 and 5.2) separates the islands from this chain into two groups, with most of the samples from Tabar, Lihir and Tanga having higher $^{206}Pb/^{204}Pb$ than samples from the Feni islands.

In Figure 5-1c, the Tabar-Feni samples plot as a tightly clustered group within and slightly above the Pacific MORB field, showing that an additional component with higher $^{207}Pb/^{204}Pb$, which could be OIB or sediments, is required if MORB is assumed to be an endmember component in the Feni lavas. The recycling of continental crust in the form of subducted sediments and as sediments within the arc crust is usually assumed to be at most a few percent (Tera et al. 1986, Sun 1980, White and Patchett 1984, Thirwall and Graham 1984). This amount of sediment/crust is sufficient to eliminate any overlap between MORB and IAB in Sr and Nd isotopes and to produce the characteristic $^{207}Pb/^{204}Pb$ of arc magmas. The high Pb abundances of the Tabar-Feni lavas can be used to argue for no sediment or crustal contamination. If the high Pb concentrations resulted from contamination by a crustal or sedimentary component in the magma source, the Pb isotopic signature of this component should dominate, as it does in the Grenada lavas (Thirwall and Graham 1984). High $^{207}Pb/^{204}Pb$ relative to $^{206}Pb/^{204}Pb$ is common in arc lavas (Armstrong 1981), and this can only be explained by an old component, such as sediments, or continental crustal or

lithospheric materials, or by an ancient mantle component. Pacific Ocean sediments have high $^{207}Pb/^{204}Pb$ (>15.5) and are more variable in $^{207}Pb/^{204}Pb$ and $^{208}Pb/^{204}Pb$ (Sun 1980) than the Tabar-Feni lavas. The constancy of these ratios in the Tabar-Feni lavas, and the low $^{207}Pb/^{204}Pb$ (<15.57) show that a sedimentary signature is not observable in the Tabar-Feni lavas (Figure 5-2).

The restricted range of $^{207}Pb/^{204}Pb$ and $^{208}Pb/^{204}Pb$ (Tables 2.1, 4.2, 5.2, 5.3 and Figure 5-2) indicates a common Pb component in eastern Papua New Guinea. With the exception of 3 samples, which plot just outside the edge of the Pacific MORB field, all of the Tabar-Feni samples plot within this field and the OIB field. There is no observable sedimentary Pb isotopic signature in lavas from eastern Papua New Guinea and OIB or MORB sources are sufficient.

The constancy of Sm/Nd has been discussed in chapter 2 and this indicates that the measured $^{143}Nd/^{144}Nd$ differences are much older than the arc system associated with the development of the mantle beneath these islands. In many ways, the isotopic data of the Tabar-Feni suite is divorced from the subduction process as suggested by Stern and Ito (1983).

In essence, the isotopic data from the Tabar-Feni islands does not require an old crustal or sedimentary component that has been introduced into the mantle by recent subduction processes (<100 my), and can be adequately explained as a mixture of different OIB isotopic components.

Table 5.3

Pb Isotopic composition of Rabaul and Bougainville lavas

	$^{206}Pb/^{204}Pb$	$^{207}Pb/^{204}Pb$	$^{208}Pb/^{204}Pb$
Rabaul			
R1	18.835	15.572	38.520
R2	18.778	15.529	38.313
R3	18.836	15.559	38.460
R4	18.795	15.546	38.415
Bougainville			
B1	18.657	15.543	38.404
B2	18.531	15.554	38.420
B3	18.450	15.562	38.279
	18.442	15.550	38.234

In run statistics are better than .015% amu^{-1} and reproducibility is better thank 0.05% amu^{-1} for Pb isotopes corrected for machine fractionation using average from multiple analyses of NBS 981. NBS 981 value taken as average of Todt et al. (1983) and Hamelin et al. (1985).

Figure 5.2

$^{208}Pb/^{204}Pb$ vs $^{207}Pb/^{204}Pb$ for Tabar-Feni lavas. OIB and sediment fields after Hickey et al. 1986. MORB field after White et al. 1986. The small field surrounding the Tabar-Feni data points encloses all samples from these islands and East New Britain and Bougainville. A fractionation vector giving 2 sigma errors is also shown.

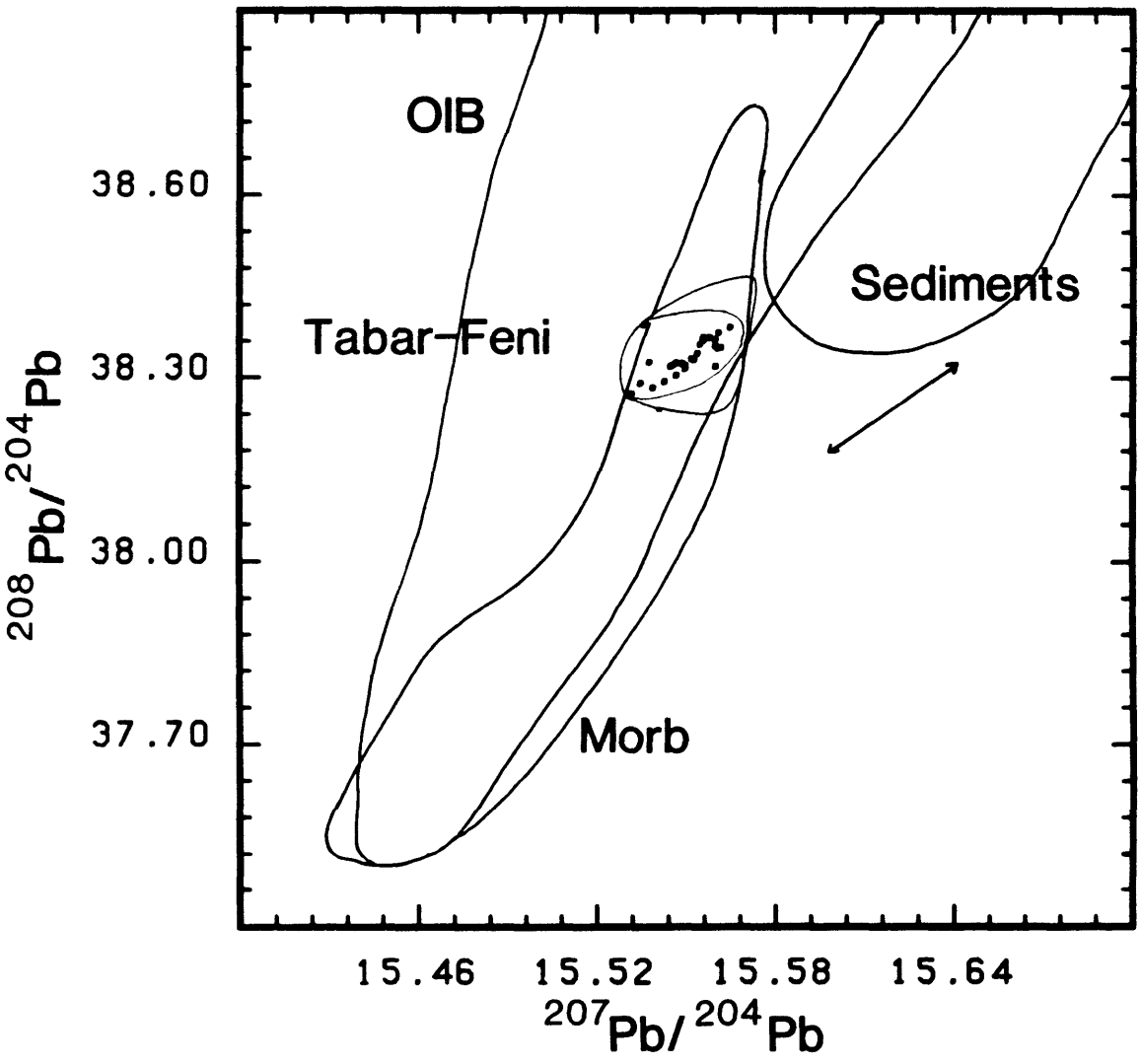
OIB
Tabar-Feni
Sediments
Morb
38.60
38.30
38.00
37.70
$^{208}Pb/^{204}Pb$
15.46
15.52
15.58
15.64
$^{207}Pb/^{204}Pb$

Since the isotopes and trace element ratios are not drastically different to those of uncontaminated arc lavas, this suite of samples demonstrate that undersaturated magmas can be generated from a "normal arc source".

The mantle source for the Tabar-Feni lavas

Modeling of the source characteristics and the melting process for the Tabar-Feni lavas requires a knowledge of the mineralogy of the mantle. However, at present there is no consensus about the primary source components of IAB, or the residual arc mantle mineralogy (Perfit and Kay 1986, Morris and Hart 1986, Green 1980, Arculus and Powell 1986, Baker and Eggler 1983, Brophy and Marsh 1986, Arculus and Powell 1986, Gust and Perfit 1987, Crawford et al. 1987). The Tabar-Feni undersaturated lavas may have been derived from an amphibole lherzolite "MORB" source (Perfit and Kay 1986, Ewart and Hawkesworth 1987), from a garnet lherzolite "OIB" source (Morris and Hart 1983), or perhaps even a phlogopite-bearing lherzolite (Varne 1986).

Major element constraints on mantle melting

The generation of undersaturated magma has been discussed at length in chapters 1 and 3, and only a short synopsis is given here. Low SiO_2 has been interpreted as an indication of either amphibole or garnet as a residual phase

in the mantle, and a greater contribution to the melt by a low SiO_2 phase (amphibole, olivine and garnet) than from orthopyroxene (Nicholls et al. 1980). High CaO/Al_2O_3 suggests spinel does not strongly influence the composition of the melt. The depth of generation of undersaturated lavas is poorly constrained by major element compositions. Thompson (1974) concluded that an alkali olivine basalt from the Isle of Skye was generated from a spinel lherzolite mantle at a depth of approximately 50 km. Wyllie (1979) has presented a projection of the composition of vapor-saturated melt compositions that showed that ne-normative melts can be generated at pressure as low as 16 kb. Higher SiO_2 and Na_2O can result from generation at lower pressures or higher water contents (Fujii and Scarfe 1985, Jaques and Green 1980).

The major element data indicates that either garnet or amphibole is present in the source of the Tabar-Feni lavas, but does not distinguish between them. The high K_2O of the primitive samples suggests a K-rich mantle which possibly contains phlogopite as a metasomatic phase.

Trace element constraints on source mineralogy

Lavas generated in equilibrium with garnet normally have variable La/Yb ratios and almost constant HREE concentrations (Shimizu and Arculus 1975, Minster and Allegre 1978, Sun and Hanson 1975b). In many Tabar-Feni lavas $(Yb/Lu)_{c.n.} < 1.0$ and

this is common in boninites (Hickey and Frey 1982) and occurs in other ne-normative arc lavas (Wyers and Barton 1987, Wheller et al. 1987). Differences in the HREE abundances of the primitive samples, given their almost identical La/Yb, and (Yb/Lu)c.n. <1, do not support residual garnet in the source. If garnet is a residual phase in the mantle during melting, the source must have unusual trace element characteristics.

The Tabar-Feni lavas have (Sm/Yb)c.n.> (Lu/Yb)c.n., concave upward curvature of REE patterns (Wallace et al. 1983) and variable HREE concentrations. This can be attributed to residual amphibole in the mantle or to high pressure fractionation of amphibole. The uniform Sm/Nd ratio of lavas from a single island could be explained by high degrees of partial melting. However, this is considered unlikely given the undersaturated nature of the lavas. The conclusion that amphibole is a residual phase is consistent with the interpretation of other researchers who have worked on arc lavas from PNG (White and Patchett 1984, Johnson et al. 1985, Johnson and Arculus 1981) and from other arcs (Whitford et al. 1979, Nicholls et al. 1980, White and Patchett 1984, Ewart and Hawkesworth 1987, Perfit et al. 1980, Perfit and Kay 1986).

Minster and Allegre (1978) suggested that phlogopite may be a residual phase during generation of undersaturated lavas from Grenada, and Varne (1985) has suggested a phlogopite-bearing mantle source for Indonesian arc lavas.

Clague and Frey (1982) calculated possible amounts of residual phlogopite to be between 2% and 7%, for highly undersaturated lavas with lower K_2O contents than Tabar-Feni lavas.

The poor correlation of K2O, Rb, and Ba with the REE, and of K, Rb and Cs, with Ba (Figure 4-5), and the large variation in the Ba/Rb (2.0-8.0) ratio of the primitive lavas can be explained by residual phlogopite controlling the partitioning of these elements (Hofmann 1986). An alternative explanation is the mobility of Rb and K_2O during post eruptive alteration (Hart 1971) of the fluid rich Tabar-Feni lavas.

Watson (1980) has shown that undersaturated lavas with SiO_2 contents similar to the Tabar-Feni lavas would require > 4% P_2O_5 to be saturated in apatite under mantle conditions. The Tabar-Feni lavas have P_2O_5 <1.0% and therefore have never been in equilibrium with residual mantle apatite.

Residual plagioclase can be ruled out by a number of facts: undersaturated lavas which have Al_2O_3 <16% cannot be generated at pressures within the plagioclase stability field (Jaques and Green 1980, and Wyllie 1979), and the high and variable Sr concentrations of the primitive lavas (1050-1900 ppm).

Melting models for Lihir lavas

Melting is undoubtedly non-modal when accessory phases

are involved (Jaques and Green 1980, Mysen and Kushiro 1977, Barton 1982, Wendlandt and Eggler 1980), but is likely to be close to invariant once accessory phases have melted (Mysen and Kushiro 1977, Presnall et al. 1979).

Modal, non-modal and continuous melting, with positive and negative proportions of phases entering the melt are used in the recent arc literature for modeling the generation of IAB. A variety of mineralogies, initial phase proportions and melting proportions are used (see for example, Perfit and Kay 1986, Morris and Hart 1983, Gill 1987, Ewart and Hawkesworth 1987, Brophy and Marsh 1986, Nicholls et al. 1980, Foden and Varne 1980).

The proportion of each phase in the source prior to melting is poorly constrained since samples of mantle xenoliths and high temperature peridotites have variable proportions of olivine, orthopyroxene, spinel, clinopyroxene, amphibole and garnet. Fortunately, three of these minerals have little effect on the partitioning of incompatible elements. The relative proportions of olivine, spinel and orthopyoxene melting are only important in terms of the major element composition of the melt. This, however, does not help with the choice of proportions of amphibole, garnet, phlogopite and clinopyroxene; the phases controlling the trace element abundances of the erupted lava.

Although the source mantle mineralogy in arcs is virtually unknown, lherzolitic xenoliths from Ichinomegata, Japan (Tanaka and Aoki 1981, Takahashi 1980, Sakuyama and

Koyaguchi 1986, Koyaguchi 1986, Takahashi 1985) give an indication of the phases and phase proportions that possibly occur in residual and fertile arc mantle. These xenoliths are found in basalts and andesites and are "relic" garnet lherzolites, and spinel lherzolites that contain pargasite (up to 9%) and small amounts of apatite and spinel. Both "garnet" bearing and fertile spinel lherzolites are LREE depleted and enriched in Ba relative to the REE. The least fertile spinel lherzolites (highest MgO) have higher La/Yb and are in some instances LREE enriched. Based on these samples, the following phase proportions were chosen.

The source oliv:opx:cpx:amp:spin:gar:phl percentages are: 1) GL, 60:23:12:0:0:5:0, 2) PAL, 60:18:12:5:0:0:5 and 3) AL, 58:20:12:10:0:0:0. The proportions of gar, phl, amp are extreme for residual mantle, however they facilitate a clear separation of calculated source characteristics. The results of these calculations are shown as source mantle REE patterns in Figure 5-3 and have been included as fields on the ratio-ratio plots (Figure 5-4).

The simplest approach to trace element modeling of source characteristics, given the above mentioned uncertainties, is back calculation of trace element abundances in the residual mantle using the equilibrium (batch) melting equations (Shaw 1970), since this requires "estimation" of the least number of variables. This approach ignores the possibility of non-uniqueness (Albarede and Tamagnanagon 1986, Hofmann 1986), the possibility of

source heterogeneity in trace element concentrations, and melt extraction problems (McKenzie 1984, Navon and Stolper 1987, Suen and Frey 1985).

Table 5.4 gives the partition coefficients used in the melting models. These values are from experimental mineral-melt and phenocryst-groundmass partitioning studies where possible, or from mineral-mineral partitioning studies in ultramafic nodules combined with the available mineral-melt partition coefficients.

In the following sections, calculated source trace element abundances for the three hypothetical source mantle mineralogies (amphibole lherzolite (AL), garnet lherzolite (GL), and phlogopite-amphibole lherzolite (PAL)) are discussed.

REE characteristic of model mantle sources

The calculated mantle source compositions (Figure 5.3) all have curved REE patterns and calculated Sm and Eu abundances that result in a pronounced hump in the REE patterns. The major differences between the AL, PAL and GL sources is in the HREE, as the LREE are highly incompatible in each of these sources. The AL and PAL sources calculated for <5% partial melting percentages have REE patterns that are similar to fertile (high CaO, low MgO) amphibole bearing spinel lherzolites from Japan (Tanaka and Aoki, 1981), West Germany (Stosch and Lugmair 1986), Nunivak, and Salt Lake

Table 5.4

Partition Coefficients

	Oliv	Opx	Cpx	Spin	Amp	Phlog	Gar
Ba	.0001	.0001	.0008	.0001	.6	6.0	.0017
Sr	.0002	.0026	.054	.0001	.1	.08	.0001
K	.0002	.0002	.002	.0001	.33	1.6	.0002
Rb	.0002	.0002	.001	.0001	.2	1.6	.0001
Pb	.0002	.0002	.01	.0001	.034	.006	.004
U	.0001	.0002	.0007	.0001	.04	.038	.003
Th	.0002	.003	.0002	.0001	.038	.04	.00004
La	.008	.0012	.058	.0001	.17	.018	.005
Ce	.008	.0016	.100	.00015	.26	.017	.02
Nd	.005	.0028	.22	.0002	.44	.016	.08
Sm	.005	.0054	.45	.0005	.76	.016	.1
Eu	.005	.015	.48	.0015	.80	.016	.2
Tb	.006	.025	.50	.0025	.85	.017	.7
Yb	.009	.070	.53	.007	.59	.018	5.0
Lu	.0095	.090	.50	.009	.51	.018	8.0
Hf	.0004	.036	.25	.08	.38	.08	.14
Nb	.008	.008	.1	.005	.5	.33	.1

Partition coefficients from experimental megacryst-host and xenolith studies from Watson et al. (1987), Irving and Frey (1984, 1985), Frey et al. (1978), Nicholls and Harris (1980), Stosch (1982), Stosch and Lugmair (1986), Dunn and McCallum (1982), Dunn (1987), Kurat et al. (1980), Dautria et al. (1987), Shimizu (1974), Shimizu and Kushiro (1975), Cohen et al. (1984), Kramers (1977), Richardson et al. (1985), Irving and Frey (1978), Fujimaki and Tatsumoto (1984), Morioka and Kigoshi (1978).

Crater, Oahu (BVSP 1981). In contrast, the reversal of curvature of the REE patterns is unusual for garnet lherzolites. Garnet lherzolites usually have LREE depleted to LREE enriched patterns which have smooth curvature. The calculated source for F12 has a chondrite normalized enrichment of Sm over Yb. The problem of a strangely distorted GL source REE pattern cannot be alleviated by the addition of garnet to the source. This would result in lower calculated La/Yb and higher HREE abundances. However, the REE pattern becomes even more distorted and the calculated (Lu/Yb)c.n. ratio is increased to unlikely values (>2). The presence of phlogopite in the source results in a minor reduction of the calculated source abundances, but otherwise produces an identical REE abundance pattern to an AL source.

Although these calculated sources cannot be used to rule out garnet as a residual mantle phase, they do point out the unusual REE abundances of a source which contains residual garnet. The enrichment of a previously depleted mantle, which results in the formation of an amphibole bearing lherzolite, and the subsequent melting of this enriched mantle is considered more likely. These models, although simple, show that the mantle source for the Tabar-Feni lavas is likely to be enriched in the MREE and, that a phlogopite bearing source cannot be distinguished from a source which does not contain this phase using only REE abundance patterns.

Figure 5.3

REE patterns for calculated mantle sources using batch melting equations of Shaw 1970 and assumed mantle mineralogies and phase proportions. Sources were taken as having oliv, opx, cpx, amp, spin, gar, phl in the proportions 1) 60:23:12:0:0:5:0, 2) 60:18:20:5:0:0:5, 3) 58:20:12:10:0:0:0. Source compositions were calculated using partition coefficients in Table 5.4 and for magma compositions F1 and F12. Shaded fields delineate the range of calculated abundances for an element within the source for F=0 to 0.1. Phlogopite-amphibole lherzolite calculated source compositions have lower REE abundances than amphibole lherzolite sources in the upper diagrams. The calculated REE fields for the garnet lherzolite sources are shown in the lower diagrams. Fields are patterned as follows. AL (///), PAL (\\\), and GL (///).

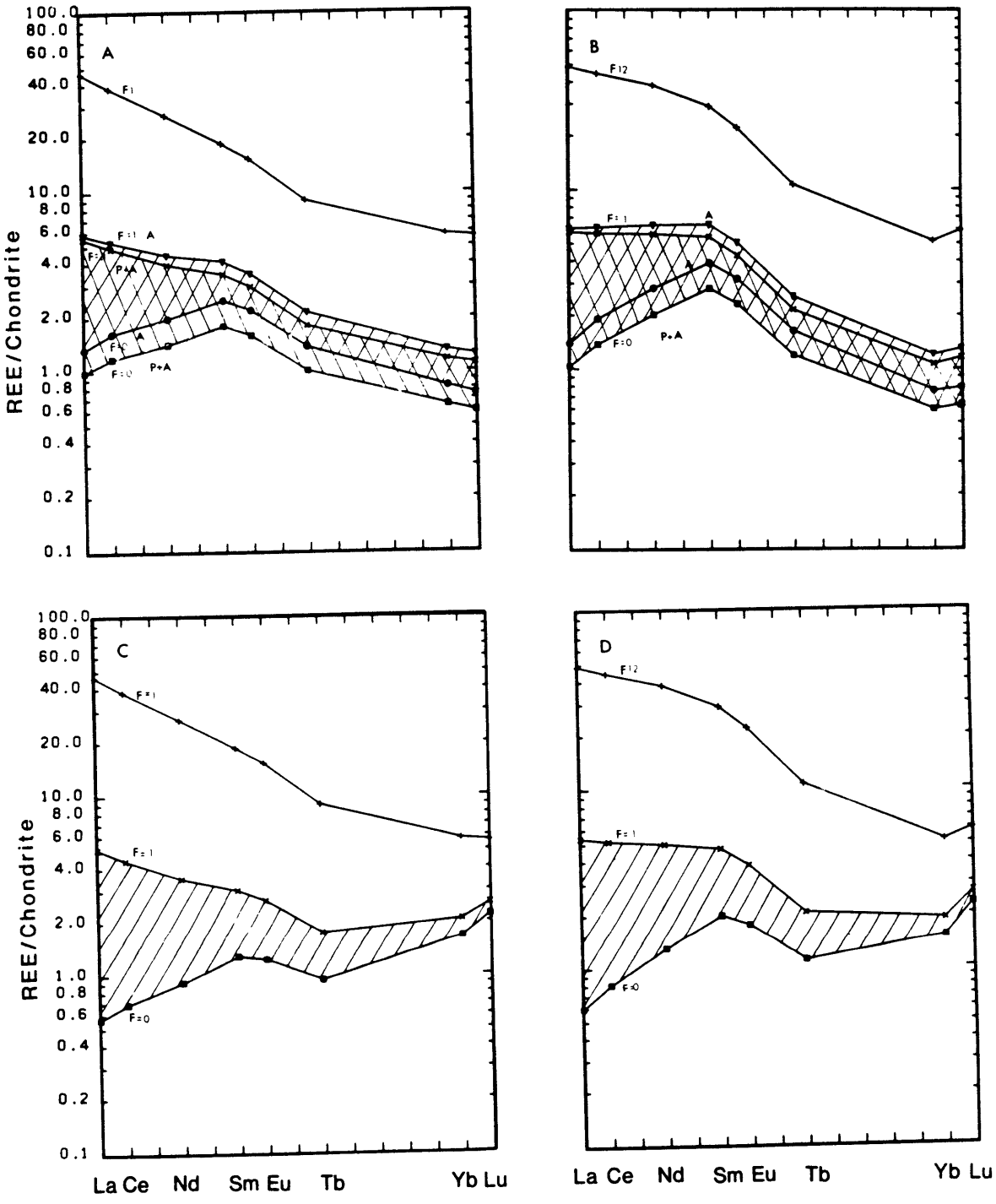
A
B
C
D
REE/Chondrite
100.0
80.0
60.0
40.0
20.0
10.0
8.0
6.0
4.0
2.0
1.0
0.8
0.6
0.4
0.2
0.1
F=1
F=0
P+A
La Ce Nd Sm Eu Tb Yb Lu

The LILE enrichments of arc lavas results from the influx of a metasomatic fluid/melt (Perfit et al. 1980, Newman et al. 1984, Morris and Hart 1983, and Davidson 1987). With this in mind, the next section examines the available information on fluids in equilibrium with mantle materials, and places it in the context of arc petrogenesis.

"Metasomatism" in the Tabar-Feni mantle

The distribution of incompatible elements within mantle materials is complex, see for example Fraser et al. (1983), Suzuki (1986, 1987), Stosch and Lugmair (1986), Menzies and Wass (1983). In many instances the enrichment of incompatible elements along grain boundaries and within xenoliths can be attributed to fluid/melt influx (Zindler and Jagoutz 1988, Stosch 1982), and the elements affected by this process include Na, Cs, Rb, K, Ba, LREE, Th and possibly the HFSE. Mantle enrichment can be produced by low density volatile-rich fluids or melts, although low percentage partial melts with their higher concentrations of incompatible elements are more efficient at producing enrichments (Schneider and Eggler 1986). At 12 kb, fluids produced by dehydration of synthetic serpentine are enriched in Cs, Rb K, Ba and Sr relative to the REE which are enriched relative to the HFSE (Tatsumi et al. 1986).

If fluids exist in the subarc mantle that are in equilibrium with mantle peridotite at depths greater than 70 km, then these fluids are likely to be H_2O-rich, containing a few percent of dissolved solute which is rich in silica and sodium (Schneider and Eggler 1986) and enriched in LILE relative to the REE.

Low density volatile-rich fluids may exist within the mantle at depths >22 kb if there is sufficient H_2O present to allow most of the K_2O to be converted into phlogopite. This requires the H_2O/K_2O ratio of the mantle to exceed 0.3 (Eggler 1987). If 3.6% K_2O is taken as the upper limit for a primary Tabar-Feni magma and 5% partial melting is assumed, the K content of the mantle would be 1500 ppm if K is highly incompatible during melting. This amount of K would amount to approx. 1% phlogopite and this would require >.05% H_2O for a separate fluid phase to exist at depths of approximately 70 km. Such a fluid phase could have a relative depletion of K when compared to the fluid emanating from the slab.

At depths <22 kb where amphibole is stable, mantle fluids are more likely to be CO_2-rich and to contain much less dissolved solute (Schneider and Eggler 1986), thus it is conceivable that the continual precipitation of alkalis and trace elements from a slab derived fluid produces an enriched zone in the sub-arc mantle close to the upper most stability limit for amphibole (Schneider and Eggler 1986, Takahashi 1986, and Tatsumi et al. 1986). Melting within the above mentioned enriched zone, or melting associated with an influx

of this fluid could produce arc magmas that have relative enrichments and depletions of the different trace element groups, LILE, REE and HFSE. CO_2 or Cl rich fluids are likely to have higher Na/Al ratios and SiO_2 contents than H_2O-rich fluids (DeFino et al. 1986, Schneider and Eggler 1986). The high Na_2O (6%), SiO_2 (52%) and Cl, and lower H_2O contents of the phonolitic tephrites is consistent with this suggestion.

The influx of a mantle fluid produces H_2O- and CO_2-rich metasomatic mantle phases such as amphibole, phlogopite, apatite, and dolomite. These phases, with the exception of apatite, are possibly present in the mantle source for the Tabar-Feni lavas and are capable of fractionating many of the ratios that are characteristic of arc and OIB lavas, such as K/Rb, K/Ba and K/Sr and Ba/La.

Partial melts within the mantle are unlikely to fractionate K, Cs, Rb, and Sr from the LREE (Wood et al. 1979) sufficiently to produce the characteristic LILE enrichment arc lavas. Partial melts within the arc mantle may result in the enrichment of zones or regions. However, this is movement or concentration of arc enrichments and not generation of them.

LILE enrichments and HFSE depletions in arc mantle

Recent experimental work has shown that the presence of a residual Ti-rich phase, such as sphene, ilmemite or rutile

in the source regions for arc magmas is highly unlikely (Green and Pearson 1986, Ryerson and Watson 1988). If there is no phase retaining the HFSE during melting then the low concentrations in erupted lavas must result from melting of a previously depleted source. Ion microprobe studies of clinopyroxene in lherzolitic nodules (Salters and Shimizu 1988) show the presence of HFSE depletions in mantle xenoliths from oceanic, continental and "arc" localities and this may be a general characteristic of lherzolites from shallow depths. This provides a simple explanation for the HFSE depletions in arc lavas; the arc mantle is depleted prior to melting. This is supported by the existence of primitive arc lavas from the New Britain region with MORB like REE abundances and HFSE depletions (Perfit et al. 1980). An OIB mantle which had previously been depleted in HFSE and subsequently enriched with LILE would make an ideal arc source.

HFSE depletions are in some instances poorly coupled to the LILE enrichments (Morris 1984, Ewart and Hawkesworth 1987). In other instances, the HFSE and LILE are coupled by the partial melting process (Varne and Foden 1986). Since the HFSE depletion is a residual mantle characteristic that is inherited by the arc source, it is unlikely that the magnitude of the HFSE depletions would be positively correlated with the magnitude of the LILE enrichment.

Correlations between HFSE depletions and LILE enrichments

The ratio-ratio plots using Ba/La, Sr/Nd, La/Nb, La/Sm, and Ce/Yb ratios of primitive and evolved lavas (Figure 5-4) show the relationship between LILE enrichments and, HFSE depletions, and REE enrichment, for the primitive and evolved Tabar-Feni lavas. The compositions listed in Table 5.1 and calculated fields for mantle source compositions (<10% batch partial melting) and bulk silicate earth (BSE) ratios are also shown. The position of the calculated source composition fields depends on the modal mineralogy and partition coefficients and these fields can only be used to qualitatively examine source characteristics. The fields were calculated for the previously given source mineralogies and partition coefficients.

There is a positive correlation between Sr/Nd and Ba/La, a negative correlation between Sr/Nd and La/Nb, and a weak positive correlation between Ba/La and La/Sm (Figures 5-4a, 5-4b and 5-4c), for both the primitive and evolved Tabar-Feni lavas. The evolved lavas are more scattered and extend to higher Ba/La (>50) and, Sr/Nd (>120) than the primitive group, although there is no systematic displacement to higher values. There is no well defined relationship between Sr/Nd and Ce/Yb (Figure 5-4d). The primitive lavas from Feni, (F1, F11 and F12) form a linear trend with negative slope on this diagram, while the majority of samples, both primitive and evolved, form an array with

Figure 5.4

Ratio-ratio plots showing the relationship between LILE enrichment and HFSE depletion, and, LILE enrichment and REE enrichment in the Tabar-Feni lavas. Evolved lavas are shown as filled squares and primitive lavas (>5.75% MgO) are shown as open circles. Samples F1, F11, F12, and L6 are labeled in each figure. Averaged composition for other arcs are shown as labeled: A, Aoba; K, Kermadec; M, Manum; B, Bagana; and P, Patmos. W is Woodlark basin N-type MORB. Bulk silicate earth ratios are marked as vertical or horizontal lines. Calculated source fields are labeled GL, garnet lherzolite, AL, amphibole lherzolite, and PAL, phlogopite-amphibole lherzolite in Figure 5-4a and 5-4c. In Figure 5-4b all three source fields overlap and a single field is shown. Within this field are marked individual fields calculated for F1, F11 and F12. In Figure 5-4d, Al and PAL fields overlap and are shown as a single field. In each diagram partial melting fractions of 0, .05 and .1 are labeled of the amphibole lherzolite field.

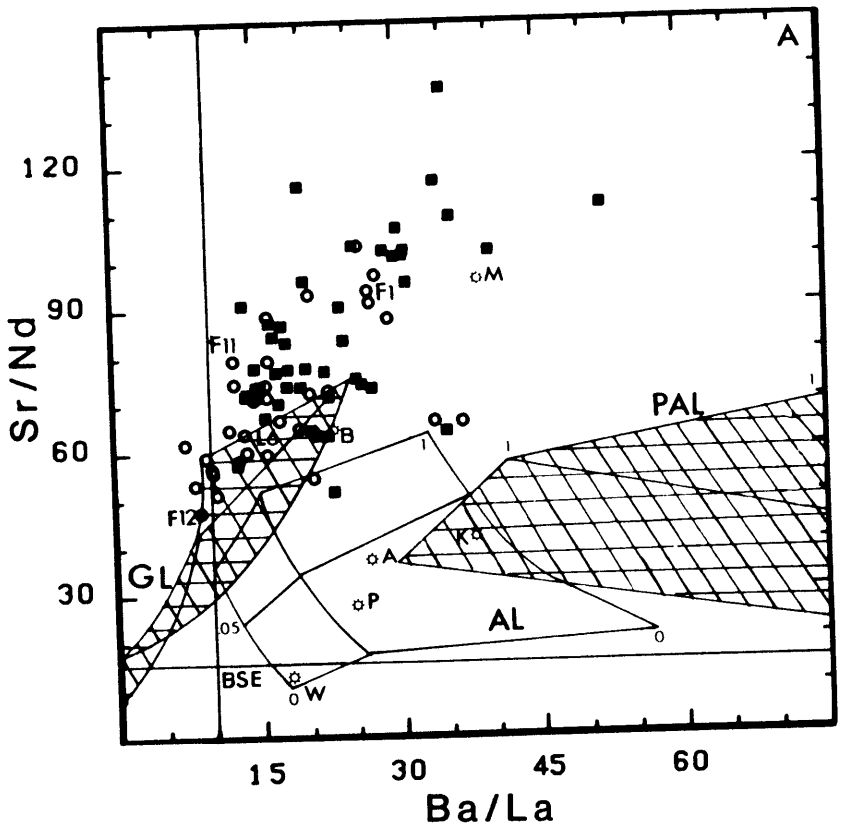
A
120
90
60
30
Sr/Nd
15
30
45
60
Ba/La
F11
F1
M
B
L6
F12
PAL
GL
AL
KC
A
P
BSE
W
0
.05
1

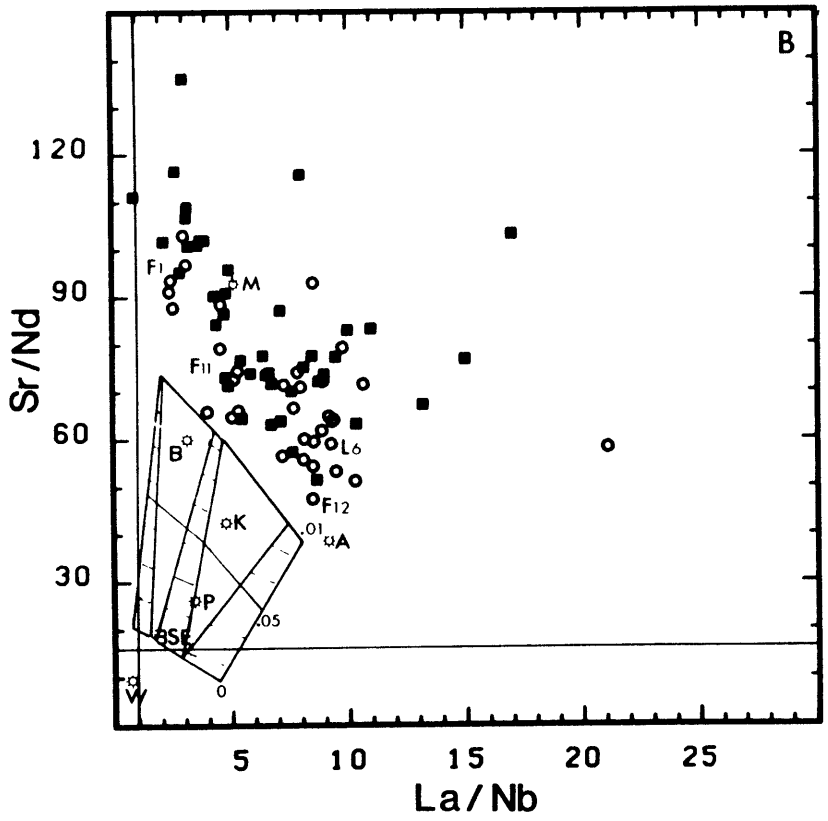
B
120
90
60
30
Sr/Nd
5
10
15
20
25
La/Nb
F1
M
F11
B
L6
F12
K
A
P
BSE
W
0
.01
.05

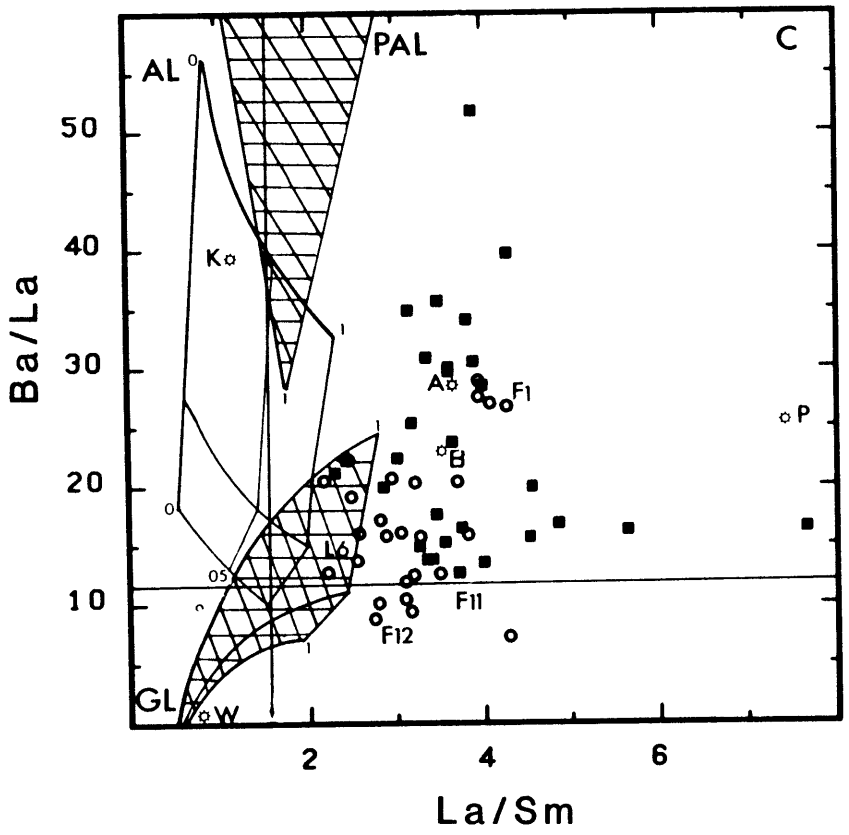
C
PAL
AL
K
GL
W
A
B
P
F1
F11
F12
L6
Ba/La
La/Sm
50
40
30
20
10
2
4
6

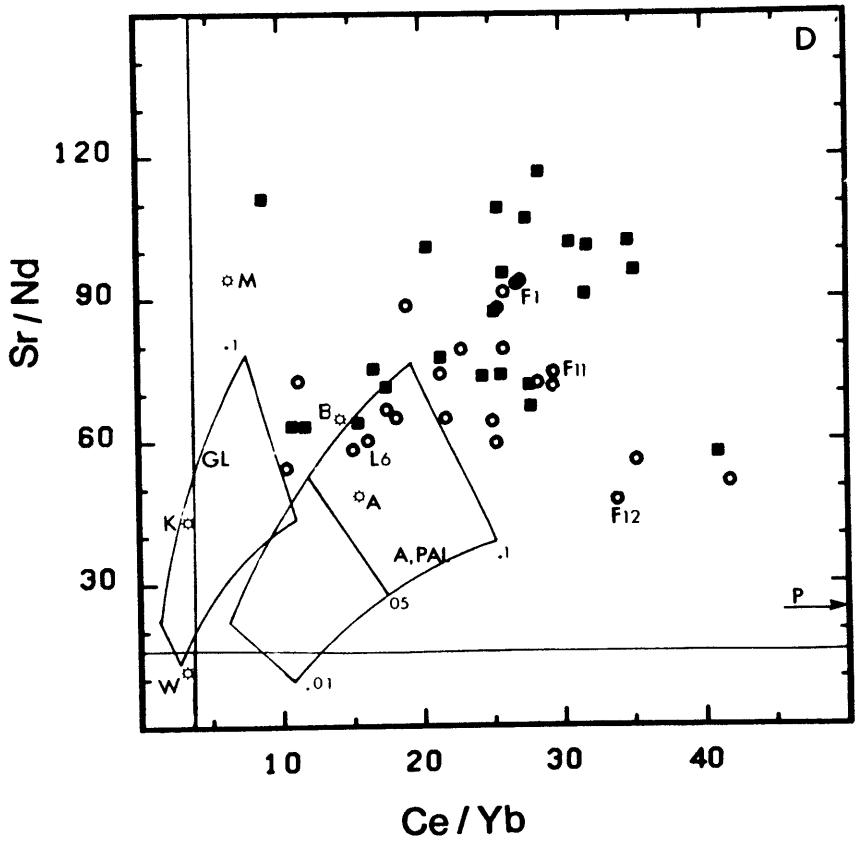
D
M
GL
K
W
B
A
A,PAL
L6
F1
F11
F12
P
Sr/Nd
Ce/Yb
120
90
60
30
10
20
30
40

positive slope. L6, the primitive Lihir lava in Table 5.1, plots at lower Ce/Yb and Sr/Nd in this figure.

The averaged data from other arcs overlap with the Tabar-Feni data in most instances, although there are exceptions for every ratio. Manam and Kermadec lavas have lower Ce/Yb and higher Ba/La. The Patmos lavas have higher La/Sm and Ce/Yb, and lower La/Nb than the Tabar-Feni samples. Of the localities listed in Table 5-1, only Manam and Bagana, the two other PNG data sets, have similar Sr/Nd to the Tabar-Feni suite. The correlations exhibited by the Tabar-Feni data are not observable among the averaged data. The averaged data from the other arcs shows that the highest Ba/La occurs in the tholeiitic suites which result from the highest degree of partial melting, also the Tabar-Feni lavas do not have unusual Ba/La, La/Nb, La/Sm, and Ce/Yb ratios when compared to calc-alkaline lavas. This figure also shows that although the Tabar-Feni lavas have correlations between LILE enrichment and HFSE depletion, samples from different islands have different REE characteristics.

The calculated mantle source fields for garnet lherzolite (GL), amphibole lherzolite (AL) and phlogopite-amphibole lherzolite (PAL) overlap to differing degrees in the ratio-ratio plots. In the plots involving Ba/La the three fields show minimal overlap, and this results from the range of the calculated bulk partition coefficient of Ba for the three sources (0.0002-0.3). If the mantle source for the Tabar-Feni lavas has residual phlogopite, the

source must have extreme Ba/La, unless either the amount of residual phlogopite is small or the degree of partial melting is high. In the Sr/Nd vs Ba/La and Ba/La vs La/Sm diagrams, the fields are separately labeled. In Figure 5-4b there is complete overlap of the GL, AL and PAL fields because of the similarity of calculated bulk partition coefficients for each of the four elements in each of the sources. In this instance, the three smaller fields within the one large field are the calculated sources for F1, F11 and F12 and each of these smaller fields contains the calculated GL, AL and PAL sources. In the Sr/Nd vs Ce/Yb diagram, the calculated AL and PAL sources are essentally identical and overlap completely, thus a single field is shown for these two source mineralogies. The GL source has lower calculated Ce/Yb and this is consistent with the previously shown calculated source REE patterns for GL and the high HREE partition coefficients of garnet. Since a garnet lherzolite source was considered unlikely on the basis of the REE patterns of the lavas and calculated sources, this type of source will not be considered further (however these fields are shown for the interested reader).

The relationship between the erupted lavas and the mantle source

Most models discussing the source characteristics of arc lavas (Kay 1980, Stern and Ito 1983, Morris and Hart 1983,

Hickey et al. 1986) rely upon the assumption that observed correlations in erupted primitive lavas can be related to the source. This is possible for incompatible element ratios in lavas that have been generated by relatively large percentages of partial melting. Relating the observed correlations in undersaturated arc lavas to the mantle source is decidedly more difficult given the possibility of residual phases, i.e. phlogopite and amphibole, which can fractionate the LILE and REE elements. If the sources that produce the primitive lavas have different residual mineralogies, it is impossible to relate lava composition to source composition.

Relating an observed correlation to the source is even further complicated by the possibility of different degrees of partial melting for the different primitive magma compositions. The change in the slope of the correlation between erupted lavas and mantle sources, with changing percent of partial melting, can be deciphered from the boundaries of the calculated sources at F=0 and F=.1, and by the tie lines connecting source compositions for F=0.05. The F=0.05 tie lines are marked in the amphibole lherzolite source field. The variation in isotopic composition in the primitive lavas prevents assessment of relative degrees of partial melting. However, the correlations in Figures 5-4a and 5-4b suggests that if the assumption of similar partial melting percentages is incorrect, there is a relationship between the degree of partial melting and the enrichment and the depletion observed in the lavas.

With the assumption of similar degrees of partial melting, it is possible to address the cause of the observed correlations. If F1, F11, and F12 are all derived from amphibole lherzolite sources, with the same residual mineralogies by 5% partial melting, the sources would also have the same correlations between ratios, but would have different slopes when plotted on the diagrams. This can be seen by the sub-parallel nature of lines connecting mantle sources which are calculated for fixed melt percentages (0, .05, and 0.1). A phlogopite bearing source would also have similar correlations to those of the erupted lavas, but with slightly different slopes. Although the above discussion of the simplest possible models shows the difficulty of relating correlations between arc enrichments and depletions to the mantle source for undersaturated lavas, and the large number of assumptions required, the Tabar-Feni data can provide some constraints on the production of these correlations in the lavas and the arc source.

Two stage models for the generation of the Tabar-Feni arc sources

There are two possible processes that could have generated the observed trends and each represent a different facet of the problem of generation of "arc" mantle. The possibilities are: 1) mixing between two arc sources to produce a spectrum of sources, and 2) modification of a

single arc mantle endmember to produce a spectrum of arc sources.

Mixing between an OIB arc source (phonolitic tephrite source) and an altered MORB arc source (calcic alkali basalt source) can explain the observed trace element correlations and the isotopic variations discussed earlier and shown in Figures 5-1abc. This model ignores the questions of how these two sources are produced and mixed and the problem of LILE enrichment in the arc source. The following discussion of the second possibility attempts to address these unanswered questions.

If amphibole is a residual mantle phase (Perfit et al. 1980 and Perfit and Kay 1986), melts derived by different degrees of partial melting should plot along curves which have negative gradients in the Ba/La va La/Sm diagram (Figure 5-4c). The weak positive correlation between these ratios in the Tabar-Feni lavas reflects changes in the curvature of the REE patterns, and La/Sm is not an adequate measure of LREE enrichment or degree of partial melting. Changes in the La/Sm ratio do not parallel changes in the Ce/Yb ratio and this is observable in Figure 5-4d where F12, a primitive group 3 lava with low La/Sm, has high Ce/Yb. If the higher P_2O_5, REE abundances and La/Yb, and lower SiO_2 of the group 3 calcic alkali basalt (F12) result from smaller degrees of partial melting than the group 2 (F11) and group 1 (F1) lavas, there is a negative correlation between Sr/Nd and LREE enrichment produced during partial melting.

Ratios formed from a LREE and a MREE are affected by differences in the mantle source enrichment of the different islands (see the discussion on source Sm/Nd ratios in chapter 2) as well as the percentage of partial melting. The scattered positive correlation between Sr/Nd and Ce/Yb reflects variations in the LREE enrichment of lavas from different islands coupled with variations in Sr/Nd. When this fact is coupled with the Pb isotopic differences between the Feni samples and samples from the other island groups, the complete data set cannot be used for discussion. For this reason, the Feni data, which encompasses the range of LILE enrichments and HFSE depletions, is focused upon for the rest of this section.

The slope of the observed correlations amongst the primitive samples are at an angle to those expected to be produced by batch melting of the mineralogies previously listed. This is apparent from the positions and change in source mantle composition with melting that were calculated for samples F1, F11, and F12. Melts generated from these source fields would produce a trend that crosses the observed data trend. Thus, melting of sources similar to those used here cannot produce the observed correlations.

The negative correlation between LILE enrichment (Sr/Nd) and HFSE depletions (La/Nb) shows that a relative enrichment of Sr is accompanied by a relative enrichment in Nb (Figure 5-5b). In the Feni lavas, and by analogy their source, Sr and the LREE decrease in abundance between F12 and

F1, and Nb increases, with the relative decrease in Sr being less than the decrease in LREE. This change is accompanied by increasing $^{87}Sr/^{86}Sr$ and decreasing $^{206}Pb/^{204}Pb$ and $^{143}Nd/^{144}Nd$. As the isotopic composition becomes more depleted, the LILE enrichment decreases and the HFSE depletion increases. The change from the source for F12 to the source for F1 is consistent with the addition of a component that has high Sr/Nd, Ba/La and low La/Nb relative to the F12 source. This component must, when added to a source similar to the source of F12, increase the abundance of Nb and produce a slight reduction of the HFSE depletion. The decrease in LREE, predicted for the calculated sources, is difficult to explain simply by the influx of a fluid phase. Experimental and xenolith studies (Schneider and Eggler 1986, Tatsumi et al. 1986, and Stosch 1982) indicate mantle fluids are enriched in LREE relative to MREE and HFSE, and the influx of such fluids should increase the relative abundances of the LREE. The decrease in Sr is hard to explain by the influx of a fluid, as mantle fluids should have high Sr/REE (Eggler 1987). The lower REE of F1 could result from larger percentages of melting than F12. Thus, variable melt percentages and influx of fluids into a previously depleted mantle is required by the observed relationships if mixing is ignored. Subtle differences in Pb isotopes and REE require such a fluid to have changing isotopic, trace element, and major element composition. Although this possibility cannot be eliminated, the simple

mixing process proposed earlier seems a more likely alternative.

Summary

The Tabar-Feni lavas have isotopic composition and trace element ratios that are similar to those found in calc-alkaline, tholeiitic and undersaturated arc lavas that have no identifiable crust/sediment isotopic signature. The Tabar-Feni lavas have high Pb, low Th and high P_2O_5/Ce, which is unusual when compared to the other arcs. The REE patterns, calculated for hypothetical source compositions and mineralogies suggest garnet is unlikely to be a residual phase. Amphibole or phlogopite-amphibole lherzolite are more likely source mineralogies. However, these possibilities are not separable with the present data set. The combined data from all island groups produces a negative correlation between La/Nb (HFSE depletion) and Sr/Nd (LILE enrichment). This correlation could not have resulted from melting of mantle sources similar to those used to examine the REE abundances of the source. Two alternatives exist for the generation of the observed correlations which are: 1) mixing between two arc source components, with both derived from OIB or one derived from MORB, or 2) influx of a fluid/melt into a MORB type source which has been previously depleted in HFSE. This latter alternative requires unusual alkali element ratios and variable isotopic composition within the fluid/melt.

There has been no plate subduction for >20 my in the T-F region and there is no seismic evidence for a detached plate beneath these islands. Therefore, magmas with arc signatures can be generated in a tectonic setting where there is no subducting slab and there is no present influx of fluids from a slab.

Albarede F. (1985) Regime and trace-element evolution of open magma chambers. Nature 318-358.

Albarede F. and Bottinga Y. (1972) Kinetic disequilibrium in trace element partitioning between phenocrysts and host lava. Geochim. Cosmochim. Acta 36, 141-146.

Albarede F. and Provost A. (1977) Petrological and geochemical mass-balance equations: an algorithm for least-squares fitting and general error analysis. Comput. Geosci. 3, 309-326.

Albarede F. and Tamagnan U. (1986) Trace element composition of mantle magma sources: applications of inverse methods to the Piton de la Fournaise volcano (Reunion Island). Terra Cognita 6, 138.

Albee A.L., and Ray L. (1970) Correction factors for electron microprobe microanalysis of silicates, oxides, carbonates, phosphates and sulfates. Anal. Chem. 42, 1408-1414.

Allegre C.J., Treuil M., Minster J.F., Minster B. and Albarede F. (1977) Systematic use of trace element in igneous process, Part I: fractional crystallization processes in volcanic suites. Contrib. Miner. Petrol. 60, 57-75.

Anders E. and Ebihara M. (1982) Solar-system abundances of the elements. Geochim. Cosmochim. Acta 46, 2363-2380.

Angus-Leppan P.V., Allman J.S. and Sloane B. (1983) Crustal movement from satellite observations in the Australian region. Tectonophysics, 97, 87-93.

Arculus R.J. (1976) Geology and geochemistry of the alkali basalt-andesite association of Grenada, Lesser Antilles island arc. Geol. Soc. Amer. Bull. 87, 612-624.

Arculus R.J. and Johnson R.W. (1981) Island-arc magma sources: A geochemical assessment of the roles of slab-derived components and crustal contamination. Geochim. J., 15, 109-133.

Arculus R.J. and Johnson R.W. (1981) Mineralogy of strongly silica-undersaturated volcanic rocks from the Tabar, Lihir, Tanga, and Feni Islands, Papua New Guinea. Abstracts Vol. 1981 IAVCEI 'Arc Volcanism' Symposium, Tokyo and Hakone, 18-19.

Arculus R.J. Johnson R.W., Chappell B.W., McKee C.O. and Sakai, H. (1983) Ophiolite-contaminated andesites, trachybasalts, and cognate inclusions of Mount Lamington, Papua New Guinea: Anhydrate-Amphibole-bearing lavas and the 1951 cumulodome. J. Volcan. Geotherm. Res. 18, 215-247.

Arculus R.J. and Powell R. (1986) Source component mixing in the regions of arc magma generation. J. Geophys. Res. 91, 5913-5926.

Arculus R.J. and Wills K.J.A. (1980) The petrology of plutonic blocks and inclusions from the Lesser Antilles Island Arc. J. Petrol. 21, 743-799.

Armstrong R.L. (1981) Radiogenic isotopes: the case for crustal recycling on a near-steady-state no-continental growth. Earth. Philos. Trans. R. Soc. London, Ser. A, 301, 443-472.

Bacon C.R. (1986) Magmatic inclusions in silicic and intermediate volcanic rocks. J. Geophys. Res. 91, 6091-6112.

Bailey J.C., Larsen O. and Frolova T.I. (1987) Strontium isotope variations in Lower Tertiary-Quaternary volcanic rocks from the Kurile island arc. Contrib. Mineral. Petrol. 95, 155-165.

Baker D.R., and Eggler D.H. (1983) Fractionation paths of Atka (Aleutians) high-alumina basalts: Constraints from phase relations. J. Volc. Geoth. Res., 18, 387-404.

Baker D.R. and Eggler D.H. (1987) Compositions of anhydrous and hydrous melts coexisting with plagioclase, augite, and olivine or low-Ca pyroxene from 1 atm to 8 kbar: Application to the Aleutian volcanic center of Atka. Amer. Mineral. 72, 12-28.

Baldridge W.S., Carmichael I.S.E. and Albee A.L. (1981) Crystallization paths of leucite-bearing lavas: examples from Italy. Contrib. Mineral. Petrol. 76, 321-335.

Banks R. (1979) The use of linear programming in the analysis of petrological mixing models. Contrib. Mineral Petrol. 70, 237-244.

Barsdell M., Smith I.E.M. and Sporli K.B. (1982) The origin of reversed geochemical zoning in the Northern New Hebrides Volcanic Arc. Contrib. Mineral. Petrol. 81, 148-155.

Barton M. and van Bergen M.J. (1981) Green clinopyroxenes and associated phases in a potassium-rich lava from Leucite Hills, Wyoming, Contrib. Mineral. Petrol. 77, 101-114.

Barton M. and Hamilton D.L. (1982) Water-undersaturated melting experiments bearing upon the origin of potassium-rich magmas. Mineralogical Magazine, 45, 267-278.

Barton M., Varekamp J.C. and van Bergen M.J. (1982) Complex zoning of clinopyroxenes in the lavas of Vulsini, Latium, Italy: Evidence for magma mixing. J. Volc. Geoth. Res. 14, 361-388.

Bence A.E. and Albee A.L. (1968) Empirical correction factors for the electron microanalysis of silicates and oxides. J. Geol. 76, 382-403.

Bergman S.C. and Dubessy J. (1984) CO_2 CO fluid inclusions in a composite peridotite xenolith: implications for upper mantle oxygen fugacity. Contr. Miner. Petrol. 85, 1-13.

Bielski-Zyskind M., Wasserburg G.J. and Nixon P.H. (1984) Sm-Nd and Rb-Sr systematics in volcanics and ultramafic xenoliths from Malaita, Solomon Islands and the nature of the Ontong-Java Plateau. J. Geophys. Res. 89, 2415-2424.

Biggar G.M. (1972) Diopside, lithium metasilicate and the 1968 temperature scale. Mineral. Mag. 38, 768-770.

Boettcher A.L., Burnham C.W., Windom K.E. and Bohlen S.R. (1982) Liquids, glasses and the melting of silicates to high pressures. J. Geol. 90, 127-138.

Bottinga Y. and Weill D.F. (1972) The viscosity of magmatic silicate liquids: a model for calculation. Am. J. Sci. 272, 438-475.

Brearley M. and Scarfe C.M. (1986) Dissolution rates of upper mantle minerals in an alkali basalt melt at high pressure: An experimental study and implications for ultramafic xenolith survival. J. Petrology, 27, pt. 5, 1157-1182.

Brey G. and Green D.H. (1977) Systematic study of liquidus phase relations in olivine melilitite + H_2O + CO_2 at high pressures and petrogenesis of an olivine melilitite magma, Contrib. Mineral. Petrol. 61, 141-162.

Brophy J.G. and Marsh B.D. (1986) On the origin of high-alumina arc basalt and the mechanics of melt extraction. J. Petrology, 27, pt. 4, 763-789.

Brown G.M. and Holland J.G. (1977) Geochemistry of the Lesser Antilles volcanic island arc. Geochim. Cosmochim. Acta, 41, 785-801.

Bryan W.B. (1969) Materials balance in igneous rock suites. Ann. Rep. Dir. Geophys. Lab. Carnegie Inst. Wash. 67, 241-243.

Bryan W.B. (1986) Linked evolutionary data arrays: A logical structure for petrologic modeling of multisource, multiprocess magmatic systems. J. Geophys. Res. 91, 5891-5900.

Bultitude R.J. and Green D.H. (1968) Experimental study at high pressures on the origin of olivine nepheline and olivine melilite nephelinite magmas. Earth Plane. Sci. Lett. 3, 325-337.

Bultitude R.J., Johnson R.W., Chappel B.W. (1978) Andesites of Bagana volcano, Papua New Guinea; chemical stratigraphy and a reference andesite composition. BMJR Aust. Geol. Geophys. 3, 281-289.

Byers C.D., Christie D.M., Muenow D.W. and Sinton J.M. (1984) Volatile contents and ferric-ferrous ratios of basalt, ferrobasalt, andesite and rhyolite glasses from the Galapagos 95.5°W propagating rift. Geochim. Cosmochim. Acta 48, 2234-2245.

Cameron K.L. (1984) Bishop Tuff revisited: New rare earth element data consistent with crystal fractionation. Science 224, 1338-1340.

Cameron K.L. and Cameron M. (1986) Whole-rock/groundmass differentiation trends of rare earth elements in high-silica rhyolites. Geochim. Cosmochim. Acta 50, 759-769.

Candela P.A. (1986) The evolution of aqueous vapor from silicate melts: Effect on oxygen fugacity. Geochim. Cosmochim. Acta 50, 1205-1211.

Cann J.R. (1982) Rayleigh fractionation with continuous removal of liquid. Earth Planet. Sci. Lett. 60, 114-116.

Carmichael J.S.E. and Ghiorso M.S. (1986) Oxidation-reduction relations in basic magma: a case for homogeneous equilibria. Earth Planet. Sci. Lett. 78, 200-210.

Carmichael J.S.E., Turner F.J. and Verhoogen J. (1974) Igneous Petrology, New York, McGraw-Hill.

Cawthorn R.G., Curran E.B. and Arculus R.J. (1973) A petrogenetic model for the origin of the calc-alkaline suite of Grenada. Earth Planet. Sci. Lett. 18, 237-246.

Chauvel C. and Bor-Ming J. (1984) Nd-Sr isotope and REE geochemistry of alkali basalts from the Massif Central, France. Geochim. Cosmochim. Acta 48, 93-110.

Chayes F. (1960) On correlation between varibles of constant sum. J. Geophys. Res. 65, 4185-4193.

Chayes F. (1962) Numerical correlation and petrographic variation. J. Geol. 70, 440-452.

Chayes F. (1968) A least square approximation for estimating the amounts of petrographic partition products. Mineral. Petrogr. Acta 14, 111-114.

Chen C.-Y. and Frey F.A. (1985) Trace element and isotopic geochemistry of lavas from Haleakala volcano, East Maui, Hawaii: Implications for origin of Hawaiian basalts. J. Geophys. Res. 90, 8743-8768.

Chen C.-H. and Pallister J.S. (1981) Lead isotopic studies of the Semail ophiolite, Oman. J. Geophys. Res. 86, 2699-2708.

Christie D.M., Carmichael I.S.E. and Langmuir C.H. (1986) Oxidation states of mid-ocean ridge basalt glasses. Earth Planet. Sci. Lett. 79, 397-411.

Clague D.A., and Frey F.A. (1982) Petrology and trace element geochemistry of the Honolulu volcanics, Oahu: Implications for the oceanic mantle beneath Hawaii. J. Petrol. 23, 447-504.

Coleman P.J. and Packham G.H. (1976) The Melanesian borderlands and India-Pacific plates' boundary. Earth Sci. Rev. 12, 197-233.

Conrad W.K. and Kay R.W. (1984) Ultramafic and mafic inclusions from Adak Island: Crystallization history, and implications for the nature of primary magmas and crustal evolution in the Aleutian Arc. J. Petrol., 25, 88-125.

Crawford A.J., Falloon T.J. and Eggins S. (1987) The origin of island arc high-alumina basalts. Contrib. Mineral. Petrol. 97, 417-430.

Curtis J.W. (1973a) The spatial seismicity of Papua-New Guinea-Solomon Islands. J. Geol. Soc. Aust., 20, 21-36.

Curtis J.W. (1973b) Plate tectonics of the Papua-New Guinea-Solomon Islands region. J. Geol. Soc. Aust. 20, 21-36.

Dautria J.M., Liotard J.M., Cabanes N., Girod M. and Briqueu L. (1987) Amphibole-rich xenoliths and host alkali basalts: petrogenetic constraints and implications on the recent evolution of the upper mantle beneath Ahaggar (Central Sahara, Southern Algeria). Contrib. Mineral. Petrol. 95, 133-144.

Davidson J.P. (1987) Crustal contamination versus subduction zone enrichment: examples from the Lesser Antilles and implications for mantle source compositions of island arc volcanic rocks. Geochim. Cosmochim. Acta 51, 2185-2198.

DeFino M., LaVolpe L., Peccerillo A., Piccarreta G. and Poli G. (1986) Petrogenesis of Monte Vulture volcano (Italy): inferences from mineral chemistry, major and trace elemetn data. Contrib. Mineral. Petrol. 92, 135-145.

DeLong S.E. and Fox P.J. (1977) Geological consequences of ridge subduction. In: M. Talwani and W.C. Pitman, III (eds.) Island Arcs, Deep Sea Trenches and Back-Arc basins. Am. Geophys. Union. Maurice Ewing Ser. 1, 221-228.

DeLong S.E., Schwarz W.M. and Anderson R.N. (1979) Thermal effects of ridge subduction. Earth Planet. Sci. Lett. 44, 239-246.

DeMulder M., Hertogen J., Deutsch S. and Andre L. (1986) The role of crustal contamination in the potassic suite of the Karisimbi volcano (Virunga, African Rift Valley). Chem. Geol. 57, 117-136.

Denham D. (1973) Seismicity, focal mechanisms and the boundaries of the Indian-Australian plate, in Coleman, P.J. (ed.), The Western Pacific: island arcs, marginal seas, geochemistry, Univ. W. Aust. Press, pp. 35-53.

DePaolo D.J. (1981) Trace element and isotopic effects of combined wall-rock assimilation and fractional crystallization. Earth Planet. Sci. Lett. 53, 189-202.

DePaolo D.J. and Johnson R.W. (1979) Magma genesis in the New Britain island arc: constraints from Nd and Sr isotopes and trace-element-patterns, Contrib. Mineral. Petrol. 70, 367-380.

DePaolo D.J. and Wasserburg G.J. (1977) The source of island arcs as indicated by Nd and Sr isotope studies. Geophys. Res. Lett. 4, 465-468.

Devey C.W. and Cox K.G. (1987) Relationship between crustal contamination and crystallization in continental flood basalt magmas with special reference to the Deccan Traps of Western Ghats, India, Earth Planet. Sci. Lett. 84, 59-68.

Dickinson J.E. and Hess P.C. (1985) Rutile solubility and titanium coordination in silicate melts. Geochim. Cosmochim. Acta 49, 2289-2296.

Dostal J., Dupuy C., Carron J.P., Le Guen de Kerneizon M. and Maury C. (1983) Partition coefficients of trace elements - application to volcanic rocks of St. Vincent, West Indies. Geochim. Cosmochim. Acta. 47, 525-533.

Downes H. (1984) Sr and Nd isotope geochemistry of coexisting alkaline magma series, Cantal, Massif Central, France. Earth Planet. Sci. Lett. 69, 321-334.

Downes M.J. (1974) Sector and oscillatory zoning in calcic augites from Mt. Etna, Sicily. Contrib. Mineral. Petrol. 47, 187-196.

Drake M.J. and Weill D.F. (1975) Partition of Sr, Ba, Ca, Y, Eu^{2+}, Eu^{3+} and other REE between plagioclase feldspar and magmatic liquid: an experimental study. Geochim. Cosmochim. Acta 39, 689-712.

Duda A. and Schmincke H.U. (1985) Polybaric differentiation of alkali basaltic magmas: evidence from green-core clinopyroxenes (Eifel FRG). Contrib. Mineral. Petrol. 91, 340-353.

Duke J.M. (1974) The effect of oxidation on the crystallization of an alkali basalt from the Azores. J. Geol. 82, 524-528.

Dunn T. (1987) Partitioning of Hf, Lu, Ti, and Mn between olivine, clinopyroxene and basaltic liquid. Contrib. Mineral. Petrol., 96, 476-484.

Dunn T. and McCallum I.S. (1982) The partitioning of Zr and Nb between diopside and melts in the system diopside-albite-anorthite. Geochim. Cosmochim. Acta, 46, 623-629.

Eggler D.H. (1972) Water-saturated and undersaturated melting regulations in a Paricutin andesite and an estimate of water content in the natural magma. Contrib. Mineral. Petrol. 34, 261-271.

Eggler D.H. (1987) 2. Solubility of major and trace elements in mantle metasomatic fluids: experimental constraints. In Mantle Metasomatism, Academic Press, 21-41.

Eggler D.H. and Holloway J.R. (1977) Oregon Dept. Geology Mineral Industries Bull. 96, 15-36.

Eiche G.E., and Francis D.M. and Ludden J.N. (1987) Primary alkaline magmas associated with the Quaternary Alligator Lake volcanic complex, Yukon Territory, Canada. Contrib. Miner. Petrol. 95, 191-201.

Erlank A.J., Waters F.G., Hawkesworth C.J., Haggerty S.E., Allsopp H.L., Rickard R.S. and Menzies M. (1987) Evidence for mantle metasomatism in peridotite nodules from the Kimberley Pipes, South Africa. In Mantle Metasomatism, eds. M.A. Menzies and C.J. Hawkesworth, Academic Press.

Ewart A. (1982) The minerology and petrology of Tertiary-Recent orogenic volcanic rocks: with special reference to the andesitic-basaltic compositional range. In Andesites (R.S. Thorpe, ed.), p. 26-95, John Wiley and Sons.

Ewart A. and Hawkesworth C.J. (1987) The Pleistocene-Recent Tonga-Kermadec Arc lavas: interpretation of new isotopic and rare earth data in terms of a depleted mantle source model. J. Petrol. 28, 495-530.

Exon N.F. and Tiffin D.L. (1982) Geology and petroleum prospects of offshore New Ireland basin in Northern Papua, New Guinea. 3108, 623-630.

Falvey D.A., and Pritchard T. (1982) Preliminary paleomagnetic results from Northern Papua New Guinea: Evidence for large microplate rotations. 3106, 593-599.

Feigenson M.D., Hofmann A.W. and Spera F.J. (1983) Case studies on the origin of basalt II. The transition from tholeiitic to alkalic volcanism on Kohala volcano, Hawaii. Contrib. Mineral. Petro. 84, 390-405.

Finlayson D.M. and Cull J.P. (1973) Structural profiles in the New Britain-New Ireland region. J. Geol. Soc. Aust. 20, pp. 37-48.

Foden J.D. and Varne R. (1980) The petrology and tectonic setting of Quaternary-Recent volcanic centres of Lombok and Sumbawa, Sunda Arc. Chem. Geol. 30, 201-226.

Fodor R.V., Bauer G.R., Jacobs R.S. and Bornhorst T.J. (1987) Kahoolawe Island, Hawaii: Tholeiitic, alkalic and unusual hydrothermal "enrichment" characteristics. J. Volcanol. Geotherm. Res. 31, 171-176.

Foley S.F., Taylor W.R. and Green D.H. (1986) The role of fluorine and oxygen fugacity in the genesis of ultrapotassic rocks. Contrib. Mineral. Petrol. 94, 183-192.

Ford C.E. and Macdonald R. (1978) Melting relations of a midland valley alkali basalt. In Progr. Exp. Petrol. (N.E.R.C. Publications, Series B London), 196-197.

Francalanci L., Peccerillo A. and Poli G. (1987) Partition coefficients for minerals in potassium-alkaline rocks: Data from Roman Province (Central Italy), Geochem. Jour. 21, 1-10.

Fraser D.G., Watt F., Grime G.W., and Takacs J. (1984) Direct determination of strontium enrichment on grain boundaries in a garnet lherzolite xenolith by proton microprobe analysis. Nature, 312, 352-354.

Frey F.A. (1983) Rare element abundances in upper mantle rocks. Rare earth element geochemistry. Develop. in Geochem. 2, 153-203.

Frey F.A., Green D.H. and Roy S.D. (1978) Integrated models of basalt petrogenesis: a study of quartz tholeiites to olivine melilites from South Eastern Australia utilizing geochemical and experimental petrological data. J. Petrol. 19, 463-513.

Frey F.A., Garcia M.O., Kennedy A.K., Wise W. and Kwon S.-T. (1988) The evolution of Mauna Kea volcano, Hawaii: The relationship between tholeiitic and alkalic shield basalts. Contrib. Mineral. Petrol. (submitted).

Frey F.A., Suen C.J. and Stockman H.W. (1985) The Ronda high temperature peridotite: geochemistry and petrogenesis. Geochim. Cosmochim. Acta 49, 2469-2491.

Fujimaki H. (1986) Partition coefficients of Hf, Zr, and REE between zircon, apatite and liquid. Contrib. Mineral. Petrol. 94, 42-45.

Fujimaki H. and Tatsumoto M. (1984) Partition coefficients of Hf, Zr, and REE between phenocrysts and groundmasses. Proc. 14th Lunar and Planet. Sci. Conf., Pt. 2, J. Geophys. Res., 89, Suppl., B662-B672.

Galer S.J.G. and O'Nions R.K. (1985) Residence time of thorium, uranium and lead in the mantle with implications for mantle convection. Nature, 316, 778-782.

Galer S.J.G. and O'Nions R.K. (1986) Magmagenesis and the mapping of chemical and isotopic variations in the mantle. Chem. Geol. 56, 45-61.

Gast P.W. (1968) Trace element fractionation and the origin of tholeiitic and alkaline magma types, Geochim. Cosmochim. Acta 32, 1057-1086.

Gill J.B. (1981) Orogenic andesites and plate tectonics. Springer Berlin, Heidelberg, New York, 390 p.

Gill J.B. (1984) Sr, Pb, Nd isotopic evidence that both MORB and OIB sources contribute to oceanic island arc magmas in Fiji. Earth Planet. Sci. Lett. 68, 443-458.

Gill J.B. (1987) Early geochemical evolution of an oceanic island arc and backarc: Fiji and the South Fiji basin. J. Geology, 95, 5, 589-615.

Gorton M.P. (1977) The geochemistry and origin of the Quaternary volcanism in the New Hebrides: Geochemica et Cosmochimica Acta, 41, 1257-1270.

Graham A.M. (1980) Melting relations of island arc lavas from Grenasda, Lesser Antilles in Progr. Exp. Petrol. (N.E.R.C. Publications, Series D 18; London) 5, 126-132.

Gray N.H. (1973) Estimation of parameters in petrologic materials balance equations. J. Int. Assoc. Math. Geol. 5, 225-236.

Green T.H. (1980) Island arc and continent-building magmatism - a review of petrogenetic models based on experimental petrology and geochemistry. J. Volc. Geotherm. Res. 10, 405-422.

Green T.H. and Pearson N.J. (1986) Ti-rich accessory phase saturation in hydrous mafic-felsic compositions at high P, T. Chem. Geol. 54, 185-201.

Green T.H. and Pearson N.J. (1987) An experimental study of Nb and Ta partitioning between Ti-rich minerals and silicate liquids at high pressure and temperature. Geochim. Cosmochim. Acta, 51, 55-62.

Gromet L.P. and Silver L.T. (1983) Rare earth element dislocations among minerals in a granodiorite and their petrogenetic implications. Geochim. Cosmochim. Acta, 47, 925-939.

Grove T.L. and Baker M.B. (1984) Phase equilibrium controls o the tholeiitic versus calc-alkaline differentiation trends. J. Geophys. Res. 89, B5, 3253-3274.

Grove T.L. and Bence A.E. (1976) Experimental study of pyroxene-liquid interaction in quartz-normative basalt 15597. Proc. Luncar Sci. Conf. 8th, p. 1549-1579.

Grove T.L. and Bryan W.B. (1983) Fractionation of pyroxene-phyric MORB at low pressure: An experimental study. Contrib. Mineral Petrol. 84, 293-309.

Grove T.L. and Donnelly-Nolan J.M. (1986) The evolution of young silicic lavas at Medicine Lake volcano, California: Implications for the origins of compositional gaps in calc-alkaline series lavas. Contrib. Mineral Pegrol. 92, 281-302.

Grove T.L., Gerlach D.C. and Sando T.W. (1982) Origin of calc-alkaline series lavas at Medicine Lake volcano by fractionation, assimilation and mixing. Contrib. Mineral. Petrol. 80, 160-182.

Grove T.L. and Kinzler R.J. (1986) Petrogenesis of andesites. Ann. Rev. Earth Planet. Sci. 14, 417-454.

Hamelin B., Marches G., Albarede F., and Allegre C.J. (1985) Precise lead isotope measurements by the double spike technique: A reconsideration. Geochim. Cosmochim. Acta 49, 173-182.

Hamilton P.J., Johnson R.W., MacKenzie D.E. and O'Nions R.K. (1983) Pleistocene volcanic rocks from the Fly-Highlands province of western Papua, New Guinea: a note on new Sr and Nd isotopic data and their petrogenetic implications. J. Volcanol. Geotherm. Res. 18, 449-460.

Hanson G.N. (1978) The application of trace elements to the petrogenesis of igneous rocks of granitic composition. Earth Planet. Sci. Lett. 38, 26-43.

Harrison T.M. and Watson E.B. (1984) The behavior of apatite during crustal anatexis: Equilibrium and kinetic considerations. Geochim. Cosmochim. Acta 48, 1467-1477.

Hart S.R. (1971) K, Rb, Cs, Sr, and Ba contents, and isotope ratios of ocean floor basalts. Phil. Trans. Roy. Soc., London, A, 268, 573.

Hart S.R. (1984) A large-scale isotopic anomaly in the Southern hemisphere mantle. Nature 309, 753-757.

Hart S.R. and Brooks C. (1977) The geochemistry of early Precambrian mantle. Contrib. Mineral. Petrol. 61, 109-128.

Hart S.R. and Davis K.E. (1978) Nickel partitioning between olivine and silicate melt. Earth Planet. Sci. Lett. 40, 203-219.

Hart S.R. and Staudigel H. (1986) Ocean crust vein mineral deposition: Rb/Sr ages, U-Th-Pb geochemistry, and duration of circulation at sites 261, 462 and 516. Geochem. Cosmochim. Acta 50, 2751-2761.

Hart S.R. and Zindler A. (1986) In search of a bulk-earth composition. Chem. Geol. 57, 247-267.

Haskin L.A. (1983) Petrogenetic modelling-use of rare earth elements. Rare Earth Element Geochemistry. Developments in Geochemistry, 2,115-152.

Haskin L.A. and Korotev R.L. (1977) Test of a model for trace element partition during closed-system solidification of a silicate liquid. Geochim. Cosmochim. Acta 41, 921-939.

Hawkesworth C.J., (1982) Isotopic characteristics of magmas erupted along destructive plate margins in R.S. Thorpe, ed. Andesites: Orogenic Andesites and Related Rocks, pp. 549-574.

Helz R.T. (1976) Phase relations of basalts in their melting ranges at P_{H_2O}=5 kb. Part II. Melt compositions. J. Petrol. 17, 139-193.

Heming R.F. (1974) Geology and petrology of Rabaul Caldera, Papua New Guinea. Geol. Soc. Amer. Bull., 85, 1253-1264.

Heming R.F. (1979) Undersaturated lavas from Ambittle Island, Papua New Guinea, Lithos 12, 173-186.

Heming R.F. and Rankin P.C. (1979) Ce-anomalous lavas from Rabaul caldera, Papua New Guinea. Geochim. Cosmochim. Acta 43, 1351-1355.

Henderson P. and Williams C.T. (1979) Variation in trace element partition (crystal/magma) as a function of crystal growth rate. In Origin and Distribution of the Elements. Pergamon Press, 34, 191-198.

Hess P.L. (1980) Polymerization models for silicate melts. In Physics of magmatic processes. Princeton Univ. Press, 3-48.

Hickey R.L. and Frey F.A. (1982) Geochemical characteristics of boninite series volcanics: implications for their source. Geochim. Cosmochim. Acta, 46, 2099-2115.

Hickey R.L., Frey F.A., and Gerlach D.C. (1986) Multiple sources for basaltic arc rocks from central south Chile: Trace element and isotopic evidence for contributions from subducted oceanic crust, mantle, and continental crust. J. Geophys. Res. 91, 5963-5983.

Hofmann A.W. (1980) Diffusion in natural silicate melts: a critical review. In: Hargraves R.B. (ed.) Physics of Magmatic Processes. Princeton Univ. Press, 585 pp.

Hofmann A.W. (1986) Nb in Hawaiian magmas: constraints on source composition and evolution. Chem. Geol. 57, 17-30.

Hofmann A.W. and Feigenson M.D. (1983) Case studies on the origin of basalt I. Theory and reassessment of Grenada basalts. Contrib. Mineral. Petrol. 84, 382-389.

Hofmann A.W., Feigenson M.D., Raczek I. (1987) Kohala revisited. Contrib. Mineral Petrol. 95, 114-122.

Hofmann A.W. and Hart S.R. (1978) An assessment of local and regional isotopic equlibrium in the mantle, Earth Planet. Sci. Lett. 38, 44-62.

Hofmann A.W., Jochum K.P., Seufert M., White W.M. (1986) Nb and Pb in oceanic basalts: new constraints on mantle evolution. Earth Planet. Sci. Lett., 79, 33-45.

Hofmann A.W., and White W.M. (1983) Ba, Rb and Cs in the Earth's mantle. Z. Naturforsch, 38a, 256-266.

Hohnen P.D. (1978) Geology of New Ireland, Papua, New Guinea. Bureau of Mineral Resources, Australia, Bull. 194.

Hole M.J., A.D. Saunders, G.F. Marriner and J. Tarney (1984) Subduction of pelagic sediments: implications for the origin of Ce-anomalous basalts from the Mariana Islands. J. Geol. Soc. London 141, 453-472.

Holloway J.R. and Burnham C.W. (1972) Melting relations of basalt with equilibrium. Water pressure less than total pressure. J. Petrol. 13, 1-29.

Humphries D.J. (1980) Melting behaviour of some Reunion igneous rocks, In Progr. Exp. Petrol. (N.E.R.C. Publications, Series D 18; London) 5, 132-133.

Huppert H.E. and Sparks R.S.J. (1985) Cooling and contamination of mafic and ultramafic magmas during ascent through continental crust. Earth Planet. Sci. Lett. 74, 371-386.

Ila P. and Frey F.A. (1984) Utilization of neutron activation analysis in the study of geologic materials. Atomkernenergie Kerntechnik, 44, Suppl. 710-716.

Irving A.J. (1978) A review of experimental studies of crystal liquid trace element partitioning. Geochim. Cosmochim. Acta 42, 743-770.

Irvine T.N. and Baragar W.R.A. (1978) A guide to the chemical classification of the common volcanic rocks. Can. J. Earth Sci. 8, 523-548.

Irving A.J. and Frey F.A. (1978) Distribution of trace elements between garnet megacrysts and host volcanic liquids of kimberlitic to rhyolitic composition. Geochim. Cosmochim. Acta, 42, 771-787.

Irving A.J. and Frey F.A. (1984) Trace element abundances in megacrysts and their host basalts: Constraints on partition coefficients and megacryst genesis. Geochim. Cosmochim. Acta, 48, 1201-1221.

Irving A.J. and Price R.C. (1981) Geochemistry and evolution of lherzolite-bearing phonolitic lavas from Nigeria, Australia, East Germany and New Zealand. Geochim. Cosmochim. Acta 45, 1309-1320.

Jacobsen S.B. and Wasserburg G.J. (1979) Nd and Sr isotopic study of the Bay of Islands ophiolite complex and the evolution of the source of midocean ridge basalts, J. Geophys. Res. 84, 7429-7445.

Jagoutz, E., Palme H., Badenhausen H., Blum K., Cendales M., Dreibus G., Spettel G., Lorenz V. and Wanke H. (1979) The abundances of major, minor and trace elements in the Earth's mantle as derived from primitive ultramafic nodules, Proc. Lunar Planet. Sci. Conf. 10th, 2031-2050.

James D.E. (1982) A combined O, Sr, Nd and Pb isotopic and trace element study of crustal contamination in central Andean lavas, I., Local geochemical variations. Earth Planet. Sci. Lett. 57, 47-62.

Jaques A.L. and Green D.H. (1980) Anhydrous melting of peridotite at 0-15 kb pressure and the genesis of tholeiitic basalts. Contrib. Mineral. Petrol. 73, 287-310.

Jenner G.A., Cawood P.A., Rautenschlein M. and White W.M. (1987) Composition of back-arc basin volcanics, Valufa Ridge, Lau Basin: Evidence for a slab-derived component in their mantle source. J. Volcanol. Geotherm. Res. 32, 209-222.

Jochum K.P., Hofmann A.W., Ito E., Seufert H.M. and White W.M. (1983) K, U, and Th in mid-ocean ridge basalt glasses - The terrestrial K/U and K/Rb ratios and heat production in the depleted mantle. Nature (London), 306: 431-436.

Jochum K.P., Seufert H.M., Spettel B. and Palme H., (1986) The solar-system abundances of Nb, Ta and Y, and the relative abundances of refractory lithophile elements in differentiated planetary bodies. Geochim. Cosmochim. Acta, 50, 1173-1183.

Johannes W. (1978) Melting of plagioclase in the system Ab-An-H_2O and Qz-Ab-An-H_2O at P_{H_2O} = 5 kbars, an equilibrium problem. Contrib. Mineral. Petrol., 66, 295-303.

Johnson R.W. (1979) Geotectonics and volcanism in Papua New Guinea. J. Aust. Geol. Geophys. 4, 181-207.

Johnson R.W. and R.J. Arculus (1978) Volcanic rocks of Witu Islands, Papua New Guinea: The origin of magmas above the deepest part of the New Britain Benioff zone, Bull. Volcanol., 41, 609-655.

Johnson R.W., Jaques A.L., Hickey R.L., McKee C.O. and Chappell B.W. (1985) Manam Island, Papua New Guinea: Petrology and Geochemistry of a low-TiO_2 Basaltic Island-Arc volcano. J. Petrol. 26, 283-323.

Johnson R.W., Mackenzie D.E. and Smith I.E.M. (1978) Volcanic rock associations at convergent plate boundaries: Reappraisal of the concept using case histories from Papua New Guinea. Geol. Soc. Amer. Bull., 89, 96-106.

Johnson R.W., Wallace D.A. and Ellis D.J. (1976) Feldspathoid-bearing potassic rocks and associated types from volcanic islands off the coast of New Ireland, Papua, New Guinea: a preliminary account of geology and petrology. In Johnson, R.W. (ed.), Volcanism in Australasia, 297-316. Elsevier, Amsterdam.

Johnson T. and Molnar P. (1972) Focal mechanisms and plate tectonics of the southwest Pacific. J. Geophys. Res. 77, 5000-5032.

Jones J.H. (1984) Temperature and pressure-independent correlations of olivine/liquid partition coefficients and their application to trace element partitioning. Contrib. Mineral. Petrol. 88, 126-132.

Jones J.H. and Burnett D.S. (1987) Experimental geochemistry of Pu and Sm and the thermodynamics of trace element partitioning. Geochim. Cosmochim. Acta 51, 769-782.

Katsura T. and Nagashima S. (1974) Solubility of sulfur in some magmas at 1 atmosphere. Geochim. Cosmochim. Acta 38, 517-532.

Kay R.W. (1980) Volcanic arc magmas: implications of a melting-mixing model for element recycling in the crust-upper mantle system, J. Geol. 88, 497-522.

Kay R.W., Rubenstone J.L. and Kay S.M. (1986) Aleutian terranes from Nd isotopes. Nature 322, 605-609.

Kay R.W., Sun S.-S., and Lee-Hu C.-N. (1978) Pb and Sr isotopes in volcanic rocks from the Aleutian island and Pribiloff Islands, Alaska. Geochim. Cosmochim. Acta 42, 263-273.

Kay S.M. and Kay R.W. (1985) Aleutian tholeiitic and calc-alkaline magma series I: the mafic phenocrysts. Contrib. Mineral. Petrol. 90, 276-290.

Kelemen P.B. and Ghiorso M.S. (1986) Assimilation of peridotite in calc-alkaline plutonic complexes: evidence from the Big Jim complex Washington Cascades. Contrib. Mineral. Petrol. 94, 12-28.

Keller J. (1983) Potassic lavas in the orogenic volcanism of the Mediterranean Area. J. Volcan. Geoth. Res. 18, 321-335.

Kennedy A.K. (1986) Pb-Sr-Nd isotopic evidence for mixing in undersaturated arc volcanics. Terra Cognita 6. 197.

Kennedy A.K., Hart S.R. and Frey F.A. (1987) Trace element and isotopic constraints on the genesis and evolution of the Lihir lavas, Papua New Guinea. J. Geophys. Res. (submitted).

Kennedy A.K., Hart S.R., Grove T.L. and Johnson R.W. (1987) Experimental and geochemical constraints on the evolution of undersaturated lavas from Lihir Island, Papua New Guinea. EOS 68, 463.

Kilinc A., Carmichael I.S.E., Rivers M.L. and Sack R.O. (1983) The ferric-ferrous ratio of natural silicate melts equilibrated in air. Contrib. Mineral. Petrol., 83, 136-140, 1983.

Klein E.M. and Langmuir C.H. (1987) Global correlations of ocean ridge basalt chemistry with axial depth and crustal thickness. J. Geophys. Res. 92, B8, 8089-8115.

Kostal G., Eastman M.P., and Pingitore N.E. (1985) Geological applications of simplex optmization. Computers and Geosciences 11, 2, 235-247.

Kouchi A., Sugawara Y., Kashima K. and Sunagawa N. (1983) Laboratory growth of sector zoned clinopyroxenes in the system $CaMgSi_2O_6$-$CaTiAl_2O_6$. Contrib. Mineral. Petrol. 83, 177-184.

Koyaguchi T. (1986) Life-time of a stratified magma chamber recorded in ultramafic xenoliths from Ichinomegata volcano, northeastern Japan. Bull. Volcanol. 48, 313-323.

Koyaguchi T. (1986) Textural and compositional evidence for magma mixing and its mechanism, Abu volcano group, Southwest Japan. Contrib. Mineral. Petrol. 93, 33-45.

Kramers J.D. (1977) Lead and strontium isotopes in Cretaceous kimberlites and mantle-derived xenoliths from southern Africa. Earth Planet. Sci. Lett. 34, 419-431.

Kuno H. (1968) Differentiation of basaltic magmas. In: Basalts (H.H. Hess and A. Poldervaart, eds.) 2, 623-688, John Wiley & Sons.

Kurat G. et al. (1980) Geochemistry of ultramafic xenoliths from Kapfenstein, Austria: evidence for a variety of upper mantle processes. Geochim. Cosmochim. Acta, 44, 45-60.

Kushiro I. (1972) Partial melting of synthetic and natural perioditites at high pressures. Carnegie Inst. Wash. Yearb. 71, 357-362.

Kwon S.-T. and Tilton G. (1987) U/Pb and Th/U ratios of bulk silicate earth. EOS Translations AGU 68, p. 1551.

Larsen L.M. (1981) Sector zoned aegirine from the Himaussaq alkaline intrusion, South Greenland. Contrib. Mineral. Petrol. 76, 285-291.

Le Maitre R.W. (1984) A proposal by IUGS Subcommission on the systematics of igneous rocks for a chemical classification of volcanic rocks based on the total alkali silica (TAS) diagram. Aust. J. Earth Sciences, 31, 243-255.

Langmuir C.H. (1988) Geochemical consequences of the solidification of magma chambers through "in situ" crystallization in a boundary layer. Nature, submitted.

Langmuir C.H., Bender J.F., Bence A.E., and Hanson G.N. (1977) Petrogenesis of basalts from the FAMOUS area: Mid-Atlantic Ridge. Earth Planet. Sci. Lett. 36, 133-156.

Langmuir C.H., Vocke Jr., R.D., Hanson G.N., and Hart S.R. (1978) A general mixing equation with application to Icelandic basalts. Earth Planet. Sci. Lett. 37, 380-392.

Lanphere M.A. and Frey F.A. (1987) Geochemical evolution of Kohala volcano, Hawaii. Contrib. Mineral. Petrol. 95, 100-113.

Leeman W.P., Budahn J.R., Gerlach D.C., Smith D.R., Powell B.N. (1980) Origin of hawaiian tholeiites: trace element constraints. Am. J. Sci. 280-A, 794-819.

Leeman W.P. and Hawkesworth C.J. (1986) Open magma systems: trace element and isotopic constraints. J. Geophys. Res. 91, 5901-5912.

Le Maitre R.W. (1979) A new generalised petrological mixing model. Contrib. Mineral Petrol. 71, 133-137.

Le Maitre R.W. (1982) Numerical Petrology: Statistical Interpretation of Geochemical Data, Elsevier 281 pp.

Lemarchand F., Villemant B. and Calas G. (1987) Trace element distribution coefficients in alkaline series. Geochim. Cosmochim. Acta 51, 1071-1082.

Lindsley D.H. and Andersen D.J. (1983) A two-pyroxene thermometer. J. Geophys. Res. 88, A887-A906.

Luhr J.F. and Carmichael I.S.E. (1985) Jorullo Volcano, Michoacan, Mexico (1759-1774): The earliest stages of fractionation in calc-alkaline magmas. Contrib. Mineral. Petrol. 90, 142-161.

Maaloe S., Sorensen I., and Hertogen J. (1986) The trachybasaltic suite of Jan Mayen. J. Petrol. 27, 439-466.

MacDougall J.D. and G.W. Lugmair (1986) Sr and Nd isotopes in basalts from the East Pacific Rise: significance for mantle heterogeneity. Earth Planet. Sci. Lett. 77, 273-284.

Mahood G.A. (1984) Pyroclastic rocks and calderas associated with strongly peralkaline magmatism. J. Geophys. Res. 89, 8540-8552.

Mahood G.A. and Baker D.R. (1986) Experimental constraints on depths of fractionation of mildly alkalic basalts and associated felsic rocks: Pantelleria, Strait of Sicily. Contrib. Mineral. Petrol. 93, 251-264.

Manhes C., Minster J.F. and Allegre C.J. (1978) Comparative uranium-thorium-lead and rubidium-strontrium of St. Severin amphoterite: consequences for early solar system chronology. Earth Planet. Sci. Lett. 39, 14-29.

Marcelot C., Dupuy C., Girod M. and Maury R.C. (1983) Petrology of Futuna Island lavas (New Hebrides): An example of the calc-alkaline magmatism associated with the initial stages of back arc spreading. Chem. Geol. 38, 23-37.

Marsh B.D. and Kantha L.H. (1978) On the heat and mass transfer from an ascending magma. Earth Planet. Sci. Lett 39, 435-443.

McBirney A.R. (1980) Effects of assimilation in the Evolution of the igneous rocks: Fiftieth Anniversary Perspectives. Princeton University Press, 307-338.

McBirney A.R. (1987) Paricutin re-examined: a classic example of crustal assimilation in calc-alkaline magma. Contrib. Mineral. Petrol. 95, 4-20.

McCulloch M.T., Gregory R.T., Wasserburg G.J., Taylor H.P., Jr. (1980) A neodymium, strontium and oxygen isotopic study of the Cretaceous Samail ophiolite and implications for the petrogenesis and seawater-hydrothermal alteration of oceanic crust. Earth Planet. Sci. Lett. 46, 2721-2735.

McCulloch M.T. and Perfit M.R. (1981) $^{143}Nd/^{144}Nd$, $^{87}Sr/^{86}Sr$ and trace element constraints on the petrogenesis of Aleutian island arc magmas. Earth Planet. Sci. Lett. 56, 167-179.

McKenzie D. (1984) The generation and compaction of partially molten rock. J. Petrol. 25, pt. 3, 713-765.

McNeil A.M. and Edgar A.D. (1987) Sodium-rich metasomatism in the upper mantle: implications of experiments on the pyrolite-Na_2O-rich fluid system at 950°C, 20 kbar. Geochim. Cosmochim. Acta, 51, 2285-2294.

Meijer A. (1976) Pb and Sr isotopic data bearing on the origin of volcanic rocks from the Mariana island-arc system. Bull. Geol. Soc. Am. 187, 1358-1369.

Menzies M. (1983) Mantle ultramafic xenoliths in alkaline magmas: evidence for mantle heterogeneity modified by magmatic activity, In: "Continental Basalts and Mantle Xenoliths", C.J. Hawkesworth and M.J. Norry, eds. Shiva Publishing Ltd., Cheshire, England.

Menzies M., Rogers N., Tindle A. and Hawkesworth C. (1987) Metasomatic and enrichment processes in lithospheric peridotites, an effect of asthenosphere-lithosphere interaction. in Mantle Metasomatism, Academic Press, London.

Menzies M.A. and Wass S.Y. (1983) CO_2-and LREE-rich mantle below eastern Australia: a REE and isotopic study of alkaline magmas and apatite-rich mantle xenoliths from the Southern Highlands Province, Australia, Earth and Planet. Sci. Lett. 65, 287-302.

Mertes H. and Schminke H.-H. (1985) Mafic potassic lavas of the Quaternary West Eifel volcanic field. Contrib. Mineral. Petrol. 89, 330-345.

Michael P.J. (1983) Chemical differentiation of the Bishop Tuff and other high-silica magmas through crystallization processes. Geology 11, 31-34.

Minster J.F. and Allegre C.J. (1978) Systematic use of trace elements in igneous processes, part III. Inverse problem of batch melting in volcanic suites. Contrib. Mineral. Petrol. 68, 37-52.

Morioka M. and Kigoshi K. (1978) Lead isotopes in mantle derived xenoliths from Japan and South Africa. Geochem. J., 12, 223-228.

Morris J.D. (1984) Enriched geochemical signatures in Aleutian and Indonesian Arc lavas: An isotopic and trace element investigation, Ph.D. Thesis, MIT, p. 320.

Morris J.D. and Hart S.R. (1983) Isotopic and incompatible element constraints on the genesis of island arc volcanics, Cold Bay and Amak Island. Aleutians. Geochim. Cosmochim. Acta, 47, 2015-2030.

Morris J.D., Jezek P.A., Hart S.R., and Gill J.B. (1982) The Halmahera Island Arc, Molucca Sea Collision Zone, Indonesia: A geochemical survey. In The Tectonics and Geologic Evolution of the Southeast Asian Seas and Islands II. AGU Monograph Series 27, 373-387.

Myers J.D. and Marsh B.D. (1981) Geology and petrogenesis of the Edgecumbe volcanic field, SE Alaska: the interaction of basalt and sialic crust. Contrib. Mineral. Petrol. 77, 272-287.

Myers J.D. and Marsh B.D. (1987) Aleutian lead isotopic data: Additional evidence for the evolution of lithospheric plumbing systems. Geochim. Cosmochim. Acta 51, 1833-1842.

Myers J.D., Marsh B.D., and Sinha A.K. (1986) Geochemical and strontium isotopic characteristics of parental Aleutian Arc magmas: evidence from the basaltic lavas of Atka. Contrib. Mineral Petrol. 94, 1-11.

Myers J.D. and Sinha A.K. (1985) A detailed Pb isotopic study of crustal contamination/assimilation: the Edgecumbe volcanic field, SE Alaska. Geochim. Cosmochim. Acta 49, 1343-1355.

Mysen B.O. and Kushiro I. (1977) Compositional variation of coexisting phases with degree of melting of peridotite in the upper mantle. Am. Mineral. 62, 843-865.

Mysen B.O. and Virgo D. (1985) Iron-bearing silicate melts: relations between pressure and redox equilibria. Phys. Chem. Minerals 12, 191-200.

Mysen B.O., Virgo D. and Seifert F.A. (1984) Redox equilibria of iron in alkaline earth silicate melts: Relationships between melt structure, oxygen fugacity, temperature and properties of iron-bearing silicate liquids. Am. Mineral. 69, 834-847.

Nakamura Y. (1973) Origin of sector-zoning of igneous clinopyroxenes. Amer. Mineral. 58, 986-990.

Navon O. and Stolper E. (1987) Geochemical consequence of melt percolation: the upper mantle as a chromatographic column. J. Geol. 95, 285-308.

Newman S., Macdougall J.D., and Finkel R.C. (1984) ^{230}Th-^{238}U disequilibrium in island arcs: evidence from the Aleutians and the Marianas. Nature, 308, 268-270.

Newman S., Macdougall J.D., and Finkel R.C. (1986) Petrogenesis and ^{230}Th-^{238}U and disequilibrium at Mt. Shasta, California, and in the Cascades. Contrib. Mineral. Petrol. 93, 195-206.

Newsom H.E., White W.M., Jochum K.P. and Hofmann A.W. (1987) Siderophile and chalcophile element abundances in oceanic basalts, Pb isotope evolution and growth of the Earth's core. Earth Planet. Sci. Lett. 80, 299-313.

Nicholls I.A. and Harris K.L. (1980) Experimental rare earth element parition coefficients for garnet, clinopyroxene and amphibole coexisting with andesitic and basaltic liquids. Geochim. Cosmochim. Acta, 44, 287-308.

Nicholls I.A., Whitford D.J., Harris K.L., and Taylor S.R. (1980) Variation in the geochemistry of mantle sources for tholeiitic and calc-alkaline mafic magmas, western Sunda volcanic arc, Indonesia. Chemical Geology, 30, 177-199.

Nielsen R.L. and Dungan M.A. (1983) Low pressure mineral melt equilibria in natural anhydrous mafic systems. Contrib. Mineral. Petrol. 84, 310-326.

Neumann H., Mead J. and Vitaliano C.J. (1954) Trace element variation during fractional crystallization as calculated from the distribution law. Geochim. Cosmochim. Acta 6, 90-99.

Nye C.J. and Reid M.R. (1986) Geochemistry of primary and least fractionated lavas from Okmok volcano, central Aleutians: Implications for arc magmagenesis. J. Geophys. Res. 91, 10271-10287.

O'Hara M.J. and Matthews R.E. (1981) Geochemical evolution in an advancing periodically replenished, periodically and tapped, continuously fractionated magma chamber. J. Geol. Soc. London 138, 237-277.

Oversby V.M. and Ewart A. (1972) Lead isotopic compositions of Tonga Kermadec volcanics and their petrogenetic significance, Contrib. Mineral. and Petrol. 37, 181-210.

Page R.W. and Johnson R.W. (1974) Strontium isotope ratios of Quaternary volcanic rocks from Papua New Guinea. Lithos. 7, 91-100.

Palacz Z. and Saunders A.D. (1986) Coupled trace element and isotope enrichment in the Cook-Austral Islands, S.W. Pacific. Earth Planet. Sci. Lett. 79, 270-280.

Papike J.J., Cameron K.L. and Baldwin K. (1974) Amphiboles and pyroxenes: Characterization of other than quadrilateral components and estimates of ferric iron from microprobe data. EOS, Trans. Am. Geophys. Union, 60, 420-421.

Patchett P.J. (1980) Thermal effects of basalt on continental crust and crustal contamination of magmas. Nature 283, 559-561.

Patchett R.J., Kouvo O., Hedge C.E. and Tatsumoto M. (1981) Evolution of continental crust and mantle heterogeneity: evidence from Hf isotopes. Contrib. Mineral. Petrol. 78, 279-297.

Peccerillo A., Poli G. and Tolomeo L. (1984) Genesis, evolution and tectonic significance of K-rich volcanics from the Alban Hills (Roman comagmatic region) as inferred from trace element geochemistry. Contrib. Mineral. Petrol. 86, 230-240.

Pegram W.J. (1986) The isotope, trace element, and major element geochemistry of the Mesozoic Appalachian tholeiite province. PhD Thesis, Mass. Inst. Tech.

Perfit M.R. and Gust D.A. (1987) Phase relations of a high-Mg basalt from the Aleutian island Arc: Implications for primary island arc basalts and high-Al basalts. Contrib. Mineral. Petrol. 97, 7-18.

Perfit M.R., Gust D.A., Bence A.R., Arculus R.J. and Taylor R. (1980) Chemical characteristics of island arc basalts: implications for mantle sources. Chem. Geol. 30, 227-289.

Perfit M.R., Johnson R.W. and Chappell B.W. (1981) Geochemistry and isotopic compositions of volcanic rocks from an alkalic island arc: Tabar-to-Feni Islands, Papua New Guinea. Abstracts Vol. 1981 IAVCEI 'Arc Volcanism', Symposium, Tokyo and Hakone, 290-291.

Perfit M.R., Langmuir C.H. and Baekisapa M. (1987) Geochemistry and petrology of volcanic rocks from the Woodlark Basin: Addressing questions of ridge subduction. In: Seafloor spreading, Ridge subduction volcanism and sedimentation in the offshore Woodlark Solomons Region.

Perfit M. and McCulloch M. T. (1982) Isotopic and trace element differences in late Cainozoic volcanic rocks from west Melanesia. EOS, 63, 586.

Powell R. (1984) Inversion of the assimilation and fractional crystallization (AFC) equations: characterization of contaminants from isotope and trace element relationships in volcanic suites. J. Geol. Soc. Lond. 141, 447-452.

Presnall D.C., Dixon J.R., O'Connell T.H. and Dixon S.A. (1979) Generation of mid-ocean ridge tholeiites. J. Petrol. 20, 3-35.

Prinzhofer A. and Allegre C.J. (1985) Residual peridotites and the mechanisms of partial melting. Earth Planet. Sci. Lett. 74, 251-265.

Ray G.L., Shimizu N. and Hart S.R. (1983) An ion microprobe study of the partitioning of trace elements between clinopyroxene and liquid in the system diopside-albite-anorthite. Geochim. Cosmochim. Acta 47, 2131-2140.

Reagan M.K., Gill J.B., Malavassi E. and Garcia M.O. (1987) Changes in magma composition at Arenal volcano, Costa Rica, 1968-1985: Real-time monitoring of open-system differentiation. Bull. Volcanol. 49, 415-434.

Reid M.J., Gancarz A.J. and Albee A.L. (1973) Constrained least-squares analysis of petrologic problems with an application to lunar sample 12040. Earth Planet. Sci. Lett. 17, 433-445.

Rhodes J.M. (1983) Homogeneity of lava flows: Chemical data for historic Mauna Loan eruptions. J. Geophys. Res. 88, A869-879.

Richard P., Shimizu N. and Allegre C.J. (1976) $^{143}Nd/^{144}Nd$, a natural tracer; application to oceanic basalts. Earth Planet. Sci. Lett. 31, 269-278.

Richardson S.H., Erlank A.J., Duncan A.R., and Reid D.L. (1982) Correlated Nd, Sr and Pb isotope variation in Walvis Ridge basalts and implications for the evolution of their mantle source. Earth Planet. Sci. Lett. 59, 327-342.

Richardson S.H., Erlank A.J., and Hart S.R. (1985) Kimberlite-borne garnet peridotite xenoliths from old enriched subcontinental lithosphere. Earth Planet. Sci. Lett., 75, 116-128.

Richter F.M. (1986) Simple models for trace element fractionation during melt segregation. Earth Planet. Sci. Lett. 77, 333-344.

Roden M.F., Hart S.R., Frey F.A., and Melson W.G. (1984) Sr, Nd and Pb isotopic and REE geochemistry of St. Paul's Rocks: The metamorphic and metasomatic development of an alkali basalt mantle source. Contrib. Mineral. Petrol. 85, 376-390.

Roden M.F. and Murthy V.R. (1985) Mantle metasomatism. Ann. Rev. Earth Planet. Sci. 13, 264-296.

Roedder P.L. and Emslie R.F. (1970) Olivine-liquid equilbrium. Contrib. Mineral. Petrol. 29, 275-289.

Rutter M.J. (1987) Evidence for crustal assimilation by turbulently convecting, mafic alkaline magmas. Geochemistry of mantle xenolith-bearing lavas from Northern Sardinia. J. Volcan. Geotherm. Res. 32, 343-354.

Ryabchikov I.D., Schreyer W., and Abraham K. (1982) Compositions of aqueous fluid in equilibrium with pyroxene and olivines at mantle pressures and temperature. Contrib. Mineral. Petrol. 79, 80-84.

Ryerson F.J. and Watson E.B. (1988) Rutile saturation in magmas: implications for Ti-Nb-Ta depletion in island arc basalts. Earth Planet. Sci. Lett. (in press).

Sack R.O. (1982) Spinels as petrogenetic indicators: Activity-composition relations at low pressures. Contrib. Mineral. Petrol. 79, 169-186.

Sack R.O., Carmichael I.S.E., Rivers M., Ghiorso M.S. (1980) Ferric-ferrous equilibria in natural silicate liquids at 1 bar. Contrib. Mineral. Petrol. 75, 369-376.

Sack R.O., Walker D. and Carmichael I.S.E. (1987) Experimental petrology of alkalic basalts at 1 atmosphere: Constraints on cotectics of multiple saturation in natural basalt liquids. Contrib. Mineral. Petro., 96, 1-23.

Sakuyama M. (1981) Petrological study of the Myoko Kuroshime volcanoes, Japan: crystallization sequence and evidence for magma mixing. J. Petrol. 22, 553-583.

Sakuyama M. and Koyaguchi T. (1984) Magma mixing in mantle xenolith-bearing calc-alkalic ejecta, Ichinomegata volcano, Northeastern Japan. J. Volcanol. Geotherm. Res., 22, 199-224.

Salters V.J.M. (1988) Characteristics of the mantle beneath the Carpathians, Hungary, as inferred from calc-alkaline and alkaline volcanics. Crust/Mantle Recycling at Convergence Zones, L. Gulen and S.R. Hart, eds., NATO ASI Series, D. Reidel Publishing Co., The Netherlands, in press.

Salters V. and Shimizu N. (1988) World-wide occurrence of HFSE-depleted mantle. Submitted to GCA.

Saunders A.D., Rogers G., Marriner G.F., Terrell D.J., and Verma S.P. (1987) Geochemistry of Cenozoic volcanic rocks, Baja California, Mexico: Implications for the petrogenesis of post-subduction magmas. J. Volcan. Geotherm. Res. 32, 223-245.

Sawka W.N., Chappell B.W. and Norrish K. (1984) Light-rare-earth-element zoning in sphene and allamite during granitoid fractionation. Geology 12, 131-134.

Schneider M.E. and Eggler D.H. (1986) Fluids in equilibrium with peridotite minerals: Implications for mantle metasomatism. Geochim. Cosmochim. Acta, 50, 711-724.

Sekine T., Katsura T. and Aramaki S. (1979) Water saturated phase relations of some andesites with application to the estimation of the initial temperature and water pressure at the time of eruption. Geochim. Cosmochim. Acta 43, 1367-76.

Shaw D.M. (1970) Trace element fractionation during anatexis. Geochim. Cosmochim. Acta 34, 237-243.

Shimizu N. (1974) An experimental study of the partitioning of K, Rb, Cs, Sr and Ba between clinopyroxene and liquid at high pressures. Geochim. Cosmochim. Acta, 38, 1789-1798.

Shimizu N. (1975) The partitioning of rare earth elements between garnet and liquid at high pressures: preliminary experiments. Geophys. Res. Lett. 2, 413-416.

Shimizu N. (1981) Trace element incorporation into growing augite phenocryst. Nature 289, 575-577.

Shimizu N. (1983) Interface kinetics and trace element distribution between phenocrysts and magma. In: The significance of trace elements in solving petrogenetic problems and controversies. Theophrastus Publications, Greece.

Shimizu N. and Arculus R.J. (1975) Rare earth element concentrations in a suite of basanitoids and alkali olivine basalts from Grenada, Lesser Antilles. Contrib. Mineral. Petrol. 50, 231-240.
793-811.

Singer B.S. and Kudo A.M. (1986) Assimilation-fractional crystallization of Polvadera Group rocks in the Northwestern Jemez Volcanic Field, New Mexico. Contrib. Mineral. Petrol. 94, 374-386.

Spear F.S. and Kimball K.L. (1984) RECAMP - a FORTRAN IV program for estimating Fe^{3+} contents in amphiboles. Comp. Geosci. 10, 317-325. Spencer, K.J. and Lindsley, D.H. (1981) A solution model for coexisting iron-titanium oxides. Am. Mineral. 66, 1189-1201.

Spera F.J. (1987) Dynamics of translithospheric migration of metasomatic fluid and alkaline magma, in: Mantle Metasomatism, Academic Press, London, 1-20.

Spulber S.D. and Rutherford M.J. (1983) The origin of rhyolite and plagiogranite in oceanic crust: an experimental study. J. Petrol., 24, 1-25.

Staudigel H., McCulloch M., Zindler A. and Perfit M. (1988) Complex ridge subduction and island arc magmatism: an isotopic study of the New Georgia forearc and the Woodlark basin, in: Marine Geology and Geophysics of the Woodlark Basin-Solomon Islands Region, B. Taylor and N. Exon, eds., in press.

Stern R.J. and Ito E. (1983) Trace-element and isotopic constraints on the source of magmas in the active Volcano and Mariana island Arcs, western Pacific. J. Volcanol. Geotherm. Res. 18, 461-482.

Stolper E.M. (1980) A phase diagram for mid-ocean ridge basalts: Preliminary results and implications for petrogenesis. Contrib. Mineral. Petrol. 74, 13-27.

Stolper E.M. and Walker D. (1980) Melt density and the average composition of basalt. Contrib. Mineral. Petrol. 74, 7-12.

Stormer J.C. and Nicholls J. (1978) XLFRACL: a program for the interactive testing of magmatic differentiation models. Comput. Geosci. 4, 143-159.

Stosch H.-G. (1982) Rare earth element partitioning between minerals from the anhydrous spinel peridotite xenoliths. Geochim. Cosmochim. Acta, 46,

Stosch H.-G. and Lugmair G.W. (1986) Trace element and Sr and Nd isotope geochemistry of peridotite xenoliths from the Eifel (West Germany) and their bearing on the evolution of the subcontinental lithosphere. Earth Planet. Sci. Lett. 80, 281-298.

Sun S.-S. (1980) Lead isotopic study of young volcanic rocks from mid-ocean ridges, ocean islands and island arcs. Philos. Trans. R. Soc. London, Ser. A, 297, 409-445.

Sun S.-S. (1987) Chemical composition of Archean Komatiites: implications for early history of the Earth and mantle evolution. J. Volc. Geoth. Res. 32, 67-82.

Sun S.-S. and Hanson G.N. (1975a) Evolution of the mantle: Geochemical evidence from alkali basalt. Geology 3, 297-302.

Sun S.-S. and Hanson G.N. (1975b) Origin of Ross Island basanitoids and limitations upon the heterogeneity of mantle sources for alkali basalts and nephelinites. Contrib. Mineral. Petrol. 52, 77-106.

Suzuki K. (1981) Grain boundary concentration of rare earth elements in a hornblende cumulate. Geochem. J., 15, 295-303.

Suzuki K. (1986) Enrichment of incompatible elements at grain-boundaries of olivine in an olivine-nephelinite. Geochem. J., 20, 17-27.

Suzuki K. (1987) Grain-boundary enrichment of incompatible elements in some mantle peridotites. Chem. Geol. 63, 319-334.

Takahashi E. (1980) Thermal history of lherzolite xenoliths-I. Petrology of lherzolite xenoliths from the Ichinomegata crater, Oga peninsula, northeast Japan. Geochim. Cosmochim. Acta, 44, 1643-1658.

Takahashi E. (1985) Genesis of calc-alkali andesite magma in a hydrous mantle-crust boundary: petrology of lherzolite xenoliths from the Ichinomegata crater, Oga peninsula, Northeast Japan, Part II. J. Volcanol. Geotherm. Res., 29, 355-395.

Takahashi E. and Kushiro I. (1983) Melting of a dry peridotite at high pressures and basalt magma genesis. Am. Mineral., 68, 859-879.

Tanaka T., and Aoki K.-I. (1981) Petrogenetic implications of REE and BA data on mafic and ultramafic inclusions from Itinome-Gata, Japan. J. Geol. 89, 369-390.

Tatsumi Y., Hamilton D.L., and Nesbitt R.W. (1986) Chemical characteristics of fluid phase released from a subducted lithosphere and origin of arc magmas: Evidence from high-pressure experiments and natural rocks. J. Volcanol. Geotherm. Res. 29, 293-309.

Tatsumoto M. (1978) Isotopic composition of lead in oceanic basalt and its implication to mantle evolution. Earth and Planet. Sci. Lett. 38, 63-87.

Taylor Jr., H.P. (1980) The effects of assimilation of country rocks by magmas on $^{18}O/^{16}O$ and $^{87}Sr/^{86}Sr$ systematics in igneous rocks. Earth Planet. Sci. Lett. 47, 243-254.

Taylor B.E., Eichelberger J.C., Westrich H.R. (1983) Hydrogen isotopic evidence of rhyolitic magma degassing during shallow intrusion and eruption. Nature 306, 541-545.

Tera F., Brown L., Morris J., Sacks I.S., Klien J., and Middleton R., (1986) Sediment incorporation in island-arc magmas: Inferences from ^{10}Be. Geochim. Cosmochim. Acta 50, 535-550.

Thirwall M.F. and Graham A.M. (1984) Evolution of high-Ca, high Sr C-series basalts from Grenada Lesser Antilles: the effect of intra-crustal contamination, J. Geol. Soc. Lond. 141, 427-445.

Thirwall M.F. and Jones N.W. (1983) Isotope geochemistry and contamination mechanics of Tertiary lavas from Skye, northwest Scotland, In Continental Basalts and Mantle Xenoliths. Shiva Press, 186-208.

Thompson R.N. (1974) Primary basalts and magma genesis. I. Skye, North-West Scotland. Contrib. Mineral. Petrol. 45, 317-341.

Todt W., Dupre B. and Hofmann A.W. (1983) Pb isotope measurements using a multicollection: application to standard and basalts, Terra Cognita, 3.

Tormey D.R., Grove T.L. and Bryan W.B. (1987) Experimental petrology of normal MORB near the Kane Fracture Zone: 22°-25°N, mid-Atlantic ridge. Contrib. Mineral. Petrol. (submitted).

Troll G., and Gilbert M.C. (1974) Stability of fluorine tremolite. Trans. Am. Geophys. Union, 55, 481.

Tronnes R.G., Edgar A.D., and Arima M. (1985) A high pressure-high temperature study of TiO_2 solubility in Mg-rich phlogopite: implications to phlogopite chemistry. Geochim. et Cosmochim. Acta, 49, 2323-2329.

Tsuchiyama A. (1981) Experimental studies on crystallization kinetics in the system diopside-anorthite and their application to crystallization of natural magmas. D. Sc. Thesis, Univ. Tokyo, 178 p.

Varne R. (1985) Ancient subcontinental mantle: a source for K-rich orogenic volcanics. Geology, 13, 405-408.

Varne R. and Foden J.D. (1986) Chemical and isotopic systematics of Eastern Sunda Arc Volcanics: Implications for mantle sources and mantle mixing processes. In The Origin of Arcs (F.-C. Wezel, Ed.), p. 154-189, Elsevier, Amsterdam.

Veizer J. (1983) Trace elements and isotopes in sedimentary carbonates, in Rev. Mineral. Vol. 11, Carbonates: Mineralogy and Chemistry, 265-299.

Villemant B., Jaffrezic H., Joron J. and Treuil M. (1981) Distribution coefficients of major and trace elements: fractional crystallization in the alkali basalt series of Chaine des Puys (Massif Central, France). Geochim. Cosmochim. Acta 45, 1997-2016.

Vogel T.A., Ryerson F.J., Noble D.C. and Yorinken L.W. (1986) Limits to magma mixing based on chemistry and mineralogy of pumice fragments erupted from a chemically zoned magma body. J. Geol. 95, 654-670.

Volpe A.M., MacDougall J.D., Hawkins J.W. (1987) Mariana Trough basalts (MTB): trace element and Sr-Nd isotopic evidence for mixing between MORB-like and Arc-like melts. Earth Planet. Sci. Lett. 82, 241-254.

von Drach V., Marsh B.D., and Wasserburg G.J. (1986) Nd and Sr isotopes in the Aleutians: multicomponent parenthood of island-arc magmas. Contrib. Mineral. Petrol., 92, 13-34.

Wallace D.A., Johnson R.W. Chappell B.W. Arculus R.J. Perfit M.R. and Crick I.H. (1983) Cainozoic volcanism of the Tabar, Lihir, Tanga and Feni Islands, Papua New Guinea. B.M.R. Rept. 243.

Walker D., Shibata T. and Delong S.E. (1979) Abyssal tholeiites from the Oceanographer Fracture Zone II: Phase equilibria and mixing. Contrib. Mineral Petrol., 70, 111-125.

Walker D., Tsugio S. and Delong S.E. (1979) Abyssal tholeiites from the Oceanographer Fracture Zone. Contrib. Miner. Petrol. 70, 111-125.

Wallace D.A., Johnson R.W., Chappell B.W., Arculus R.J., Perfit M.R. and Crick I.H. (1983) Cainozoic volcanism of the Tabar, Lihir, Tanga and Feni Islands, Papua New Guinea, B.M.R. rept. 243.

Watson E.B. (1980) Apatite and phosphorus in mantle source regions: an experimental study of apatite/melt equilibria at pressures to 25 kbar. Earth Planet. Sci. Lett. 40, 322-335.

Watson E.B. (1982) Basalt contamination by continental crust: some experiments and models. Contrib. Mineral Petrol. 80, 73-87.

Watson E.B. (1985) Henry's law behavior in simple systems and in magmas: Criteria for discerning concentration-dependent partition coefficients in nature. Geochim. Cosmochim. Acta 49, 917-923.

Watson E.B. and Green T.H. (1981) Apatite/liquid partition coefficients for the rare earth elements and strontium. Earth Planet. Sci. Lett. 56, 405-421.

Watson E.B., Othman D.B., Luck J.-M., and Hofmann A.W. (1987) Partitioning of U, Pb, Cs, Yb, Hf, Re and Os between chromian diopsidic pyroxene and haplobasaltic liquid. Chemical Geology, 62, 191-208.

Weissel J.K., Taylor B. and Karner G.D. (1982) The opening of the Woodlark Basin, subduction of the Woodlark spreading system, and the evolution of northern Melanesia since mid-Pliocene time. Tectonophysics 87, 253-277.

Wendlandt R.F. and Eggler D.H. (1980) The origins of potassic magmas: 2. Stability of phlogopite in natural spinel lherzolite and in the system $KAlSiO_4$-MgO-SiO_2-H_2O-CO_2 at high pressures and high temperatures. Amer. J. Sci., 280, 421-458.

Wheller G.E., Varne R., Foder J.D. and Abbott M.J. (1987) Geochemistry of Quaternary volcanism in the Sunda-Banda Arcs, Indonesia, and three-component genesis of island-arc basaltic magmas. J. Volcan. Geotherm. Res. 32, 137-160.

White W.M., Hofmann A.W. and Puchett H. (1987) Isotope geochemistry of Pacific mid-ocean ridge basalt. J. Geophys. Res. 92, 4881-4893.

White W.M. and Patchett J. (1984) Hf-Nd-Sr isotopes and incompatible element abundance in island arcs: Implications for magma origins and crust-mantle evolution. Earth Planet. Sci. Lett. 67, 167-185.

White W.M. and Dupre B. (1986) Sediment subduction and magma genesis in the Lesser Antilles: Isotopic and trace element constraints. J. Geophys. Res. 91, 5927-5941.

Whitford D.J. and Nicholls I.A. (1976) Potassium variation in lavas across the Sunda arc in Java and Bali. In: Volcanism in Australia (R.W. Johnson, Ed.) p. 63-76, Elsevier, Amsterdam.

Wiebenga W.A. (1973) Crustal structure of the New Britain-New Ireland region in the Western Pacific: island arcs, marginal seas, geochemistry (Coleman P.J., ed.) Univ. of W. Aust. Press 163-177.

Wilkinson J.F.G. and LeMaitre R.W. (1987) Upper mantle amphiboles and micas and TiO_2, K_2O, and P_2O_5 abundances and 100 $Mg/(Mg+Fe^{2+})$ ratios of common basalts and andesites: Implications for modal mantle metasomatism and undepleted mantle compositions. J. Petrology, 28, pt. 1, 37-73.

Wood D.A. (1978) Major and trace element variation in the Tertiary lavas of eastern Iceland with respect to the Iceland geochemical anomaly. J. Petrol. 19, 393-436.

Wood D.A., Joron J.-L., Treuil M., Norry M. and Tarney J. (1979) Elemental and Sr isotope variations in basic lavas from Iceland and the surrounding ocean floor. Contrib. Mineral. Petrol. 70, 319-339.

Worner G., Beusen J.-M., Duchateau N., Gijbels R. and Schmincke H.-U. (1983) Trace element abundance and mineral/melt distribution coefficients in phonolites from the Laacher See Volcano (Germany). Contrib. Mineral. Petrol. 84, 152-173.

Wright T.L. and Doherty P.C. (1970) A linear programming and least squares computer method for solving petrological mixing problems. Bull. Geol. Soc. Am. 81, 1995-2008.

Wright E. and White W.M. (1987) The origin of Samoa: New evidence from Sr, Nd, and Pb isotopes, Earth Planet. Sci. Lett. 81, 151-162.

Wyers G.P. and Barton M. (1987) Geochemistry of a transitional ne-trachybasalt-Q-trachyte lava series from Patros (Dodecanesos), Greece: further evidence for fractionation, mixing and assimilation. Contrib. Mineral. Petrol. 97, 279-291.

Wyllie P.J. (1979) Magmas and volatile components. Amer. Mineral. 64, 469-500.

Yoder H.S. and Tilley C.E. (1962) Origin of basalt magmas: an experimental study of natural and synthetic rock systems. J. Petrol. 3, 342-532.

Zindler A. and Hart S. (1986) Chemical Geodynamics. Ann. Rev. Earth Planet. Sci. 14, 493-571.

Zindler A. and Jagoutz E. (1988) Mantle cryptology. Geochim. Cosmochim. Acta, in press.

Zindler A., Staudigel H., and Batiza R., (1984) Isotope and trace element geochemistry of young Pacific seamounts: implications for the scale of upper mantle heterogeneity, Earth Planet. Sci. Lett. 70, 175-195.